

**Development of new physical and chemical tools for studying bacterial physiology**

By

**Ye-Jin Eun**

Dissertation submitted in partial fulfillment of  
the requirements for the degree of

Doctor of Philosophy  
(Biochemistry)

at the

UNIVERSITY OF WISCONSIN-MADISON

2013

Date of final oral examination: December 13<sup>th</sup>, 2012

Members of the Final Oral Committee:

Douglas B. Weibel, Assistant Professor, Biochemistry and Biomedical  
Engineering

James L. Keck, Professor, Biomolecular Chemistry

Helen E. Blackwell, Professor, Chemistry

Katherine D. McMahon, Associate Professor, Civil and Environmental  
Engineering and Microbiology

Ronald T. Raines, Professor, Biochemistry

## TABLE OF CONTENTS

<b>Acknowledgements</b> .....	iv
<b>Abstract</b> .....	vi
<b>Chapter 1: Dissecting microbiological systems using materials science</b> .....	1
Abstract .....	2
Introduction .....	3
Nanostructures .....	5
Microstructures: elastomeric polymers .....	9
Mesostructures: hydrogels .....	14
Conclusions and future perspectives .....	17
Acknowledgements .....	21
Figures .....	22
Tables .....	28
References .....	31
<b>Chapter 2: Encapsulating bacteria in agarose microparticles using microfluidics for high-throughput cell analysis and isolation</b> .....	37
Abstract .....	38
Introduction .....	39
Experimental methods .....	45
Results and Discussion .....	55
Conclusion .....	64
Acknowledgements .....	68
Figures .....	69
Tables .....	82
References .....	84
<b>Chapter 3: Fabrication of microbial biofilm arrays by geometric control of cell adhesion</b> .....	92
Abstract .....	93
Introduction .....	94
Experimental methods .....	97
Results and Discussion .....	106
Conclusion .....	113
Acknowledgements .....	116
Figures .....	117
References .....	123

<b>Chapter 4: Chemical biological studies of sub-cellular organization in bacteria .....</b>	<b>127</b>
Abstract .....	128
Abbreviations .....	129
Introduction .....	130
Peptidoglycan .....	132
Lipids .....	141
Conclusion .....	147
Acknowledgements .....	148
Figure .....	149
Tables .....	151
References .....	154
<b>Chapter 5: DCAP, a broad-spectrum antibiotic that targets the bacterial membrane .....</b>	<b>161</b>
Abstract .....	162
Introduction .....	163
Experimental methods .....	165
Results and Discussion .....	179
Conclusion .....	187
Acknowledgements .....	188
Figures .....	189
Tables .....	203
References .....	207
<b>Chapter 6: A bacterial division inhibitor that targets the assembly of the divisome .....</b>	<b>210</b>
Abstract .....	211
Introduction .....	212
Experimental methods .....	215
Results .....	227
Discussion .....	236
Conclusion .....	238
Acknowledgements .....	239
Figures .....	240
Tables .....	263
References .....	270
<b>Chapter 7: Conclusions and future directions .....</b>	<b>274</b>
References .....	283
<b>Appendix: Deterministic and stochastic modeling of the bipolar MipZ gradient in <i>Caulobacter crescentus</i> .....</b>	<b>285</b>

Abstract .....	286
Introduction .....	287
The model .....	290
Results and Discussion .....	291
Conclusion .....	296
Acknowledgements .....	298
Figures .....	299
Table .....	304
References .....	305

## Acknowledgements

I am quite lucky that I have always had a great mentor at every turn of my life. Prof. Doug Weibel is one of them, and I would not have grown as a scientist without his support. There are many things that I have learned and gained from him; I list a few of them here. First, he has an infectious enthusiasm for science. I am thankful that I was able to rush into his office whenever I had exciting, weird, and fun observations to share. Second, Doug has made me a better writer. To teach someone how to write is no trivial task, and it was through the countless drafts we exchanged over the years that had given me the practice I needed to learn. Third, Doug trusted me to be independent and encouraged me to collaborate with other scientists. This trust enabled me to explore new things without being afraid of failures, and to develop my own networks within the scientific community. Lastly, Doug has supported my participation in the Physiology Course at the Marine Biological Laboratory where I learned cutting-edge techniques, built lasting friendships, and became convinced about my love for science. Attending the course at MBL was one of the most transformative and profound experiences in my life.

In addition to the support from Doug, I am grateful to my committee members who have given me productive feedback on my work over the years. I am also indebted to the members of the Weibel lab, especially Hannah Tuson, Matt Copeland, and Marie Foss. All past and present lab members were a critical component in my scientific training, and they made the long hours in lab fun and enjoyable.

I would like to acknowledge two research collaborators, Andrew Utada and Martin Thanbichler. Andy worked with me in making agarose microparticles using

microfluidics, and I am grateful for the friendship and mentorship Andy has given me. Martin helped me learn molecular biology and genetics in *Caulobacter crescentus*, and I thank him for answering my unending questions about *C. crescentus*. Also, Martin generously invited me to visit his lab several times, which helped me gain hands-on experiences with *C. crescentus* and become friends with members of his lab.

I would not be here without Profs. Silvia Cavagnero, Tom Record, and Bill Reznikoff. My undergraduate education at Madison was the foundation for my graduate training, and Silvia provided much of that foundation. Particularly, she taught me how to rigorously analyze biochemical and biophysical data. Tom's class on biophysical chemistry was the best science class I took during undergraduate, and I am grateful for the many hours of discussion and coffee he shared in the lunchroom. Bill has rescued me on several occasions – once when I felt defeated about my future and another time when I was stranded in the Boston Logan airport.

I thank my friends (including those in Village Health Project and Ulssu) who have helped me keep my sanity intact and given me opportunities to do things other than science! There are so many to name individually here but I am truly grateful for their friendship and support.

Lastly, I am thankful to my family who has given me unlimited support whenever and wherever. Without my parents, I would not have come to the U.S. from Korea to study abroad. I thank my little sister for being the little sister and my other half.

## **Development of new physical and chemical tools for studying bacterial physiology**

Ye-Jin Eun

Under the supervision of Douglas B. Weibel, Ph. D.

Department of Biochemistry

University of Wisconsin – Madison, Madison, WI.

Throughout the history of science, new tools and techniques have advanced our understanding of nature. In microbiology, the demand for new tools has increased to keep pace with new discoveries, which include the prevalence of bacterial communities. In these microbial communities, heterogeneity and chemical signaling is essential to adaptation and fitness. These discoveries have stimulated research projects that aim to control heterogeneity in bacterial populations, understand variations at the single cell level, and introduce chemicals that modulate biological processes. New tools can have a transformative impact on these areas of microbiology. Each chapter in this thesis introduces a new physical or chemical tool for studying microbial physiology. Chapter 2 describes a biofilm stencil fabricated in a biocompatible polymer. This material serves as a physical scaffold for patterning biofilms on surfaces, and growing them reproducibly in a high-throughput manner. Chapter 3 introduces a microfluidic device for encapsulating microbial cells in agarose microparticles. Encapsulation enables isolation and manipulation cells with rare phenotypes (e.g. drug resistance) in a large population. Chapter 5 describes DCAP, a small molecule that targets bacterial membranes, reduces their transmembrane potential, and increases membrane permeability. The biological activity of DCAP makes it a potent antibiotic against slow-

growing and biofilm-associated cells, which are frequently associated with persistent bacterial infections. Chapter 6 introduces the small molecule divin, which targets the assembly and maturation of divisome, a multi-protein complex that drive bacterial cytokinesis. This mechanism of divin makes it a valuable tool for studying the dynamics of the divisome and the function of its protein components. These chemical and physical tools present new capabilities for isolating, manipulating and studying bacteria, and are poised to transform microbiology.

## CHAPTER 1

### **Dissecting microbiological systems using materials science**

Adapted from:

Abishek Muhalimohan, Ye-Jin Eun, Basu Bhattacharyya, and Douglas B. Weibel (2009)

*Trends in Microbiology* 17(3):100-108.

## ABSTRACT

Materials science offers microbiologists a wide variety of organic and inorganic materials with chemical and physical properties that can be precisely controlled. These materials present new capabilities for isolating, manipulating and studying bacteria and other microorganisms and are poised to transform microbiology. This chapter summarizes three classes of materials that span a range of length scales (nano, micro and meso) and describes several areas in microbiology where these materials can be beneficial for research.

## INTRODUCTION

Materials science is a field that is positioned at the intersection of the physical sciences and engineering; in it, organic, inorganic and polymeric materials are routinely synthesized and fabricated with an extraordinary spectrum of dimensions and properties. Biocompatible structures that match the intrinsic length scale of a wide variety of structures found in microbiology (e.g. proteins, chromosomes, organelles, individual cells and multicellular structures) can be tailored to study a range of processes that might be difficult to explore using the techniques of classical physiology-driven microbiology, genetics, genomics and biochemistry (Figure 1). In contrast to microbiology and materials science, which are just beginning to converge, eukaryotic cell biology has been implementing new materials for at least a decade. Eukaryotic cell biology and materials science have become intertwined to the point where cell biologists routinely synthesize materials for their studies and materials scientists are experienced in cell culture and genetics. What does materials science and engineering bring to eukaryotic cell biology that it cannot also bring to microbiology? We believe that the implementation of new materials will benefit the study of microbes just as it has transformed eukaryotic cell biology.

In this chapter, we draw connections between recent advances in materials science and unanswered questions in microbiology by focusing on two aims that will stimulate research at the interface of these two fields: (i) a discussion of several 'classes' of structures organized according to physical length scale (nano to meso) that we anticipate will be particularly useful for microbiological studies, and (ii) a review of examples from the literature that demonstrates or indicates their potential application

in these areas. We conclude by suggesting several questions in microbiology for which material science may have an impact and stimulate further research.

## NANOSTRUCTURES

'Nano' is typically used to define structures with a length scale of 1–100 nm. To put the dimensions of nanoscale objects in perspective: a structure that is 1 nm wide consists of tens of atoms. Nanoscale materials are not just another step in miniaturization – they are a unique class of materials with characteristics that are not found in their macroscopic counterparts, including a large surface-to-volume ratio in which the majority of the atoms are present on the surface of a particle or structure; tunable optical properties (e.g. excitation and emission wavelengths and plasmon resonance); and extraordinary mechanical, thermal and conductive properties (1). The length scale and properties of nanoscale materials make them particularly applicable to exploring phenomena occurring within bacteria at the subcellular level. Below, we introduce this class of materials and elaborate on its application to the study of intracellular structures in bacterial cells.

A wide variety of nanostructured materials (e.g. surfaces, thin films, wires, spheres, rods, prisms and other particles) have applications in biology. Nanoparticles (NPs) are arguably the class of nanostructured materials that have been most frequently applied to the study of biological systems (1). NPs can be synthesized in monodisperse form – that is, the particles have a small coefficient of variance in their mean diameter – which makes it possible to control and predict their properties. The diameter of NPs (>1 nm) is equivalent to or smaller than the cross-section (hydrodynamic radius) of many proteins and other biological structures. NPs have been synthesized in a variety of organic and inorganic materials (Table 1). Finally, several classes of NPs are photostable and have optical parameters that can be tuned by controlling their dimensions during

their synthesis. We believe that semiconductor nanocrystals (quantum dots, or 'QDs') and gold NPs are two classes of nanostructures that will illuminate the structure of microbes. A summary of the most salient features of these materials is discussed below.

### *Quantum dots*

QDs are photostable, bright and resistant to metabolic degradation (2). The emission spectrum of QDs is narrow and can be controlled by varying the diameter of particles (Figure 2b). QDs are particularly useful as donors for Förster resonance energy transfer (FRET) (3). In vivo studies of mammalian cells using QDs as tracers and FRET donors have taken advantage of their photostability and fluorescence intensity. The ability to coat the surface of particles with ligands that target their localization within the cell (Figure 2a) has made them particularly useful for studying the subcellular structure of mammalian cells (4). QDs are typically microinjected into mammalian cells, and their temporal and spatial location is measured using epifluorescence microscopy over a range of time scales (1, 2). NPs can also be introduced in mammalian cells by attaching transport sequences to their surface (3).

In contrast to their application to the study of mammalian cell biology, QDs are still emerging as probes for studying microbes (5). One of the major hurdles of using QDs to study bacteria is the difficulty of transporting them into the cytoplasm. The cell dimensions of most strains of bacteria make microinjection unfeasible. The peptidoglycan (PG) layer of the cell wall limits the passive transport of QDs into cells; this material can range from 10 to 80 nm thick in Gram-negative and Gram-positive bacteria (6). The average pore size of the mesh-like PG is believed to be constant in bacteria and is ~2 nm in cells of *Bacillus subtilis* and *Escherichia coli* (7). The porosity of

the PG is smaller than the diameter of most commercially available QDs (~3–6 nm) and makes it unlikely that QDs will passively diffuse through the PG into the cytoplasm.

Although the PG presents a physical barrier for the efficient uptake of QDs by bacteria, several groups have started exploring the transport of QDs into bacterial cells. Li and coworkers (8) transformed  $\text{Ca}^{2+}$ -induced competent cells of *E. coli* with 3–4 nm diameter QDs as tracers for studying chemical competence. An interesting approach for transforming cells with QDs might be to take advantage of the native transport machinery in the bacterial cell wall. Kloepfer et al. (9) have found that adenine- and adenosine monophosphate (AMP)-coated QDs are internalized by adenine auxotrophs of *B. subtilis* and *E. coli* (Figure 2c,d). They suggest that the uptake of QDs occurs via purine-dependent transport mechanisms. Hirschey et al. (10) described the transport of QDs coated with organic di- and tricarboxylic acids (e.g. citrate, isocitrate, succinate and malate) into the cytoplasm of cells of *E. coli*. It is unclear how the QDs cross the PG en route to the cytoplasm, particularly if the PG is a continuous polymer network with 2-nm wide pores. The systematic study of QDs decorated with ligands that target the transport systems of bacterial cells might introduce new materials and mechanisms for studying transport processes in bacteria and techniques for improving their transformation.

### ***Gold nanoparticles***

Gold NPs are frequently used as contrast agents for imaging bacterial cells using transmission electron microscopy (TEM). The application of gold NPs to the study of bacteria, however, is not limited to TEM and might also be useful for imaging the subcellular localization of proteins and nucleic acid within cells using optical

microscopy. Gold NPs exhibit a phenomenon referred to as localized surface plasmon resonance (LSPR), in which gold NPs scatter visible light at a specific wavelength (11). When the surface chemistry of a gold NP changes, the wavelength of light scattered by the particle is red-shifted and provides a color-based biological sensor. The application of a related technique to study the localization of proteins in live cells might be possible using gold NPs coated with small molecules that are substrates for enzymes. The basis for this approach is a recent study by Liu et al. (12), in which the authors used an LSPR-based technique to monitor b-lactamase activity. In this assay, gold NPs were coated with cephalosporin. Cleavage of cephalosporin by b-lactamase caused the NPs to cluster, which produced a measurable optical signal. A similar concept has been applied to the development of an optical sensor of bacterial growth that depends on the crosslinking of dextran-coated gold NPs in the presence of concanavalin A and carbohydrates in the growth medium. During periods of growth, the concentration of free carbohydrates in solution decreases and the size of gold NP clusters is reduced (13).

## MICROSTRUCTURES: ELASTOMERIC POLYMERS

Microstructures have a size scale similar to that of individual or small groups of microorganisms and typically range from 100 nm to 100 microns. The overlap in these length scales makes it possible to design and implement microstructured materials to isolate, manipulate and study individual bacteria or small multicellular structures.

Microstructures can be used to control the interface between cells and their microenvironment – the region that is sensed by a cell and is typically defined by molecular contact, mass transport and diffusion – and, ultimately, the internal organization and physiology of the cell. In the next section, we describe a class of microstructured materials for controlling small volumes of fluids that provide access to a variety of experimental conditions that are not available using traditional techniques of microbiology.

Microfluidic systems have channels with micron-scale dimensions and are used to manipulate small volumes of fluids (from fL to mL). Microchannels have a large surface-to-volume ratio that facilitates rapid mass and heat transfer. These systems offer predictable and reproducible control over conditions for experiments with bacteria by minimizing the effects of environmental fluctuations (e.g. temperature and aeration) (14). The concentration of molecules in microchannels can also be controlled with a high degree of accuracy in space and time (15). Microfluidic systems also have several practical characteristics: they consume small quantities of samples and reagents, they can be multiplexed to perform several assays simultaneously and they are inexpensive. Most bacteria live in low Reynolds-number environments, and microfluidic systems, in which fluids flow in the laminar regime, can reproduce such environments precisely.

Microchannels have been created in a variety of materials, including glass, silicon, poly(methyl methacrylate) (PMMA) and other polymers (Table 2). The simplicity of embossing the elastomeric polymer, poly(dimethylsiloxane) (PDMS), with channels and the unique properties of this polymer make it widely used for microfluidics (16). Below, we briefly discuss the areas of microbiology in which microstructured materials have been particularly useful and presented a clear potential to further research.

### *Single cell analysis*

Microstructured surfaces are useful for the isolation and study of single bacterial cells and might be particularly relevant to bacterial communities in environmental samples (17). One of the challenges facing microbial ecology is the difficulty of culturing a heterogeneous population of microorganisms extracted from their environment, which makes it difficult to quantitatively determine their composition, genotype and function. Recent advances in PDMS microfluidic systems make it possible to analyze the genotype and phenotype of a single bacterium, which obviates the necessity for culturing cells and bypasses the limitations of their isolation and growth in the laboratory. The Quake group has developed several techniques based on microfluidics for isolating single bacteria from sparse environmental samples, including the hind gut of termites (18) and the human oral cavity (19). They have integrated multiplex PCR into these microfluidic systems to amplify and sequence entire genomes from single bacteria and have used these devices to genotype and identify several new species of bacteria.

The greatest impact of microstructured materials in microbiology might be in the area of single-cell analysis (20, 21). Single-cell analysis overcomes biases in sampling

that arise from ensemble averaging of data from bulk measurements (22), which makes it a powerful tool to illuminate minor phenotypic differences among clonal populations of cells. However, data from traditional single-cell experiments (e.g. microscopy) are inherently noisy because of variations in the age of cells, the stochastic nature of metabolism and transcription, and fluctuations in the microenvironment of cells. Microstructured materials make it possible to average data collected from thousands of isolated cells in parallel under identical conditions. For example, Balaban and coworkers (23, 24) used microfluidic channels to keep track of progenies of single bacterial cells over several life cycles after treatment with antibiotics and derived a mathematical model of bacterial persistence to (Figure 3b).

### *Cell shape*

The molecular details of the coordination of cell growth, division, asymmetry and the cytoskeleton in bacteria are just beginning to emerge (25-27). Microstructured tools provide a unique capability for the study of polarity, division, and cell wall remodeling in bacterial cells. For example, Renner and Weibel (28) tested the hypothesis that the intrinsic curvature of poles in bacterial cells is responsible for organization of membrane lipids. They fabricated circular holes with varying curvatures in agarose using a PDMS mold, and confined *E. coli* spheroblasts inside the holes. The authors observed that cardiolipin, an anionic lipid in the *E. coli* membrane, preferred to localize to the region of high curvature.

The idea that bacterial cells utilize physical parameters to organize and modify their biological processes was tested in another study by Mannik et al (29). The authors confined *E. coli* cells in a PDMS channel whose height is smaller than the width of the

cell, squeezing the cells down to a 'pancake' shape. Then they asked how cell division responds to altered cell shape. Remarkably, the bacterial cells continue to grow and divide into two equal halves while trapped in the channel. By testing different mutants under identical conditions, they concluded that the nucleoid occlusion is responsible for the robust division of mis-shaped bacterial cells.

The robustness of division in 'pancake' shaped cells demonstrates how flexible and dynamic cell sculpting process is in prokaryotes. Takeuchi et al. (30) used embossed agarose structures to exert mechanical forces on growing bacterial filaments. As the cells grow, the deposition of the cell wall during filamentation is controlled and the filaments become permanently deformed in the shape of the channels (Figure 3a). Cabeen et al. (31) recently used this technique to study the mechanism of crescentin, a homolog of eukaryotic intermediate filaments that polymerizes into filaments in cells of *Caulobacter crescentus* and influences cell curvature.

### ***Bacterial motility***

The study of bacterial motility is another area of microbiology in which microchannels are playing an important part. The dimensions and properties of channels can be tailored to create new conditions or mimic the native environment of bacterial cells. DiLuzio et al. (32) studied the motility of cells of motile strains of *E. coli* in microchannels in which the porosity of the channel surfaces was varied. They observed that bacteria preferably swim in hydrodynamic contact with the surface of hydrogels. This phenotype is particularly evident when cells are in channels with a hydrogel 'floor' – the cells move along the channel in contact with the right-hand wall because of the clockwise rotation of the cell body (viewed from behind the cell) during

their translation through fluids. Hulme et al. (33) have taken advantage of this phenotype to develop a microfluidic system of ratchets that sorts motile strains of bacteria based on cell length. Microfluidics might also provide insight into bacterial chemotaxis. Traditional capillary-based chemotaxis assays are incapable of producing gradients that are temporally stable, complex and non-linear. Microfluidic systems overcome these limitations and make it possible to study concentration gradients of chemoattractants and chemorepellants at the nanomolar level (34).

## MESOSTRUCTURES: HYDROGELS

Mesostructured materials typically have features with length scales from 500 microns to several millimeters, which we refer to as ‘mesoscopic’. These structures provide mechanisms of controlling populations of microbial cells and confining them in geometries to study population dynamics and collective behavior. Mesostructured materials might provide a unique platform for culturing bacteria, in which the user can control the spatial organization of colonies and manipulate cell–cell and cell–environment interactions (35).

In this section, we introduce mesostructured polymers with properties that provide several advantages over traditional materials used for bacterial cell culture. Hydrogels are polymers that absorb and retain a large volume fraction of bound water. Agar is an example of this class of materials that has been used in microbiology as a substrate for bacterial growth. It is widely available, inexpensive, and easy to prepare and use. Agar has many useful properties: it provides a ‘wet’ environment for bacterial growth; it is relatively ‘transparent’ to the diffusion of nutrients, ions and metabolic waste; it is biocompatible; and it is not degraded by bacteria. Several characteristics of agar limit its applicability to addressing certain microbiological questions, including chemical and physical properties that are typically not well defined. Agar offers limited control over parameters such as surface chemistry, porosity, wetness, wettability and stiffness. Agarose is chemically defined and provides better control over some parameters relevant to bacterial culture. Poly(ethylene glycol) (PEG) and polyacrylamide (PAA) are hydrogels that might be excellent alternatives to agar and agarose for bacterial culture because their physical properties can be tuned precisely

during their synthesis (36) (Table 3). The surface of these polymers can be topographically patterned and functionalized to present different molecules (37), including chemistry that makes them responsive to light, pH, temperature and molecules secreted by cells. These modifications change the pore size, water content and diffusion of molecules through the polymer and might affect the growth rate of microbes on the surfaces. Below, we describe applications of hydrogels in microbiology.

### *Microbial culturing*

Cell culture is arguably one of the most fundamental techniques in microbiology and can benefit considerably from the implementation of new materials. Most organisms in the biosphere have not been cultured by conventional microbiology to date, and many of these seem to be refractory to routine culture. Polymers might be useful for culturing and isolating these organisms which, in turn, will provide insights into the mechanisms of sensory transduction between the cell and its environment (38). Mesostructured polymeric structures have recently been used to control the length scale of interactions between different microorganisms, making it possible to engineer syntrophic interactions (39, 40). Kaehr and Shear (41) have developed protein-based hydrogels that respond to chemical stimuli by undergoing changes in their hydration state, making it possible to dynamically control the volume of the polymer. Using this technique, the Shear and Whiteley labs have collaborated to create 'lobster' traps and investigated the relationship between quorum sensing, virulence factor expression, and environmental parameters of growth. These three-dimensional structures for microbial culturing would further assist the study of sociomicrobiology.

Bacterial microarrays, like their DNA and protein counterparts, have applications in high-throughput phenotypic (42) and genotypic screens (43). Reproducibility and the ability to catalog (store) and replicate thousands of parallel microcolonies while maintaining a form factor no larger than a postage stamp make bacterial microarrays an excellent alternative to conventional techniques of streaking and plating colonies. Weibel et al. (44) have developed a technique for directly printing patterns of bacterial colonies on surfaces using hydrogel stamps for cataloging strains and studying cell-cell interaction (Figure 3d).

### *Population dynamics and evolution*

Mesostructured materials can also be used to address questions of population dynamics and microbial evolution. Cho et al. (45) and Flickinger et al. (46) recently used mesostructures to identify the role of chemotaxis, quorum sensing and spatial confinement in the formation of biofilms (Figure 3c). The systematic variation of parameters that affect biofilm growth (47) (including surface chemistry, microenvironment and mechanical stresses due to flow and geometry) will make it possible to study the interaction of cells, the establishment of spatial heterogeneity and the differentiation of cells within biofilms (48). Mathematical models that describe complex multicellular behavior (such as cooperation (49) and the predator-prey model of *E. coli* behavior (50)) can now be verified experimentally using this class of materials.

## CONCLUSION AND FUTURE PERSPECTIVES

Many of the materials that are currently used to study microbes have evolved little since their introduction, even after a century or more of routine use. Have these materials stuck around because they are convenient, or do they offer unique capabilities or an ideal solution? A relevant example is the agar plate. Agar surfaces are still the most frequently used platform for culturing and isolating the vast majority of bacterial strains grown in the laboratory. Slants, stabs, plates and other forms of solid media that incorporate agar are used for the routine propagation and storage of bacterial colonies. However, based on the diverse environments that microbes inhabit, it seems unlikely that the surface of an agar plate is a faithful reproduction of their microhabitat (38). Because there are hundreds of other polymer gels with chemical and physical properties that can be precisely tuned – in contrast to agar – and used for this application, it seems likely that the popularity of agar might be a matter of convenience.

New materials and techniques for studying microbes will make it possible to control their microenvironment and study cell physiology and behavior at a new level of detail by interfacing these capabilities with the techniques of genetics, genomics and biochemistry. Materials scientists know how to control the physical and chemical properties of materials that will have key roles in this area; they might not fully appreciate the capabilities that microbiologists need. Physical scientists and engineers that design and fabricate materials, and end users, who might be microbiologists seeking new capabilities for studying microbes, have historically not worked closely together. Over the past several years, however, the gap between these fields has narrowed as materials scientists have ventured into microbiology in search of new

applications for materials and microbiologists have been introduced to materials with new capabilities. Materials science is poised to have an important impact on microbiology, and we pose several questions below that we believe will stimulate further research at the interface of microbiology and materials science.

*What is the fate of individual bacteria in multicellular communities?*

Fluorescence microscopy has been instrumental in advancing our understanding of microorganisms. Commonly used fluorescent probes are limited by their low photostability and occasional cytotoxicity. Quantum dots (QDs) are fluorescent semiconductor nanoparticles that can be designed to overcome these problems. QDs can be used to label subpopulations of bacteria and can be tracked over several generations (4).

*What is the role of physical interactions between individual bacterial cells in multicellular structures?*

Most bacteria are too small and intractable to be used with micromanipulation techniques commonly used with larger eukaryotic cells. Microfluidics offers a platform for precisely controlling the position of single bacterial cells and engineering reproducible interactions between cells, thereby making it possible to study cell-cell interactions.

*How does asymmetry arise in bacteria?*

The manipulation of single microbial cells might be also an important capability for studying the intracellular organization of bacteria. Rather than a simplistic view of

the cytosol as a collection of freely diffusing molecules, it is now recognized that there is a remarkable amount of subcellular organization and asymmetry in bacterial cells. Microfluidic techniques such as PARTCELL (51) make it possible to 'paint' domains of a cell with reagents by taking advantage of laminar fluid flow. This method, and others, might be particularly useful for studying the origins of asymmetry and its role in bacterial physiology.

*How do interactions arise between different bacterial species?*

Bacteria in their natural habitats exhibit a rich variety of interspecies interactions including symbiosis, competition, parasitism and commensalism. The systematic study of these interactions is complicated by the challenge of accurately mimicking the conditions for their growth. The physical and chemical properties of certain biocompatible hydrogels can be tuned to present a spatially heterogeneous substrate that resembles natural substrates more closely than the surface of an agar plate does.

The merger of material science and microbiology fields will almost certainly drive the emergence of exciting new questions and directions in biology, chemistry, and materials science and engineering. In the next two chapters, I describe two physical tools I have developed to study multicellular behaviors and interspecies interactions in bacteria. Specifically, I discuss a new method to spatially control biofilm formation using PDMS stencils (52) in Chapter 2. This method allows us to form multicellular communities on various surfaces reproducibly and makes it possible to study the communities in a high-throughput manner. In Chapter 3, I discuss the fabrication of hydrogel microparticles using microfluidic devices to encapsulate bacterial cells (53).

The flexibility of the technique allows for separation of individual cells from a heterogeneous population for single-cell analysis and co-encapsulation of different cell types to study dynamics of cell-to-cell interaction within a microparticle.

## ACKNOWLEDGEMENTS

The United States Department of Agriculture (WISO1192), the National Science Foundation under Grant No. DMR-0520527, a 3M Non-tenured Faculty Award and a Searle Scholar Award support research in our laboratory at the interface of materials science and microbiology.

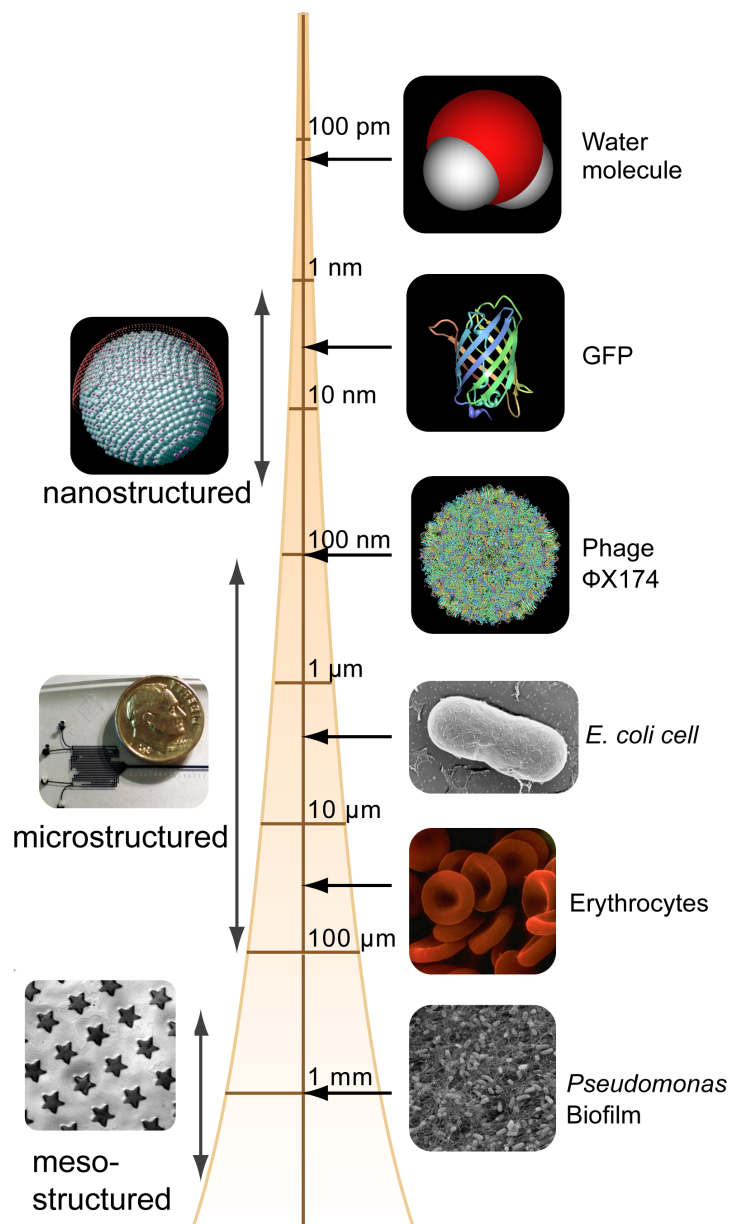


**Figure 1.** Length scales in materials science and biology. Nano-, micro- and mesostructured materials are represented by a quantum dot (54), a microfluidic device and patterns of star-shaped bacterial colonies of *E. coli* (left column) (44). Common biological structures are shown for size comparison (right column). Images of protein structures were generated from PDB entries 1EMA and 1CDR using Pymol

(<http://www.pymol.org/>). The structure of the quantum dot was reproduced, with permission, from Ref. (54).

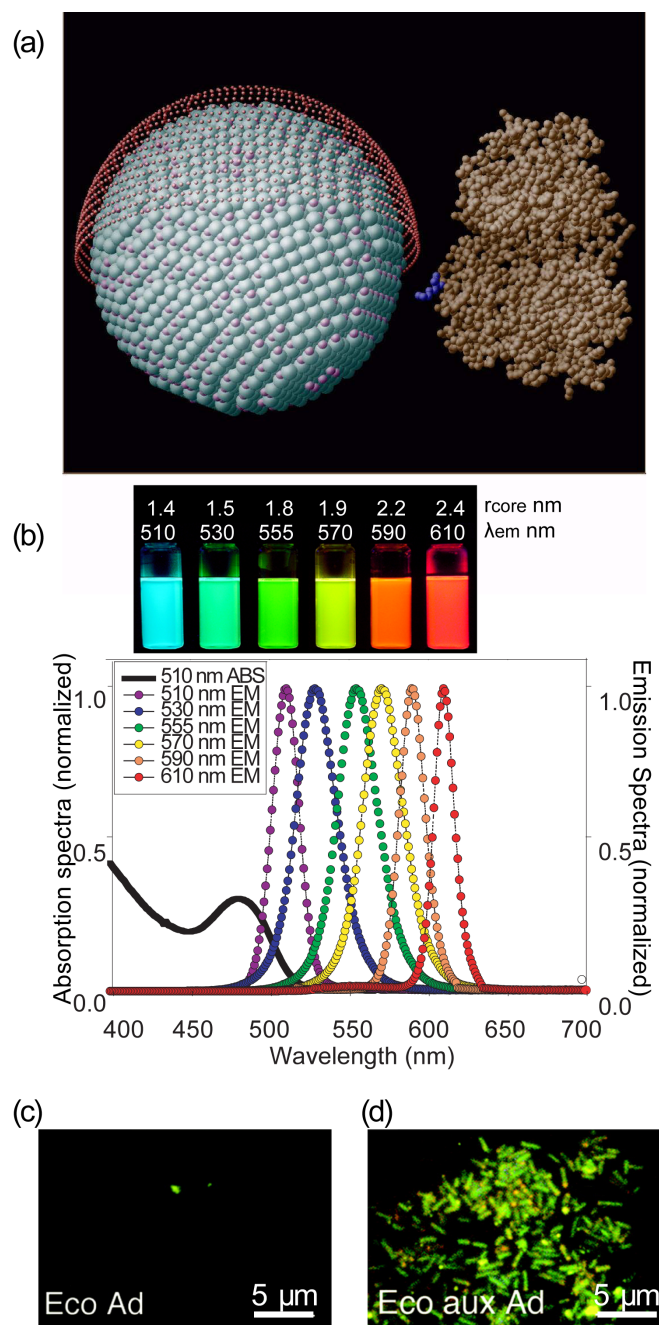


**Figure 2.** Properties of quantum dots (QDs). (a) A cartoon depicting a QD (55). The inner CdSe core particle (diameter = 60Å) is encapsulated by a ZnS shell. The zinc atoms are shown in pink, and the sulfur atoms are shown in teal. The QD surface is

functionalized with dihydrolipoic acid (red). A maltose-binding protein is shown to the right of the QD for size comparison. (b) A plot of the fluorescence emission of QDs versus the radius of the core particle (55). (c,d) QDs labeled with adenine or AMP are internalized by *E. coli* adenine auxotrophs (Eco aux Ad, right image); no internalization is observed in wild-type *E. coli* (Eco Ad, left image) (9). Figures were reproduced, with permission, from Refs (9, 54, 55).

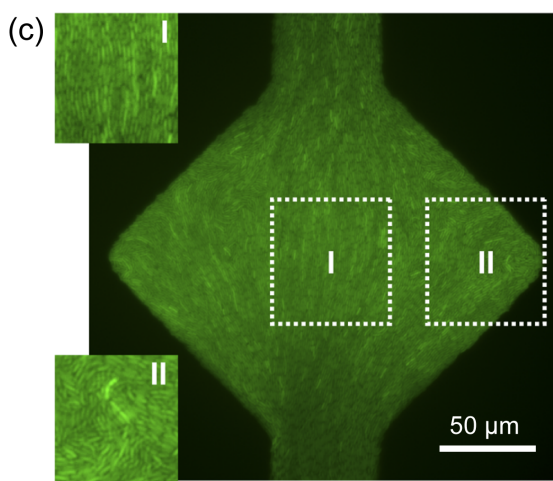
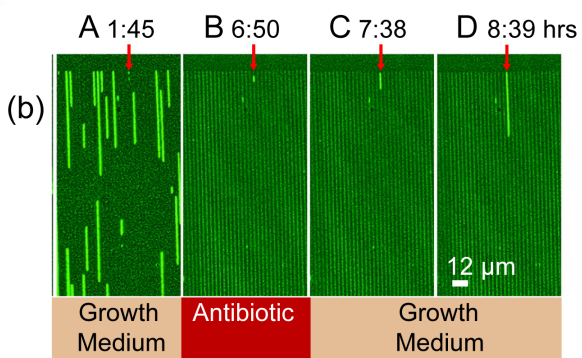
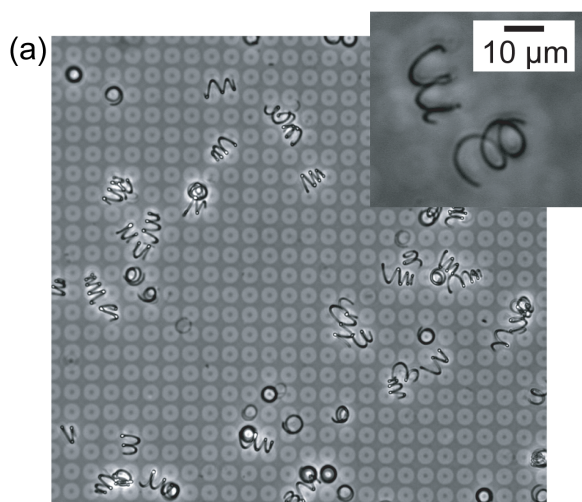


**Figure 3.** Examples of micro- and mesostructured materials. (a) A micropatterned agarose surface used to engineer bacterial cell shape. The image inset shows helical, filamentous cells of *E. coli* that were released from the microchambers and retain the imposed shape (30). (b) Microchannels used for single-cell analysis of bacterial persistence (23). Cells form linear microcolonies in the microchannels that were used to link persistence to heterogeneity in bacterial populations. (c) The spatial self-organization of bacteria is observed when grown in confined geometries (45). Cells in region I were distributed almost exclusively perpendicular to the long axis of the mesostructure, whereas cells in region II were randomly distributed. (d) Bacteria-shaped structures of photoluminescent *Vibrio fischeri* patterned on the surface of agar to form the word 'ink' (44). Figures (a), (b) and (c) were reproduced, with permission, from Refs (23, 30, 45).

**Table 1.** Properties of nanoparticles

<b>Material</b>	<b>Composition</b>	<b>Preparation</b>	<b>Properties</b>	<b>Refs</b>
Dendrimers	Polymer	Chemical synthesis	Hyper-branched network Porous	(56)
Nanocages	DNA	Self-assembly	Hybridization to dsDNA	(57)
Metal nanoparticles	Gold, silver	Nucleation	Surface plasmon resonance Can be functionalized	(12, 13, 58)
Quantum dots	CdSe, CdTe, PbSe, InAs	Nucleation, crystallization	Fluorescent Photostable Narrow emission spectra Can be functionalized	(55, 59)

**Table 2.** Properties of common microstructured materials

<b>Material</b>	<b>Fabrication methods</b>	<b>Optical properties</b>	<b>Young's modulus</b>	<b>Other properties</b>
Silicon	Electron-beam lithography Chemical etching Photolithography	Opaque; reflective <500 nm	129-186 GPa	Resistant to most solvents Scratch resistant Expensive Brittle
Glass	Electron-beam lithography Chemical etching	Transparent >195 nm	~100 GPa	Resistant to most solvents Scratch resistant Expensive
PMMA	Electron-beam lithography Photolithography Hot embossing	Transparent >350 nm	2-3 GPa	Acid sensitive Organic-solvent sensitive
PDMS	Drop casting Rapid prototyping	Transparent >280 nm	~2 MPa	Resistant to alcohols Reversible swelling in organic solvents Flexible Gas permeable Hydrophobic

**Table 3.** Properties of hydrogels

<b>Material</b>	<b>Synthesis</b>	<b>Physical properties</b>	<b>Surface chemistry</b>	<b>Stimulus response</b>	<b>Refs</b>
Agar	Gels upon cooling	Pore size is undefined Permits diffusion of macromolecules	Hydroxyl groups	None	
Agarose	Gels upon cooling	Pore size varied from 200-500 nm (5-1% gel) Stiffness is 400 kPa (2.5% gel)	Hydroxyl groups	None	(60, 61)
Alginate	Crosslinks with Ca <sup>+2</sup>	Pore size and stiffness varied	Guluronic acid groups	None	(62)
PEG	Photo-crosslinking	Pore size is 1-10 nm Stiffness varied	Ether linkages	Volume expands upon water absorption	(63)
PAA	Free-radical polymerization	Pore size is 19-142 nm Stiffness ~10 GPa	Various	Responsive to temperature (NIPAM) and pH (chitosan-PAA)	(64,65)
Protein-based	Photo-crosslinking	Unknown	Amino acids	Responsive to temperature, pH, and ionic strength	(41)

## REFERENCES

1. Grainger, D. W., and Castner, D. G. (2008) Nanobiomaterials and nanoanalysis: Opportunities for improving the science to benefit biomedical technologies, *Advanced Materials* 20, 867-877.
2. Jaiswal, J. K., and Simon, S. M. (2004) Potentials and pitfalls of fluorescent quantum dots for biological imaging, *Trends in Cell Biology* 14, 497-504.
3. Alivisatos, A. P., Gu, W. W., and Larabell, C. (2005) Quantum dots as cellular probes, In *Annual Review of Biomedical Engineering*, pp 55-76.
4. Michalet, X., Pinaud, F. F., Bentolila, L. A., Tsay, J. M., Doose, S., Li, J. J., Sundaresan, G., Wu, A. M., Gambhir, S. S., and Weiss, S. (2005) Quantum dots for live cells, in vivo imaging, and diagnostics, *Science* 307, 538-544.
5. Helmick, L., de Mayolo, A. A., Zhang, Y., Cheng, C.-M., Watkins, S. C., Wu, C., and LeDuc, P. R. (2008) Spatiotemporal response of living cell structures in *Dictyostelium discoideum* with semiconductor quantum dots, *Nano Letters* 8, 1303-1308.
6. Vollmer, W., Blanot, D., and de Pedro, M. A. (2008) Peptidoglycan structure and architecture, *Fems Microbiology Reviews* 32, 149-167.
7. Demchick, P., and Koch, A. L. (1996) The permeability of the wall fabric of *Escherichia coli* and *Bacillus subtilis*, *Journal of Bacteriology* 178, 768-773.
8. Li, W. H., Me, H. Y., Xie, Z. X., Lu, Z. X., Ou, J. H., Chen, X. D., and Ping, S. (2004) Exploring the mechanism of competence development in *Escherichia coli* using quantum dots as fluorescent probes, *Journal of Biochemical and Biophysical Methods* 58, 59-66.
9. Kloepfer, J. A., Mielke, R. E., and Nadeau, J. L. (2005) Uptake of CdSe and CdSe/ZnS quantum dots into bacteria via purine-dependent mechanisms, *Applied and Environmental Microbiology* 71, 2548-2557.
10. Hirschey, M. D., Han, Y. J., Stucky, G. D., and Butler, A. (2006) Imaging *Escherichia coli* using functionalized core/shell CdSe/CdS quantum dots, *Journal of Biological Inorganic Chemistry* 11, 663-669.
11. Aslan, K., Lakowicz, J. R., and Geddes, C. D. (2005) Plasmon light scattering in biology and medicine: new sensing approaches, visions and perspectives, *Current Opinion in Chemical Biology* 9, 538-544.

12. Liu, R., Liew, R., Zhou, H., and Xing, B. (2007) A simple and specific assay for real-time colorimetric visualization of beta-lactamase activity by using gold nanoparticles, *Angewandte Chemie-International Edition* 46, 8799-8803.
13. Nath, S., Kaittanist, C., Tinkharn, A., and Perez, J. M. (2008) Dextran-coated gold nanoparticles for the assessment of antimicrobial susceptibility, *Analytical chemistry* 80, 1033-1038.
14. Atencia, J., and Beebe, D. J. (2005) Controlled microfluidic interfaces, *Nature* 437, 648-655.
15. Whitesides, G. M. (2006) The origins and the future of microfluidics, *Nature* 442, 368-373.
16. Xia, Y. N., and Whitesides, G. M. (1998) Soft lithography, *Annual Review of Materials Science* 28, 153-184.
17. Costerton, B. (2004) Microbial ecology comes of age and joins the general ecology community, *Proceedings of the National Academy of Sciences of the United States of America* 101, 16983-16984.
18. Ottesen, E. A., Hong, J. W., Quake, S. R., and Leadbetter, J. R. (2006) Microfluidic digital PCR enables multigene analysis of individual environmental bacteria, *Science* 314, 1464-1467.
19. Marcy, Y., Ouverney, C., Bik, E. M., Loesekann, T., Ivanova, N., Martin, H. G., Szeto, E., Platt, D., Hugenholtz, P., Relman, D. A., and Quake, S. R. (2007) Dissecting biological "dark matter" with single-cell genetic analysis of rare and uncultivated TM7 microbes from the human mouth, *Proceedings of the National Academy of Sciences of the United States of America* 104, 11889-11894.
20. Mihalcescu, I., Hsing, W. H., and Leibler, S. (2004) Resilient circadian oscillator revealed in individual cyanobacteria, *Nature* 430, 81-85.
21. Rosenfeld, N., Young, J. W., Alon, U., Swain, P. S., and Elowitz, M. B. (2005) Gene regulation at the single-cell level, *Science* 307, 1962-1965.
22. Brehm-Stecher, B. F., and Johnson, E. A. (2004) Single-cell microbiology: Tools, technologies, and applications, *Microbiology and Molecular Biology Reviews* 68, 538-559.
23. Balaban, N. Q., Merrin, J., Chait, R., Kowalik, L., and Leibler, S. (2004) Bacterial persistence as a phenotypic switch, *Science* 305, 1622-1625.
24. Gefen, O., Gabay, C., Mumcuoglu, M., Engel, G., and Balaban, N. Q. (2008) Single-cell protein induction dynamics reveals a period of vulnerability to antibiotics in persister bacteria, *Proceedings of the National Academy of Sciences of the United States of America* 105, 6145-6149.

25. Cabeen, M. T., and Jacobs-Wagner, C. (2005) Bacterial cell shape, *Nature Reviews Microbiology* 3, 601-610.
26. Shapiro, L., McAdams, H. H., and Losick, R. (2002) Generating and exploiting polarity in bacteria, *Science* 298, 1942-1946.
27. Shapiro, L., McAdams, H. H., and Losick, R. (2009) Why and How Bacteria Localize Proteins, *Science* 326, 1225-1228.
28. Renner, L. D., and Weibel, D. B. (2011) Cardiolipin microdomains localize to negatively curved regions of Escherichia coli membranes, *Proceedings of the National Academy of Sciences of the United States of America* 108, 6264-6269.
29. Mannik, J., Wu, F., Hol, F. J., Bisicchia, P., Sherratt, D. J., Keymer, J. E., and Dekker, C. (2012) Robustness and accuracy of cell division in Escherichia coli in diverse cell shapes, *Proc Natl Acad Sci U S A* 109, 6957-6962.
30. Takeuchi, S., DiLuzio, W. R., Weibel, D. B., and Whitesides, G. M. (2005) Controlling the shape of filamentous cells of Escherichia coli, *Nano Letters* 5, 1819-1823.
31. Cabeen, M. T., Charbon, G., Vollmer, W., Born, P., Ausmees, N., Weibel, D. B., and Jacobs-Wagner, C. (2009) Bacterial cell curvature through mechanical control of cell growth, *The EMBO journal* 28, 1208-1219.
32. DiLuzio, W. R., Turner, L., Mayer, M., Garstecki, P., Weibel, D. B., Berg, H. C., and Whitesides, G. M. (2005) Escherichia coli swim on the right-hand side, *Nature* 435, 1271-1274.
33. Hulme, S. E., DiLuzio, W. R., Shevkoplyas, S. S., Turner, L., Mayer, M., Berg, H. C., and Whitesides, G. M. (2008) Using ratchets and sorters to fractionate motile cells of Escherichia coli by length, *Lab on a chip* 8, 1888-1895.
34. Mao, H. B., Cremer, P. S., and Manson, M. D. (2003) A sensitive, versatile microfluidic assay for bacterial chemotaxis, *Proceedings of the National Academy of Sciences of the United States of America* 100, 5449-5454.
35. Ingham, C. J., Sprenkels, A., Bomer, J., Molenaar, D., van den Berg, A., Vlieg, J. E. T. v. H., and de Vos, W. M. (2007) The micro-Petri dish, a million-well growth chip for the culture and high-throughput screening of microorganisms, *Proceedings of the National Academy of Sciences of the United States of America* 104, 18217-18222.
36. Mrksich, M. (2002) What can surface chemistry do for cell biology?, *Current Opinion in Chemical Biology* 6, 794-797.

37. Kim, D., and Beebe, D. J. (2007) Hydrogel-based reconfigurable components for microfluidic devices, *Lab on a chip* 7, 193-198.
38. Kaeberlein, T., Lewis, K., and Epstein, S. S. (2002) Isolating "uncultivable" microorganisms in pure culture in a simulated natural environment, *Science* 296, 1127-1129.
39. Choi, W. S., Kim, M., Park, S., Lee, S. K., and Kim, T. (2012) Patterning and transferring hydrogel-encapsulated bacterial cells for quantitative analysis of synthetically engineered genetic circuits, *Biomaterials* 33, 624-633.
40. Kim, H. J., Boedicker, J. Q., Choi, J. W., and Ismagilov, R. F. (2008) Defined spatial structure stabilizes a synthetic multispecies bacterial community, *Proceedings of the National Academy of Sciences of the United States of America* 105, 18188-18193.
41. Kaehr, B., and Shear, J. B. (2008) Multiphoton fabrication of chemically responsive protein hydrogels for microactuation, *Proceedings of the National Academy of Sciences of the United States of America* 105, 8850-8854.
42. Xu, C. W. (2002) High-density cell microarrays for parallel functional determinations, *Genome Research* 12, 482-486.
43. Narayanaswamy, R., Niu, W., D Scouras, A., Hart, G. T., Davies, J., Ellington, A. D., Iyer, V. R., and Marcotte, E. M. (2006) Systematic profiling of cellular phenotypes with spotted cell microarrays reveals mating-pheromone response genes, *Genome Biology* 7.
44. Weibel, D. B., Lee, A., Mayer, M., Brady, S. F., Bruzewicz, D., Yang, J., DiLuzio, W. R., Clardy, J., and Whitesides, G. M. (2005) Bacterial printing press that regenerates its ink: Contact-printing bacteria using hydrogel stamps, *Langmuir : the ACS journal of surfaces and colloids* 21, 6436-6442.
45. Cho, H., Jonsson, H., Campbell, K., Melke, P., Williams, J. W., Jedynek, B., Stevens, A. M., Groisman, A., and Levchenko, A. (2007) Self-organization in high-density bacterial colonies: Efficient crowd control, *Plos Biology* 5, 2614-2623.
46. Flickinger, S. T., Copeland, M. F., Downes, E. M., Braasch, A. T., Tuson, H. H., Eun, Y. J., and Weibel, D. B. (2011) Quorum sensing between *Pseudomonas aeruginosa* biofilms accelerates cell growth, *J Am Chem Soc* 133, 5966-5975.
47. Lee, J.-H., Kaplan, J. B., and Lee, W. Y. (2008) Microfluidic devices for studying growth and detachment of *Staphylococcus epidermidis* biofilms, *Biomedical Microdevices* 10, 489-498.
48. Little, A. E. F., Robinson, C. J., Peterson, S. B., Raffa, K. E., and Handelsman, J. (2008) Rules of Engagement: Interspecies Interactions that Regulate Microbial Communities, In *Annual Review of Microbiology*, pp 375-401.

49. Nowak, M. A. (2006) Five rules for the evolution of cooperation, *Science* 314, 1560-1563.
50. Balagadde, F. K., Song, H., Ozaki, J., Collins, C. H., Barnet, M., Arnold, F. H., Quake, S. R., and You, L. (2008) A synthetic *Escherichia coli* predator-prey ecosystem, *Molecular Systems Biology* 4.
51. Takayama, S., Ostuni, E., LeDuc, P., Naruse, K., Ingber, D. E., and Whitesides, G. M. (2003) Selective chemical treatment of cellular microdomains using multiple laminar streams, *Chemistry & Biology* 10, 123-130.
52. Eun, Y. J., and Weibel, D. B. (2009) Fabrication of microbial biofilm arrays by geometric control of cell adhesion, *Langmuir : the ACS journal of surfaces and colloids* 25, 4643-4654.
53. Eun, Y. J., Utada, A. S., Copeland, M. F., Takeuchi, S., and Weibel, D. B. (2011) Encapsulating bacteria in agarose microparticles using microfluidics for high-throughput cell analysis and isolation, *ACS Chem Biol* 6, 260-266.
54. Medintz, I. L., Konnert, J. H., Clapp, A. R., Stanish, I., Twigg, M. E., Mattoussi, H., Mauro, J. M., and Deschamps, J. R. (2004) A fluorescence resonance energy transfer-derived structure of a quantum dot-protein bioconjugate nanoassembly, *Proceedings of the National Academy of Sciences of the United States of America* 101, 9612-9617.
55. Medintz, I. L., Uyeda, H. T., Goldman, E. R., and Mattoussi, H. (2005) Quantum dot bioconjugates for imaging, labelling and sensing, *Nature Materials* 4, 435-446.
56. Klajnert, B., and Bryszewska, M. (2001) Dendrimers: properties and applications, *Acta Biochimica Polonica* 48, 199-208.
57. Erben, C. M., Goodman, R. P., and Turberfield, A. J. (2006) Single-molecule protein encapsulation in a rigid DNA cage, *Angewandte Chemie-International Edition* 45, 7414-7417.
58. Daniel, M. C., and Astruc, D. (2004) Gold nanoparticles: Assembly, supramolecular chemistry, quantum-size-related properties, and applications toward biology, catalysis, and nanotechnology, *Chemical Reviews* 104, 293-346.
59. Clapp, A. R., Goldman, E. R., and Mattoussi, H. (2006) Capping of CdSe-ZnS quantum dots with DHLA and subsequent conjugation with proteins, *Nature Protocols* 1, 1258-1266.
60. Maaloum, M., Pernodet, N., and Tinland, B. (1998) Agarose gel structure using atomic force microscopy: Gel concentration and ionic strength effects, *Electrophoresis* 19, 1606-1610.

61. Normand, V., Lootens, D. L., Amici, E., Plucknett, K. P., and Aymard, P. (2000) New insight into agarose gel mechanical properties, *Biomacromolecules* 1, 730-738.
62. Augst, A. D., Kong, H. J., and Mooney, D. J. (2006) Alginate hydrogels as biomaterials, *Macromolecular Bioscience* 6, 623-633.
63. Kim, D. H., Kim, P., Song, I., Cha, J. M., Lee, S. H., Kim, B., and Suh, K. Y. (2006) Guided three-dimensional growth of functional cardiomyocytes on polyethylene glycol nanostructures, *Langmuir* 22, 5419-5426.
64. Bonina, P., Petrova, T., and Manolova, N. (2004) pH-sensitive hydrogels composed of chitosan and polyacrylamide - Preparation and properties, *Journal of Bioactive and Compatible Polymers* 19, 101-116.
65. Zhang, X. Z., Sun, G. M., Wu, D. Q., and Chu, C. C. (2004) Synthesis and characterization of partially biodegradable and thermosensitive hydrogel, *Journal of materials science. Materials in medicine* 15, 865-875.

## CHAPTER 2

### **Fabrication of Microbial Biofilm Arrays by Geometric Control of Cell Adhesion**

Adapted from:

Ye-Jin Eun and Douglas B. Weibel (2009) *Langmuir* 25(8):4643-4654.

## ABSTRACT

This chapter presents a technique for patterning arrays of microbial biofilms on a wide range of different substrates using thin polymer stencils. The stencils function as 'scaffolds' that provide geometric control over cell adhesion on surfaces and confine biofilm growth to specific regions of a substrate. We demonstrate the fabrication of biofilm arrays with features (e.g. individual biofilms) as small as 50  $\mu\text{m}$  in diameter with physiological characteristics that are reproducible. Biofilm arrays of a range of microorganisms can be produced using this technique, including: *P. aeruginosa*, *B. subtilis*, *S. epidermidis*, *V. fischeri*, *E. coli*, and *C. albicans*. This approach provides a simple, user-configurable, and relatively inexpensive method for growing biofilms in both static and flow conditions. The method described in this chapter makes it possible to study the chemical, physical, and environmental factors that affect biofilm development in a statistically relevant and reproducible format.

## INTRODUCTION

In this chapter, I describe the use of freestanding, elastomeric stencils with microfabricated 'holes' with different shapes and dimensions to control the spatial adhesion and growth of bacterial cells on surfaces. Using this approach, we demonstrate the fabrication of arrays of patterned microbial biofilms on a variety of substrates. This technique presents a simple and inexpensive method for patterning biofilms of various microorganisms including *Pseudomonas aeruginosa*, an opportunistic pathogen in humans and a model organism widely used for biofilm studies. The arrays created using this method make it possible for the user to test how different environmental factors affect biofilm growth, maturation, and removal under defined and reproducible conditions.

Biofilms are communities of microbial cells adhered to a surface and encapsulated in extracellular matrix (ECM), which usually consists of DNA, proteins, and polysaccharides (1). The composition of the ECM varies greatly between microbes, and even strains within the same species, and is influenced by nutrient availability and growth conditions (2-5). It has been suggested that most microbial communities exist as biofilms (6, 7), and fossil records indicate that biofilms may have existed more than three billion years ago (8, 9). In nature, biofilms provide an environment that facilitates beneficial interactions in a population of cells that may contain different species of microbes (10, 11). These multicellular structures have an impact on a variety of biomedical and industrial processes, including fluid transport, wastewater management, marine biofouling, food processing and storage, and medical implants. Several strategies (12-15) have been developed to prevent biofilm formation and to

remove biofilms on surfaces (16, 17). Despite these efforts, the complete inhibition of biofilm formation is difficult to achieve. The physiological heterogeneity of these communities and their resistance to antibiotics provides cells with a mechanism of survival in response to environmental stresses (18-20). Mature biofilms adhere tightly to surfaces and are resistant to fluid flow and shear stress, which makes it difficult to remove them (4). Understanding the formation, development, and homeostasis of biofilms is a critical step toward developing practical strategies to prevent their formation and facilitate their removal.

Several different techniques are currently used to grow and study biofilms. One of the most common techniques involves culturing cells in glass tubes in which cells adhere to the walls and form a 'pellicle' (e.g. a buoyant biofilm at the air-liquid interface) (21). Glass microscope coverslips can be introduced into the tube to provide a surface for bacteria to adhere and grow. After biofilm formation, the coverslip may be removed and analyzed directly using microscopy. These examples of batch-culture methods are relatively simple to set up and are typically used for studying biofilm growth in the absence of fluid flow (i.e. 'static' conditions), but they provide poor reproducibility, which makes it difficult to compare data between experiments (22, 23). There have been several efforts to control and maintain the chemical composition of the growth environment in order to improve the reproducibility of these methods (24).

Cells in biofilms are sensitive to their microenvironment (25)—that is the chemical and physical region sensed by a cell and typically defined by molecular contact, mass transport, and diffusion—and respond to the flow of fluid within and around the multicellular structure. Fluid flow influences several characteristics of biofilms including: 1) development and dispersal (3); 2) architecture (26); 3) the amount

(27) and composition of the ECM (2, 28); 4) heterogeneity and cell density in biofilms (29); and 5) the susceptibility of cells to biocides (30). To increase the reproducibility of biofilms (31), and to cultivate biofilms in conditions of fluid flow, several approaches have been developed, including: 1) chemostats/bioreactors; 2) modified Robbins devices (mRD); 3) flow cells; and 4) perfused biofilm fermenters. Several reviews (24, 32-36) have covered these techniques in detail; below we briefly summarize each method.

Chemostats (i.e. bioreactors) make it possible for users to control the chemical components in the culture medium and the rate of cell growth. The manipulation of these characteristics improves the reproducibility between experiments. Several different designs of chemostats of varying complexity have been introduced (37). Chemostats that have removable surface substrates (e.g. CDC bioreactors) are commercially available. Recently, a microchemostat was developed to observe biofilm formation in a sub-microliter volume of fluid based on a microfluidic platform (38).

mRDs consist of polyacrylate tube (tens of cm in length) with removable 'cups' that have a porous surface for the initial inoculation of cells and to facilitate nutrient exchange, and may contain different substrates for cell adhesion and biofilm formation (33, 39). These devices have been used frequently to test different surfaces for cell adhesion and biofilm development in conditions that simulate pipes for transporting fluids. Contamination and leakage are common issues with mRDs since the devices cannot be autoclaved (23), and the surface substrates that biofilms are adhered to must be removed from the 'cups' for the analysis of biofilms.

Flow cells have been widely used for studying biofilms. These devices are typically several cm in length and incorporate several channels for growing biofilms. In

contrast to test tube methods and mRDs, flow cells are typically constructed such that one side of the device is a glass coverslip, which makes it possible to monitor biofilms in real time using microscopy. There are disadvantages to using these devices. Several of the materials incorporated into flow cells cannot be autoclaved, and care must be exercised to prevent contamination from residual debris from previous experiments (34). Biofilms grown inside flow cells can be difficult to access physically, and destructive methods such as sonication are often required to remove multicellular structures.

Perfused biofilm fermenters are devices that combine several key characteristics of flow cells and mRDs: the size of a fermenter resembles a flow cell and its mechanism of operation is similar to an mRD. The fermenter has a single channel with five 'cups' that hold different substrates for studying cell adhesion and biofilm growth. The device enables the user to monitor biofilm development in real time via microscopy and to avoid many of the disadvantages of mRDs (40).

96-well plates also make it possible to analyze biofilm growth in static conditions. The major advantage of this platform is that the plates are designed for high-throughput spectrometric analysis and they support the study of biofilms in parallel (e.g. one biofilm per well). This technique has been widely used to screen genes that affect biofilm development; for example, O'Toole and Kolter isolated a transposon mutant of *P. aeruginosa* that was unable to adhere to the bottom of 96-well plate and initiate biofilm formation (41). This technique is only suitable for studying the initial stages of biofilm development (8). For example, assays commonly used to analyze biofilms grown in the wells of plates (e.g. crystal violet assay) make it possible to quantify the adhesion of cells on surfaces, which represents only the first step in the

process of biofilm development (42). Many of the techniques for imaging biofilms are not compatible with 96-well plates (e.g. confocal microscopy and scanning electron microscopy), and thus it is difficult to study mid- and late-stages of biofilm development (i.e. maturation, and dispersion).

The methods that are currently available for creating and studying biofilms do not provide reproducible, parallel biofilms in large numbers for comparative analysis and high-throughput experimentation. The introduction of a method for growing and studying biofilms in both static and flow conditions, in which the device can be easily configured by the user to address particular experimental needs, would be an important addition to this field. To the best of our knowledge, no systems are available that make it possible to study all of the stages of biofilm formation in a format that can be configured by the end-user and provides parallel samples in a quantity that is suitable for quantitative analysis.

To address these limitations, we have developed a technique for fabricating hundreds or thousands of parallel microbial biofilms using elastomeric stencils. The stencils consist of a thin layer of the biocompatible silicone elastomer, poly(dimethylsiloxane) (PDMS), which is impermeable to bacterial cells and contains an array of holes that controls the geometric adhesion of cells on substrates and their growth into biofilms. One of the most important features of this technique is that it defines the position on substrates where microbial cells adhere and where they do not. This approach overcomes a limitation of traditional methods in which biofilms are typically grown from cells that have adsorbed to surfaces through a process that is largely stochastic and nearly impossible to reproduce. We demonstrate an approach for creating parallel and reproducible biofilms in a statistically relevant manner, opening

new doors for studying the chemical, physical and environmental factors that govern biofilm development by combining microstructured polymers and microscopy.

## EXPERIMENTAL METHODS

### *Materials.*

PDMS elastomer base and curing agent were purchased from Dow Corning (Midland, MI). SU-8 2050 photoresist was from MicroChem (Newton, MA). Ammonium chloride, diisopropylamine, formaldehyde (37 % w/w in water), potassium hydrogen phosphate, iron (II) sulfate heptahydrate, sodium hydrogen phosphate heptahydrate, sodium chloride, magnesium sulfate, 3-(N-morpholino)propanesulfonic acid (MOPS), polyallylamine hydrochloride (average molecular weight = 240,000 g/mol), polyacrylic acid (average molecular weight = 60,000 g/mol) and 1,2-propanediol monoethyl ether acetate were from Alfa Aesar (Ward Hill, MA). Heptadecafluoro-1,1,2,2-tetrahydrodecyl trichlorosilane was from Gelest (Morrisville, PA). Tryptic soy broth (TSB), yeast extract, agar, agarose, Bacto peptone, casamino acids, yeast nitrogen base, and polystyrene petri dishes were purchased from BD Biosciences (Franklin Lakes, NJ). N-2-hydroxyethylpiperazine-N'-2-ethanesulfonic acid (Hepes), ethyl acetate, acetone, ampicillin, potassium chloride, calcium chloride, polyvinyl chloride slides, dextrose, Rosell Park Memorial Institute (RPMI) 1640 media, D-glucose, and a solution of 10x phosphate-buffered saline (PBS) were from Fisher Scientific (Pittsburgh, PA). Dodecyl- $\beta$ -D-maltoside (DDM), 4',6-diamidino-2-phenylindole (DAPI), isopropyl- $\beta$ -D-thiogalactopyranoside (IPTG), osmium tetroxide, and fluorescent brightener 28 (a.k.a. calcofluor white) were from Sigma (St. Louis, MO). 11-amino-1-undecanethiol hydrochloride was purchased from Asemblon (Redmond, WA). BacLight LIVE/DEAD kit, gentamycin and agarose were from Invitrogen (Carlsbad, CA). 5-Cyano-2,3-ditolyl tetrazolium chloride was obtained from Polysciences (Warrington, PA). Gold-coated

coverslips were from EMF corporation (Ithaca, NY). These substrates consist of glass coverslips (22 x 22 mm wide and 160  $\mu\text{m}$  thick) coated with a 1-nm thick layer of Cr followed by a 25-nm thick layer of gold; the layers were deposited by electron-beam evaporation. Teflon tubing for microfluidic devices was purchased from Small Parts (Miramar, FL). Sheets of polycarbonate, polyethylene, and stainless steel with a thickness of 1.6 mm were obtained from McMaster-Carr (Santa Fe Springs, CA).

### *Fabrication of micropatterned stencils.*

Stencils (50-80  $\mu\text{m}$  thick) were fabricated in PDMS using soft lithography (43, 44). Briefly, we used photolithography to fabricate a 'master' consisting of a pattern in SU-8 photoresist in bas-relief on a silicon wafer. The master was silanized by vapor deposition of heptadecafluoro-1,1,2,2-tetrahydrodecyl trichlorosilane for 3 hr at 25 °C. A thin layer of PDMS pre-polymer was applied to the surface of the wafer by spin coating; the layer of PDMS was not thick enough to coat the top of the features of photoresist. The PDMS prepolymer was cured for 12 hr at 75 °C, and the resulting stencil was peeled away from the silicon wafer and contained a pattern of 'holes' transferred from the photomask into the resist during photolithography. We demonstrate that bacterial biofilms can be fabricated in various sizes and shapes, including a diamond, heart, and circle; in principle, this technique makes it possible to create patterns of any arbitrary shape. Unpolymerized siloxane oligomers were extracted from micropatterned PDMS stencils by soaking the stencil consecutively in diisopropylamine, ethyl acetate, and acetone (45). Stencils were immersed in each solvent for at least 1 hr and dried in air; this process improved conformal contact and adhesion of the stencil to the surface of a

substrate. Stencils were stored in ethanol to keep them sterile. After stencils were used in biofilm experiments, they were soaked in bleach, rinsed with water, autoclaved, and stored in a solution of ethanol before their reuse. In order to reduce the non-specific adhesion of cells to PDMS surfaces, stencils were coated with a solution of DDM (46) (0.1 % w/w in 1x PBS) or Pluronic F-127 (47) (0.2% w/w in 1x PBS) for 12 hr and rinsed with 1x PBS before use.

### ***Microbial cell culture and growth conditions.***

Several bacterial strains and one fungal strain were used in this study. A list of organisms, their genotype, and the conditions used for their growth is summarized in Table 1. Lauria-Bertani (LB) media (10 g/L tryptone, 10 g/L NaCl, 5 g/L yeast extract, pH 7.2) was used to grow *Escherichia coli* strain MG1655. *Bacillus subtilis* strain 168 was grown in LB media supplemented with 20 g/L  $(\text{NH}_4)_2\text{SO}_4$ , 12 g/L  $\text{KH}_2\text{PO}_4$ , 2.3 g/L  $\text{K}_2\text{HPO}_4$ , 120.4 mg/L  $\text{MgSO}_4$ , 10 g/L sodium citrate, and 1 mg/L glucose (48). Growth media for *Vibrio fischeri* strain ES114 (49) contained 1.5 mg/L  $\text{FeSO}_4$ , 52 mg/L  $\text{KH}_2\text{PO}_4$ , 1 g/L  $\text{NH}_4\text{Cl}$ , 3 mg/L casamino acids, 2 mg/L glucose, and artificial seawater (11.7 g/L NaCl, 6.02 g/L  $\text{MgSO}_4$ , 0.745 g/L KCl, and 1.1 g/L  $\text{CaCl}_2$ ) in 50 mM Hepes buffer at pH 7. *P. aeruginosa* strain PAO1 and a PAO1 derivative with a plasmid encoding green fluorescent protein (GFP) (50) were grown in M8 minimal media (241 mg/L  $\text{MgSO}_4$ , 4 mg/L glucose, 5 mg/L casamino acids, 12.8 g/L of  $\text{Na}_2\text{HPO}_4 \cdot 7\text{H}_2\text{O}$ , 3 g/L of  $\text{KH}_2\text{PO}_4$ , and 0.5 g/L of NaCl). A final concentration of 200  $\mu\text{g}/\text{mL}$  of ampicillin and 1 mM of isopropyl  $\beta$ -D-1-thiogalactopyranoside was added to the M8 media for GFP-expressing cells. *Staphylococcus epidermidis* was grown in TSB media supplemented with 2.5 mg/L

glucose (51). *Candida albicans* strain SC5314 was grown in yeast peptone dextrose (YPD) media (10 g/L yeast extract, 2 g/L peptone, and 2 g/L dextrose). Cells from overnight cultures of *C. albicans* were centrifuged for 4 min at 6000 rpm and resuspended in 1x PBS buffer. After three cycles of centrifugation and washing, the fungal cells were resuspended in Rosell Park Memorial Institute (RPMI) 1640 media (RPMI 1640 powder containing L-glutamine) prepared in 0.1 M MOPS, pH 7 for biofilm experiments (52). All overnight cultures were grown at 37 °C except for *V. fischeri* (25 °C) and *C. albicans* (30 °C). Biofilms of all organisms were grown at 37 °C except for *V. fischeri*, which was grown at 25 °C. Microfluidic experiments to observe the architecture of *P. aeruginosa* biofilms grown with different carbon sources used FAB medium (53) (2 g/L  $(\text{NH}_4)_2\text{SO}_4$ , 9 g/L  $\text{Na}_2\text{HPO}_4 \cdot 7\text{H}_2\text{O}$ , 3 g/L  $\text{KH}_2\text{PO}_4$ , 3 g/L NaCl, 93 mg/L  $\text{MgCl}_2$ , and 11 mg/L  $\text{CaCl}_2$ ). The medium was supplemented with either glucose or succinate to a final concentration of 10 mM as the sole source of carbon. A solution of 1x trace metals (1000x trace metal solution: 200 mg/L  $\text{CaSO}_4 \cdot 2\text{H}_2\text{O}$ , 200 mg/L  $\text{FeSO}_4 \cdot 7\text{H}_2\text{O}$ , 20 mg/L  $\text{MnSO}_4 \cdot \text{H}_2\text{O}$ , 20 mg/L  $\text{CuSO}_4 \cdot 5\text{H}_2\text{O}$ , 20 mg/L  $\text{ZnSO}_4 \cdot 7\text{H}_2\text{O}$ , 10 mg/L  $\text{CoSO}_4 \cdot 7\text{H}_2\text{O}$ , 10 mg/L  $\text{NaMoO}_4 \cdot \text{H}_2\text{O}$ , and 5 mg/L  $\text{H}_3\text{BO}_3$ ) was added to the medium.

### ***Patterning biofilms on surfaces.***

A rectangular PDMS jig was created with dimensions slightly larger than the PDMS stencils. The jig was pressed into conformal contact with the surface of a substrate. A PDMS stencil was immersed in ethanol for 30 sec before bringing it into contact with the substrate inside of the jig. The solvent was evaporated in a biological safety cabinet to maintain sterility. A suspension of bacterial cells (typically 1-2 mL) was

placed on the stencil. The device was stored and incubated in a sterile Petri dish during biofilm formation.

*Preparation of surfaces for biofilm formation.*

Glass coverslips were coated with several layers of polyelectrolyte (PEL) to enhance bacterial cell adhesion (54-56). The first layer of PEL was deposited on clean coverslips that had been treated with an oxygen plasma. Oxidized coverslips were incubated in a solution of polyallylamine hydrochloride (30 mg/L in 0.01 M NaCl) for 5 min. The coverslips were then washed with a solution of NaCl (0.01 M) and dried with a stream of nitrogen gas. Polyacrylic acid was added as the next PEL layer by incubating the amine-coated glass coverslips in a solution of polyacrylic acid (30 mg/L in 0.01M NaCl) for 5 min. The deposition cycle of polyallylamine and polyacrylic acid was repeated until at least five consecutive layers of these materials were deposited.

We used polystyrene Petri dishes and pieces (6 cm x 3 cm) of stainless steel, polyethylene, polycarbonate, and polyvinylchloride as substrates for growing biofilms; the materials were used without any modification. 11-Amino-1-undecanethiol hydrochloride was used to prepare a self-assembled monolayer (SAM) on gold. The thiol was dissolved in ethanol to a final concentration of 1 mM, and gold-coated glass cover slips were incubated in the solution for 10 hr at 25 °C. At the end of the incubation period, the coverslips were rinsed with ethanol and dried under a stream of nitrogen. Tweezers used to handle the coverslips were sonicated in acetone and ethanol for 10 min each prior to use.

### *Scanning electron microscopy.*

Biofilms were grown for 3 days in PDMS stencils and fixed with a solution of formaldehyde (5 % w/v) or glutaraldehyde (2.5 % w/v) in 1x PBS buffer for 2 hr and treated with a solution of osmium tetroxide (2 % w/v) in 1x PBS buffer for 2 hr at 25 °C. After fixing the cells, the samples were rinsed with buffer or water (1 mL). The samples were soaked in a series of ethanol solutions (a step gradient of 30%, 50%, 70% and 90% in water for 10 min per step), ending with 100% ethanol. After dehydration, the samples were dried in a critical point dryer (Tousimis Samdri 780) and subsequently coated with a 60:40 gold-palladium alloy (approximately 10-nm thick; SeeVac Auto Conductavac IV; 30 mA; 120 mTorr; sputtering duration of 3 min). Scanning electron microscopy was performed using a Hitachi S-570 electron microscope at an accelerating voltage of 10 kV.

### *Fluorescence microscopy.*

GFP expressed in *P. aeruginosa* was excited at 488 nm, and its emission was detected at 515/30 nm. Calcofluor white (80  $\mu\text{g}/\text{mL}$ ;  $\lambda_{\text{excite}} = 408 \text{ nm}$  and  $\lambda_{\text{emit}} = 450/35 \text{ nm}$ ) was used to visualize polysaccharide in the extracellular matrix of biofilms (57). To stain polysaccharide with calcofluor white, a solution of dye was admixed with the suspension of cells just before inoculating the PDMS stencil; the dye was present during biofilm growth. After staining, the biofilm arrays in the PDMS stencil were rinsed three times with 1x PBS to remove unbound dye. A Nikon Eclipse TE2000E inverted microscope with a Perfect Focus system and an encoded z-stage was used for phase contrast and epifluorescence microscopy. A Nikon Eclipse TE2000U (diode laser for 408 nm and Ar laser for 488 nm) was used for confocal microscopy, and TE2000U

microscope equipped Bio-Rad Radiance 2100 MP Rainbow was used for confocal scanning laser microscopy (CSLM).

To quantify live and dead cells in arrays of biofilms in PDMS stencils, we used the BacLight LIVE/DEAD kit from Molecular Probes (58). The protocol provided by Molecular Probes with the kit was used to stain the cells. The fluorescence emission from Syto 9 ( $\lambda_{\text{excite}} = 484 \text{ nm}$  and  $\lambda_{\text{emit}} = 520 \text{ nm}$ ) and propidium iodide ( $\lambda_{\text{excite}} = 484 \text{ nm}$  and  $\lambda_{\text{emit}} = 620 \text{ nm}$ ) was imaged separately for each biofilm. The resulting images were analyzed using MacBiophotonics Image J (version 1.41a); a circle with a diameter that matched the diameter of the holes in the stencil was superimposed on the image and the mean gray scale intensity of the entire circular area was calculated using Image J. The ratio between the mean intensity of the gray scale for Syto 9 and propidium iodide was determined and used to calculate the relative amount of live and dead cells in individual holes in a PDMS stencil.

The quantum yield for Syto 9 and propidium iodide was corrected by using the following procedure: an overnight culture of *P. aeruginosa* was divided into two equal volumes, centrifuged, and a solution of either 0.01M NaCl or isopropanol was added to each tube. The cells incubated in the salt solution remained alive; the cells in isopropanol were dead after 1 hr at 25°C. We resuspended cells in biofilm growth media (i.e. M8 media) and stained them with Syto 9 (e.g. live) and propidium iodide (e.g. dead) using the same concentrations of reagents used for biofilm assays. At least 7 cells stained with each dye were imaged and analyzed using ImageJ. The difference in fluorescence emission (e.g. quantum yield) from each dye was used to correct the values of fluorescence intensity obtained from imaging the biofilm arrays.

To observe metabolically active cells in biofilm arrays, we used 5-cyano-2,3-ditoyl tetrazolium chloride (CTC) (59, 60). CTC is reduced in cells due to respiration and becomes fluorescent(61) ( $\lambda_{\text{excite}} = 484 \text{ nm}$  and  $\lambda_{\text{emit}} = 620 \text{ nm}$ ). A stock solution of 50 mM CTC was prepared in water and diluted to a final concentration of 5 mM in M8 media before the assay. The CTC solution (1 mL) was added to biofilm arrays, and the devices were incubated for 1 hr at 37 °C. At the end of incubation, biofilm arrays in the stencil were imaged and analyzed using ImageJ.

### *Interferometry.*

A Zygo interferometer (Middlefield, CT) running the MetroPro software (version 8.1.5) was used to measure and analyze the height of nascent biofilms formed on 11-amino-1-undecanethiol SAMs on gold coverslips. The resolution of the instrument was approximately 550 nm using a 20x objective. Eighteen ‘mini-biofilms’ were imaged and analyzed: the wavelength and frequency of the filter were fixed during analysis (high filter wavelength = 2  $\mu\text{m}$  at a frequency of 0.5  $\mu\text{m}^{-1}$ ; low filter wavelength = 200  $\mu\text{m}$  at a frequency of 0.005  $\mu\text{m}^{-1}$ ). Height values less than the normal thickness of a bacterial cell (e.g. < 700 nm) were discarded.

### *Interfacing PDMS stencils with microfluidic systems.*

PDMS stencils and microfluidic devices were coated with a solution of Pluronic (0.2 % w/v) prior to interfacing the two components. PEL-coated glass coverslips were prepared as described. After the stencil was adhered to the glass surface, the stencil on glass and slab of PDMS embossed with the microchannels were plasma oxidized and covalently bonded by bringing the oxidized surfaces into contact. The PEL was

probably etched away in this step, and the likely PEL damage can be avoided by oxidizing the jig and attaching it to the substrate without oxidizing the membrane. Immediately after interfacing the stencil with microfluidic device, a sterile solution of 1x PBS buffer was introduced into the channels to keep the walls hydrophilic. Devices were sterilized by UV exposure for 30 min. Liquid growth media was pumped through the channel using a syringe pump (PHD2000, Harvard, Holliston, MA) at a flow rate of 1.4 or 50  $\mu\text{L}/\text{min}$  (approximate Reynolds numbers were 0.01 and 0.33, respectively) at 37 °C.

#### ***Growing *P. aeruginosa* biofilms with different carbon sources.***

An overnight culture of *P. aeruginosa* PAO1 grown in FAB media supplemented with either 10 mM of glucose or succinate was diluted to an optical density of 0.3 (wavelength, 600 nm), and the suspension of cells was injected into a microfluidic biofilm device. The inoculated device was incubated for 30 min for cells to adhere to the glass surface before starting the flow of liquid (a flow rate of 50  $\mu\text{L}/\text{min}$ ) for 40 hrs at 30 °C. To observe the structure of biofilms, biofilms in the microfluidic device were stained with Syto 9 (a final concentration of 3  $\mu\text{M}$  in sterile water) and imaged using CSLM. Cross-sectional images of biofilms were obtained by analyzing microscopy data using ImageJ.

#### ***Statistical analysis on the quantitative characterization of biofilms grown in PDMS stencils.***

We performed statistical analysis on the data collected to quantitatively characterize *P. aeruginosa* biofilms grown in PDMS stencils. The characterization

included physiological parameters such as the ratio of live and dead cells and metabolic activity of cells in biofilms, as described in the Materials and Methods section and Figure 6. We used the coefficient of variation (CV) function to analyze the data, which is the ratio of the standard deviation and the mean value of the data set. We chose this tool because it is scale-free and therefore allows unbiased comparison with other data sets. The CV was calculated for the data sets included in Figure 6, and the values are tabulated in Table 2.

## RESULTS AND DISCUSSION

### *Fabrication of biofilm arrays on surfaces.*

The general procedure for patterning biofilms is illustrated in Figure 1. A jig consisting of a slab of PDMS (3 – 7 mm thick) with a rectangular cavity slightly larger than the PDMS stencil was placed in contact with the substrate. A PDMS stencil was brought in conformal contact with the surface of a substrate. A suspension of microbial cells was added on top of the stencil, and the device was incubated at a defined temperature for the growth of biofilms (see experimental section). The surface of the substrate on which cells could adsorb and form biofilms was restricted by the pattern of holes in the PDMS stencil. At the end of the incubation period, the culture medium was removed, and the stencil was gently washed three times with fresh media to remove planktonic cells adsorbed on the surface of the PDMS. The resulting layer of PDMS contained biofilms in the holes of the stencil.

Typical incubation times for growing biofilms were 1-3 days. Incubating the devices for different periods of time made it possible to grow and analyze biofilms during different stages of development. Figure 2 shows biofilms of *P. aeruginosa* that were created using this process, including structures that are formed at an early stage of development where a thin layer of cells have irreversibly adhered to a substrate ('nascent' biofilms grown for 20 hrs; Fig. 2A, B and C) and those formed at longer incubation times ('mature' biofilms grown for 3 days; Fig. 2D).

Nascent biofilms remained intact after peeling off the PDMS stencil at the end of 20 hr incubation (Figure 2A and B). They could be grown into mature structures by adding more liquid media and incubating the substrates. The array of biofilms was

stable to the flow of liquid media and was not removed at flow rates below 1.7 mL/min (i.e. the maximum flow rate we tested). Peeling away the stencil after longer incubation times (e.g. 45 hrs) to leave freestanding mature biofilms on substrates was complicated by the adhesion of the ECM to the walls of the PDMS stencil, which usually caused the biofilms to lift off of the substrate and remain intact in the holes of the stencil. We found that coating the stencil surface with DDM (46) or Pluronic (47) was moderately effective in reducing the adhesion of biofilms to PDMS. Leaving the stencil in place made it possible to study different stages of biofilm growth without perturbing these structures. Biofilms were imaged directly by mounting the devices on an inverted, upright, or confocal microscope. Alternatively, stencils were loaded on a stub and imaged using scanning electron microscopy (SEM). Biofilms grown in the holes of stencils are 'exposed' and can be physically manipulated—for example, cells or ECM could be removed using a micromanipulator and imaged.

The thickness of the biofilms formed in the PDMS stencils varied from 1.6 to 40  $\mu\text{m}$  as observed by confocal microscopy (data not shown), and depended on the incubation time and formulation of the culture broth; it may be possible to grow taller structures using longer incubation times. Arrays of circular biofilms for many experiments were 100  $\mu\text{m}$  in diameter; we also created biofilms that ranged 50–400  $\mu\text{m}$  in diameter (e.g. biofilms that are 50  $\mu\text{m}$  in diameter are shown in Fig. 2D). The range we tested is by no means the limits of the technique; arrays of smaller or larger features in stencils can be created using soft-lithography (44, 62, 63). The ability to use stencils to produce patterns of bacteria with features  $<100 \mu\text{m}$  would also be an advantage over

other methods for patterning multicellular structures of bacteria on surfaces using microcontact printing techniques (64, 65).

### ***Biofilm arrays of different organisms.***

We tested whether biofilms of different organisms could be patterned using this technique. We selected six model microorganisms representing Gram-negative bacteria, Gram-positive bacteria, and a species of fungi. The growth conditions and details for each strain are summarized in Table 1. Biofilms of *E. coli*, *P. aeruginosa*, *V. fischeri*, *B. subtilis*, *S. epidermidis*, and *C. albicans* grew in the holes of PDMS stencils for three days. Figure 3 shows electron micrographs of biofilms embedded in the holes of PDMS stencils. The amount of ECM secreted by the cells depended on the strain and the culture media. We observed that the biofilms remained intact in the holes of the stencils even after several vigorous washing steps. These results demonstrate that this approach for patterning biofilms is applicable to a range of different microorganisms, including other Gram-negative and Gram-positive strains of bacteria.

### ***Patterning biofilms on different surfaces.***

We took advantage of the flexibility and adhesive property of PDMS to bring the stencil in conformal contact with different surfaces, including: PEL-coated glass, polycarbonate, polystyrene, polyvinylchloride, polyethylene, stainless steel, and SAMs of 11-amino-1-undecanethiol on gold coverslips. We also used this approach to pattern multicellular structures of bacteria on agar and agarose (see Supporting Information). After growing for three days, patterned *P. aeruginosa* biofilm arrays were imaged using confocal microscopy. Figure 4 shows 3-D image reconstructions of biofilm arrays

imaged using confocal microscopy; GFP-expressing cells are green and the biofilm matrix, which was stained with calcofluor dye, is red. By exploiting the flexibility of PDMS stencils, it may be possible to pattern biofilms on surfaces that are rough, corrugated or topographically textured. The study of biofilm growth, development, and organization on topography is an area that has not been studied. The fabrication of surfaces with texture and surface chemistry that mimics the natural environment for biofilms may provide new insight into multicellular structure and homeostasis.

Nascent biofilms (i.e. biofilms grown for 20 hr) of *P. aeruginosa* were patterned on 11-amino-1-undecanethiol SAMs on gold coverslips; this thiol was chosen because its positively charged amino group promotes cell adhesion to surfaces through electrostatic interactions with the negatively charged lipopolysaccharides on the cell wall. Thiols presenting different functional groups have been used to study bacterial cell adhesion and biofilm development (16, 66, 67). Using interferometry, we measured the height of nascent biofilms on SAM-coated gold coverslips after peeling off the PDMS stencil. The mean height of the 18 biofilms analyzed was  $880 \pm 170$  nm, which suggested that the nascent biofilms were monolayer of cells and were consistent with images from light microscopy (Figure 2A and B). By using longer periods of growth, we created mature biofilms of *P. aeruginosa* on SAMs (Figure 4A). We are currently studying how surface chemistry affects the organization of cells and ECM in biofilms.

### ***Growing biofilm arrays in a microfluidic device.***

As we mentioned in the introduction, the flow of fluids affects biofilm growth, development, dispersal, and organization. To grow biofilms in the presence of fluid flow, we interfaced PDMS stencils with microfluidic systems. A schematic illustration of

the fabrication process and an image of a microfluidic biofilm device are shown in Figure 5. Microfluidic devices were embossed in PDMS using soft lithography (44). The microfluidic device (Figure 5A) had four identical channels that were 5.5 mm wide, 36.4 mm long and 130  $\mu\text{m}$  in height: the volume of each channel was approximately 25  $\mu\text{L}$ . Eight small PDMS posts (1 mm diameter) were incorporated in each channel during fabrication to prevent the channel from collapsing irreversibly on the 'floor' during the assembly of the device, and an inlet and outlet for each channel were created using a biopsy punch (1 mm in diameter) (Figure 5B). We fabricated PDMS stencils with a footprint that matched the dimensions of the microfluidic system so that the two components could be easily interfaced.

The flow of fluid in these devices was in the laminar regime and was characterized by a low Reynolds number ( $Re$ ).  $Re$  is a unit-less parameter that describes the ratio of inertial and viscous forces acting on a particle moving through a fluid, and is expressed as  $Re = dv\rho/\mu$ , where  $d$  is the hydraulic diameter of the channel ( $\mu\text{m}$ ), which depends on the cross-sectional geometry of the channel,  $v$  is the velocity ( $\mu\text{m}\cdot\text{sec}^{-1}$ ),  $\rho$  is the density ( $\text{g}\cdot\text{cm}^{-3}$ ), and  $\mu$  is the viscosity ( $\text{kg}\cdot\text{m}^{-1}\cdot\text{sec}^{-1}$ ). Laminar flow occurs at  $Re < 2100$  and in this regime all mixing occurs by diffusion. In our experiments the  $Re$  was 0.01–0.3. The rate of flow of fluid we used produced very low shear on the biofilms (i.e. the shear stress on the surface of the biofilms was less than 40 mPa). Since the liquid flowing inside the channels was in the laminar regime, the velocity approached zero at the surface of biofilms, and the effect of the fluid on the growing biofilms was primarily to supply nutrients to the biofilms and to remove metabolic waste by diffusion.

Using this approach, a stencil containing an array of 650 holes was isolated in each channel of the fluidic device. The holes in the device were inoculated by introducing a suspension of cells through tubing connected to the inlet using a syringe (Figure 5C). After inoculation, the device was incubated for 30 min at 37 °C in the absence of fluid flow so that cells could adhere to the surface of the substrate. Fluid was pumped through the devices at different flow rates using a syringe pump during incubation of the biofilm arrays at 37 °C.

#### *Characterization of biofilm arrays in fluid flow.*

We used fluorescence-based assays to characterize the arrays and determined whether individual biofilms in an array closely resembled each other physiologically and whether these characteristics could be reproduced in separate experiments at different flow rates of culture media. We used two fluorescent assays to test the reproducibility of biofilms: 1) BacLight Live/Dead staining was used to measure the ratio of live and dead cells; and 2) a cell metabolism assay using a redox indicator, 5-cyano-2,3-ditolyl tetrazolium chloride (CTC), which becomes fluorescent when it is reduced in the cytoplasm and reports the metabolic activity of cells. We used fluorescence microscopy to characterize *P. aeruginosa* biofilms after 20 hr of growth in static and flow conditions (volumetric flow rate = 1.4 and 50  $\mu\text{L}/\text{min}$ ) using these assays; three independent experiments were performed for each assay and for each growth condition. For experiments in the absence of fluid flow, the same PDMS jig and stencil was used in the three replicate experiments to ensure that the variability between experiments was not due to differences in the materials. The fluorescence intensity from imaging the ratio of live/dead cells (i.e. emission from Syto 9 and propidium iodide,

respectively) and the metabolic activity of cells (i.e. emission from CTC) was analyzed in these parallel biofilm arrays. At least 100 biofilms were analyzed for each array by using ImageJ to measure the total fluorescence emission data for each hole in a stencil. The fluorescence emission from Syto 9 and propidium iodide was corrected for their respective quantum yield as described in the Methods section. Figure 6 shows a plot of the measured fluorescence intensities for biofilms grown using different conditions. The mean ratio of live vs. dead cells in biofilm arrays were  $0.18 \pm 0.02$  (no flow),  $0.37 \pm 0.02$  (flow rate =  $1.4 \mu\text{L}/\text{min}$ ), and  $0.36 \pm 0.08$  (flow rate =  $50 \mu\text{L}/\text{min}$ ) (Figure 6A). The data suggest that the ratio of live vs. dead cells increases with increasing flow (and shear rate) of growth media, which we interpret as arising from the availability of nutrients and the rapid removal of metabolic waste. The mean fluorescence intensity that indicates cell metabolism was similar in all three growth conditions tested:  $145 \pm 4$  (no flow),  $108 \pm 3$  (flow rate =  $1.4 \mu\text{L}/\text{min}$ ), and  $127 \pm 21$  (flow rate =  $50 \mu\text{L}/\text{min}$ ) (Figure 6B). Using the results from these experiments, we performed a statistical analysis (i.e. coefficient of variation) to investigate the degree of variation in the data sets presented in Figure 6. The coefficients obtained from this analysis are tabulated in Table 2, and they ranged from 0.03 to 0.22, indicating that the variation in the data was relatively small.

Relatively small standard deviations and coefficients of variation calculated for the three independent experiments suggest a similar level of cell death and metabolic activity between the structures in an array. We have also found that the physiological characteristics of biofilms grown in static and flow conditions are reproducible between experiments.

### *Morphology of P. aeruginosa biofilms cultured in microfluidic devices.*

The structure of a biofilm depends on gene expression, mutations (2, 26), and nutrients in the growth medium (53). For example, several studies have demonstrated that FAB media supplemented with citrate, succinate, or glutamate as the sole carbon source promote a carpet-like biofilm structure (53, 68), whereas glucose-containing media produce biofilms with a characteristic mushroom shape (53, 68-70). *P. aeruginosa* biofilms exhibit at least two types of biofilm morphology / architecture: structured and flat (68). We explored whether *P. aeruginosa* biofilms grown in the holes of stencils in microfluidic devices would form different structures depending on the carbon sources present.

*P. aeruginosa* PAO1 biofilms were grown under fast liquid flow (i.e. 50  $\mu\text{L}/\text{min}$ ) with either glucose or succinate as the primary carbon source in FAB media to generate the two structural phenotypes. At the end of 40 hr of growth, biofilms grown in the holes of PDMS stencils were imaged using CSLM. The microscopy data was reconstructed in 3-D and a cross-section through the center of the structures was created using ImageJ (Figure 7). Glucose-fed biofilms (Figure 7A) exhibited a structure consisting of a monolayer of cells punctuated by cell aggregates similar to the morphology reported by Shrout et al (68). In contrast, biofilms grown in the presence of media supplemented with succinate had a flat and relatively uniform appearance with the majority of the cells spread evenly on the surface (Figure 7B). The morphologies that we observed are reproducible and suggest that the architecture of biofilms is not influenced by the spatial confinement of these structures in the holes of PDMS stencils (i.e. stencil holes with a diameter of 100  $\mu\text{m}$ ) and that they are dependent on nutrient conditions.

We subjected the biofilms of different morphologies to an antibiotic challenge (i.e. flowing a solution of gentamycin in FAB media for 8 hrs), and quantified the ratio of live and dead cells using the BacLight LIVE/DEAD kit. The relative amount of dead cells increased when a solution of gentamycin was added to the microfluidic device, regardless of the biofilm architecture; however, we did not observe a difference in relative antibiotic susceptibility when biofilms of two different phenotypes were compared. More details on the antibiotic susceptibility test are found in the Supporting Information.

## CONCLUSION

In this chapter, we introduce a new technique for the reproducible growth of parallel biofilms in arrays by geometrically confining the adhesion and growth of cells on surfaces using thin PDMS stencils. We have demonstrated that this technique is compatible with a variety of organisms and makes it possible to study the chemical, physical, and environmental factors that influence biofilm development in a statistically relevant experimental format.

There are several improvements that can be made to this technique. One drawback of the microfluidic devices introduced in this paper is that they cannot be reused. The ability to rapidly prototype structures in PDMS makes it possible to overcome this limitation as replica devices are easily prepared using soft lithography (71). The non-specific adhesion of cells on PDMS is difficult to prevent. This phenomenon may be particularly problematic if cells adsorbed on the top of the PDMS stencil grow into a biofilm and spread into the holes, thereby complicating analyses. We observed that treating the polymer with a surfactant reduced non-specific adhesion of cells on PDMS but did not prevent adhesion. The adhesion of ECM and cells to the walls of the PDMS was also a problem that made it very difficult to peel away the stencil and leave freestanding biofilms after long periods of growth (e.g. >45 hr). The covalent grafting of passivating layers of material to the PDMS surface or the fabrication of stencils from a different polymer (e.g. crosslinked poly(ethyleneglycol)) may minimize or prevent adhesion of cells and ECM to the surface of the stencil (72). Stencils fabricated in hydrogels may also provide a platform for studying chemical communication between multicellular structures. These materials would provide a

mechanism for physically separating biofilms while permitting the diffusion of small molecules and ions through the 'transparent' walls. The effects of sharing nutrients and secondary metabolites may have interesting consequences on the growth and phenotypes of neighboring multicellular structures. For example, Kim et al. recently described how to engineer syntrophy between physically isolated, unrelated communities of different bacteria that were in fluidic contact (e.g. chemical communication) by manipulating their spatial organization (73). The growth of arrays consisting of different microbial biofilms using this technique is currently untested, but seems feasible, and may shed insight into the evolution of symbiotic interactions.

There are several advantages to this technique. The PDMS stencils are straightforward to fabricate with holes that are as small as  $\sim 5 \mu\text{m}$  and with shapes and patterns that are easily controlled using soft lithographic techniques. This technique makes it possible to address how the geometry of biofilms affects the organization, physiology, and homeostasis of cells (and ECM) in multicellular structures. The patterns of multicellular structures produced using this and related techniques should be of interest to scientists studying biofilm development and removal (42), microbial ecology (e.g. interspecies interaction in biofilms (74, 75)), and the influence of quorum sensing (76, 77), surface chemistry (78), and chemical gradients on biofilm formation (79).

One of the first steps in biofilm growth is the formation of 'microcolonies' (8). The definition of a microcolony is not specific and typically refers to small clumps of bacterial cells attached to the surface. Since bacterial communication (e.g. quorum sensing) within and between multicellular structures plays an important role in biofilm

formation and maturation (76), it would be helpful to understand the relationship between the size of biofilm microcolonies and biofilm development. Distributed spatial networks of bacterial populations interact with neighboring patches of cells (80). These interactions may be related to the interactions between microcolonies and their development of mature biofilms. In these spatial networks, the increase in the population density of bacterial cells over time stimulates the self-organization of cells within their environment (81, 82). The study of the distribution, crowding, and self-organization of bacterial cells in biofilms confined in various shapes may provide insight into this phenomena of population interaction. . Using the technique described in this paper, it should be possible to create patterns of microcolonies of bacteria on surfaces with defined size, shape, and pitch between multicellular structures. This capability may shed insight into the development of biofilms and other multicellular structures of bacteria.

Using stencils it is possible to pattern biofilms over relatively large areas ( $< 16 \text{ cm}^2$ ) and the stencils may be reused indefinitely. The technique is conceptually simple, inexpensive, and easy to combine with optical and electron microscopy. Furthermore, the flexibility and adhesive property of PDMS make it possible to pattern biofilms on a range of surface substrates and study how the physical (e.g. topography, porosity, stiffness) and chemical properties (e.g. surface energy, presentation of ligands that target the outer membrane of cells) of surfaces affect biofilm formation and removal.

Another method for creating multicellular patterns of bacteria is based on microcontact printing (64). While this method utilizes soft materials such as agar that support cell growth and thus 'regenerate' its ink for printing, it is limited to producing patterns of bacteria with features  $>150 \text{ }\mu\text{m}$  in diameter. 'Dynamic patterns' created by

microcontact printing typically become distorted as the cells grow into colonies and consume nutrients and produce waste. In contrast, the multicellular patterns fabricated using PDMS stencils have stable lateral dimensions as the stencil confines the structure during growth and have smaller feature sizes than those created by microcontact printing techniques. Although we have only tested the lateral stability of biofilms grown in stencils for up to three days, we anticipate that the structures should be stable for longer periods of time.

## ACKNOWLEDGEMENTS

This research was supported by a grant from the USDA (142-L192), 3M Corporation, a Steenbock Career Award, and a Searle Scholar Award. We thank Helen Blackwell for *P. aeruginosa* strains, Timothy Pautian for *S. epidermidis* strains, and Christina Hull for *C. albicans* strains. We thank Tom Martin for the use of his confocal microscope.

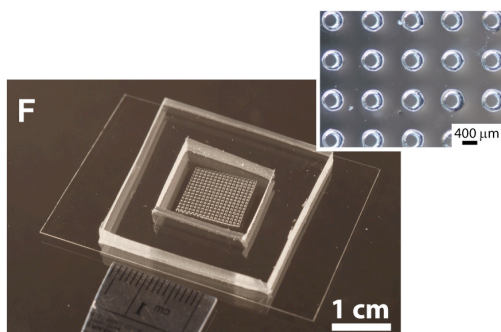
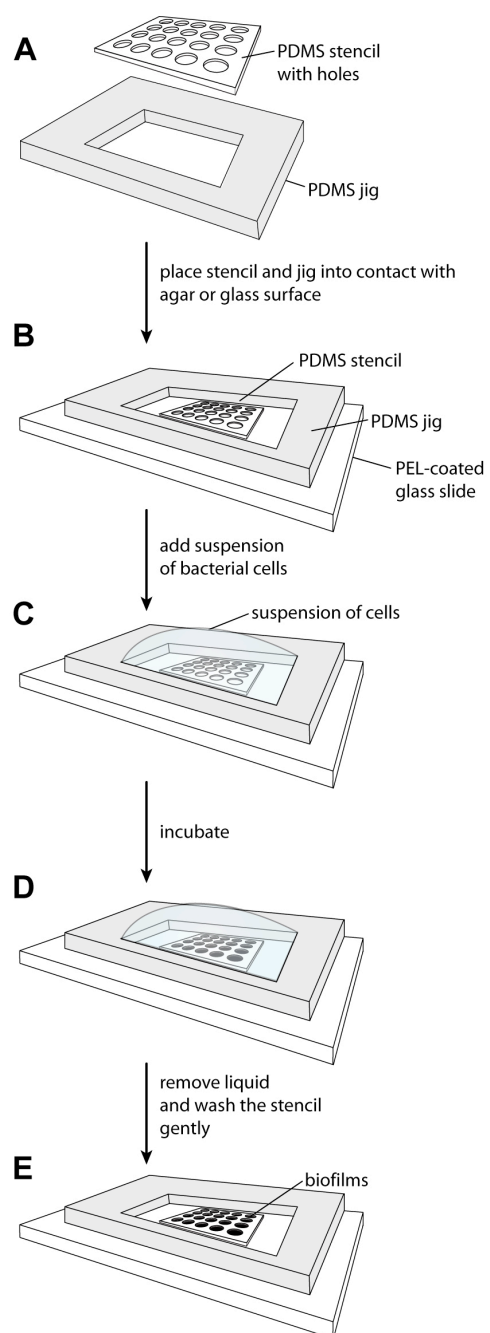


**Figure 1.** A schematic diagram depicting the process of patterning bacterial cells using thin, PDMS stencils. A) A sterile PDMS stencil and jig. B) The stencil and jig are pressed into contact with a PEL-coated glass coverslip or another substrate. C) A suspension of bacterial cells diluted from an overnight culture is added on top of the stencil. D) The device is placed in a sterile Petri dish and incubated to promote biofilm formation on the substrate surface. Cells make contact with the surface through the holes in the PDMS stencil and biofilms therefore grow in the area defined by the patterns in the stencil. E) At the end of the growth period, excess liquid is removed and the stencil containing biofilm arrays is gently washed with fresh media to remove planktonic cells from the surface of the polymer. An array of biofilms is patterned on the surface of the substrate. At this stage, the PDMS stencil can be removed, if necessary, to leave free standing biofilm arrays on the surface as shown in Figure 2A and 2B. Alternatively, the stencil can be left in place to grow biofilms in the holes. F) A typical device consisting of a PDMS stencil, jig, and glass coverslip is shown. The image inset is a PDMS stencil imaged using stereomicroscopy.

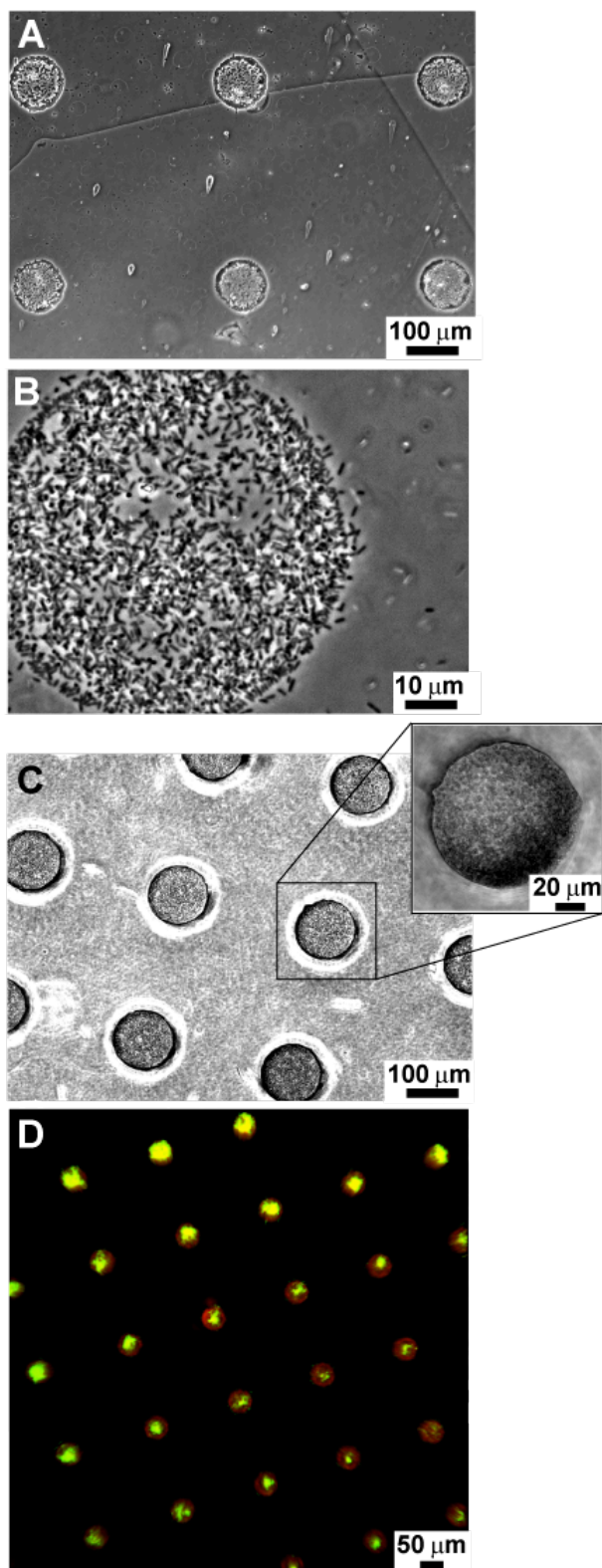


**Figure 2.** *P. aeruginosa* PAO1 biofilms were patterned on PEL-coated glass coverslips using PDMS stencils with circular holes that were 50  $\mu\text{m}$  (D) or 100  $\mu\text{m}$  in diameter (A, B and C). A) A section of an array of nascent free-standing *P. aeruginosa* biofilms. The patterned biofilms remained adhered on the substrate surface after the PDMS stencil was peeled away. B) A nascent *P. aeruginosa* biofilm imaged at a higher magnification. All optical images were acquired using phase contrast microscopy. C) Nascent biofilms filled the holes in the PDMS stencils after 20 hrs of growth as shown in this phase contrast image. D) Biofilms of GFP-expressing PAO1 cells were grown for 3 days in a PDMS stencil. The image is an overlay of two epifluorescence images: bacterial cells are green, and the polysaccharide biofilm matrix, which was stained with calcofluor, appears red.

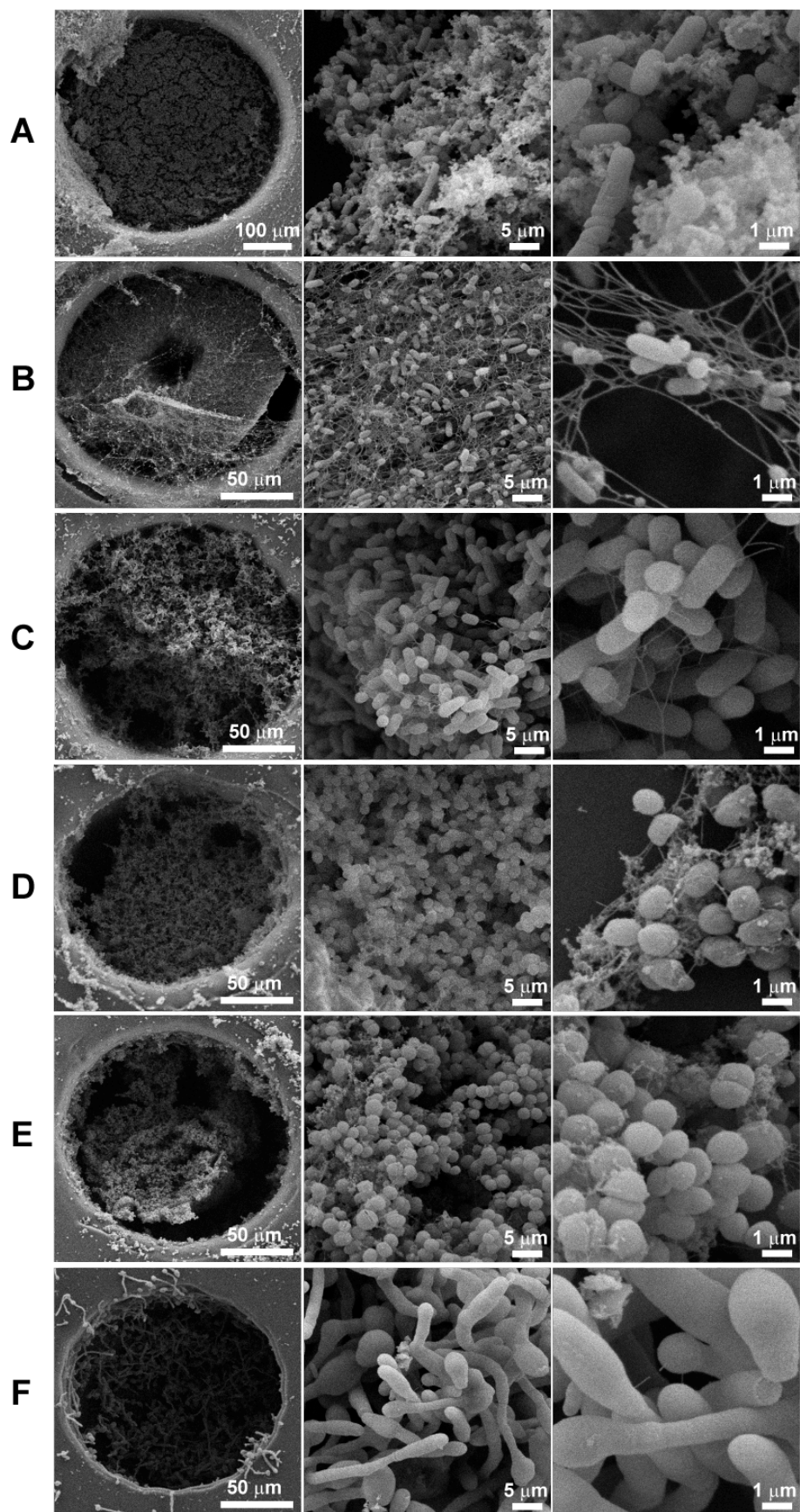


**Figure 3.** Scanning electron micrographs (SEM) of biofilms fabricated in PDMS stencils. Each row of images corresponds to biofilms of the following organisms grown on PEL-coated glass coverslips: A) *B. subtilis*, B) *P. aeruginosa*, C) *E. coli*, D) *V. fischeri*, E) *S. epidermidis*, and F) *C. albicans*. The biofilms were grown for 72 hr using the conditions described in the experimental section. The cells were prepared for SEM by fixing and critical point drying the cells in the stencils. Peeling the biofilm-embedded stencils away from surface substrates distorted the biofilm structure and frequently promoted its detachment from the walls of the stencil (e.g. B-E).

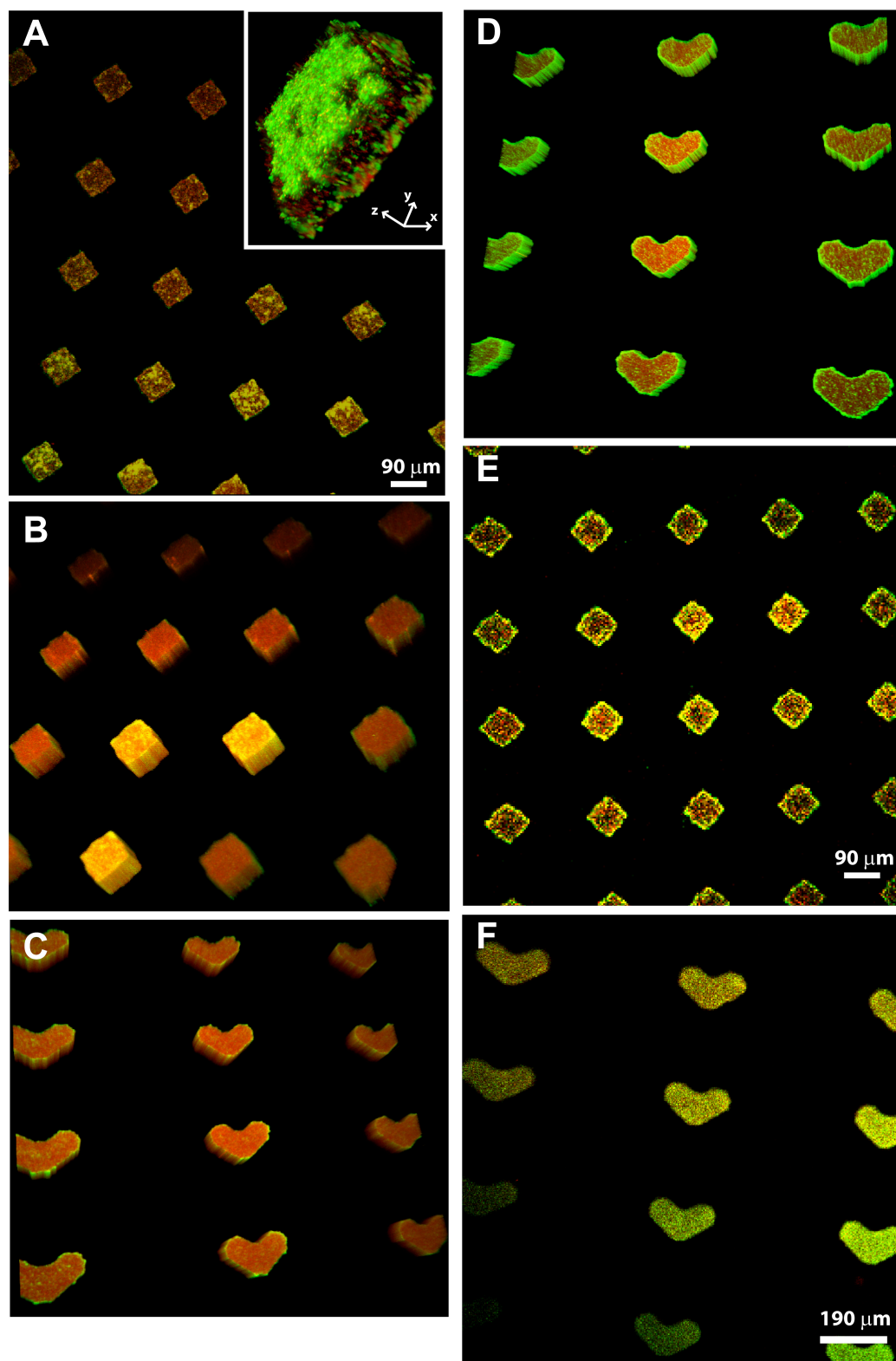


**Figure 4.** Arrays of *P. aeruginosa* biofilms patterned on the surface of various substrates. A) Biofilm arrays were grown on an 11-amino-1-undecanethiol hydrochloride SAM on a gold-coated coverslip using a stencil with diamond-shaped holes. The image inset shows a 'mini-biofilm' in an array at a higher magnification in 3-D after rotating the image along the y-axis. Biofilm arrays fabricated on B) polyvinylchloride, C) polycarbonate, D) polystyrene, E) polyethylene, and F) stainless steel. *P. aeruginosa* biofilms were grown for 72 hr. The lateral dimensions of biofilms were 90  $\mu\text{m}$  in panel B and 190  $\mu\text{m}$  in panels C and D. All images, except A, E, and F for which only one plane was captured by epifluorescence microscopy, are 3-D reconstructions of confocal microscopy images. Stencils with diamond-shaped holes (panels A, B, and E) and heart-shaped holes (panels C, D, and F) were used for these experiments. The 3-D images do not have scale bars as the images are rotated and viewed at an oblique angle. Green and red indicate bacterial cells and biofilm matrix, respectively. The thickness of biofilms grown on various surfaces ranged between 15 and 25  $\mu\text{m}$ .

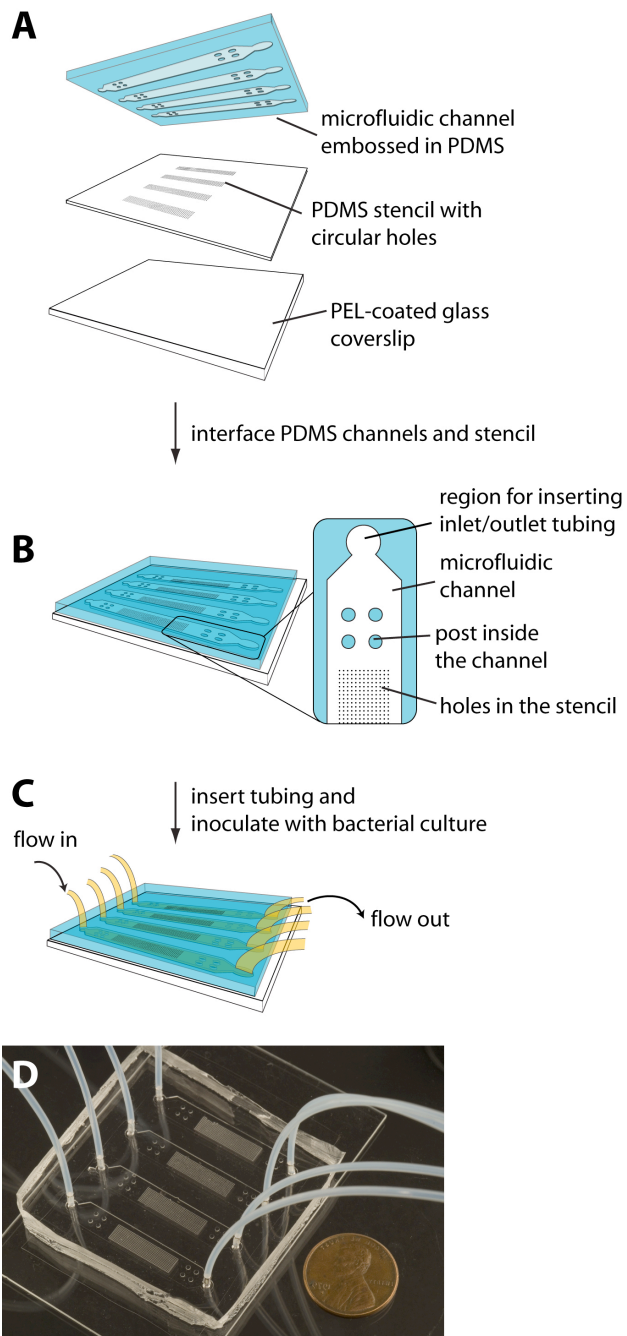


**Figure 5.** A schematic diagram illustrating the process of interfacing PDMS microfluidic devices and stencils. A) Microfluidic channels are embossed in a slab of PDMS. A thin layer of PDMS stencil has an array of holes with dimensions that fit

within the microfluidic channels. B) The PDMS slab with microfluidic channels and the PDMS stencil are brought into contact with the surface of a substrate. A close-up of a channel is shown on the right. Each channel has eight 'posts'—four at each end of the channel—to prevent the channel from collapsing on to the surface of the stencil. C) A suspension of cells diluted from an overnight culture is introduced into each channel through an inlet tubing, and the effluent from the channel is removed through an outlet tubing. D) An image of an assembled device: microfluidic channels and a PDMS stencil on a PEL-coated glass coverslip with inlet/outlet tubing attached. A penny is included in the image to provide a reference of the length scale.

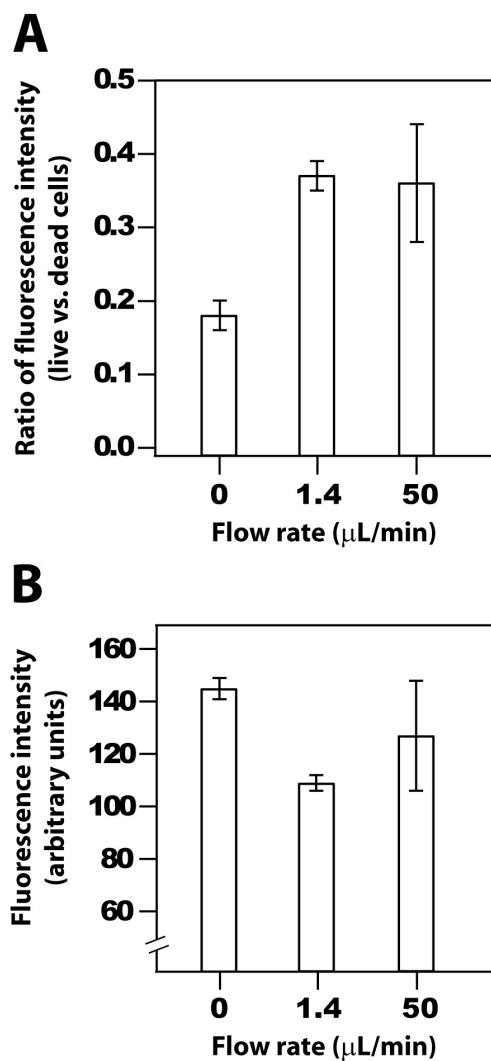


**Figure 6.** Physiological characterization of biofilms grown in PDMS stencils at different flow rates of culture media. A) Ratio of fluorescence emission from live *vs.* dead cells in biofilms. Live cells (stained with a 6  $\mu\text{M}$  solution of Syto 9) and dead cells (stained with a 30  $\mu\text{M}$  solution of propidium iodide) in biofilms were visualized using a BacLight LIVE/DEAD kit. B) The fluorescence emission from metabolically active cells was probed using CTC. The mean fluorescence intensity from CTC, Syto 9, and propidium iodide was calculated using Image J, and the values for the live and dead staining were

corrected for the difference in quantum yield as described in the Materials and Methods section. For each assay, *P. aeruginosa* biofilms were grown in static condition or under liquid flow for 20 hr at 37 °C. Two different flow rates (1.4 and 50  $\mu\text{L}/\text{min}$ ) were tested. Three independent experiments were performed for each condition, and at least 100 biofilms were imaged and analyzed for each experiment. A statistical analysis (i.e. coefficient of variation) of the data is summarized in Table 2.

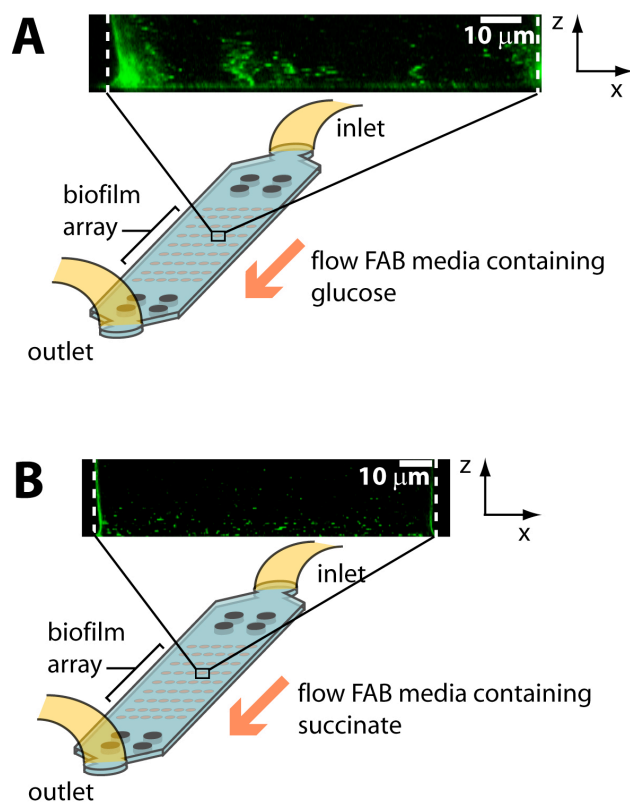


**Figure 7.** Observation of two types of biofilm architecture (i.e. flat and structured) resulting from cell growth in the presence of different carbon sources. A) Biofilms grown in media supplemented with glucose and B) with succinate. Biofilms were grown in microfluidic devices using PDMS stencils with 100  $\mu\text{m}$  diameter holes. The fabrication of the microfluidic devices is analogous to that described in Figure 5. Dashed lines indicate the edges of the hole. The multicellular structures embedded in the stencils were imaged using CSLM, and the images were reconstructed and vertically sliced using ImageJ to provide a cross section of the biofilms.

**Table 1.** Strains and culture conditions used in this study. \*Cell cultures were diluted as indicated before inoculating for biofilm experiments. Optical density at 600 nm and overnight culture are abbreviated as OD<sub>600</sub> and OC, respectively.

Strain	Media used	Genotype	Biofilm experiments*	References
<i>P. aeruginosa</i> PAO1	M8 and FAB	wild type	OD <sub>600</sub> = 0.1 (M8) and 0.3 (FAB)	(83)
<i>P. aeruginosa</i> pTdK-GFP	M8, 200 µg/mL ampicillin	<i>Plac-gfp, amp<sup>R</sup></i>	OD <sub>600</sub> = 0.1	(50)
<i>E. coli</i> MG1655	LB	<i>rph-1, LAM-, F-</i>	1/200 dilution of OC	CGSC# 8237
<i>V. fischeri</i> ES114	Hepes minimal media	wild type	1/100 dilution of OC	(84)
<i>S. epidermidis</i> 3004	TSB	wild type	1/100 dilution of OC	This study
<i>B. subtilis</i> 168	modified LB	<i>trpC2</i>	OD <sub>600</sub> = 0.5	(85)
<i>C. albicans</i> SC5314	YPD	wild type	OD <sub>600</sub> = 1	(86)

**Table 2.** Statistical analysis of the physiological parameters characterized for biofilms grown in PDMS stencils.

<b>Parameter quantified</b>	<b>Flow rate used for biofilm growth (uL/min)</b>	<b>Mean</b>	<b>Standard Deviation</b>	<b>Coefficient of Variation</b>
Ratio of live over dead cells	0	0.18	0.02	0.11
	1.4	0.37	0.02	0.05
	50	0.36	0.08	0.22
Cellular metabolic activity	0	145	4	0.03
	1.4	108	3	0.03
	50	127	21	0.17

## REFERENCES

1. Davey, M. E., and O'Toole, G. A. (2000) Microbial biofilms: from ecology to molecular genetics, *Microbiology and Molecular Biology Reviews* 64, 847-867.
2. Davies, D. G., and Geesey, G. G. (1995) Regulation of the Alginate Biosynthesis Gene *AlgC* in *Pseudomonas-Aeruginosa* during Biofilm Development in Continuous-Culture, *Applied and Environmental Microbiology* 61, 860-867.
3. Costerton, J. W., Lewandowski, Z., Caldwell, D. E., Korber, D. R., and Lappinscott, H. M. (1995) Microbial Biofilms, *Annual Review of Microbiology* 49, 711-745.
4. Sutherland, I. W. (2001) The biofilm matrix - an immobilized but dynamic microbial environment, *Trends in Microbiology* 9, 222-227.
5. Danese, P. N., Pratt, L. A., and Kolter, R. (2000) Exopolysaccharide production is required for development of *Escherichia coli* K-12 biofilm architecture, *Journal of Bacteriology* 182, 3593-3596.
6. Costerton, J. W., Cheng, K. J., Geesey, G. G., Ladd, T. I., Nickel, J. C., Dasgupta, M., and Marrie, T. J. (1987) Bacterial Biofilms in Nature and Disease, *Annual Review of Microbiology* 41, 435-464.
7. Lawrence, J. R., Korber, D. R., Hoyle, B. D., Costerton, J. W., and Caldwell, D. E. (1991) Optical Sectioning of Microbial Biofilms, *Journal of Bacteriology* 173, 6558-6567.
8. Hall-Stoodley, L., Costerton, J. W., and Stoodley, P. (2004) Bacterial biofilms: From the natural environment to infectious diseases, *Nature Reviews Microbiology* 2, 95-108.
9. Westall, F., de Wit, M. J., Dann, J., van der Gaast, S., de Ronde, C. E. J., and Gerneke, D. (2001) Early Archean fossil bacteria and biofilms in hydrothermally-influenced sediments from the Barberton greenstone belt, South Africa, *Precambrian Research* 106, 93-116.
10. Little, R., Peterson, Raffa, and Handelsman. (2008) Rules of Engagement: Interspecies Interactions that Regulate Microbial Communities, *Annual Review of Microbiology* 62, 375-401.
11. Tyson, G. W., Chapman, J., Hugenholtz, P., Allen, E. E., Ram, R. J., Richardson, P. M., Solovyev, V. V., Rubin, E. M., Rokhsar, D. S., and Banfield, J. F. (2004) Community structure and metabolism through reconstruction of microbial genomes from the environment, *Nature* 428, 37-43.

12. Antoci, V., King, S. B., Jose, B., Parvizi, J., Zeiger, A. R., Wickstrom, E., Freeman, T. A., Cornposto, R. J., Ducheyne, P., Shapiro, I. M., Hickok, N. J., and Adams, C. S. (2007) Vancomycin covalently bonded to titanium alloy prevents bacterial colonization, *Journal of Orthopaedic Research* 25, 858-866.
13. Zhang, L. H., and Dong, Y. H. (2004) Quorum sensing and signal interference: diverse implications, *Molecular Microbiology* 53, 1563-1571.
14. Valle, J., Da Re, S., Henry, N., Fontaine, T., Balestrino, D., Latour-Lambert, P., and Ghigo, J. M. (2006) Broad-spectrum biofilm inhibition by a secreted bacterial polysaccharide, *Proceedings of the National Academy of Sciences of the United States of America* 103, 12558-12563.
15. Beckloff, N., Laube, D., Castro, T., Furgang, D., Park, S., Perlin, D., Clements, D., Tang, H., Scott, R. W., Tew, G. N., and Diamond, G. (2007) Activity of an antimicrobial peptide mimetic against planktonic and biofilm cultures of oral pathogens, *Antimicrobial Agents and Chemotherapy* 51, 4125-4132.
16. Ista, L. K., Perez-Luna, V. H., and Lopez, G. P. (1999) Surface-grafted, environmentally sensitive polymers for biofilm release, *Applied and Environmental Microbiology* 65, 1603-1609.
17. Lu, T. K., and Collins, J. J. (2007) Dispersing biofilms with engineered enzymatic bacteriophage, *Proceedings of the National Academy of Sciences of the United States of America* 104, 11197-11202.
18. Drenkard, E., and Ausubel, F. M. (2002) Pseudomonas biofilm formation and antibiotic resistance are linked to phenotypic variation, *Nature* 416, 740-743.
19. Costerton, W., Veeh, R., Shirtliff, M., Pasmore, M., Post, C., and Ehrlich, G. (2003) The application of biofilm science to the study and control of chronic bacterial infections, *Journal of Clinical Investigation* 112, 1466-1477.
20. Lynch, A. S., and Robertson, G. T. (2008) Bacterial and fungal biofilm infections, *Annual Review of Medicine* 59, 415-428.
21. Friedman, L., and Kolter, R. (2004) Genes involved in matrix formation in Pseudomonas aeruginosa PA14 biofilms, *Molecular Microbiology* 51, 675-690.
22. McLean, R. B., C.; Barnes, M; McGowin, C.; and Aron, G. (2004) Methods of studying biofilms, In *Microbial biofilms* (O'Toole, M. G. a. G. A., Ed.), p 398, American Society for Microbiology Press, Washington, D.C.
23. Mack, D., Bartscht, K., Fischer, C., Rohde, H., De Grahl, C., Dobinsky, S., Horstkotte, M. A., Kiel, K., and Knobloch, J. K. M. (2001) Genetic and biochemical

- analysis of *Staphylococcus epidermidis* biofilm accumulation, In *Methods in Enzymology - Microbial Growth in Biofilms, Pt A*, pp 215-239.
24. Ramos, C., Licht, T. R., Sternberg, C., Krogfelt, K. A., and Molin, S. (2001) Monitoring bacterial growth activity in biofilms from laboratory flow chambers, plant rhizosphere, and animal intestine, In *Methods in Enzymology - Microbial Growth in Biofilms, Pt B*, pp 21-42.
  25. Stewart, P. S., and Franklin, M. J. (2008) Physiological heterogeneity in biofilms, *Nature Reviews Microbiology* 6, 199-210.
  26. Purevdorj, B., Costerton, J. W., and Stoodley, P. (2002) Influence of hydrodynamics and cell signaling on the structure and behavior of *Pseudomonas aeruginosa* biofilms, *Applied and Environmental Microbiology* 68, 4457-4464.
  27. Hawser, S. P., Baillie, G. S., and Douglas, L. J. (1998) Production of extracellular matrix by *Candida albicans* biofilms, *Journal of Medical Microbiology* 47, 253-256.
  28. Mangalappalli-Illathu, A. K., Lawrence, J. R., Swerhone, G. D. W., and Korber, D. R. (2008) Architectural adaptation and protein expression patterns of *Salmonella enterica* serovar Enteritidis biofilms under laminar flow conditions, *International Journal of Food Microbiology* 123, 109-120.
  29. Beyenal, H., and Lewandowski, Z. (2002) Internal and external mass transfer in biofilms grown at various flow velocities, *Biotechnology Progress* 18, 55-61.
  30. Simoes, M., Pereira, M. O., and Vieira, M. J. (2005) Action of a cationic surfactant on the activity and removal of bacterial biofilms formed under different flow regimes, *Water Research* 39, 478-486.
  31. Rupp, M. E., and Fey, P. D. (2001) In vivo models to evaluate adhesion and biofilm formation by *Staphylococcus epidermidis*, In *Methods in Enzymology - Microbial Growth in Biofilms, Pt A*, pp 206-215.
  32. Allison, D., Maira-Litran, T., and Gilbert, P. (1999) Perfused biofilm fermenters, In *Methods in Enzymology - Biofilms*, pp 232-248.
  33. Kharazmi, A., Giwerzman, B., and Hoiby, N. (1999) Robbins device in biofilm research, In *Methods in Enzymology - Biofilms*, pp 207-215.
  34. Palmer, R. J. (1999) Microscopy flowcells: Perfusion chambers for real-time study of biofilms, In *Methods in Enzymology - Biofilms*, pp 160-166.
  35. Zinn, M. S., Kirkegaard, R. D., Palmer, R. J., and White, D. C. (1999) Laminar flow chamber for continuous monitoring of biofilm formation and succession, In *Methods in Enzymology - Biofilms*, pp 224-232.

36. Millar, M. R., Linton, C. J., and Sheriff, A. (2001) Use of a continuous culture system linked to a modified Robbins device or flow cell to study attachment of bacteria to surfaces, In *Methods in Enzymology - Microbial Growth in Biofilms, Pt B*, pp 43-62.
37. Buswell, C. M., Nicholl, H. S., and Walker, J. T. (2001) Use of continuous culture bioreactors for the study of pathogens such as *Campylobacter jejuni* and *Escherichia coli* O157 in biofilms, In *Methods in Enzymology - Microbial Growth in Biofilms, Pt B*, pp 70-78.
38. Balagadde, F. K., You, L. C., Hansen, C. L., Arnold, F. H., and Quake, S. R. (2005) Long-term monitoring of bacteria undergoing programmed population control in a microchemostat, *Science* 309, 137-140.
39. McCoy, W. F., Bryers, J. D., Robbins, J., and Costerton, J. W. (1981) Observations of Fouling Biofilm Formation, *Canadian Journal of Microbiology* 27, 910-917.
40. Allison, D., Maira-Litran, T., and Gilbert, P. (1999) Methods in Enzymology - Perfused biofilm fermenters, In *Biofilms*, pp 232-248.
41. O'Toole, G. A., and Kolter, R. (1998) Initiation of biofilm formation in *Pseudomonas fluorescens* WCS365 proceeds via multiple, convergent signalling pathways: a genetic analysis, *Molecular Microbiology* 28, 449-461.
42. Sauer, K., Camper, A. K., Ehrlich, G. D., Costerton, J. W., and Davies, D. G. (2002) *Pseudomonas aeruginosa* displays multiple phenotypes during development as a biofilm, *Journal of Bacteriology* 184, 1140-1154.
43. Ostuni, E., Kane, R., Chen, C. S., Ingber, D. E., and Whitesides, G. M. (2000) Patterning mammalian cells using elastomeric membranes, *Langmuir : the ACS journal of surfaces and colloids* 16, 7811-7819.
44. Xia, Y. N., and Whitesides, G. M. (1998) Soft lithography, *Angewandte Chemie-International Edition* 37, 551-575.
45. Lee, J. N., Park, C., and Whitesides, G. M. (2003) Solvent compatibility of poly(dimethylsiloxane)-based microfluidic devices, *Analytical Chemistry* 75, 6544-6554.
46. Huang, B., Wu, H. K., Kim, S., and Zare, R. N. (2005) Coating of poly(dimethylsiloxane) with n-dodecyl-beta-D-maltoside to minimize nonspecific protein adsorption, *Lab on a Chip* 5, 1005-1007.
47. Gomez-Sjoberg, R., Leyrat, A. A., Pirone, D. M., Chen, C. S., and Quake, S. R. (2007) Versatile, fully automated, microfluidic cell culture system, *Analytical Chemistry* 79, 8557-8563.

48. Bais, H. P., Fall, R., and Vivanco, J. M. (2004) Biocontrol of *Bacillus subtilis* against infection of *Arabidopsis* roots by *Pseudomonas syringae* is facilitated by biofilm formation and surfactin production, *Plant Physiology* 134, 307-319.
49. Yip, E. S., Geszvain, K., DeLoney-Marino, C. R., and Visick, K. L. (2006) The symbiosis regulator RscS controls the *syp* gene locus, biofilm formation and symbiotic aggregation by *Vibrio fischeri*, *Molecular Microbiology* 62, 1586-1600.
50. De Kievit, T. R., Gillis, R., Marx, S., Brown, C., and Iglewski, B. H. (2001) Quorum-sensing genes in *Pseudomonas aeruginosa* biofilms: Their role and expression patterns, *Applied and Environmental Microbiology* 67, 1865-1873.
51. Heilmann, C., Gerke, C., PerdreauRemington, F., and Gotz, F. (1996) Characterization of Tn917 insertion mutants of *Staphylococcus epidermidis* affected in biofilm formation, *Infection and Immunity* 64, 277-282.
52. Ramage, G., vande Walle, K., Wickes, B. L., and Lopez-Ribot, J. L. (2001) Standardized method for in vitro antifungal susceptibility testing of *Candida albicans* biofilms, *Antimicrobial Agents and Chemotherapy* 45, 2475-2479.
53. Heydorn, A., Nielsen, A. T., Hentzer, M., Sternberg, C., Givskov, M., Ersboll, B. K., and Molin, S. (2000) Quantification of biofilm structures by the novel computer program COMSTAT, *Microbiology-Uk* 146, 2395-2407.
54. Decher, G. (1997) Fuzzy nanoassemblies: Toward layered polymeric multicomposites, *Science* 277, 1232-1237.
55. Eriksson, M., Notley, S. M., and Wagberg, L. (2005) The influence on paper strength properties when building multilayers of weak polyelectrolytes onto wood fibres, *Journal of Colloid and Interface Science* 292, 38-45.
56. Shim, H. W., Lee, J. H., Hwang, T. S., Rhee, Y. W., Bae, Y. M., Choi, J. S., Han, J., and Lee, C. S. (2007) Patterning of proteins and cells on functionalized surfaces prepared by polyelectrolyte multilayers and micromolding in capillaries, *Biosensors & Bioelectronics* 22, 3188-3195.
57. Doherty, D., Leigh, J. A., Glazebrook, J., and Walker, G. C. (1988) *Rhizobium-Meliloti* Mutants That Overproduce the R-Meliloti Acidic Calcofluor-Binding Exopolysaccharide, *Journal of Bacteriology* 170, 4249-4256.
58. Webb, J. S., Thompson, L. S., James, S., Charlton, T., Tolker-Nielsen, T., Koch, B., Givskov, M., and Kjelleberg, S. (2003) Cell death in *Pseudomonas aeruginosa* biofilm development, *Journal of Bacteriology* 185, 4585-4592.
59. Pyle, B. H., Broadaway, S. C., and McFeters, G. A. (1995) Factors Affecting the Determination of Respiratory Activity on the Basis of Cyanoditolyl Tetrazolium Chloride Reduction with Membrane Filtration, *Applied and Environmental Microbiology* 61, 4304-4309.

60. Rodriguez, G. G., Phipps, D., Ishiguro, K., and Ridgway, H. F. (1992) Use of a Fluorescent Redox Probe for Direct Visualization of Actively Respiring Bacteria, *Applied and Environmental Microbiology* 58, 1801-1808.
61. Manz, W., Wagner, M., and Kalmbach, S. (2001) Assessment of metabolic potential of biofilm-associated bacteria, In *Methods in Enzymology - Microbial Growth in Biofilms, Pt a R Biological Aspects*, pp 265-276.
62. Jackman, R. J., Duffy, D. C., Ostuni, E., Willmore, N. D., and Whitesides, G. M. (1998) Fabricating large arrays of microwells with arbitrary dimensions and filling them using discontinuous dewetting, *Analytical Chemistry* 70, 2280-2287.
63. Weibel, D. B., DiLuzio, W. R., and Whitesides, G. M. (2007) Microfabrication meets microbiology, *Nature Reviews Microbiology* 5, 209-218.
64. Weibel, D. B., Lee, A., Mayer, M., Brady, S. F., Bruzewicz, D., Yang, J., DiLuzio, W. R., Clardy, J., and Whitesides, G. M. (2005) Bacterial printing press that regenerates its ink: Contact-printing bacteria using hydrogel stamps, *Langmuir : the ACS journal of surfaces and colloids* 21, 6436-6442.
65. Xu, L. P., Robert, L., Qi, O. Y., Taddei, F., Chen, Y., Lindner, A. B., and Baigl, D. (2007) Microcontact printing of living bacteria arrays with cellular resolution, *Nano Letters* 7, 2068-2072.
66. Cheng, G., Zhang, Z., Chen, S. F., Bryers, J. D., and Jiang, S. Y. (2007) Inhibition of bacterial adhesion and biofilm formation on zwitterionic surfaces, *Biomaterials* 28, 4192-4199.
67. Hou, S. Y., Burton, E. A., Simon, K. A., Blodgett, D., Luk, Y. Y., and Ren, D. C. (2007) Inhibition of Escherichia coli biofilm formation by self-assembled monolayers of functional alkanethiols on gold, *Applied and Environmental Microbiology* 73, 4300-4307.
68. Shrout, J. D., Chopp, D. L., Just, C. L., Hentzer, M., Givskov, M., and Parsek, M. R. (2006) The impact of quorum sensing and swarming motility on Pseudomonas aeruginosa biofilm formation is nutritionally conditional, *Molecular Microbiology* 62, 1264-1277.
69. Klausen, M., Aaes-Jorgensen, A., Molin, S., and Tolker-Nielsen, T. (2003) Involvement of bacterial migration in the development of complex multicellular structures in Pseudomonas aeruginosa biofilms, *Molecular Microbiology* 50, 61-68.
70. Klausen, M., Heydorn, A., Ragas, P., Lambertsen, L., Aaes-Jorgensen, A., Molin, S., and Tolker-Nielsen, T. (2003) Biofilm formation by Pseudomonas aeruginosa wild type, flagella and type IV pili mutants, *Molecular Microbiology* 48, 1511-1524.

71. McDonald, J. C., and Whitesides, G. M. (2002) Poly(dimethylsiloxane) as a material for fabricating microfluidic devices, *Acc Chem Res* 35, 491-499.
72. Khademhosseini, A., Yeh, J., Jon, S., Eng, G., Suh, K. Y., Burdick, J. A., and Langer, R. (2004) Molded polyethylene glycol microstructures for capturing cells within microfluidic channels, *Lab on a Chip* 4, 425-430.
73. Kim, H. J., Boedicker, J. Q., Choi, J. W., and Ismagilov, R. F. (2008) From the Cover: Defined spatial structure stabilizes a synthetic multispecies bacterial community, *Proc Natl Acad Sci U S A* 105, 18188-18193.
74. Dietrich, L. E. P., Teal, T. K., Price-Whelan, A., and Newman, D. K. (2008) Redox-active antibiotics control gene expression and community behavior in divergent bacteria, *Science* 321, 1203-1206.
75. Hansen, S. K., Rainey, P. B., Haagensen, J. A. J., and Molin, S. (2007) Evolution of species interactions in a biofilm community, *Nature* 445, 533-536.
76. Hardie, K. R., and Heurlier, K. (2008) Establishing bacterial communities by 'word of mouth': LuxS and autoinducer 2 in biofilm development, *Nature Reviews Microbiology* 6, 635-643.
77. Kirisits, M. J., and Parsek, M. R. (2006) Does *Pseudomonas aeruginosa* use intercellular signalling to build biofilm communities?, *Cellular Microbiology* 8, 1841-1849.
78. Lichter, J. A., Thompson, M. T., Delgadillo, M., Nishikawa, T., Rubner, M. F., and Van Vliet, K. J. (2008) Substrata mechanical stiffness can regulate adhesion of viable bacteria, *Biomacromolecules* 9, 1571-1578.
79. Ista, L. K., Callow, M. E., Finlay, J. A., Coleman, S. E., Nolasco, A. C., Simons, R. H., Callow, J. A., and Lopez, G. P. (2004) Effect of substratum surface chemistry and surface energy on attachment of marine bacteria and algal spores, *Applied and Environmental Microbiology* 70, 4151-4157.
80. Keymer, J. E., Galajda, P., Muldoon, C., Park, S., and Austin, R. H. (2006) Bacterial metapopulations in nanofabricated landscapes, *Proceedings of the National Academy of Sciences of the United States of America* 103, 17290-17295.
81. Cho, H., Jonsson, H., Campbell, K., Melke, P., Williams, J. W., Jedynek, B., Stevens, A. M., Groisman, A., and Levchenko, A. (2007) Self-organization in high-density bacterial colonies: efficient crowd control, *PLoS Biol* 5, e302.
82. Volfson, D., Cookson, S., Hasty, J., and Tsimring, L. S. (2008) Biomechanical ordering of dense cell populations, *Proceedings of the National Academy of Sciences of the United States of America* 105, 15346-15351.
83. Holloway, B. W., Krishnapillai, V., and Morgan, A. F. (1979) Chromosomal

Genetics of *Pseudomonas*, *Microbiological Reviews* 43, 73-102.

84. Boettcher, K. J., and Ruby, E. G. (1990) Depressed Light-Emission by Symbiotic *Vibrio-Fischeri* of the Sepiolid Squid *Euprymna-Scolopes*, *Journal of Bacteriology* 172, 3701-3706.
85. Carballido-Lopez, R., Formstone, A., Li, Y., Ehrlich, S. D., Noirot, P., and Errington, J. (2006) Actin homolog MreBH governs cell morphogenesis by localization of the cell wall hydrolase LytE, *Developmental Cell* 11, 399-409.
86. Hull, C. M., Raisner, R. M., and Johnson, A. D. (2000) Evidence for mating of the "asexual" yeast *Candida albicans* in a mammalian host, *Science* 289, 307-310.

## CHAPTER 3

### **Encapsulating bacteria in agarose microparticles using microfluidics for high-throughput cell analysis and isolation**

Adapted from:

Ye-Jin Eun, Andrew Utada, Matthew F. Copeland, Shoji Takeuchi, and Douglas B.

Weibel (2011) *ACS Chemical Biology* 6(3):260-266.

## ABSTRACT

This chapter describes the high-throughput analysis and isolation of bacterial cells encapsulated in agarose microparticles using fluorescence-activated cell sorting (FACS). Flow-focusing microfluidic systems were used to create monodisperse microparticles that were ~30  $\mu\text{m}$  in diameter. The dimensions of these particles made them compatible with flow cytometry and FACS, and the sensitivity of these techniques reduced the incubation time for cell replication before analyses were carried out. The small volume of the microparticles (~1-50 picoliters) minimized the quantity of reagents needed for bacterial studies. This platform made it possible to screen and isolate bacteria, and apply a combination of techniques to rapidly determine the target of biologically active small molecules. As a pilot study, *Escherichia coli* cells were encapsulated in agarose microparticles, incubated in the presence of varying concentrations of rifampicin, and analyzed using FACS. The minimum inhibitory concentration of rifampicin was determined, and spontaneous mutants that had developed resistance to the antibiotic were isolated via FACS and characterized by DNA sequencing. The  $\beta$ -subunit of RNA polymerase, RpoB, was confirmed as the target of rifampicin, and Q513L was the mutation most frequently observed. Using this approach, the time and quantity of antibiotics required for the isolation of mutants was reduced by 8- and 150-fold, respectively, compared to conventional microbiological techniques using nutrient agar plates. We envision that this technique will have an important impact on research in chemical biology, natural products chemistry, and the discovery and characterization of biologically active secondary metabolites.

## INTRODUCTION

This chapter describes a microfluidic technique for encapsulating, growing, and analyzing bacteria in agarose microparticles to rapidly screen and isolate cells that display phenotypes of interest. As a proof-of-principle, we used the bacterial RNA polymerase inhibitor rifampicin and identified spontaneous mutations in *Escherichia coli* (*E. coli*) that conveyed resistance to this antibiotic. We created agarose microparticles using microfluidic flow-focusing devices fabricated in poly(dimethylsiloxane) (PDMS). The microparticles are mechanically stable and have a user-defined diameter that ranges from 20 to 150  $\mu\text{m}$ ; these characteristics enable us to use flow cytometry (FC) and fluorescence-activated cell sorting (FACS) for the high-throughput analysis, selection, and isolation of encapsulated cells based on phenotypes.

Microbiologists frequently culture bacterial cells on agar plates to screen, select, and isolate monoclonal populations of cells. ‘Agar plates, toothpicks, and logic’ (1) played a central role in microbiology over the past century; however, approaches based on the growth of cells on agar nutrient media have significant drawbacks for culturing organisms that grow slowly or require environmental cues (2). The most common techniques for identifying targets of biologically active small molecules in bacteria involve large-scale screens to isolate mutants that have spontaneous resistance to the compounds, isolation and amplification of their genomic DNA, and sequencing to identify genetic changes responsible for the acquired resistance. The isolation of mutants by growing bacteria on agar typically requires large quantities of the chemical(s) of interest and multiple iterations of screening, which can make these assays

expensive and slow. These requirements can be particularly problematic if the reagents are difficult to obtain and are only available in small quantities (e.g. structurally complex secondary metabolites and natural products that are not yet available through total syntheses) or when the exposure of users to hazardous compounds should be minimized. Furthermore, the time required for each cycle is constrained by the growth of an individual cell into a colony that is large enough to visualize and pick. This characteristic limits the throughput of assays for the rapid screening of biological and chemical targets.

To address these limitations, several different methods have been proposed for encapsulating bacterial cells in aqueous droplets (3-5), liquid plugs (6, 7), or hydrogels (8-13) for high-throughput analysis. The most widely used of these techniques encapsulate cells in agarose (2, 14-17) and have been used to study a variety of phenomena, including: (1) antibiotic susceptibility (18, 19); (2) bacterial uptake of small molecules by electroporation (20); (3) enrichment of slow-growing bacteria (21, 22); and (4) growth of 'uncultured' bacteria for phylogenetic analyses (2).

Despite their demonstrated applications, the methods currently available for fabricating agarose particles provide limited control over the diameter of particles and produce particles with a large coefficient of variance (e.g.,  $\geq 40\%$ ) (12, 23-26). The large variance in the diameter of these particles can be problematic when studying cells that are present at a low frequency in a heterogeneous population of cells. Large particles with diameters that are incompatible with FC or FACS are removed by filtration prior to analysis. Strains that are underrepresented in a mixed population of cells may be encapsulated in large particles and removed before they are analyzed, which biases the

composition of the sample and poses a challenge for the detection and analysis of 'rare' cells in a mixed population.

To transcend the limitations of conventional techniques for encapsulating bacteria in agarose, we used PDMS flow-focusing microfluidic systems to form monodisperse microparticles (27, 28). The mechanism of drop formation in these microfluidic junctions is well understood and can be exploited to create monodisperse droplets and bubbles (29-31). We isolated single cells in microparticles and demonstrated rapid determination of the minimum inhibitory concentration (MIC) of rifampicin to *E. coli* strain MG1655 and screening and isolation of spontaneous mutants that are resistant to the antibiotic. This approach makes it possible to isolate strains of bacteria based on changes in genotype and phenotype and will be useful for evolving and engineering proteins in microbes (4).

## EXPERIMENTAL METHODS

### *Materials.*

Mineral oil, Span 80, low-melting point agarose IX-A, and anhydrotetracycline hydrochloride were purchased from Sigma Aldrich. Tryptone, sodium chloride, potassium chloride, magnesium chloride, magnesium sulfate, glucose, isopropyl- $\beta$ -D-thiogalactopyranoside (IPTG), ampicillin, yeast extract, peptone, dextrose, kanamycin, rifampicin, phosphate-buffered saline (PBS), and tetracycline were purchased from Fisher Scientific. Nylon mesh with 60  $\mu\text{m}$  diameter pores was from Small Parts. Sylgard 184 PDMS elastomer base and curing agent were from Dow Corning . Heptadecafluoro-1,1,2,2-tetrahydrodecyl trichlorosilane was from Gelest.

### *Fabrication of microfluidic devices.*

We used photolithography to fabricate a master copy of the desired microchannels in a layer of SU-8 photoresist on a silicon wafer(32). We designed the microchannel patterns with a CAD program, printed a photomask, and used photolithography techniques to transfer the channel pattern from the photomask to a layer of photoresist; the resulting master contained the microchannel pattern in bas-relief. We silanized the master by vapor deposition of heptadecafluoro-1,1,2,2-tetrahydrodecyl trichlorosilane. We poured a mixture of degassed PDMS (a 10:1 ratio of base:crosslinker) on the silanized master and cured the polymer by heating at 60 °C for 3 h. After curing the PDMS, we cut out the region containing the embossed microchannels with a scalpel and gently peeled it away from the wafer. A biopsy punch

was used to create the inlet and outlet holes. We oxidized a glass slide and the PDMS channel layer and covalently bonded them together by pressing them into conformal contact. The microfluidic channels that we fabricated had PDMS walls and ceiling and a glass floor.

### *Fabrication of microparticles.*

We dissolved agarose in water or growth media at a final concentration of 2% v/v and used light mineral oil as the continuous phase for the emulsification of the agarose solution. To stabilize the pre-gelled agarose droplets and prevent coalescence, we added 4% (v/v) of the surfactant Span80 to the mineral oil. We filtered the agarose solutions and oil through 0.22  $\mu\text{m}$  pore size syringe filters and loaded them into glass gas-tight syringes. We used positive displacement syringe pumps (Harvard Apparatus) to control the flow rate of fluids in the microfluidic devices. To prevent gelation of the agarose in the syringe and in the device during the production of microparticles, we heated the syringes on the pumps with heating tape to maintain a temperature of 40 °C; we heated the microfluidic device to 37 °C.

### *Characterization of agarose microparticles.*

We imaged the formation of agarose droplets inside microfluidic devices using a stereomicroscope (Nikon SMZ1500) with a video-rate CCD (Marshall MTV1802CA). Microparticles were imaged with an inverted microscope (Nikon Eclipse TE2000E) equipped with an Andor iXon EMCCD.

To determine the range of sizes of microparticles produced in our PDMS devices, we varied the relative flow rates of the liquid agarose solution and oil. In this device, the height of all of the channels was 25  $\mu\text{m}$ . The dispersed phase channel was 50- $\mu\text{m}$  wide; orthogonal to this channel were two opposing 25- $\mu\text{m}$  wide channels for the continuous phase (e.g. mineral oil). Just beyond the intersection of these three channels was an outlet channel with a 15- $\mu\text{m}$  wide constriction to constrict the liquids. The flow of the opposing streams of mineral oil sheared the agarose stream, causing it to break up into droplets. The newly formed droplets flowed out of the outlet channel and were cooled to 4  $^{\circ}\text{C}$  to induce gelation of the agarose. After adjusting the ratio of flow rates, we equilibrated the system for 15 min before collecting samples from the outlet tubing.

### ***Microbial cell culture and growth conditions.***

We encapsulated two *E. coli* K12 strains in microparticles. The *E. coli* strains were derived from the strain MG1655 and expressed enhanced green fluorescent protein (EGFP) from a plasmid. One *E. coli* strain was transformed with a Clontech pEGFP vector that contained an ampicillin resistance cassette and a *lac* promoter for controlling the transcription of *egfp*. We refer to this strain as MG1655-*plac*EGFP. The other *E. coli* strain contained a plasmid modified from a pASK-IBA3plus vector with an ampicillin resistance cassette and a *tet* operon for controlling the transcription of *egfp* (MG1655-*ptet*EGFP). We created vector *ptet*EGFP by cloning the EGFP ORF from *plac*EGFP into pASK-IBA3plus. Specifically, the EGFP ORF was PCR amplified using primers M226 (5'-TACAAGtctagaAGCAGGAGGACGCCACCATGGTGAGC-3') and M227 (5'-TGCGACctcgagGCTTTACTTGTACAGCTCGTC-3') and Pfu Ultra II fusion Hot Start

DNA polymerase. The resulting amplicon and pASK-IBA3plus vector were digested with the restriction enzymes XbaI and XhoI (recognition sites for XbaI and XhoI are bolded in the M226 and M227 primers, respectively), gel-extracted, ligated together, and transformed into electrocompetent DH5 $\alpha$  cells. Restriction enzymes and T4 DNA ligase were from Promega Corporation. We selected transformants on LB agar containing 100  $\mu\text{g mL}^{-1}$  ampicillin and verified clones containing *ptetEGFP* by a double restriction enzyme digest XbaI and XhoI. Production of EGFP by DH5 $\alpha$  *ptetEGFP* clones was confirmed by inducing expression using Lauria-Bertani media (LB) containing 200 ng  $\text{mL}^{-1}$  of anhydrotetracycline and observing EGFP fluorescence using a Nikon TE2000 inverted scope equipped with 484/15x and 520/30m excitation and emission filters from Chroma Technology Corporation.

Overnight cultures of MG1655-*placEGFP* and MG1655-*ptetEGFP* strains were grown in LB media (10 g  $\text{L}^{-1}$  tryptone, 10 g  $\text{L}^{-1}$  NaCl, 5 g  $\text{L}^{-1}$  yeast extract, pH 7.2) containing 100  $\mu\text{g mL}^{-1}$  ampicillin. Strain MG1655 *placEGFP* was induced by adding IPTG at a final concentration of 1 mM to the media. We induced strain MG1655 *ptetEGFP* by adding anhydrotetracycline to LB media at a final concentration of 200 ng  $\text{mL}^{-1}$ .

#### ***Encapsulation of bacterial cells in agarose microparticles.***

To encapsulate bacterial cells in agarose microparticles, we prepared a 2% agarose solution (w/v) in SOC media (20 g  $\text{L}^{-1}$  tryptone, 5 g  $\text{L}^{-1}$  yeast extract, 10 mM NaCl, 2.5 mM KCl, 10 mM  $\text{MgCl}_2$ , 10 mM  $\text{MgSO}_4$ , and 20 mM glucose) or in PBS buffer. We filtered the warm solution of agarose containing antibiotics and the appropriate

small molecule transcriptional inducer through a sterile 0.22  $\mu\text{m}$  filter and incubated it at 30  $^{\circ}\text{C}$  before adding the cells. We diluted an overnight culture of bacteria into the agarose solution to produce a final concentration of  $\sim 1 \times 10^7$  cells  $\text{mL}^{-1}$ . To grow the encapsulated cells, we incubated the gel microparticles suspended in the mineral oil phase in a water bath at 37  $^{\circ}\text{C}$ . To measure the growth rate of encapsulated cells in microparticles suspended in mineral oil, we took a timelapse at every 2 min using a Nikon TE2000 inverted scope and Photometrics CCD camera with a 60x oil immersion objective. The objective and the microscope stage were heated to 37  $^{\circ}\text{C}$  during the acquisition of the timelapse.

***Using a Poisson distribution to encapsulate single cells in agarose microparticles.***

To guide the dilution of cells to encapsulate one cell per microparticle, we used the Poisson equation. For cells randomly distributed in a sample, the fraction of microparticles containing  $n$  cells ( $P$ ) is described by a Poisson distribution as shown in Equation 1,

$$P(n, \bar{n}) = \frac{\bar{n}^n e^{-\bar{n}}}{n!} \quad (1)$$

where  $\bar{n}$  is the average number of cells per microparticle). The expression for  $\bar{n}$  is defined in Equation 2,

$$\bar{n} = \rho V_{\text{microparticle}} \quad (2)$$

where  $\rho$  is the concentration of cells in suspension (e.g. number of cells mL<sup>-1</sup>) and  $V_{\text{microparticle}}$  is the average volume of a microparticle in mL. For empty microparticles ( $n=0$ ) and single-cell microparticles ( $n=1$ ), we used Equation 3 and 4, respectively:

$$P(0, \bar{n}) = e^{-\bar{n}} \quad (3)$$

$$P(1, \bar{n}) = \bar{n} e^{-\bar{n}} \quad (4)$$

The average diameter of microparticles—consisting of agarose dissolved in water—was 26  $\mu\text{m}$  when using flow rates of 150 and 50  $\mu\text{L h}^{-1}$  for oil and agarose, respectively. We imaged the microparticles using an inverted microscope, measured the surface area of microparticles from two-dimensional images using ImageJ, and used these data to determine the diameter of the microparticles; we calculate the mean diameter of 103 microparticles to be 26  $\mu\text{m}$ , which corresponds to an average volume of 9 pL.

### *Flow cytometry and fluorescence-activated cell sorting.*

We used FACS to sort the population of microparticles containing EGFP-expressing cells into the wells of 96-well microplates, culture tubes, or onto LB agar plates. For these experiments, we used a SORP BD FACS Aria instrument at the Flow Cytometry Facility at the UW Carbone Cancer Center. Prior to analyzing the microparticles using FACS, we extracted the microparticles from the oil phase and transferred them into a solution of PBS or growth medium containing the appropriate antibiotics and small molecule inducers. To transfer the microparticles from oil to the

buffer, we rinsed the microparticles with pure mineral oil seven times to remove the surfactant. For the first three rinse cycles, we spun the microparticles in microcentrifuge tubes at  $100 \times g$  for 3 min; we reduced the centrifugation time to 30 s for the subsequent four cycles. After rinsing with mineral oil, we carefully pipetted the microparticle-oil emulsion on top of 700  $\mu\text{L}$  of growth medium or PBS in a microcentrifuge tube. The density of the microparticles was higher than the oil and the particles gradually moved into the aqueous solution. To prevent the possibility of clogging the FC or FACS, we filtered the aqueous suspension of microparticles through a Nylon filter with 60- $\mu\text{m}$  diameter pores. This step was not necessary but was carried out at the request of the FACS facility. We acquired FC data by collecting  $>10,000$  data points for each sample; for FACS, we used an 85  $\mu\text{m}$  diameter nozzle tip at a liquid pressure of 45 psi.

#### *Determination of the minimum inhibitory concentration.*

We determined the minimum inhibitory concentration (MIC) of rifampicin that prevents the growth of strain MG1655-*ptetEGFP* in liquid cultures (i.e. macrodilution method) (33) and in agarose microparticles. For both methods, the concentration range of rifampicin we tested was 0.3 to 80  $\mu\text{M}$ ; the antibiotic was serially diluted into a suspension of cells in growth media. We used a final concentration of  $10^5$  cells  $\text{mL}^{-1}$  for the macrodilution method and  $10^7$  cells  $\text{mL}^{-1}$  for single-cell encapsulation in microparticles. We encapsulated the cells in microparticles as previously described, suspended the resulting microparticles in growth medium, and serially diluted the suspension. All samples were incubated at 37 °C while shaking. After 10 h incubation, we examined the turbidity of the macrodiluted cell suspensions to determine the MIC.

We performed the macrodilution experiment in triplicate. For the encapsulated cells in microparticles, we incubated the samples for 3 h and induced the cells with anhydrotetracycline for 45 min prior to using FC.

*Isolation and characterization of spontaneous mutants resistant to rifampicin.*

To increase the probability of isolating spontaneous mutants to rifampicin, we incubated 480 independent cultures of strain MG1655-*placEGFP* in 96-well microplates (200  $\mu\text{L}$  per well). We grew the cultures in microplates to saturation prior to isolating spontaneous mutants; the absorbance of the culture was initially 0.001 at  $\lambda$ , 600 nm. After the culture became saturated, we removed 2  $\mu\text{L}$  from each culture and combined the fractions into 2 mL of PBS. We centrifuged the suspension of cells, removed the supernatant, and resuspended the pellet in a warm solution (500  $\mu\text{L}$ ) of 2% agarose (w/v) in PBS. We estimated that the absorbance of the suspension of cells in agarose was  $\sim 10$  ( $\lambda$ , 600 nm). To increase the probability of finding a mutant we used a high concentration of cells ( $10^8$ ) to compensate for the low frequency of mutations. We suspended the cells in a solution of warm agarose and encapsulated them in a microfluidic device. We transferred the microparticles containing encapsulated cells into a solution of SOC media containing 80  $\mu\text{M}$  rifampicin. We filtered the microparticle suspension through a sterile Nylon mesh with 60  $\mu\text{m}$  holes and incubated for 3 h at 37 °C. After incubation, we induced the expression of EGFP in encapsulated cells by adding anhydrotetracycline to a concentration of 200  $\text{ng mL}^{-1}$  and incubated for 1 h at 37 °C. We sorted the microparticles using FACS and isolated those containing EGFP-expressing cells into a tube with 1 mL of SOC medium. We incubated the suspension

for 13 h at 37 °C. The incubation period was chosen to be excessively long so that cells eventually grow out of the microparticles and freely replicated in the liquid media within the tube.

Following overnight growth, 1 mL of the incubated suspension was diluted into LB and 100 µL of the diluted cells were plated on LB agar plates containing 80 µM rifampicin. After overnight incubation at 37°C, ten single colonies were selected and streaked on LB agar containing 80 µM rifampicin. An isolated colony from each of the ten streaks was cultured overnight at 37°C in LB broth containing 80 µM rifampicin. A 703 bp region of the *rpoB* gene was amplified from each rifampicin resistant strain using primers M245 (5'-CGGTGAAAGAGCGTCTGTCT-3') and M246 (5'-ACAGCACGTTCCATAACCAGTAC-3') and Pfu Ultra II fusion Hot Start DNA polymerase. Amplicons were confirmed on a 1% (w/v) agarose gel in tris/acetate/EDTA buffer and purified using a QIAquick PCR purification kit. Purified *rpoB* dsDNA fragments were sequenced using the nested primers M247 (5'-TGTTTCGCACCCATCAATGC-3') and M248 (5'-ATACCCTGATGCCACAGGA-3') and BigDye Terminator v3.1. The University of Wisconsin-Madison Biotechnology Center DNA Sequencing Facility performed Sanger sequencing. Sequencing data was analyzed using DNASTAR Lasergene software version 8.

## RESULTS AND DISCUSSION

The flow-focusing microfluidic devices consisted of a cross-junction with three inputs and one outlet channel through which microparticles flowed out of the device and were collected. The dispersed phase liquid admixed with cells was pumped into the junction through an inlet channel where it met the continuous phase, mineral oil, which was flowing from two orthogonally oriented channels. This geometry caused the mineral oil streams to focus the dispersed phase into a thin stream that broke into droplets as it flowed through a constriction into the outlet channel (Figure 1). The geometry of the device and the physics of fluids at the micron-scale ensured the stable and reproducible breakup of the dispersed phase into uniform droplets (34).

### *Characterization of microparticles.*

We measured the diameter of the agarose microparticles produced in the PDMS microfluidic devices at different ratios of flow rates of the mineral oil and solution of agarose. Although we fabricated microfluidic channels with a range of different dimensions, we present data from one set of devices with critical dimensions that are described in Experimental Methods. As we increased the ratio of the flow rates of oil to agarose, the diameter of the microparticles decreased to  $\sim 20 \mu\text{m}$  (Figure 1C). The coefficient of variance for the microparticle diameter at each ratio of flow rates was 10% and indicated that the microparticles were moderately monodisperse. To analyze microparticles using FACS or FC, we fabricated colloids that were  $\sim 30 \mu\text{m}$  in diameter; we chose this diameter for the particles to accommodate a standard core size of  $40 \mu\text{m}$

in most FC and FACS instruments. Microparticles with a diameter of 60–160  $\mu\text{m}$  or larger can be created by fabricating channels / nozzles with dimensions that are larger than those described here.

### *Growth and analysis of encapsulated cells.*

To visualize cells in microparticles via microscopy, FC, and FACS, we used a strain of *E. coli* MG1655 with a plasmid encoding an ampicillin resistance and a *lac* operon for controlling the transcription of *egfp* (we refer to this strain as MG1655-*placEGFP*). Using the Poisson equation as a guide, we diluted a cell culture such that ~10% of a population of agarose microparticles would contain single cells and the majority of the remaining microparticles would be empty.

We gated the data in FC experiments and analyzed the fluorescence emission of the microparticles (Figure 2). To differentiate between the autofluorescence of empty agarose microparticles (red data points in Figure 2a) and the fluorescence emitted from EGFP-expressing cells encapsulated in microparticles (black data points), we excited the sample at  $\lambda=488$  nm and compared the fluorescence emission at two wavelengths: 525 nm and 710 nm. The fluorescence emission of EGFP is high at  $\lambda=525$  nm and low at  $\lambda=710$  nm. Using this guideline, we gated the population of microparticles to determine the percentage containing fluorescent cells, and found that approximately 11% of the microparticles contained EGFP at the initial time point (Figure 2a). This percentage of fluorescent microparticles agreed well with our calculation using the Poisson distribution, indicating that most of the fluorescent microparticles contained single cells. When we imaged the microparticles using epifluorescence microscopy, we found that

some microparticles contained more than one cell, which may have arisen from four experimental variables: (1) the Poisson distribution predicts that ~1% of the microparticles contain more than one cell; (2) aggregates of cells formed in the overnight culture were not dispersed completely in the agarose solution; (3) cells aggregated in the syringe during the formation of the microparticles in the microfluidic device; and (4) single cells encapsulated in microparticles replicated during sample collection from the microfluidic outlet channel. For example, a microparticle (top left) in image for the 'time zero' sample (Figure 2a) probably contained an aggregate of multiple cells.

The incubation of microparticles containing single cells led to the formation of microcolonies within the agarose and demonstrated that the nutrients in the microparticles and gas exchange through the mineral oil were sufficient for cell growth. We have found that the growth rate of *E. coli* cells in agarose microparticles suspended in mineral oil was very similar to their growth on an agarose pad. The microencapsulated cells reproduced with a doubling time of  $17 \pm 3$  min at 37 °C, which is comparable to the doubling time of  $19 \pm 5$  min at 37 °C on an agarose pad. We observed that the doubling time increased after 1.5 h when cells were encapsulated in 36- $\mu$ m diameter microparticles that were suspended in oil. However, the maximum time of growth in particles will depend on the medium in which they are suspended (oil vs. nutrient broth), the size of the particles, and the number of cells encapsulated per particle.

We also observed a time-dependent increase in the percentage of microparticles containing EGFP-expressing cells during the incubation of an unsorted collection of

microparticles suspended in mineral oil at 37 °C without shaking (Figure 2). After 8 h of incubation in mineral oil, 24% of the microparticles were fluorescent (compared to 11% at 0 h), and after 13 h of incubation the number of fluorescent microparticles increased to 40%. We hypothesized that the increase in the number of fluorescent microparticles over time was due to the released cells from ruptured microparticles, which led to attachment of the freed cells to the surface of intact microparticles that were initially empty.

Cells formed microcolonies that were 5 – 20  $\mu\text{m}$  in diameter within 30  $\mu\text{m}$  (diameter) microparticles after 5 h of growth in mineral oil. It was difficult to determine the size of these colonies with precision using 2D optical microscopy due to the influence of the orientation of the colony / particle (Figure 2). A more reliable and sensitive approach was to use FACS to analyze the total fluorescence intensity of the encapsulated cells in the microparticles. For FACS, we transferred the colloids from mineral oil to an aqueous buffer. Some of the particles containing large colonies became mechanically unstable and released cells into the buffer during their transfer from the mineral oil. We suspected that these cells adsorbed to the surface of agarose microparticles and increased the number of fluorescent microparticles in our samples. To confirm this hypothesis we fabricated empty microparticles and admixed them with a suspension of MG1655-*placEGFP* cells. We immediately analyzed the sample by FC and found that ~40% of the empty microparticles were fluorescent.

The release of cells from microparticles can be an issue in some applications; however, it can be avoided by using short incubation times for cell growth and taking advantage of the sensitivity of the detectors in FC and FACS instruments. When

microparticles were incubated for  $\leq 5$  hrs, we rarely observed cells released from microparticles. For applications that require larger microencapsulated communities, the optimization of the microparticle size, agarose concentration, and transfer of the microparticles from mineral oil to buffer will decrease colony heterogeneity that may arise from non-specific adsorption of cells to other microparticles.

*Determination of the minimum inhibitory concentration.*

We used agarose microparticles to determine the MIC of rifampicin and compared the result to measurements made using techniques based on the macrodilution of batch cultures. In batch culture techniques, the MIC is the lowest concentration of antibiotic that inhibits visual growth of bacteria. These culture techniques require incubating cells for long periods of time (typically 12-18 h for *E. coli*, and  $> 24$  h for slower-growing species) and consume significant amounts of the antibiotic (e.g.  $> 10$  mg) as the cultures are typically grown in a dilution series and require several replicates at each concentration of compound. To decrease the amount of compound required for assay, the MIC can be determined using 96-well microtiter plates. However, performing assays in microtiter plates does not reduce the experimental time. In contrast, the microencapsulation technique we describe requires very small amounts of compounds ( $< 1$  mg) and short incubation times ( $\leq 3$  h), as FC makes it possible to quantitatively measure growth by measuring small changes in the fluorescence of microparticles. We anticipated that the determination of MICs using microfluidic encapsulation would provide a useful alternative to batch culture methods.

To measure an MIC of rifampicin against *E. coli* MG1655 we constructed a strain that contained a plasmid encoding an ampicillin resistance cassette and a *tet* operon for

controlling the transcription of *egfp* (MG1655-*ptetEGFP*). We encapsulated single cells of MG1655-*ptetEGFP* in agarose microparticles and analyzed fluorescence using FC. To analyze FC data from microparticles, we included two controls without rifampicin: (1) uninduced; and (2) induced with anhydrotetracycline. Using these controls, we created a gate for the GFP-positive population of microparticles and used a percent population of the uninduced control that fell into the GFP-positive gate as a threshold to determine the concentration of rifampicin that completely inhibited the growth of bacteria. As we increased concentration of antibiotic the number of microparticles in the GFP-positive gate decreased (Figure 3). At 10  $\mu\text{M}$  rifampicin, the percentage of the GFP-positive population approached the uninduced controls (1.1-1.2%), indicating that at this concentration, growth was inhibited. The MIC we determined using microparticles (10  $\mu\text{M}$ ) closely matches the value determined using a dilution technique (10-12.5  $\mu\text{M}$ ) (35, 36). The agar dilution method required 24-48 h of incubation after inoculating several plates of agar with cells and would have consumed at least 600 mL of solid media and 10 mg of antibiotic. By contrast, the microfluidic technique for determining the MIC of rifampicin reduced the total amount of reagents used by 60-fold and the experimental time by 16-fold.

### *Screening and isolation of spontaneous mutants.*

The encapsulation of bacterial cells in microparticles combined with FACS may be a powerful tool for rapidly isolating strains of bacteria via changes in genotype and phenotype. To explore this application, we used this technique to isolate and characterize spontaneous mutants that are resistant to rifampicin. Although rifampicin is commercially available in large quantities, we used it as a surrogate of structurally

complex natural products that are not readily available and for which screening and isolation of resistant mutants using conventional microbiological techniques may be challenging. The frequency of spontaneous mutants for resistance against small molecules in the rifamycin family is between  $10^{-8}$ - $10^{-9}$  per bacterium per cell division (37, 38). Traditionally these mutants are selected on agar plates that contain growth media and an antibiotic at a concentration above its MIC. The isolation of spontaneous mutants using conventional approaches typically requires liters of solid media containing a high concentration of the target antibiotic (typically tens of milligrams per liter), and takes 2-4 days of incubation to obtain visible colonies on plates from which cells are isolated. A high-throughput approach using agarose microparticles with a picoliter volume combined with FACS should make it possible to reduce the time and amount of antibiotic for the isolation of mutants.

We encapsulated cells of strain MG1655-*ptet*EGFP in agarose microparticles and dosed them with rifampicin. As expected, most of the cells in microparticles did not express EGFP (99.8% of microparticles), indicating their sensitivity to rifampicin (37). A small sub-population of microparticles (0.2%; approximately  $8 \times 10^3$  out of the  $4 \times 10^6$  microparticles that we analyzed) was GFP-positive and was sorted into a tube containing liquid nutrient media. From these microparticles we isolated mutants, sequenced them, and identified an A1538T base-pair mutation in the *rpoB* ORF (Figure 4). This mutation results in a Q513L substitution, which has been described previously as conferring resistance to rifampicin (35, 36). Overall, the screen used a total of 65  $\mu$ g of rifampicin and took 6 h to complete, compared to 15 mg of compound that would have been required for a 48 h screen using a traditional approach with agar plates (36).

## CONCLUSION

The microencapsulation technique offers several advantages over conventional, Petri dish approaches for isolating bacteria based on phenotypes. (1) The volume of the microparticles (e.g. several picoliters) minimizes the experimental time and consumption of reagents. Encapsulating cells in agarose microparticles makes it possible to grow the cells through only a few cycles of division and detect them by FACS. In contrast, a typical colony on an agar plate contains  $\sim 10^9$  bacterial cells (39); a visible colony requires  $\sim 20$  h of growth from a single cell that has a doubling time of 40 min. (2) FACS is a sensitive technique, which can detect low levels of fluorescence in a colloidal sample. This characteristic can be used to detect changes in fluorescence in individual encapsulated cells (40, 41). Using FACS for the analysis of cells expands the number of genotypes and phenotypes that can be simultaneously quantified in a high-throughput screen, as each can be coupled to a fluorescent reporter. Many FACS instruments can simultaneously measure up to 16 different fluorophores in a sample, which makes it possible to multiplex analyses. (3) The encapsulation and growth of cells in microparticles that are suspended in oil can protect the user from toxic reagents that are either incorporated into the colloids or are produced by cells. These compounds only diffuse out of the colloids if they are soluble in mineral oil. Replacing the mineral oil as the continuous phase with fluoruous liquids, such as perfluorodecalin, will improve the insulation of the user from these compounds by reducing their solubility in the continuous phase fluid (8). This characteristic may be particularly useful in research with biosafety level two and three organisms and select chemicals. (4) The use of agarose as the hydrogel has several advantages, including biocompatibility, a gelling

temperature that is close to the optimal growth temperatures for bacteria, relatively low cost, and availability in most biological laboratories. (5) PDMS devices are straightforward to fabricate and operate and users can easily manipulate the layout and dimensions of the systems using soft lithographic techniques (28). The devices described in this manuscript produce agarose microparticles at a frequency of  $>500$  Hz. Droplet formation at frequencies of  $10^3 - 10^4$  Hz have been reported in the literature for similar microfluidic systems (29, 31), which will reduce the time required to encapsulate a large population of cells for analysis and selection. The devices presented in this chapter produce monodisperse microparticles with a user-defined diameter, enabling sample analysis by FACS without preliminary filtering to remove particles that are too large for the instrument. The ability to omit the filtration step avoids sample bias.

There are several characteristics of this approach that currently limit its application. Measuring the fluorescence emission of cells encapsulated in microparticles requires that cells produce fluorescent molecules or proteins. In many cases this criteria is not an issue and can be solved by genetic engineering. A fundamental limitation is that it may be difficult to rely on fluorescence detection when isolating and amplifying bacteria that have not been previously cultured or which are genetically intractable. A potential solution is to use forward light scattering for measuring cell growth in microparticles. In addition, long incubation periods can lead to release of cells from microparticles, which will be eliminated from analysis or which may adsorb on the surface of other colloids and contaminate them. The optimization of growth time and conditions can transcend this limitation. Finally, the small molecule we tested is an antibiotic and provides an obvious phenotype for screening as it prevents cell replication. The biological target of other small molecules may be more difficult to

discern using this approach and may require the development of more sophisticated methods of analysis.

In addition to its application in the high-throughput screen for studying target proteins of biologically active small molecules in microorganisms, we anticipate that encapsulating and analyzing single bacterial cells in agarose microparticles will have a variety of applications in environmental microbiology and for studying the human microbiome. Since encapsulation of cells makes it possible to detect and analyze slow-growing and rare species in a mixed population by using FACS, bacterial strains that are isolated and amplified in microparticles can be sequenced to catalog microbes associated with a particular ecological niche. Manipulating the liquid in which the microparticles are dispersed and incubated provides control over the diffusion of secondary metabolites in and out of the colloids, which may promote growth of species that are otherwise difficult to culture using standard media (2, 42). Finally, this technique may find applications in areas that require phenotypic screening of bacteria, including biosensing, biological engineering, and synthetic biology.

## ACKNOWLEDGEMENTS

This manuscript is based upon work supported by the National Science Foundation under Grant No. DMR-0520527. ASU acknowledges the Japan Society for the Promotion of Science (JSPS) for support. YJE acknowledges a Genentech Graduate Fellowship and a William R. & Dorothy E. Sullivan Wisconsin Distinguished Graduate fellowship. MFC is funded by an NIH biotechnology training grant (grant 5T32GM08349). DBW acknowledges support from the Searle Scholar Program, DARPA, the Human Frontiers Science Program (RGY0069/2008-C), and USDA (WIS00974). We thank J. Weisshaar for vector pASK-IBA3plus.

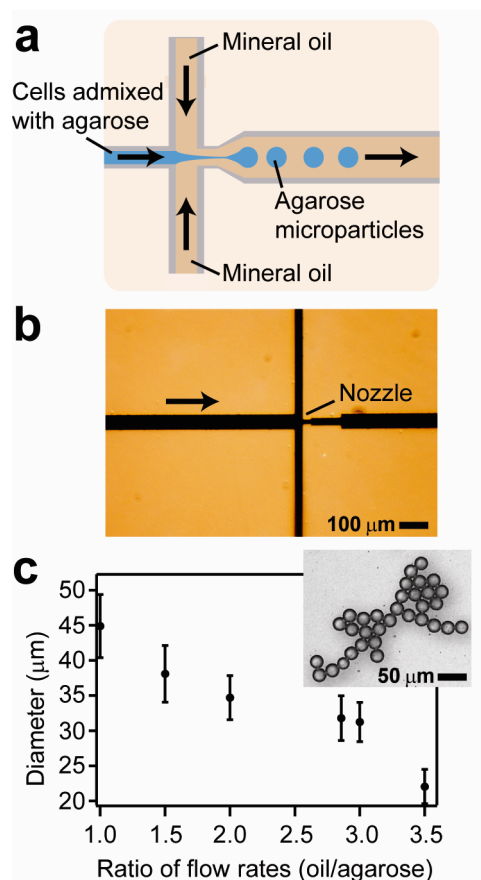


**Figure 1.** Production of microparticles in PDMS flow-focusing microfluidic devices. a) A schematic diagram of the PDMS device depicting the direction of fluid flow and formation of agarose droplets suspended in mineral oil at the nozzle. b) An image of a PDMS microfluidic device showing the nozzle region of the device; the channels were filled with black ink to increase the contrast. The arrow shows the direction of flow of the agarose solution admixed with cells. c) A plot showing the relationship between the ratio of flow rates of mineral oil and agarose and the resulting diameter of microparticles that were formed. The error bars represent the coefficient of variance for each ratio tested. The image inset shows agarose microparticles produced using flow rates of 150 (oil) and 50 (agarose)  $\mu\text{L h}^{-1}$ .

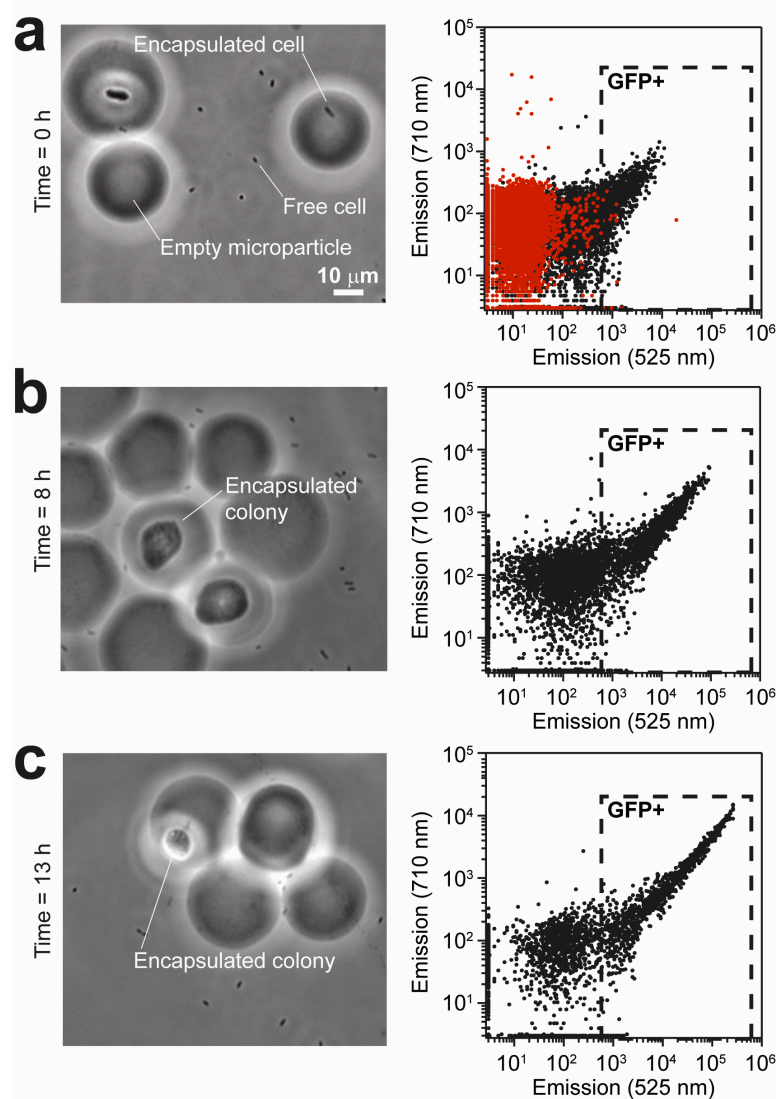


**Figure 2.** Growth of *E. coli* cells in agarose microparticles. Samples were collected, analyzed, and imaged at three time points:  $t = 0, 8,$  and  $13$  h. Images of microparticles are shown in the left column, corresponding to these time points. The right column contains plots of fluorescence from FC for each corresponding time point. The dotted rectangle shows the gate drawn for the GFP-positive population. Red dots in the scatter plot for the  $t = 0$  h sample indicate background fluorescence emission from empty

microparticles. Black dots indicate fluorescence signal from *E. coli* cells encapsulated in microparticles.

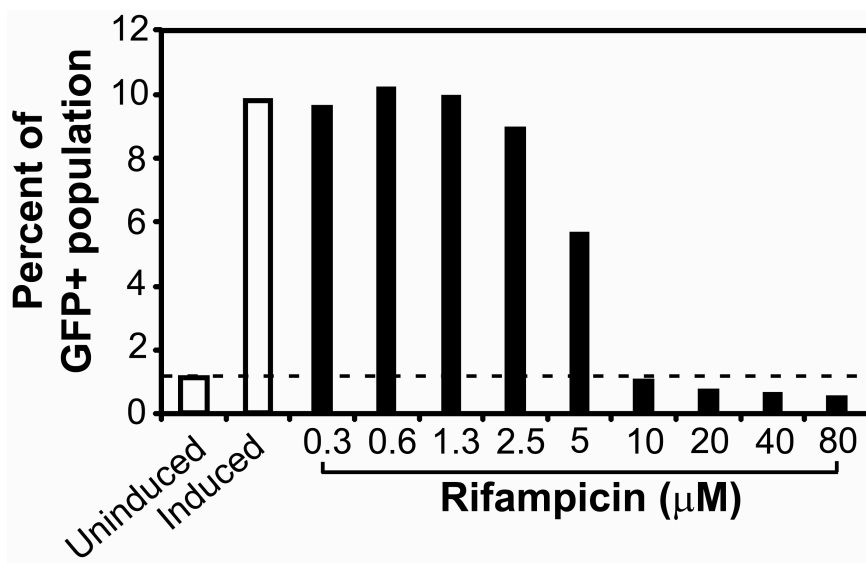


**Figure 3.** Determination of the minimum inhibitory concentration by encapsulating cells in agarose microparticles. The plot shows the percentage of a microparticle population that fell into the GFP-positive gate (GFP+) at various concentrations of the antibiotic (filled bars). Control samples (open bars) without antibiotic were either induced or uninduced to determine the lowest and highest percentages of cells in the GFP-positive gate. A dashed line was drawn to indicate the percent of GFP+ population from the uninduced control.

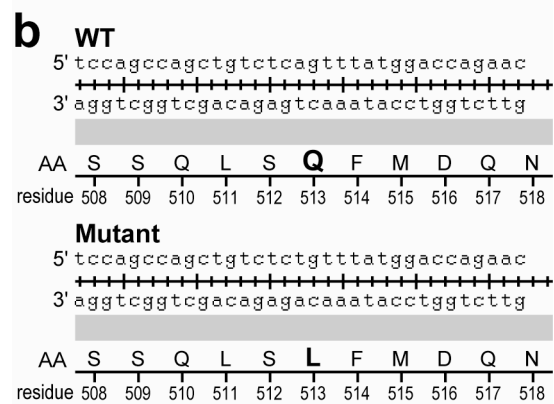
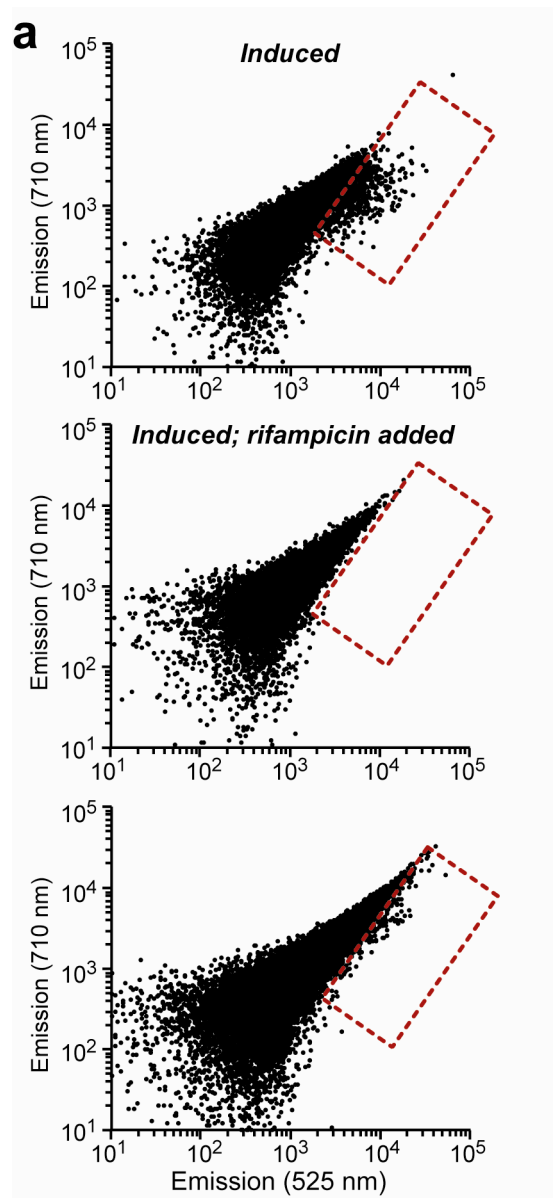


**Figure 4.** Spontaneous mutant screen of *E. coli* cells in agarose microparticles. a) We analyzed the microparticles using FC. By comparing the fluorescence emission at wavelengths of 525 nm and 710 nm, we differentiated a subpopulation with a positive EGFP signal for the induced control (the uppermost plot). The GFP-positive gate is drawn as a dashed box. As a negative control, we analyzed microparticles containing both inducer and rifampicin (the middle plot). The negative control had negligible emission in the GFP-positive gate since a monoculture of wildtype *E. coli* cells was sensitive to the antibiotic. By contrast, a small population of microparticles that contained cells from a pool of 480 independent cultures showed fluorescence emission in the GFP-positive gate despite the presence of rifampicin (the bottom plot). This GFP-positive subpopulation were isolated via FACS. b) Mutants that were isolated by FACS contained a mutation in the *rpoB* gene, resulting in a Q513L substitution. The panel shows the DNA sequence of the region, the corresponding amino acids (AA), and residue numbers. The mutant locus is indicated with a bold letter.

## REFERENCES

1. Shuman, H. A. (2003) Just toothpicks and logic: How some labs succeed at solving complex problems, *Journal of Bacteriology* 185, 387-390.
2. Zengler, K., Toledo, G., Rappe, M., Elkins, J., Mathur, E. J., Short, J. M., and Keller, M. (2002) Cultivating the uncultured, *Proceedings of the National Academy of Sciences of the United States of America* 99, 15681-15686.
3. Huebner, A., Bratton, D., Whyte, G., Yang, M., Demello, A. J., Abell, C., and Hollfelder, F. (2009) Static microdroplet arrays: a microfluidic device for droplet trapping, incubation and release for enzymatic and cell-based assays, *Lab Chip* 9, 692-698.
4. Agresti, J. J., Antipov, E., Abate, A. R., Ahn, K., Rowat, A. C., Baret, J. C., Marquez, M., Klivanov, A. M., Griffiths, A. D., and Weitz, D. A. (2010) Ultrahigh-throughput screening in drop-based microfluidics for directed evolution, *Proc Natl Acad Sci U S A* 107, 4004-4009.
5. Granieri, L., Baret, J. C., Griffiths, A. D., and Merten, C. A. (2010) High-throughput screening of enzymes by retroviral display using droplet-based microfluidics, *Chem Biol* 17, 229-235.
6. Boedicker, J. Q., Li, L., Kline, T. R., and Ismagilov, R. F. (2008) Detecting bacteria and determining their susceptibility to antibiotics by stochastic confinement in nanoliter droplets using plug-based microfluidics, *Lab on a Chip* 8, 1265-1272.
7. Liu, W. S., Kim, H. J., Lucchetta, E. M., Du, W. B., and Ismagilov, R. F. (2009) Isolation, incubation, and parallel functional testing and identification by FISH of rare microbial single-copy cells from multi-species mixtures using the combination of chemistride and stochastic confinement, *Lab on a Chip* 9, 2153-2162.
8. Baret, J. C., Miller, O. J., Taly, V., Ryckelynck, M., El-Harrak, A., Frenz, L., Rick, C., Samuels, M. L., Hutchison, J. B., Agresti, J. J., Link, D. R., Weitz, D. A., and Griffiths, A. D. (2009) Fluorescence-activated droplet sorting (FADS): efficient microfluidic cell sorting based on enzymatic activity, *Lab Chip* 9, 1850-1858.
9. Morimoto, Y., Tan, W. H., Tsuda, Y., and Takeuchi, S. (2009) Monodisperse semi-permeable microcapsules for continuous observation of cells, *Lab on a Chip* 9, 2217-2223.
10. Panda, P., Ali, S., Lo, E., Chung, B. G., Hatton, T. A., Khademhosseini, A., and Doyle, P. S. (2008) Stop-flow lithography to generate cell-laden microgel particles, *Lab Chip* 8, 1056-1061.

11. Pereira, T., Millar, T. J., and Chuck, J. A. (2005) Viability analysis of alginate encapsulated micro-organisms using fluorescent stains, *Journal of Microencapsulation* 22, 787-792.
12. Weaver, J. C., Williams, G. B., Klibanov, A., and Demain, A. L. (1988) Gel Microdroplets - Rapid Detection and Enumeration of Individual Microorganisms by Their Metabolic-Activity, *Bio-Technology* 6, 1084-1089.
13. Workman, V. L., Dunnett, S. B., Kille, P., and Palmer, D. D. (2008) On-chip alginate microencapsulation of functional cells, *Macromolecular Rapid Communications* 29, 165-170.
14. Bernath, K., Hai, M. T., Mastrobattista, E., Griffiths, A. D., Magdassi, S., and Tawfik, D. S. (2004) In vitro compartmentalization by double emulsions: sorting and gene enrichment by fluorescence activated cell sorting, *Analytical Biochemistry* 325, 151-157.
15. Katsuragi, T., Tanaka, S., Nagahiro, S., and Tani, Y. (2000) Gel microdroplet technique leaving microorganisms alive for sorting by flow cytometry, *Journal of Microbiological Methods* 42, 81-86.
16. Luo, D. W., Pallela, S. R., Marquez, M., and Cheng, Z. D. (2007) Cell capsules with tunable transport and mechanical properties, *Biomicrofluidics* 1.
17. Nir, R., Yisraeli, Y., Lamed, R., and Sahar, E. (1990) Flow-Cytometry Sorting of Viable Bacteria and Yeasts According to Beta-Galactosidase Activity, *Applied and Environmental Microbiology* 56, 3861-3866.
18. Akselband, Y., Cabral, C., Shapiro, D. S., and McGrath, P. (2005) Rapid mycobacteria drug susceptibility testing using Gel Microdrop (GMD) Growth Assay and flow cytometry, *Journal of Microbiological Methods* 62, 181-197.
19. Ryan, C., Nguyen, B. T., and Sullivan, S. J. (1995) Rapid Assay for Mycobacterial Growth and Antibiotic Susceptibility Using Gel Microdrop Encapsulation, *Journal of Clinical Microbiology* 33, 1720-1726.
20. Gift, E. A., and Weaver, J. C. (2000) Simultaneous quantitative determination of electroporative molecular uptake and subsequent cell survival using gel microdrops and flow cytometry, *Cytometry* 39, 243-249.
21. Akselband, Y., Cabral, C., Castor, T. P., Chikarmane, H. M., and McGrath, P. (2006) Enrichment of slow-growing marine microorganisms from mixed cultures using gel microdrop (GMD) growth assay and fluorescence-activated cell sorting, *Journal of Experimental Marine Biology and Ecology* 329, 196-205.
22. Manome, A., Zhang, H., Tani, Y., Katsuragi, T., Kurane, R., and Tsuchida, T. (2001) Application of gel microdroplet and flow cytometry techniques to

- selective enrichment of non-growing bacterial cells, *Fems Microbiology Letters* 197, 29-33.
23. Nilsson, K., Birnbaum, S., Flygare, S., Linse, L., Schroder, U., Jeppsson, U., Larsson, P. O., Mosbach, K., and Brodelius, P. (1983) A General-Method for the Immobilization of Cells with Preserved Viability, *European Journal of Applied Microbiology and Biotechnology* 17, 319-326.
  24. Nir, R., Lamed, R., Gueta, L., and Sahar, E. (1990) Single-Cell Entrapment and Microcolony Development within Uniform Microspheres Amenable to Flow-Cytometry, *Applied and Environmental Microbiology* 56, 2870-2875.
  25. Williams, G. B., Weaver, J. C., and Demain, A. L. (1990) Rapid Microbial Detection and Enumeration Using Gel Microdroplets and Colorimetric or Fluorescence Indicator Systems, *Journal of Clinical Microbiology* 28, 1002-1008.
  26. Tumarkin, E., and Kumacheva, E. (2009) Microfluidic generation of microgels from synthetic and natural polymers, *Chemical Society Reviews* 38, 2161-2168.
  27. McDonald, J. C., Duffy, D. C., Anderson, J. R., Chiu, D. T., Wu, H. K., Schueller, O. J. A., and Whitesides, G. M. (2000) Fabrication of microfluidic systems in poly(dimethylsiloxane), *Electrophoresis* 21, 27-40.
  28. Xia, Y. N., and Whitesides, G. M. (1998) Soft lithography, *Angewandte Chemie-International Edition* 37, 551-575.
  29. Garstecki, P., Fuerstman, M. J., Stone, H. A., and Whitesides, G. M. (2006) Formation of droplets and bubbles in a microfluidic T-junction - scaling and mechanism of break-up, *Lab on a Chip* 6, 437-446.
  30. Hashimoto, M., Shevkoplyas, S. S., Zasonska, B., Szymborski, T., Garstecki, P., and Whitesides, G. M. (2008) Formation of Bubbles and Droplets in Parallel, Coupled Flow-Focusing Geometries, *Small* 4, 1795-1805.
  31. Xu, S., Nie, Z., Seo, M., Lewis, P., Kumacheva, E., Stone, H. A., Garstecki, P., Weibel, D. B., Gitlin, I., and Whitesides, G. M. (2005) Generation of monodisperse particles by using microfluidics: Control over size, shape, and composition (vol 44, pg 724, 2005), *Angewandte Chemie-International Edition* 44, 3799-3799.
  32. Duffy, D. C., McDonald, J. C., Schueller, O. J. A., and Whitesides, G. M. (1998) Rapid Prototyping of Microfluidic Systems in Poly(dimethylsiloxane), *Analytical Chemistry* 70, 4974-4984.
  33. Ferraro, M. J. (2000) Methods for dilution antimicrobial susceptibility tests for bacteria that grow aerobically, (Institute, C. a. L. S., Ed.) 5 ed., pp 7-12, Wayne.

34. Nie, Z., Xu, S., Seo, M., Lewis, P. C., and Kumacheva, E. (2005) Polymer particles with various shapes and morphologies produced in continuous microfluidic reactors, *J Am Chem Soc* 127, 8058-8063.
35. Jin, D. J., Cashel, M., Friedman, D. I., Nakamura, Y., Walter, W. A., and Gross, C. A. (1988) Effects of rifampicin resistant rpoB mutations on antitermination and interaction with nusA in Escherichia coli, *J Mol Biol* 204, 247-261.
36. Reynolds, M. G. (2000) Compensatory evolution in rifampin-resistant Escherichia coli, *Genetics* 156, 1471-1481.
37. Floss, H. G., and Yu, T. W. (2005) Rifamycin-mode of action, resistance, and biosynthesis, *Chemical Reviews* 105, 621-632.
38. Wehrli, W., and Staehelin, M. (1971) Actions of the rifamycins, *Bacteriol Rev* 35, 290-309.
39. Mashimo, K., Nagata, Y., Kawata, M., Iwasaki, H., and Yamamoto, K. (2004) Role of the RuvAB protein in avoiding spontaneous formation of deletion mutations in the Escherichia coli K-12 endogenous tonB gene, *Biochem Biophys Res Commun* 323, 197-203.
40. Davey, H. M., and Kell, D. B. (1996) Flow cytometry and cell sorting of heterogeneous microbial populations: the importance of single-cell analyses, *Microbiol Rev* 60, 641-696.
41. Czechowska, K., Johnson, D. R., and van der Meer, J. R. (2008) Use of flow cytometric methods for single-cell analysis in environmental microbiology, *Curr Opin Microbiol* 11, 205-212.
42. Kaeberlein, T., Lewis, K., and Epstein, S. S. (2002) Isolating "uncultivable" microorganisms in pure culture in a simulated natural environment, *Science* 296, 1127-1129.

## CHAPTER 4

### **Chemical tools for studying the subcellular organization of the bacterial cell envelope**

Adapted from:

Marie H. Foss\*, Ye-Jin Eun\*, and Douglas B. Weibel (2011) *Biochemistry* 50(36):7719-7734.

\*Co-first authors.

## ABSTRACT

The subcellular organization of biological molecules is a critical determinant of many bacterial processes, including growth, replication of the genome, and division. However, the details of many mechanisms that control intracellular organization remain unknown. Decoding this information will impact the field of bacterial physiology and can provide insight into eukaryotic biology, including related processes in mitochondria and chloroplasts. Small molecule probes provide unique advantages to study these mechanisms and to manipulate the organization of biomolecules in live bacterial cells. This chapter describes small molecules that are available for investigating subcellular organization in bacteria, specifically targeting peptidoglycan and lipid bilayers. We discuss how these probes have been used to study microbiological questions and conclude by providing suggestions of important areas in which chemical biological approaches will have a revolutionary impact on the study of bacterial physiology.

**ABBREVIATIONS**

Peptidoglycan (PG); penicillin binding protein (PBP); phosphatidylethanolamine (PE); phosphatidylglycerol (PGL); cardiolipin (CL); 10-N-nonyl acridine orange (NAO); fluorescence resonance energy transfer (FRET)

## INTRODUCTION

Analogous to human skin protecting the internal organs, the bacterial cell envelope encapsulates the cytoplasm. This envelope consists of several layers, including the inner and outer membrane, peptidoglycan, and periplasm in Gram-negative bacteria. Some organisms also have a coat of S-layer, which is a crystalline layer of glycoproteins. The extensive layers independently or together serve a number of critical functions: 1) they form a semi-permeable physical and chemical barrier, 2) they provide a physical base for different appendages such as pili and flagella, and 3) they serve as a determinant of cell shape (1). The performance of these essential functions by the heterogeneous envelope begs the question of how their structure/organization is related to the biological functions.

The first study on the organization of the cell envelope was aided by transmission electron microscopy on whole cells, which showed the layer-by-layer organization of the envelope (1). While the technique was instrumental in understanding the overall organization of the envelope, it did not reveal much insight into the organization *within* a single layer. As many discoveries have been made in the past 15 years about the subcellular organization of bacterial cytoplasm, it is now evident that each layer in the cell envelope is also organized at the level of proteins, peptidoglycan, and lipid domains (2). The ongoing challenge is to discover more organized components and investigate how their spatiotemporal organization is created, maintained, and changed.

To study the organization of the envelope, many studies relied on the technique of forward genetics, and this tool has led to numerous insightful findings. However, the

technique has been mainly useful for investigating the roles of protein components in the envelope, and has made little contribution to understanding the organization of non-protein components. Complex networks of enzymes synthesize the non-protein molecules such as lipids and peptidoglycan, and their synthesis routes are often linked with other metabolic networks (3). The intertwined connections in the synthesis pathway make it difficult to modify a particular property of peptidoglycan or lipid membrane while leaving other aspects unchanged.

The unpredictability and pleiotropic effects in using forward genetics have made the way to develop chemical tools that allow specific recognition and perturbation of non-protein components in the envelope. Small molecules offer several advantages including their rapid effect on the target, ability to reverse its effect, and dose-dependent modulation of their activity. In this chapter, I describe several small molecules that have been developed to target peptidoglycan and lipids, how they have been applied to study the subcellular organization of the bacterial envelope, and remaining questions that might benefit from the use of small molecule tools.

## PEPTIDOGLYCAN

The peptidoglycan consists of a network of polysaccharides (i.e. the glycan) that are linked together by peptides. The subunit of this co-polymer is a disaccharide tetrapeptide in which *N*-acetylglucosamine and *N*-acetylmuramic acid form the disaccharide monomer; the most common sequence of the mature tetrapeptide consists of L-Ala, D-Glu, *meso*-2,6-diaminopimelic acid, and D-Ala. The subunits are connected through  $\beta$ -1,4 glycosidic bonds to form glycan strands, and amide groups between tetrapeptides link strands together. The composition of the peptidoglycan subunit and the linkage site between glycan strands vary among different bacterial species. Other factors that influence peptidoglycan diversity include the three-dimensional structure and organization of the peptidoglycan network. In Gram-positive bacteria, the meshwork of peptidoglycan forms the outermost layer of the cell, contains associated teichoic acids, and is thicker than the peptidoglycan layer found in Gram-negative organisms. In Gram-negative bacteria, the peptidoglycan is positioned between the inner and outer membranes. A visual comparison of Gram-positive and Gram-negative peptidoglycan structure is provided in Figure 1B. For detailed information on the chemistry, physical properties, and structure of peptidoglycan, we suggest several excellent reviews (4-6).

### *Antibiotics that target the peptidoglycan.*

A currently accepted model of the spatial organization of peptidoglycan synthesis entails the cytoskeletal proteins as the shape determining factors that guide

peptidoglycan synthesis, and peptidoglycan as the scaffold that physically maintains the cell shape (7, 8). In the past decade of research that led to this model, several different methods were used to probe peptidoglycan synthesis and correlate its localization with cell division, growth, cytoskeletal proteins and their interacting partners. These methods include metabolic labeling, antibody labeling, and fluorescent antibiotics that specifically bind to nascent peptidoglycan substrates. In this section, we focus our discussion on peptidoglycan-specific antibiotics and their use in studying subcellular organization in bacteria.

The inhibition of cell wall synthesis was among the earliest targets for developing new antibiotics. Thus, there is a long list of antibiotics that target different stages of peptidoglycan synthesis, and several of these compounds have been useful in studying subcellular organization (Table 1). Using tunicamycin as a probe, ManA was determined to play a role in cell shape maintenance (9). Fosfomycin was used to investigate the hierarchy of protein-protein interactions in cytoskeleton-guided peptidoglycan synthesis (10). These and other examples demonstrate how antibiotics can provide insight into the spatial and temporal organization of peptidoglycan synthesis (11).

In addition to their use in modulating protein activity *in vivo*, antibiotics can be covalently modified with fluorescent probes for visualizing cellular organization using epifluorescence microscopy. Three antibiotics—vancomycin, ramoplanin, and phenoxymethylpenicillin (penicillin V; also referred to as bocillin)—have been derivatized with fluorophores for studying peptidoglycan (12-14). Vancomycin binds the nascent pentapeptide of a peptidoglycan subunit and prevents its maturation into a disaccharide tetrapeptide to block peptidoglycan assembly (15). Since the maturation

step from penta- to tetrapeptide is rapid, labeling of Gram-positive bacteria with fluorescent vancomycin derivatives indicates regions of nascent peptidoglycan synthesis (7). Similar to vancomycin, ramoplanin also inhibits the maturation of peptidoglycan (13). The antibiotic inhibits transglycosylation by binding to lipid II (16). Ramoplanin is arguably a more specific probe for visualizing nascent peptidoglycan, as the pentapeptide substrate of vancomycin is also present in mature peptidoglycan (13). The third derivatized antibiotic, bocillin blocks cell wall synthesis by inhibiting transpeptidases (14). Radiolabeled penicillin derivatives have been used to identify and characterize penicillin-binding proteins (PBPs). Bocillin was introduced as a non-radioactive alternative for visualizing functional PBPs on polyacrylamide gels. It is unclear whether the localization of the probe specifically indicates the sites of peptidoglycan synthesis; however its labeling is comparable to fluorescent vancomycin in cells of *Corynebacterium glutamicum* (11).

A significant advantage of using fluorescent derivatives of antibiotics is the high temporal resolution that they provide in contrast to metabolic and antibody labeling methods. Fluorescent antibiotics can be used in conjunction with proteins that are translationally fused to fluorescent proteins, thereby enabling multi-color live cell imaging experiments. This combination of strategies for labeling has been an important tool in studying the dynamics of peptidoglycan synthesis and the involvement of cytoskeletal proteins in cell shape determination.

Fluorescent antibiotics have several useful characteristics, including their specificity, rapid binding, and compatibility with in vivo imaging; however these probes are relatively impermeable to the cell wall of Gram-negative bacteria. Bulky glycopeptides cannot penetrate across the outer membrane, and the cell wall of Gram-

negative bacteria contains multiple sites for vancomycin binding; these characteristics make it difficult to distinguish between old and new peptidoglycan (7). However, Gober and co-workers (17) have successfully used fluorescent vancomycin to probe the localization of peptidoglycan synthesis in *C. crescentus*.

### *Applications of fluorescent vancomycin probes.*

The advantages of using fluorescent vancomycin derivatives far outweigh their limitations and have made them widely used probes for studying peptidoglycan synthesis. This class of small molecules has been particularly useful for studying two general areas of cellular organization in bacteria: 1) the spatial organization of bacterial growth and division; and 2) the investigation of the involvement of cytoskeletal proteins and their associated proteins in peptidoglycan synthesis. In this section, we summarize findings from both of these areas of research.

The first use of fluorescent vancomycin revealed the location of nascent peptidoglycan in *B. subtilis*, *Streptococcus pneumoniae*, *Streptomyces coelicolor*, and *C. glutamicum* cells (12). The fluorescent antibiotic has since been used to probe the cell division patterns of several other organisms, including *C. crescentus* (17), *Mycobacterium* species (18), *Lactococcus lactis* (19), and *S. aureus* (20). This approach for studying peptidoglycan synthesis transcends the limitations of the spatial resolution of autoradiography and has enabled the discovery of previously uncharacterized phenomena, including the helical pattern of peptidoglycan synthesis in *B. subtilis* (12, 13). A recent study of *S. aureus* used the fluorescent probes to investigate how this spherical bacterium can sequentially alternate between three orthogonal planes for division (21). The authors selectively marked the first division plane with fluorescent

vancomycin, and tracked the position of the labeled peptidoglycan during the following two cycles of division. Their approach enabled the correlation between peptidoglycan labeling and the age of a cell. The results of this study suggest that remodeled peptidoglycan may serve as a physical marker (e.g. a 'landmark') of previous division planes in a spherical bacterium.

The dynamic process of peptidoglycan remodeling is frequently used as a protein positioning mechanism in the cell. For example, in *Listeria monocytogenes*, the continuous remodeling of peptidoglycan along the long axis and at the septum of the cell leads to the asymmetric polar localization of ActA (22). ActA extends from the cytoplasm to the outside of the cell and its asymmetric distribution is critical for the motility of *L. monocytogene* motility inside the host eukaryotic cells. The authors demonstrated that the localization of fluorescent ActA and vancomycin labeling is mutually exclusive, indicating that the degradation of peptidoglycan and peptidoglycan-spanning proteins drives the polar localization of ActA. Initially, the protein is randomly inserted into the cell envelope, and repeated cell growth/division spreads the patches of ActA into a more uniform distribution across the surface. The distribution of ActA becomes concentrated at one pole as some regions of peptidoglycan (e.g. the septum) are degraded more rapidly than others (e.g. cell poles). This study suggests that the uneven distribution of peptidoglycan synthesis and differential peptidoglycan dynamics can serve as a mechanism for localizing proteins in bacteria.

Fluorescent vancomycin derivatives have also been used to correlate cell wall dynamics and the localization of the cytoskeleton. Several groups have demonstrated that the depletion of one of the three MreB isoforms does not abolish the helical pattern

of fluorescent vancomycin in *B. subtilis*, suggesting that these proteins have a redundant function in determining cell shape (13, 23). *E. coli* and *C. crescentus* cells also use MreB for guiding the cylindrical growth of peptidoglycan, and FtsZ has been shown to modulate the spatial activity of MreB in this process (17, 24). *S. aureus* cells have a spherical morphology and lack a copy of *mreB* in its genome. The depletion of *S. aureus* FtsZ resulted in diffuse peptidoglycan synthesis throughout the entire cell, instead of the typical tight band in the region at which the septum forms (20). Finally, actinobacteria may have a different mechanism for the localization of peptidoglycan synthesis, as the organism does not use MreB; instead, DivIVA guides polar peptidoglycan synthesis in *S. coelicolor*, *C. glutamicum*, and mycobacterial species (25). Several lines of evidence suggest that DivIVA is required for polar growth and the rod shape of *C. glutamicum*, as fluorescently labeled vancomycin and DivIVA colocalize in these cells (26). In summary, these studies used vancomycin as a probe for nascent peptidoglycan and demonstrated the role of cytoskeletal proteins as cell shape determinants.

The bacterial cytoskeleton serves as a blueprint for the structure of the peptidoglycan; however it is unclear how these cytoplasmic proteins communicate with peptidoglycan synthesis machinery located outside of the (inner) membrane. Which molecules link the cytoskeleton to the peptidoglycan machinery? Many proteins interact with the cytoskeleton in *C. crescentus*. For example, MreC and MreD bridge MreB and the peptidoglycan machinery (27). Minor changes in cell shape and minimal vancomycin labeling accompany the depletion of MreC (17). The small change in cell shape was consistent with intact localization of MreB structures during MreC depletion. These phenotypes indicate that MreC is an integral component in transmitting the

organization of MreB to the peptidoglycan synthesis machinery and influencing cell wall assembly.

*Future studies: peptidoglycan-specific chemical tools and their application to studying bacteria.*

In this section, we discuss unanswered questions regarding the dynamic localization and interactions of proteins in bacterial cells that may be effectively probed and manipulated using small molecules. Small molecules may be advantageous over protein-based probes (e.g. antibodies or translational fusions to fluorescent proteins) when the target is heterogeneous and has a dynamic structure and position in cells (e.g. peptidoglycan, chromosome, and lipid membranes). Advances in labeling technologies, including the use of Sortase A to attach user-designed molecules to the peptidoglycan and development of synthetic cell wall precursors which can be incorporated into peptidoglycan *in vivo* will play an important role in imaging the structure and assembly of this biopolymer (28-32).

Below we summarize several areas in which chemical probes may be particularly useful tools in studying peptidoglycan-related questions in microbiology.

1. *Cytoskeletal proteins and peptidoglycan synthesis.* During cell division, the Z-ring produces a constrictive force that is hypothesized to participate in cytokinesis. How is the force generated by FtsZ transmitted to the peptidoglycan synthesis machinery? How does the helical pattern of peptidoglycan machinery establish and maintain the width of the cell? (33) Bacterial genomes contain a variety of genes encoding proteins that may be homologous to tubulin, actin, and intermediate filament. What is the role of these unexplored cytoskeletal elements in the regulation of peptidoglycan synthesis in

bacteria? The discovery of small molecule inhibitors of these proteins will be helpful in studying these questions.

2. *Cell growth and peptidoglycan synthesis.* How is the length of a cell determined, and which proteins regulate the process? How is metabolism and environmental sensing coupled to cell growth and peptidoglycan synthesis? In *M. tuberculosis*, PknA and PknB kinases may participate in the interplay between the extracellular environment and intracellular decisions. Fluorescently labeled vancomycin has been used to demonstrate that the phosphorylation state of the Pkn kinases govern its interactions with peptidoglycan synthesis machinery (34). How does a bacterium coordinate cell wall elongation and division? Both of these processes involve peptidoglycan synthesis. How do the different components interact and communicate? The labeling pattern of *B. subtilis* cells treated with vancomycin and the localization of PBP1 have provided insight into how EzrA and GpsB may coordinate FtsZ- and MreB-based machineries (35).

3. *The subcellular localization of peptidoglycan synthesis as a mechanism for storing spatial information and a force for moving MreB filaments.* Earlier, we mentioned the hypothesis that spherical bacteria may use remodeled peptidoglycan from the previous round of cell division as a mechanism for the sequential alternation between division planes. The confirmation of this hypothesis requires an understanding of how the epigenetic information in peptidoglycan is transmitted to the cytoplasm. Another cellular process that may use the organization of peptidoglycan as a landmark is the maintenance of cell polarity. Cells maintain polarity before, during, and after division. How does a daughter cell inherit polarity from the mother cell (36)? The localization of peptidoglycan synthesis may spatially guide the organization of the bacterial

chromosome. The peptidoglycan synthesis inhibitor tunicamycin caused shape defects in *B. subtilis* cells and simultaneously perturbed the morphology of the nucleoid (9). The shape of the nucleoid was studied using 4',6-diamidino-2-phenylindole (DAPI), a small molecule that fluoresces when bound to AT-rich regions of DNA. From these studies, it was proposed that chromosome conformation may follow the organization of peptidoglycan synthesis (9). Another role of peptidoglycan synthesis may be translocation of MreB-associated complexes, as three recent studies demonstrated that inhibition of peptidoglycan synthesis using antibiotics caused rapid cessation of MreB movements in vivo (37-39).

4. *Peptidoglycan architecture*. Can the optical properties of fluorescent peptidoglycan-specific probes be tailored for applications in super-resolution microscopy techniques (40, 41)? The use of these techniques for studying the organization of peptidoglycan in live cells below the diffraction limit will provide important details on peptidoglycan architecture.

## LIPIDS

Bacterial membranes consist of three major classes of phospholipids: phosphatidylethanolamine (PE), phosphatidylglycerol (PGL), and cardiolipin (CL). PE has a neutral net charge (i.e. zwitterionic) and PGL and CL are anionic at physiological conditions. All three classes of phospholipids arise from a common precursor via a branched biosynthetic pathway (42). The phospholipid composition of the membrane varies among species of bacteria and depends on growth conditions (43). A representation of lipid localization and composition is shown in Figure 1C. In *E. coli*, the cell membrane consists of 75% PE, 20% PGL, and 5% CL (44).

### *Probing lipid organization using small molecules.*

Three classes of small molecules for studying the subcellular organization of lipids are introduced and discussed below: photoactivatable crosslinkers, lipid-specific fluorophores, and inhibitors of lipid biosynthesis (Table 2).

A variety of different photoactivated lipid analogs have been synthesized to probe the environment surrounding lipids (45). For example, phosphatidylcholine can be modified with a diazirine group at the end of the sn-2 aliphatic chain. This functional group is converted to a carbene upon UV exposure and reacts rapidly with neighboring molecules to form covalent bonds (46). Some analogs also contain radioactive elements for quantitative measurements. *Micrococcus luteus* cells can metabolize radiolabeled 9-(2-anthryl)nonanoic acid and transform the lipid analog into PGL. After the photoreactive lipid is incorporated into the membrane in vivo, the cells are irradiated and lipids are extracted for radioactivity counting (47). Results from these experiments

have provided insight into the lateral distribution and diffusion of lipids in bacterial membranes.

Although crosslinking reagents are useful, they must be coupled with biochemical analyses and are not ideal for probing membrane organization in real time. Lipid-specific fluorophores and lipid synthesis inhibitors are more suitable for monitoring the dynamics of lipid domains. Several fluorescent probes have been used to label lipids in vivo (48-51). Some of these probes have been used for fluorescence microscopy (51), and others for time-resolved fluorescence spectroscopy (52, 53). Most of these probes consist of a lipid with a fluorophore attached to the head group. While many fluorophores are not specific to a particular type of lipid, 10-N-nonyl acridine orange (NAO) and Ro09-0198 bind specifically to CL and PE, respectively. Ro09-0198 is a hemolysis-inducing peptide, isolated from *Streptoverticillium griseoverticillatum* (54). Several studies have characterized the binding of Ro09-0198 to PE (54, 55). NAO binding to CL arises from intercalation between fluorophores and lipid molecules. When the fluorophores are  $\pi$ - $\pi$  stacked, their emission wavelength undergoes a large Stokes shift, which enables NAO bound to CL to be distinguished from NAO bound to peptidoglycan (49, 56).

Small molecules that inhibit the biosynthesis of particular lipids have also been used to study membrane organization. In eukaryotic cells, cholesterol has been described as a major component of lipid rafts. Compounds that sequester cholesterol or inhibit its biosynthesis (e.g. filipin, nystatin, amphotericin, methyl- $\beta$ -cyclodextrin, and statins) have been used extensively for studying lipid raft biology (57, 58). Several antibiotics target lipid biosynthesis in bacteria (59-61). Only recently have these

compounds been explored as tools for investigating lipid domains in bacteria. For example, zaragozic acid, was used to study lipid domains in *B. subtilis* cells (62).

*Insights obtained from using small molecules that bind to lipids specifically.*

Lipid-specific compounds have been useful for identification and characterization of lipid domains in bacterial membranes. Below, we examine how these small molecules provided insight into lipid organization in bacterial membranes.

Initial studies of lipid organization in bacteria detected heterogeneity in bacterial membranes using chemical biological approaches. For example, *E. coli* cells treated with laurdan, an amphipathic molecule with a fluorescent group, demonstrated the existence of two subpopulations of laurdan in the bacterial membrane (53). The organization of lipids into two distinct groups was abolished when cells were pre-treated with chloramphenicol, a protein synthesis inhibitor. The results indicate that the membrane consists of domains that are either lipid-rich or protein-rich. In a subsequent study (52) pyrene-labeled phospholipids (pyrene-PE and pyrene-PGL) were used to study *E. coli* and *B. subtilis* cells. A combination of fluorescence spectroscopy and lipid extraction methods demonstrated that pyrene-labeled PE and PGL have different local environments and suggest that presence of lipid domains in bacterial membranes.

Small molecules also enable observations of lipid organization in vivo. Two early studies reported the non-homogenous labeling of membranes with lipophilic dyes in *E. coli* and mycobacterial species (48, 51). Several groups later demonstrated that fluorophores that bind to CL and PE—NAO and Ro09-0198, respectively—localized to the septum and poles in *E. coli* and *B. subtilis* (50, 63, 64). Interestingly, Ro09-0198 has been observed to localize to the cleavage furrow of Chinese hamster ovary cells (65);

these observations suggest a connection between lipid organization and cell division in both prokaryotes and eukaryotes. Moreover, CL and PE are concentrated in the forespore membrane in *B. subtilis* cells (63), and their localization contributed to the hypothesis that some lipids may be recruited to regions of membrane curvature (66, 67).

Investigations of the organization of bacterial membranes have provided clues to the biological function of lipid domains. Lipid organization is hypothesized to play a role in many processes, including: cell division (68), DNA replication (42), sporulation (63), osmoregulation (69), protein translocation (70), peptidoglycan synthesis (71), and biofilm formation (62). Below, we describe two examples of small molecule-based studies of the biological roles of lipid domains in bacterial membranes.

In *B. subtilis*, the helical pattern of FM4-64 co-localizes with the helical pattern of MinD translationally fused to green fluorescence protein (68). To quantify the interaction between lipid spirals and MinD, fluorescence resonance energy transfer (FRET) was measured between GFP-MinD (i.e. FRET donor) and FM4-64 (i.e. FRET acceptor). These experiments indicated that the two classes of biomolecules interact within the 10-nm spatial limit of FRET. The close association between anionic lipids and MinD suggests that these lipids may participate in cell division.

The relationship between CL organization and *E. coli* membrane curvature was quantitatively measured using NAO to visualize CL (72). MinD translationally fused to a fluorescent protein colocalized with CL microdomains at regions of large, negative curvature in *E. coli* membranes. CL localization at regions of large negative curvature may be a landmark for positioning MinD at the poles of *E. coli* cells. This hypothesis is supported by the demonstration that CL modulates the polar localization of the osmosensory transporter ProP in *E. coli* cells (69). Cells expressing a chimera of a

fluorescent protein fused to ProP were labeled with NAO; the polar localization of the protein was observed to be dependent on CL organization in vivo. It was also observed that the polar localization of the mechanosensitive ion channel protein MscS is also CL-dependent (73).

***Future studies: Lipid-specific small molecules and their application to bacterial cell biology.***

In summary, chemical biological tools have been useful for probing the subcellular organization of lipids in vitro and in vivo. The discovery and characterization of new classes of compounds that bind specific lipids or substrate analogs that can be incorporated into lipids in vivo will enable this area of microbiology to move forward. Recently, fluorescent analogs of trehalose have been used in *M. tuberculosis* cells to produce fluorescent glycolipids in vivo, and these labeled glycolipids were observed to concentrate at the bacterial poles (74).

There are many unanswered questions regarding the structure and organization of bacterial membranes in which chemical probes may be particularly helpful. We highlight several areas below.

1. *Mechanism of controlling membrane organization.* Several observations suggest that negative membrane curvature stabilizes and localizes CL domains in bacteria (67). For example, a recent study of *E. coli* spheroplasts visualized CL using NAO while systematically varying membrane curvature by confining the cells in biocompatible microchambers (72). The characterization of this mechanism in cells would benefit from lipid-specific derivatives of NAO that are more photostable and compatible with super-resolution microscopy techniques.

2. *Biological function of lipid domains.* Lipid domains may function as physical landmarks for protein localization, and/or may directly modulate the activity of proteins. Several studies suggest that lipid rafts may perform both of these functions in vivo: MinD localization is perturbed in a *B. subtilis* strain that does not synthesize PGL (68) and CL stimulates the ATPase activity of EpsE, a component of type II secretion system in *V. cholerae* (75). If lipid domains directly modulate enzyme activity or participate in recruiting proteins, it will be important to address the molecular mechanism of their recognition and interaction.

3. *Relationship between cytoskeletal elements and lipid domains.* In eukaryotic cells, lipid rafts are often associated with actin filaments. Do the lipid domains in bacterial membranes interact with cytoskeletal proteins? Inhibitors of these proteins may play an important role in deciphering this relationship.

4. *Proteins associated with bacterial lipid domains.* Perturbing the organization of squalene causes delocalization of flotilin and KinC and halts the signaling cascade for biofilm formation in *B. subtilis* (62). The identification of other signaling cascades that are modulated by lipid domains and the characterization of proteins that are associated with lipid domains in bacteria will play an important role in understanding the physiological role of this mechanism in bacteria.

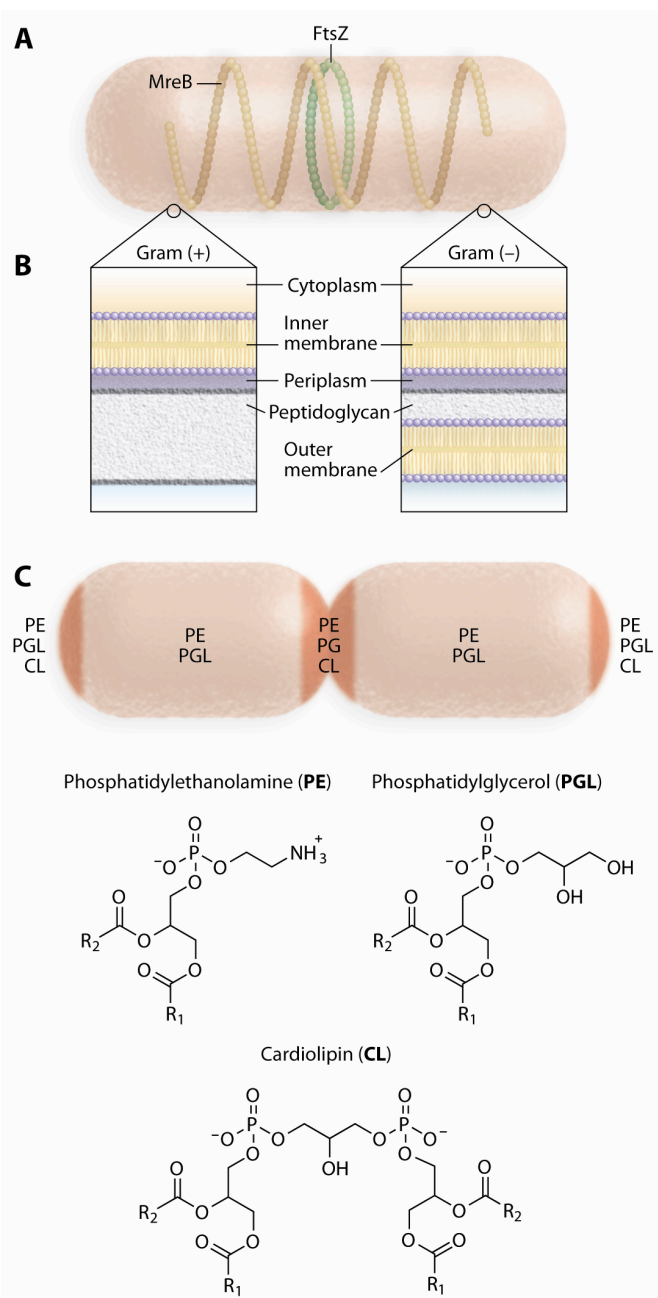
## CONCLUSIONS

With the aid of genetic and chemical tools, a burst of research in the microbiology field has shown complex, spatiotemporal organizations inside the cytoplasm and within the layers surrounding the cytoplasm. We continue to discover more molecular components participating in the subcellular organization, and different strategies utilized by bacteria to achieve organization. Comparison of the mechanisms in diverse single-cell organisms that vary across the size scale would help us understand how inherent physical properties are exploited in different cell types (76). For example, the protist *Stentor* is one of the biggest unicellular eukaryote with its length being approximately 2 mm (77). On the other hand, bacterial species in the genus *Mycoplasma* have a size of 0.3  $\mu\text{m}$  (78). It is likely that the size scale and geometrical shape of these single-cell organisms have significantly influenced the evolution of different organizational mechanisms used by the giant *Stentor* and tiny *Mycoplasma*. Studying their unique and common routes for accomplishing organization would illuminate fundamental biological principles underlying the evolution of life (77).

In the next two chapters, I describe the discovery and characterization of two small molecule tools. Chapter 5 reports the study of DCAP, a membrane-targeting antibiotic, which can be utilized to investigate the dynamic nature of bacterial membrane composition. Chapter 6 describes the study of divin, an inhibitor of cell division in Gram-negative bacteria. As the division process in Gram-negative involves coordination of all layers in the cell envelope, development of divin would help elucidate the molecular mechanism of communication between envelope layers and the cytoplasm during reproduction.

## ACKNOWLEDGEMENTS

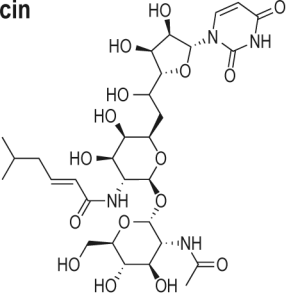
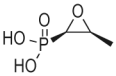
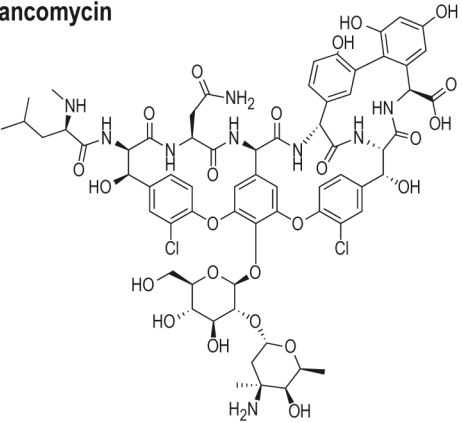
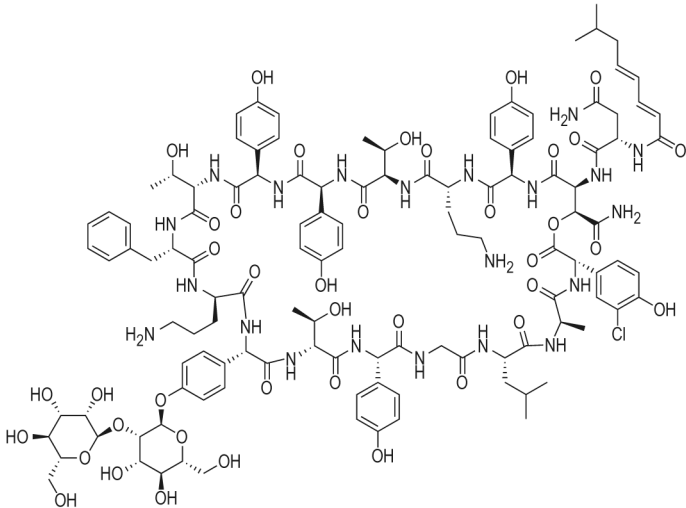
We thank Prof. Jared Shaw, Prof. David Spiegel, and Dr. Dave Anderson for insightful comments on this review. We acknowledge several agencies that fund this area of research in our lab, including: the Human Frontiers Science Program (RGY0069), USDA, a Searle Scholars Award (D.B.W.), an Alfred P. Sloan Research Fellowship (D.B.W.), Genentech Graduate Fellowship (Y.-J.E.) and the Senator Robert Caldwell Graduate Fellowship (Y.-J.E.).



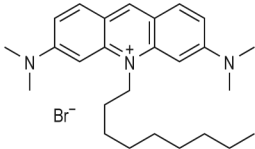
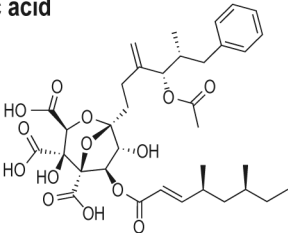
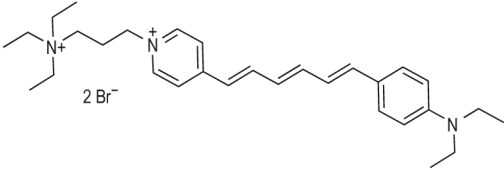
**Figure 1.** Sub-cellular localization of FtsZ, MreB, peptidoglycan, and lipids in bacterial cells. A) A cartoon depicting the localization of the tubulin homolog FtsZ and actin homolog MreB. B) The structure of the cell wall of Gram-positive and Gram-negative bacteria. The dark lines separating the peptidoglycan from adjacent layers were added

to indicate the boundaries. C) A cartoon depicting the distribution of the membrane lipids phosphatidylethanolamine (PE), phosphatidylglycerol (PGL), and cardiolipin (CL).

**Table 1.** Peptidoglycan labeling reagents. The following compounds have been described and utilized as labels for studying peptidoglycan synthesis. The structure, biomolecular targets, and fluorescence characteristics of this class of compounds are tabulated.

Compound Structure	Biomolecular target	Fluorescence properties	Refs
<p><b>Tunicamycin</b></p> 	Broad inhibitor of glycosylation	NA	(78)
<p><b>Fosfomycin</b></p> 	MurA	NA	(79)
<p><b>Vancomycin</b></p> 	Nascent PG subunit (a disaccharide pentapeptide)	BODIPY-FL conjugate; $\lambda_{ex} / \lambda_{em} = 502/510 \text{ nm}$	(81)
<p><b>Ramoplanin A2</b></p> 	Reducing end of a glycan strand	Fluorescein conjugate; $\lambda_{ex} / \lambda_{em} = 500/520 \text{ nm}$	(82)

**Table 2.** Probes for lipid studies. The following small molecules have been described and utilized in the literature as probes for studying lipid organization. The table summarizes the structure of probes, their biomolecular target or lipid specificity, and fluorescence characteristics.

Compound Structure	Biomolecular target	Fluorescence properties	Refs
<p><b>10-N-nonylacridine orange (NAO)</b></p> 	Cardiolipin	$\lambda_{ex} / \lambda_{em} = 488/628 \text{ nm}$	(114, 121)
<p><b>Ro09-0198</b>            Cys-Arg-Gln-Cys-Cys-3-NH<sub>2</sub>-Ala-Phe-Gly-Pro-Phe-(2S,3S)-2-amino-3-mercaptobutanoyl-Phe-Val-Cys-3-OH-<math>\alpha</math>-Asp-Gly-Asn-(2S,3S)-2-amino-3-mercaptobutanoyl-Lys</p>	Phosphatidyl ethanolamine	Needs to be tagged for fluorescent antibody binding (e.g. conjugated with biotin for binding with anti-streptavidin antibody)	(119, 120)
<p><b>Zaragozic acid</b></p> 	Squalene synthase	NA	(127)
<p><b>FM 4-64</b></p> 	Non-specific binding to lipids	$\lambda_{ex} / \lambda_{em} = 515/640 \text{ nm}$	(133)

## REFERENCES

1. Silhavy, T. J., Kahne, D., and Walker, S. (2010) The bacterial cell envelope, *Cold Spring Harb Perspect Biol* 2, a000414.
2. Shapiro, L., McAdams, H. H., and Losick, R. (2009) Why and How Bacteria Localize Proteins, *Science* 326, 1225-1228.
3. Vanden Boom, T., and Cronan, J. E., Jr. (1989) Genetics and regulation of bacterial lipid metabolism, *Annu Rev Microbiol* 43, 317-343.
4. Vollmer, W., Blanot, D., and de Pedro, M. A. (2008) Peptidoglycan structure and architecture, *FEMS Microbiology Reviews* 32, 149-167.
5. Vollmer, W., and Seligman, S. J. (2010) Architecture of peptidoglycan: more data and more models, *Trends in Microbiology* 18, 59-66.
6. Cabeen, M. T., and Jacobs-Wagner, C. (2007) Skin and bones: the bacterial cytoskeleton, cell wall, and cell morphogenesis, *Journal of Cell Biology* 179, 381-387.
7. Cabeen, M. T., and Jacobs-Wagner, C. (2005) Bacterial cell shape, *Nat Rev Microbiol* 3, 601-610.
8. Young, K. D. (2010) Bacterial shape: two-dimensional questions and possibilities, *Annual Review of Microbiology* 64, 223-240.
9. Elbaz, M., and Ben-Yehuda, S. (2010) The metabolic enzyme ManA reveals a link between cell wall integrity and chromosome morphology, *PLoS Genet* 6, 1-12.
10. Aaron, M., Charbon, G., Lam, H., Schwarz, H., Vollmer, W., and Jacobs-Wagner, C. (2007) The tubulin homologue FtsZ contributes to cell elongation by guiding cell wall precursor synthesis in *Caulobacter crescentus*, *Molecular Microbiology* 64, 938-952.
11. Valbuena, N., Letek, M., Ordonez, E., Ayala, J., Daniel, R. A., Gil, J. A., and Mateos, L. M. (2007) Characterization of HMW-PBPs from the rod-shaped actinomycete *Corynebacterium glutamicum*: peptidoglycan synthesis in cells lacking actin-like cytoskeletal structures, *Molecular Microbiology* 66, 643-657.
12. Daniel, R. A., and Errington, J. (2003) Control of Cell Morphogenesis in Bacteria: Two Distinct Ways to Make a Rod-Shaped Cell, *Cell* 113, 767-776.
13. Tiyanont, K., Doan, T., Lazarus, M. B., Fang, X., Rudner, D. Z., and Walker, S. (2006) Imaging peptidoglycan biosynthesis in *Bacillus subtilis* with fluorescent

- antibiotics, *Proceedings of the National Academy of Sciences of the United States of America* 103, 11033-11038.
14. Zhao, G., Meier, T. I., Kahl, S. D., Gee, K. R., and Blaszcak, L. C. (1999) BOCILLIN FL, a sensitive and commercially available reagent for detection of penicillin-binding proteins, *Antimicrobial Agents and Chemotherapy* 43, 1124-1128.
  15. Jovetic, S., Zhu, Y., Marcone, G. L., Marinelli, F., and Tramper, J. (2010) beta-Lactam and glycopeptide antibiotics: first and last line of defense?, *Trends in Biotechnology* 28, 596-604.
  16. Fang, X., Tiyanont, K., Zhang, Y., Wanner, J., Boger, D., and Walker, S. (2006) The mechanism of action of ramoplanin and enduracidin, *Mol Biosyst* 2, 69-76.
  17. Divakaruni, A. V., Baida, C., White, C. L., and Gober, J. W. (2007) The cell shape proteins MreB and MreC control cell morphogenesis by positioning cell wall synthetic complexes, *Molecular Microbiology* 66, 174-188.
  18. Thanky, N. R., Young, D. B., and Robertson, B. D. (2007) Unusual features of the cell cycle in mycobacteria: polar-restricted growth and the snapping-model of cell division, *Tuberculosis (Edinb)* 87, 231-236.
  19. Gilbert, Y., Deghorain, M., Wang, L., Xu, B., Pollheimer, P. D., Gruber, H. J., Errington, J., Hallet, B., Haulot, X., Verbelen, C., Hols, P., and Dufrene, Y. F. (2007) Single-molecule force spectroscopy and imaging of the vancomycin/D-Ala-D-Ala interaction, *Nano Lett* 7, 796-801.
  20. Pinho, M. G., and Errington, J. (2003) Dispersed mode of *Staphylococcus aureus* cell wall synthesis in the absence of the division machinery, *Molecular Microbiology* 50, 871-881.
  21. Turner, R. D., Ratcliffe, E. C., Wheeler, R., Golestanian, R., Hobbs, J. K., and Foster, S. J. (2010) Peptidoglycan architecture can specify division planes in *Staphylococcus aureus*, *Nat Commun* 1, 1-9.
  22. Rafelski, S. M., and Theriot, J. A. (2006) Mechanism of polarization of *Listeria monocytogenes* surface protein ActA, *Molecular Microbiology* 59, 1262-1279.
  23. Kawai, Y., Daniel, R. A., and Errington, J. (2009) Regulation of cell wall morphogenesis in *Bacillus subtilis* by recruitment of PBP1 to the MreB helix, *Molecular Microbiology* 71, 1131-1144.
  24. Varma, A., de Pedro, M. A., and Young, K. D. (2007) FtsZ directs a second mode of peptidoglycan synthesis in *Escherichia coli*, *J Bacteriol* 189, 5692-5704.
  25. Flardh, K. (2010) Cell polarity and the control of apical growth in *Streptomyces*, *Current Opinion in Microbiology* 13, 758-765.

26. Letek, M., Ordonez, E., Vaquera, J., Margolin, W., Flardh, K., Mateos, L. M., and Gil, J. A. (2008) DivIVA is required for polar growth in the MreB-lacking rod-shaped actinomycete *Corynebacterium glutamicum*, *Journal of Bacteriology* 190, 3283-3292.
27. White, C. L., Kitich, A., and Gober, J. W. (2010) Positioning cell wall synthetic complexes by the bacterial morphogenetic proteins MreB and MreD, *Molecular Microbiology* 76, 616-633.
28. Parthasarathy, R., Subramanian, S., and Boder, E. T. (2007) Sortase A as a novel molecular "stapler" for sequence-specific protein conjugation, *Bioconjug Chem* 18, 469-476.
29. Nelson, J. W., Chamessian, A. G., McEnaney, P. J., Murelli, R. P., Kazmierczak, B. I., and Spiegel, D. A. (2010) A biosynthetic strategy for re-engineering the *Staphylococcus aureus* cell wall with non-native small molecules, *ACS Chem Biol* 5, 1147-1155.
30. Sadamoto, R., Niikura, K., Sears, P. S., Liu, H., Wong, C. H., Suksomcheep, A., Tomita, F., Monde, K., and Nishimura, S. (2002) Cell-wall engineering of living bacteria, *J Am Chem Soc* 124, 9018-9019.
31. Yi, W., Liu, X., Li, Y., Li, J., Xia, C., Zhou, G., Zhang, W., Zhao, W., Chen, X., and Wang, P. G. (2009) Remodeling bacterial polysaccharides by metabolic pathway engineering, *Proc Natl Acad Sci U S A* 106, 4207-4212.
32. Orlachs, N. K., Aarsman, M. E., Verheul, J., Arnusch, C. J., Martin, N. I., Herve, M., Vollmer, W., de Kruijff, B., Breukink, E., and den Blaauwen, T. (2011) A novel in vivo cell-wall labeling approach sheds new light on peptidoglycan synthesis in *Escherichia coli*, *Chembiochem* 12, 1124-1133.
33. Cabeen, M. T., and Jacobs-Wagner, C. (2010) The bacterial cytoskeleton, *Annu Rev Genet* 44, 365-392.
34. Jani, C., Eoh, H., Lee, J. J., Hamasha, K., Sahana, M. B., Han, J. S., Nyayapathy, S., Lee, J. Y., Suh, J. W., Lee, S. H., Rehse, S. J., Crick, D. C., and Kang, C. M. (2010) Regulation of polar peptidoglycan biosynthesis by Wag31 phosphorylation in mycobacteria, *BMC Microbiol* 10, 327.
35. Claessen, D., Emmins, R., Hamoen, L. W., Daniel, R. A., Errington, J., and Edwards, D. H. (2008) Control of the cell elongation-division cycle by shuttling of PBP1 protein in *Bacillus subtilis*, *Molecular Microbiology* 68, 1029-1046.
36. Ebersbach, G., and Jacobs-Wagner, C. (2007) Exploration into the spatial and temporal mechanisms of bacterial polarity, *Trends Microbiol* 15, 101-108.

37. Garner, E. C., Bernard, R., Wang, W., Zhuang, X., Rudner, D. Z., and Mitchison, T. (2011) Coupled, circumferential motions of the cell wall synthesis machinery and MreB filaments in *B. subtilis*, *Science* 333, 222-225.
38. Dominguez-Escobar, J., Chastanet, A., Crevenna, A. H., Fromion, V., Wedlich-Soldner, R., and Carballido-Lopez, R. (2011) Processive movement of MreB-associated cell wall biosynthetic complexes in bacteria, *Science* 333, 225-228.
39. Teeffelen, S. v., Wang, S., Furchtgott, L., Huang, K. C., Wingreen, N. S., Shaevitz, J. W., and Gitai, Z. (2011) The bacterial actin MreB rotates and rotation depends on cell-wall assembly, *Proc Natl Acad Sci U S A* 108, 15822-15827.
40. Schermelleh, L., Heintzmann, R., and Leonhardt, H. (2010) A guide to super-resolution fluorescence microscopy, *J Cell Biol* 190, 165-175.
41. Toomre, D., and Bewersdorf, J. (2010) A new wave of cellular imaging, *Annu Rev Cell Dev Biol* 26, 285-314.
42. Mileykovskaya, E., and Dowhan, W. (2005) Role of membrane lipids in bacterial division-site selection, *Current Opinion in Microbiology* 8, 135-142.
43. Epanand, R. M., and Epanand, R. F. (2009) Domains in bacterial membranes and the action of antimicrobial agents, *Mol Biosyst* 5, 580-587.
44. Dowhan, W. (1997) Molecular basis for membrane phospholipid diversity: Why are there so many lipids?, *Annual Review of Biochemistry* 66, 199-232.
45. Radhakrishnan, R., Gupta, C. M., Erni, B., Robson, R. J., Curatolo, W., Majumdar, A., Ross, A. H., Takagaki, Y., and Khorana, H. G. (1980) Phospholipids containing photoactivable groups in studies of biological membranes, *Annals of the New York Academy of Sciences* 346, 165-198.
46. Garner, J., Durrer, P., Kitchen, J., Brunner, J., and Crooke, E. (1998) Membrane-mediated release of nucleotide from an initiator of chromosomal replication, *Escherichia coli* DnaA, occurs with insertion of a distinct region of the protein into the lipid bilayer, *Journal of Biological Chemistry* 273, 5167-5173.
47. de Bony, J., Lopez, A., Gilleron, M., Welby, M., Laneelle, G., Rousseau, B., Beaucourt, J. P., and Tocanne, J. F. (1989) Transverse and lateral distribution of phospholipids and glycolipids in the membrane of the bacterium *Micrococcus luteus*, *Biochemistry* 28, 3728-3737.
48. Fishov, I., and Woldringh, C. L. (1999) Visualization of membrane domains in *Escherichia coli*, *Molecular Microbiology* 32, 1166-1172.
49. Mileykovskaya, E., and Dowhan, W. (2009) Cardiolipin membrane domains in prokaryotes and eukaryotes, *Biochimica et Biophysica Acta* 1788, 2084-2091.

50. Nishibori, A., Kusaka, J., Hara, H., Umeda, M., and Matsumoto, K. (2005) Phosphatidylethanolamine domains and localization of phospholipid synthases in *Bacillus subtilis* membranes, *J Bacteriol* 187, 2163-2174.
51. Christensen, H., Garton, N. J., Horobin, R. W., Minnikin, D. E., and Barer, M. R. (1999) Lipid domains of mycobacteria studied with fluorescent molecular probes, *Molecular Microbiology* 31, 1561-1572.
52. Vanounou, S., Parola, A. H., and Fishov, I. (2003) Phosphatidylethanolamine and phosphatidylglycerol are segregated into different domains in bacterial membrane. A study with pyrene-labelled phospholipids, *Molecular Microbiology* 49, 1067-1079.
53. Vanounou, S., Pines, D., Pines, E., Parola, A. H., and Fishov, I. (2002) Coexistence of domains with distinct order and polarity in fluid bacterial membranes, *Photochemistry and Photobiology* 76, 1-11.
54. Choung, S. Y., Kobayashi, T., Inoue, J., Takemoto, K., Ishitsuka, H., and Inoue, K. (1988) Hemolytic activity of a cyclic peptide Ro09-0198 isolated from *Streptovorticillium*, *Biochimica et Biophysica Acta* 940, 171-179.
55. Wakamatsu, K., Choung, S. Y., Kobayashi, T., Inoue, K., Higashijima, T., and Miyazawa, T. (1990) Complex formation of peptide antibiotic Ro09-0198 with lysophosphatidylethanolamine: <sup>1</sup>H NMR analyses in dimethyl sulfoxide solution, *Biochemistry* 29, 113-118.
56. Mileykovskaya, E., Dowhan, W., Birke, R. L., Zheng, D., Lutterodt, L., and Haines, T. H. (2001) Cardiolipin binds nonyl acridine orange by aggregating the dye at exposed hydrophobic domains on bilayer surfaces, *FEBS Letters* 507, 187-190.
57. Allen, J. A., Halverson-Tamboli, R. A., and Rasenick, M. M. (2007) Lipid raft microdomains and neurotransmitter signalling, *Nat Rev Neurosci* 8, 128-140.
58. Lingwood, D., and Simons, K. (2010) Lipid rafts as a membrane-organizing principle, *Science* 327, 46-50.
59. Campbell, J. W., and Cronan, J. E., Jr. (2001) Bacterial fatty acid biosynthesis: targets for antibacterial drug discovery, *Annual Review of Microbiology* 55, 305-332.
60. Heath, R. J., White, S. W., and Rock, C. O. (2002) Inhibitors of fatty acid synthesis as antimicrobial chemotherapeutics, *Applied Microbiology and Biotechnology* 58, 695-703.
61. Wright, H. T., and Reynolds, K. A. (2007) Antibacterial targets in fatty acid biosynthesis, *Curr Opin Microbiol* 10, 447-453.

62. Lopez, D., and Kolter, R. (2010) Functional microdomains in bacterial membranes, *Genes and Development* 24, 1893-1902.
63. Kawai, F., Shoda, M., Harashima, R., Sadaie, Y., Hara, H., and Matsumoto, K. (2004) Cardiolipin domains in *Bacillus subtilis* Marburg membranes, *Journal of Bacteriology* 186, 1475-1483.
64. Mileykovskaya, E., and Dowhan, W. (2000) Visualization of phospholipid domains in *Escherichia coli* by using the cardiolipin-specific fluorescent dye 10-N-nonyl acridine orange, *Journal of Bacteriology* 182, 1172-1175.
65. Emoto, K., and Umeda, M. (2001) Membrane lipid control of cytokinesis, *Cell Structure and Function* 26, 659-665.
66. Ramamurthi, K. S., and Losick, R. (2009) Negative membrane curvature as a cue for subcellular localization of a bacterial protein, *Proceedings of the National Academy of Sciences of the United States of America* 106, 13541-13545.
67. Mukhopadhyay, R., Huang, K. C., and Wingreen, N. S. (2008) Lipid localization in bacterial cells through curvature-mediated microphase separation, *Biophysical Journal* 95, 1034-1049.
68. Barak, I., Muchova, K., Wilkinson, A. J., O'Toole, P. J., and Pavlendova, N. (2008) Lipid spirals in *Bacillus subtilis* and their role in cell division, *Molecular Microbiology* 68, 1315-1327.
69. Romantsov, T., Helbig, S., Culham, D. E., Gill, C., Stalker, L., and Wood, J. M. (2007) Cardiolipin promotes polar localization of osmosensory transporter ProP in *Escherichia coli*, *Mol Microbiol* 64, 1455-1465.
70. Gold, V. A., Robson, A., Bao, H., Romantsov, T., Duong, F., and Collinson, I. (2010) The action of cardiolipin on the bacterial translocon, *Proceedings of the National Academy of Sciences of the United States of America* 107, 10044-10049.
71. van den Brink-van der Laan, E., Boots, J. W., Spelbrink, R. E., Kool, G. M., Breukink, E., Killian, J. A., and de Kruijff, B. (2003) Membrane interaction of the glycosyltransferase MurG: a special role for cardiolipin, *Journal of Bacteriology* 185, 3773-3779.
72. Renner, L. D., and Weibel, D. B. (2011) Cardiolipin microdomains localize to negatively curved regions of *Escherichia coli* membranes, *Proceedings of the National Academy of Sciences* 108, 6264-6269.
73. Romantsov, T., Battle, A. R., Hendel, J. L., Martinac, B., and Wood, J. M. (2010) Protein localization in *Escherichia coli* cells: comparison of the cytoplasmic membrane proteins ProP, LacY, ProW, AqpZ, MscS, and MscL, *Journal of Bacteriology* 192, 912-924.

74. Backus, K. M., Boshoff, H. I., Barry, C. S., Boutureira, O., Patel, M. K., D'Hooge, F., Lee, S. S., Via, L. E., Tahlan, K., Barry, C. E., 3rd, and Davis, B. G. (2011) Uptake of unnatural trehalose analogs as a reporter for *Mycobacterium tuberculosis*, *Nat Chem Biol* 7, 228-235.
75. Camberg, J. L., Johnson, T. L., Patrick, M., Abendroth, J., Hol, W. G., and Sandkvist, M. (2007) Synergistic stimulation of EpsE ATP hydrolysis by EpsL and acidic phospholipids, *EMBO Journal* 26, 19-27.
76. Schulz, H. N., and Jorgensen, B. B. (2001) Big bacteria, *Annu Rev Microbiol* 55, 105-137.
77. Marshall, W. F. (2011) Origins of cellular geometry, *BMC biology* 9, 57.
78. Maniloff, J. (1970) Ultrastructure of *Mycoplasma laidlawii* during culture development, *J Bacteriol* 102, 561-572.

## CHAPTER 5

### **DCAP: A broad-spectrum antibiotic that targets the cytoplasmic membrane of bacteria**

Adapted from:

Ye-Jin Eun, Marie H. Foss, Daniela Kiekebusch, Daniel A. Pauw, William M. Westler, Martin Thanbichler, and Douglas B. Weibel (2012) *Journal of the American Chemical Society* 134(28):11322-11325.

## ABSTRACT

Persistent infections are frequently caused by dormant and biofilm-associated bacteria, which often display characteristically slow rates of growth. Antibiotics that require rapid cell growth may be ineffective against these organisms and thus fail to prevent reoccurring infections. In contrast to growth-based antimicrobial agents, membrane-targeting drugs effectively kill slow-growing bacteria. This communication introduces a potent antibiotic that disrupts bacterial membranes: (2-((3-(3,6-dichloro-9H-carbazol-9-yl)-2-hydroxypropyl)amino)-2-(hydroxymethyl)propane-1,3-diol), which we refer to as DCAP. DCAP is a broad-spectrum antibiotic that reduces the transmembrane potential of Gram-positive and Gram-negative bacteria and causes mislocalization of essential membrane-associated proteins, including MinD and FtsA. Importantly, DCAP kills nutrient-deprived microbes and sterilizes bacterial biofilms. DCAP is lethal against bacterial cells, has no effect on red blood cell membranes, and only decreases the viability of mammalian cells after  $\geq 6$  h. We conclude that membrane-active compounds are a promising solution for treating persistent infections. DCAP expands the limited number of compounds in this class of therapeutic small molecules and provides new opportunities for the development of potent broad-spectrum antimicrobial agents.

## INTRODUCTION

While the prevalence of multi-drug-resistant pathogens continues to rise (1), the rate at which new clinical antimicrobials are introduced has declined significantly (2). To add to this dismal picture of combating infectious diseases, the treatment of persistent infections has been complicated by the pathogen phenotypes (3). Bacteria that grow very slowly are often associated with prolonged infections, and they are particularly tolerant of many of the clinically important classes of antibiotics that inhibit rapidly growing cells. For example, the  $\beta$ -lactam family of antibiotics inhibits enzymes involved in the synthesis of peptidoglycan, and is thus most effective at targeting microbes that grow rapidly and continuously synthesize new cell wall (4, 5). Relying on antibiotics that require fast metabolism creates long-term problems, as dormant bacteria may survive antibiotic treatments, become predisposed to developing drug resistance, and cause a relapse (2).

An effective strategy for combating slow-growing bacteria is to target the lipid membrane (3). Proteomic analyses have demonstrated that approximately one third of all proteins in bacteria are associated with membranes (6). Peripheral and integral membrane proteins participate in various essential cellular processes, including: nutrient and waste transport, respiration, adhesion, mobility, cell-cell communication, and the transfer of genetic material (3, 6). Compounds that perturb these processes disrupt growth and the maintenance of cell homeostasis and may serve as potent therapeutic antimicrobial agents (3, 7).

Synthetic and naturally occurring small molecules that disrupt the bacterial membrane have been developed to treat persistent infections of mycobacterial and

staphylococcal species (3, 8). This class of compounds exhibits multiple mechanisms of action, including: inhibiting specific enzymatic processes in the membrane, decreasing the transmembrane potential ( $\Delta\Psi$ ), and increasing membrane permeability. The increase in permeability perturbs bacterial physiology and simultaneously facilitates the penetration of free radicals secreted by macrophages of the host immune system (3).

The therapeutic benefit of membrane-active drugs has been demonstrated against dormant bacteria; however, there are no clear design rules for small molecules that are specific for bacterial versus eukaryotic membranes (3). Many antibiotics in this class are ineffective against Gram-negative bacteria, presumably due to the outer membrane (8). The identification of new broad-spectrum antibiotics that target bacterial membranes and the study of their mechanism of toxicity will provide an important step forward for this field.

## EXPERIMENTAL METHODS

### *In vitro* ATPase screen with purified recombinant MipZ.

We purified recombinant MipZ for in vitro screens as described previously (9). We used two ATPase assays to screen three small molecule libraries (a total of 43,400 compounds) at the University of Wisconsin Carbone Cancer Center. One assay utilized pyruvate kinase and lactic dehydrogenase as coupling enzymes, and phosphoenolpyruvate and NADH as their substrates, respectively. A solution of coupling enzymes, their substrates, Triton X-100 and MipZ were aliquoted (22.3  $\mu$ L per well) in 384-well black plates using Biomek FX liquid handler (Beckman Colter). Plates were briefly centrifuged to pull liquids to the bottom of the wells. We used pin tools to deliver 0.2  $\mu$ L of a stock solution of unique small molecules (10 mM in DMSO) from chemical libraries to each well. The first two columns of each plate were reserved for controls and did not receive compounds from the libraries. We then added a solution of ATP (2.5  $\mu$ L per well) using a Biotek Fill instrument to all wells except the first column for each plate to initiate ATP hydrolysis. Final concentrations of assay components are: 0.01% Triton X-100, 1 mM phosphoenolpyruvate, 0.3 mM NADH, 3 U/mL pyruvate kinase, 3 U/mL lactic dehydrogenase, 7.5  $\mu$ M MipZ, and 1 mM ATP in a buffered solution of 50 mM Tris-HCl, 50 mM KCl, and 10 mM MgCl<sub>2</sub>. We gently vortexed the plates to mix the solution and incubated for 3 h at 30 °C. After incubation, we measured the fluorescence emission from NADH using a Tecan Safire II plate reader ( $\lambda_{\text{ex}} = 340/35$  nm;  $\lambda_{\text{em}} = 460/10$  nm). Measurements of the fluorescence intensity from control wells were used to calculate the Z-factor; the minimum Z-factor for all plates was 0.7. We

used the coupling enzyme assay to screen compounds from Maybridge and Life Chemicals libraries. Compounds that inhibited  $\geq 60\%$  of ATP hydrolysis compared to the positive control were identified as hits and were screened using a secondary assay to eliminate compounds that target coupling enzymes. The secondary assay consisted of the same reaction components as the primary assay, except for the omission of MipZ and ATP. A solution of ADP was added instead. The fluorescence emission of compounds that did not inhibit coupling enzymes was measured at the specified wavelengths used for NADH, and the compounds were retested for their inhibitory effect on MipZ activity in vitro.

In addition to the coupling enzyme assay, we used a fluorescence polarization (FP) assay to monitor the ATPase activity of MipZ in vitro. Reaction conditions and component concentrations were same as the coupling enzyme assay unless noted otherwise. The FP assay utilized anti-ADP antibodies and Alexa633-labeled ADP. We purchased a Transcreener ADP<sup>2</sup> FP assay kit from BellBrook Labs (Madison, WI). A solution of MipZ was aliquoted (10  $\mu$ L per well) into plates, and addition of ATP (1  $\mu$ L of 5 mM stock solution per well) initiated the reaction. After 3 h, we added 10  $\mu$ L of ADP detection mix (541  $\mu$ g/mL of antibody) to each well, and incubated the plates for 1 h at 25 °C. We used the following wavelengths for FP measurements: 635 nm for excitation and 670/20 nm for emission. The Z-factor for the FP assay was  $\geq 0.7$ . The FP assay was used for screening compounds from the Life Chemicals library and the Spectrum Collection. Hits from the FP assay were tested for inhibition of the anti-ADP antibody by repeating the assay in the absence of MipZ, and checked for their intrinsic fluorescence at the specified wavelengths used for the Alexa633 probe.

***In vivo* screen with a *Caulobacter crescentus* strain that expresses MipZ-YFP.**

Hits from *in vitro* screens were tested for activity *in vivo*. We used a *C. crescentus* strain (MT97) that expresses *mipZ-yfp* from the native *mipZ* promoter. An overnight culture of MT97 was diluted to an absorbance ( $\lambda=600$  nm) of  $\sim 0.1$ ; the diluted culture was grown further for at least 1 h prior to compound treatment. Compounds were mixed with a solution of 1% agarose in M2G media(10) to achieve a final concentration of 20  $\mu$ M. We transferred cells (1  $\mu$ L per pad) on top of the compound-containing agarose pad, and imaged the cell morphology and localization of MipZ-YFP for a period of 24 h using epifluorescence microscopy. In between microscopic observations, we incubated the inoculated pads at 30 °C to promote growth.

***Nuclear magnetic resonance (NMR) spectroscopy.***

DCAP used in all experiments described in this manuscript was purchased from Ryan Scientific (catalog number F3255-0148, Mt. Pleasant, SC). We used a Varian MercuryPlus 300 MHz instrument (Magnetic Resonance Facility in the Chemistry Department of the University of Wisconsin-Madison) to obtain 1D  $^1\text{H}$  and  $^{13}\text{C}$  NMR spectra for DCAP at 25 °C. We also used a Bruker Avance III 500 MHz instrument (National Magnetic Resonance Facility at Madison) to collect 2D  $^{13}\text{C}$ -HMBC,  $^{15}\text{N}$ -HMBC, HSQC, COSY, and TOCSY spectra for DCAP structure verification. The solvent used was deuterated dimethyl sulfoxide. We analyzed the data using Sparky (T. D. Goddard and D. G. Kneller, University of California, San Francisco) and NUTS (Acorn NMR).

***High resolution electrospray ionization.***

We analyzed DCAP using high resolution electrospray ionization mass spectrometry in positive ion mode to determine the exact mass of the compound (Mass Spectrometry Facility, Department of Chemistry at the University of Wisconsin-Madison).

### ***Bacterial strains and growth conditions.***

Organisms and strains used in this study, their genotype, and relevant references are summarized in Table 1. We used Luria-Bertani (LB) media (10 g/L tryptone, 10 g/L NaCl, 5 g/L yeast extract, pH 7.2) to grow *Bacillus subtilis* 168, *Staphylococcus aureus* FRI100, *Pseudomonas aeruginosa* K1115, *Salmonella typhimurium*, *Vibrio cholera*, *Shigella boydii*, *Klebsiella pneumonia*, *Enterobacter aerogenes*, *Acinetobacter baumannii*, *Edwardsiella tarda*, and *Morganella morganii* strains. For *P. aeruginosa* PAO1 and K1119 strains and two *E. coli* BW25113 strains, we used M8 minimal media (241 mg/L MgSO<sub>4</sub>, 4 mg/L glucose, 5 mg/L casamino acids, 12.8 g/L Na<sub>2</sub>HPO<sub>4</sub> · 7H<sub>2</sub>O, 3 g/L KH<sub>2</sub>PO<sub>4</sub>, and 0.5 g/L NaCl). PYE media (2 g/L peptone, 1 g/L yeast extract, 0.8 mM MgSO<sub>4</sub>, and 0.5 mM CaCl<sub>2</sub>) was used for culturing *C. crescentus* cells at 30 °C. All cultures were grown at 37 °C, except for *C. crescentus* (30 °C). All cultures were grown while shaking at 200 rpm with the exception of clinical pathogens, which were statically incubated.

### ***Determination of the minimum inhibitory concentration (MIC) of bacterial growth.***

We determined the MIC of *E. coli*, *P. aeruginosa*, *B. subtilis*, and *C. crescentus* strains in liquid media using the macrodilution method according to the CLSI guidelines(11). For clinical pathogenic organisms including *S. aureus*, *S. typhimurium*, *V. cholera*, *S. boydii*, *K. pneumonia*, *E. aerogenes*, *A. baumannii*, *E. tarda*, and *M. morganii*

strains, we used 96-well microplates (100  $\mu$ L/well) and the microdilution method from the NCCLS guidelines(11).

***Determination of the minimum stationary-bactericidal concentration (MSC).***

We grew cultures of *C. crescentus* (24 h incubation) and *S. aureus* cells (5 d incubation) from single colonies. Cells were collected by centrifugation (5800 g for 2.5 min) and re-suspended in M2 salt solution (for *C. crescentus*; 1.74 g/L  $\text{Na}_2\text{HPO}_4$ , 1.06 g/L  $\text{KH}_2\text{PO}_4$ , and 0.5 g/L  $\text{NH}_4\text{Cl}$ ) or phosphate-buffered saline (for *S. aureus*; PBS, Fisher Scientific). The centrifugation and re-suspension was repeated two more times. After the repeated washing steps, we diluted the cell suspension 10-fold to achieve  $\sim 10^8$  cells/mL. We transferred aliquots of the diluted cell suspension into wells of a 96-well plate (100  $\mu$ L/well), and performed 2-fold serial dilutions to test a range of antibiotic concentrations. We sealed the plate with parafilm and incubated for 24 h at room temperature in the dark. After incubation, we took 50  $\mu$ L from each well to spread on nutrient agar plates (1.5 % agar in PYE for *C. crescentus*, and LB for *S. aureus*). We counted colonies on each plate after growing the cells for 1-2 days. For determining the kinetics of bactericidal activity of DCAP on stationary cultures, we diluted the washed cells by 100-fold in appropriate solutions and tested a single concentration of the compound while including a DMSO control sample. Cell suspensions were kept in closed microcentrifuge tubes instead of the wells of 96-well plates. We removed 100  $\mu$ L of the suspensions for plating at each time point. All MSC experiments were performed in static conditions.

***Determination of the minimum biofilm inhibitory concentration of growth (bMIC) and biofilm eradication concentration (MBEC).***

We grew overnight cultures of *C. crescentus* and *S. aureus*, and diluted them 100-fold into appropriate nutrient media. We transferred aliquots of the diluted suspension into wells of 96-well plates (150  $\mu\text{L}$ /well). We performed 2-fold serial dilutions for compound-containing wells. For every experiment, we included three replicates for each compound concentration tested. After transferring aliquots of the suspension, we closed the plate with specialized lids that have protruding pins (Nunc STP System), and sealed the plates using parafilm. We incubated plates in a static incubator at 30 °C (*C. crescentus*) or 37 °C (*S. aureus*) for 24 h. After cells had formed biofilms on the surface of the pins, we rinsed the pins by dipping them in M2 (*C. crescentus*) or PBS (*S. aureus*) solutions. To rinse the pins, we used clean, sterile 96-well plates (aliquots of 200  $\mu\text{L}$ /well); each rinse lasted 10 sec. After washing away planktonic cells loosely bound to biofilms, we inserted the pins into a 96-well plate that was pre-aliquoted with nutrient media containing antibiotics (2-fold dilutions, a final volume of 150  $\mu\text{L}$ /well). We sealed the plates with parafilm, incubated them for 17 h, and measured the bMIC at the end of the incubation by visual inspection. After the bMIC run, we repeated the rinse steps to remove planktonic cells, and inserted the pins into a 96-well plate that was pre-aliquoted with drug-free nutrient media (aliquots of 150  $\mu\text{L}$ /well). We sealed the plates with parafilm, incubated for 24 h, and measured the MBEC at the end of the incubation by visual inspection.

***Rabbit red blood cell (RBC) hemolysis assay.***

We used rabbit RBCs from Lampire Biological Laboratories. Prior to preparing the RBCs, we serially diluted compound-containing PBS solutions into a 96-well plate (a final volume of 100  $\mu$ L/well). We included the RBC lysis solution (Epicentre Biotechnology) as a positive control for hemolysis. For each assay, we removed 1 mL of the RBC suspension from the stock bottle and centrifuged the cells for 2 min at 2,000 rpm. We resuspended pelleted cells in sterile PBS solution and centrifuged again. We resuspended the cells in PBS and diluted them 5-fold into the same solution. We added 100  $\mu$ L aliquots of RBCs into wells of a 96-well plate that contained an equal volume of a solution of compound in PBS. We incubated the plates for varying amounts of time depending on the microbial assay conditions that we wanted to emulate. For MIC-like conditions, we incubated plates for at least 17 h at 30 °C or 37 °C. For MSC-like conditions, the incubation time was either 2 h or 6 h at 30 °C or 37 °C. During the incubation, un-lysed RBCs settled at the bottom of the wells. At the end of the incubation, we transferred 90  $\mu$ L of the supernatant into the wells of a fresh 96-well plate, and measured the absorbance of the heme at  $\lambda=405$  nm.

***Measurement of membrane potential using fluorescence microscopy and flow cytometry.***

We used the fluorescent probe, 3,3'-diethyloxacarbocyanine iodide (DiOC<sub>2</sub>) to measure  $\Delta\Psi$  in DMSO and in compound-treated cells. To eliminate the possibility of an interaction between the probe and compounds, we measured the fluorescence intensity of solutions of DiOC<sub>2</sub> in the presence and absence of the compounds, as described in Foss et al.,(12). For experiments with *B. subtilis* cells, we used the identical procedure

described by Foss et al., to prepare and label cells(12). We measured the fluorescence of these cells using a BD LSR II flow cytometer. We used the following instrument settings for detection: low flow rate, 488 nm excitation laser, 530/30 nm emission filter for green fluorescence, and 575/26 nm emission filter for red fluorescence. We used FlowJo software to analyze flow cytometry data. First we drew a gate around the region where cells were detected in the forward versus side scatter area plot. Gating enabled us to exclude any non-cellular materials in our sample that the instrument detected. We calculated the ratio of red-to-green fluorescence for each particle within the gate using the software and exported the data to GraphPad Prism. We used this graphing software to create box plots shown in Figure 6 and calculated the statistical parameters using one-way analysis of variation (GraphPad InStat).

For experiments with *C. crescentus* cells, we prepared the cells by diluting the overnight culture 10-fold into fresh PYE medium. The diluted culture was grown for 1 h at 200 rpm and 30 °C. We treated the cells with compounds for 10 min at room temperature, added DiOC<sub>2</sub> dye at a final concentration of 30 μM, and incubated for 10 min. After labeling, we transferred small aliquots (1-2 μL) of the suspensions of cells on 1% agarose pads for fluorescence microscopy. We used a Nikon Eclipse TE2000E inverted microscope with an Andor DU-895 EMCCD camera, a Perfect Focus system, and an encoded z-stage for phase contrast and epifluorescence microscopy. For detecting green and red fluorescence of the dye, we used the following wavelengths ( $\lambda_{\text{ex}}/\lambda_{\text{em}}$ ): 484/520 nm and 555/620 nm, respectively. We analyzed acquired images using the MATLAB-based script MicrobeTracker(13). Using this software, we segmented the area of individual cells in the phase contrast images. The segmentation

was applied to the fluorescence images to calculate the fluorescence intensity for individual cells. We wrote a separate MATLAB script to process the results from MicrobeTracker, in which we calculated the cell-area normalized ratio of red to green fluorescence for each cell. This data was exported to GraphPad Prism and GraphPad InStat for creating box plots and performing statistical analysis (one-way analysis of variation), respectively. All scripts we created for image analysis are available on our laboratory website (<https://www.weibellab.org>).

***Measurement of membrane permeability using fluorescence microscopy and flow cytometry.***

We used the DNA-binding probe, propidium iodide (PI) to measure the relative membrane permeability between DMSO, ethanol (50 % v/v for *C. crescentus* and 70 % v/v for *B. subtilis*) and compound-treated cells. To eliminate the possibility of an interaction between the fluorophore and small molecules, we measured the fluorescence intensity of solutions of PI in the presence and absence of the compounds, as described(12). For experiments with *B. subtilis* cells, we used the procedure previously described(12) to prepare and label the cells. We detected the fluorescence of *B. subtilis* cells using a BD LSR II flow cytometer. We used the following instrument settings for detection: low flow rate, 488 nm excitation laser, 610/20 nm emission filter. When using FlowJo to analyze the data, we excluded auto-fluorescence from cells from PI fluorescence. Other details for the analysis are identical to the description in the previous section.

For experiments with *C. crescentus* cells, we prepared the cells by diluting the overnight culture 10-fold into fresh PYE medium. The diluted culture was grown for 1-3

h at 200 rpm and 30 °C. We treated the cells with compounds for 10 min at room temperature, added PI at a final concentration of 20 µM, and incubated for 10 min. We imaged the cells and analyzed the data as described in the previous section.

*Measurement of protein localization using fluorescence microscopy and image analysis.*

For experiments with *C. crescentus* expressing MipZ-YFP, we diluted overnight cultures by 10-fold and incubated at least 1 h prior to treatment with compounds. After adding compounds, we incubated cells at 200 rpm and 30 °C for 20 min. We imaged the cells as described in the previous section. Following cell segmentation and fluorescence signal calculation in MicrobeTracker(13), we used a separate MATLAB script to detect signal peaks within an individual cell. We catalogued the number of total peaks and peak locations (i.e. poles or mid-cell) for each cell. Poles were defined as 1-25% and 75-100% along the normalized cell length (1-100 %). We classified cells as ‘wildtype’ if its catalogued information agreed with one of the following criteria: 1) MipZ-YFP was unipolar, meaning there was one peak and the peak resides within a pole region; and 2) MipZ-YFP was bipolar, meaning there were two peaks and both peaks are within a polar region. After this classification, we created a contingency table with the total number of cells analyzed, and the number of cells with the ‘wildtype’ localization. Using InStat program, we applied the Fisher’s exact test to calculate two-sided p-values between DMSO and compound-treated cells.

For experiments with *C. crescentus* expressing Venus-FtsA, we used a synchronized population of cells. First we grew an overnight culture with kanamycin (5

$\mu\text{g}/\text{mL}$ ) and glucose (0.02 % w/v). The presence of glucose suppressed the transcription of *venus-ftsA* from its xylose-inducible promoter. We diluted 2 mL of this culture into 25 mL of fresh PYE with the antibiotic and glucose, and incubated further to achieve an absorbance of  $\sim 0.6$  ( $\lambda=600$  nm). Once the cells reached mid-exponential phase, we centrifuged the culture for 10 min at 5,400 g and 4 °C. We resuspended the cell pellet in ice-cold M2 (a final volume of  $\sim 1000$   $\mu\text{L}$ ) and added 750  $\mu\text{L}$  of this suspension to an equal-volume of sterile Percol (Sigma Aldrich). After thoroughly mixing the solution, we centrifuged it for 20 min at 9,800 g and 4 °C. Upon centrifugation, we took the bottom band (swarmer cells) and washed the cells in ice-chilled M2 solution (1 mL). The washed cell pellet was suspended in fresh PYE containing kanamycin (no glucose, 6 mL). We incubated the cell suspension for 20 min and then added xylose (0.03 % w/v) to induce the expression of *venus-ftsA*. Cells were grown for another 20 min and subsequently treated with compounds. We incubated cells for 20 min again in the presence of the compounds prior to imaging. Thus, the total time of xylose induction was 40 min, and the total time of compound treatment was 20 min. At this time point (60 min post synchrony), the majority of the cells were at the beginning of cell division. Imaging conditions and data analysis were identical to the conditions described for MipZ-YFP, except for a set of criteria used for defining 'wildtype' protein localization. We defined 'wildtype' as 1) Venus-FtsA is unipolar, meaning there was one peak, and the peak resided within a polar region; and 2) Venus-FtsA was at the mid-cell, meaning there was one peak and it was within the mid-cell region (40-60 % of the normalized cell length).

We performed protein localization experiments with *B. subtilis* expressing GFP-MinD, as described previously(12). Imaging conditions and data analysis were identical to those described for MipZ-YFP, except for the definition of poles, and a set of criteria used for defining 'wildtype' protein localization. We defined 'wildtype' as 1) GFP-MinD was bipolar, meaning there were two peaks, and both peaks were at the poles (1-20% and 80-100% of the normalized cell length); 2) GFP-MinD was at the mid-cell in addition to the bipolar localization, meaning there were three peaks with two of them at the poles and one at mid-cell; and 3) GFP-MinD was at a quaternary position (20-40% and 60-80% of the normalized cell length) in addition to the bipolar and mid-cell localization (the total number of peaks was 4 if there is one quaternary peak, and the total was 5 if there are two quaternary peaks). Because *B. subtilis* cells can initiate division prior to finishing an earlier division and the completion of septation, we found that these normal cells have peaks at quaternary positions. Any cells that did not fit these criteria were categorized as non-wildtype.

#### ***Mammalian cell viability assay.***

We measured the cytotoxicity of small molecules on human epithelial kidney (HEK) cells by using the CellTiter-Glo Luminescent Cell Viability Assay from Promega (Madison, WI). The HEK cells (293T/17; ATCC number CRL-11268) were grown in 10% heat-inactivated fetal bovine serum in Dulbecco's modified Eagle medium, supplemented with penicillin and streptomycin. Cultures were incubated in an atmosphere of 5% CO<sub>2</sub> at 37°C. To seed cells into 96-well microplates, we suspended the HEK cells in media (5 x 10<sup>4</sup> cells/mL) and aliquoted 200 μL of the suspension to each well (1 x 10<sup>4</sup> cells/well). For each condition tested, we included three replicates. Cells

were incubated in the wells of plates (white, flat-bottom, sterile, and tissue-culture treated from Nunc) for 24-30 hrs prior to treatment with small molecules. For 2-hr compound treatments, the final concentration of DMSO was 0.5 % v/v or less. For longer incubations of cells with compounds, the concentration of DMSO was 0.16% v/v or less to minimize cell death in the DMSO solvent control samples. Stock solutions of compounds in DMSO were diluted in fresh growth media to their final concentrations and then added to microplate wells (100  $\mu$ L/well). Since the growth media containing small molecules contained different amounts of DMSO, we created a separate DMSO solvent control for each compound concentration that we tested. We later used data from these DMSO controls to normalize the values from compound-treated cells. Control wells without any small molecules or solvent received fresh medium so that all wells contained fresh media dosed with or without small molecules. During the treatment of cells with compounds, cells were kept at 37 °C except the last 30 min of the incubation. Plates and CellTiter-Glo reagent were left out on the bench during this 30-min period to equilibrate to 25 °C. At the end of compound treatment, we added CellTiter-Glo solution to wells (100  $\mu$ L of reagent/well; final volume in each well was 200  $\mu$ L), and mixed the contents by pipetting. To ensure complete cell lysis, plates were shaken for 2 min using the orbital and linear shaking programs (6 mm amplitude; 1 min of each program) in a Tecan M1000 microplate reader. We incubated the plates for 10 min at 25 °C and measured the luminescence using the microplate reader.

***Measurement of mitochondrial  $\Delta\Psi$  in mammalian cells.***

We measured the mitochondrial  $\Delta\Psi$  in HEK cells in the presence of small molecules. We prepared HEK cells using an identical procedure described earlier, except black 96-well microplates with clear bottoms were used in this assay. At the end of compound treatment, we aliquoted a solution of DiOC<sub>2</sub> in growth media (50 nM) into each well, and incubated the plates for 30 min at 37 °C. After the incubation, we washed the cells once with 1x PBS solution. We measured the fluorescence of DiOC<sub>2</sub> using a Tecan M1000 microplate reader with the following instrument settings: for green fluorescence,  $\lambda=488\pm 5$  and  $530\pm 5$  nm for excitation and emission, respectively, with a gain of 200. For red fluorescence,  $\lambda= 590\pm 5$  and  $615\pm 5$  nm for excitation and emission, respectively, with a gain of 255. Other settings include 50 flashes at 400 Hz with an integration time of 20  $\mu$ s and the z-position of 20,000  $\mu$ m. After acquiring the fluorescence intensities, we calculated the ratio of green-to-red fluorescence for each sample. Ratio values from compound-treated samples were normalized against data from DMSO-treated controls.

## RESULTS AND DISCUSSION

In this chapter, we describe the discovery and characterization of a new compound that specifically targets the membranes of both Gram-positive and Gram-negative bacteria. For brevity, we refer to this compound, (2-((3-(3,6-dichloro-9H-carbazol-9-yl)-2-hydroxypropyl)amino)-2-(hydroxymethyl)propane-1,3-diol), as DCAP (Figure 1; its characterization is described in Figures 2 and 3). We identified DCAP via a high-throughput inhibitor screen of the *in vitro* activity of MipZ, which is an ATPase that regulates division site placement in *Caulobacter crescentus*(9). Using a strain of *C. crescentus* in which MipZ was translationally fused to yellow fluorescent protein (YFP), we found that the treatment of cells with DCAP (20  $\mu\text{M}$ ) caused MipZ-YFP to mislocalize (Figure 4). At high concentrations of DCAP ( $\geq 75 \mu\text{M}$ ), we observed cell lysis within minutes after treatment (Figure 5). This observation suggested to us that DCAP might not specifically inhibit MipZ in the cell but instead alter the properties of the cell envelope.

To test this hypothesis, we measured  $\Delta\Psi$  of two model bacteria, *C. crescentus* (Gram-negative) and *Bacillus subtilis* (Gram-positive), in the absence and presence of DCAP. As a positive control, we used carbonyl cyanide m-chlorophenyl hydrazone (CCCP). Hydrophobic weak acids such as CCCP transport protons and other cations across the membrane and decrease  $\Delta\Psi$  (14). CCCP dissolves into the lipid bilayer, and the acidic form associates with a cation near a leaflet of the membrane. The neutral complex moves to the other leaflet and dissociates to release the cation. After dissociation of the complex, the ionophore becomes available to bind to another cation

and transport it across the membrane(15). This increased permeability to ions dissipates  $\Delta\Psi$ . To visualize changes in the membrane potential, we used the fluorescent probe 3,3'-diethyloxacarbocyanine iodide (DiOC<sub>2</sub>). DiOC<sub>2</sub> emits green fluorescence ( $\lambda=530$  nm) in the monomeric form, and its fluorescence emission maximum is red-shifted ( $\lambda=576$  nm) upon self-association (16). Molecules of DiOC<sub>2</sub> located inside cells reside either in the membrane or the cytoplasm. In the presence of a large  $\Delta\Psi$ , the number of positively-charged molecules of DiOC<sub>2</sub> partitioned in the cytoplasm is greater than the number of molecules at the membrane(17). The high local concentration in the cytoplasm causes DiOC<sub>2</sub> to aggregate and increase the ratio of fluorescent light emitted at  $\lambda_{576}/\lambda_{530}$ . Conversely,  $\lambda_{576}/\lambda_{530}$  decreases when  $\Delta\Psi$  is dissipated in bacteria(16). Figure 6A and B illustrates  $\lambda_{576}/\lambda_{530}$  for cells treated with small molecules. A significant decrease in  $\lambda_{576}/\lambda_{530}$  was apparent after 20 min of treatment with CCCP and DCAP ( $p < 0.001$ ) and indicated that  $\Delta\Psi$  dissipated rapidly. Antibiotics that do not target the bacterial membrane can decrease the potential over a long period of exposure (e.g. 3 - 4 h) (18); however, the rapid action of DCAP suggests that the dissipation in  $\Delta\Psi$  is due to its direct effect on the inner membrane.

Next we explored the mechanism of action of DCAP. One possibility is that it functions as an ionophore similar to CCCP. Alternatively, it may increase the general permeability of the membrane. To investigate the mechanism, we used propidium iodide (PI) to label the DNA of cells with compromised membranes(16). As shown in Figure 6C and D, we observed that ethanol-treated cells were intensely labeled with PI, while the DMSO control sample was not. Treating cells with CCCP did not increase DNA labeling with PI; the fluorescence emission of these cells was similar to the DMSO

sample. Addition of DCAP to cells increased the fluorescence of cells labeled with PI, although the intensity was significantly lower than the ethanol-treated cells ( $P < 0.001$ ). These results suggest that DCAP has at least two mechanisms of antimicrobial action: it decreases  $\Delta\Psi$  by facilitating ion transport across the membrane and has a minor effect on the general permeability of the lipid bilayer. The bioactivity of DCAP may arise from its direct association with bacterial lipids or proteins in the membrane.

$\Delta\Psi$  was identified recently as an important parameter for the in vivo localization of division proteins associated with the bacterial membrane, including MinD and FtsA(19). We found that the treatment of *B. subtilis* cells with either CCCP or DCAP altered the localization of a fusion of green fluorescent protein to MinD (GFP-MinD) compared to DMSO-treated cells (Figure 7A). MinD localizes to the poles of *B. subtilis* cells and guides division plane formation at the mid-cell. As division progresses, MinD accumulates at the mid-cell and marks the sites of future cell poles(19). Treating *B. subtilis* cells expressing GFP-MinD with CCCP increased diffuse fluorescence throughout the cell but had little effect on the location of the signal compared to the DMSO control (Figure 8A). In DCAP-treated cells, GFP-MinD mislocalized—the number of fluorescent foci increased in some cells while in others the fluorescence signal became more diffuse and was no longer concentrated at the poles (Figure 8A).

In addition to perturbing the localization of MinD in *B. subtilis*, CCCP and DCAP influenced the distribution of FtsA in *C. crescentus* (Figure 7B). FtsA is a peripheral membrane protein that interacts with FtsZ and activates the recruitment of downstream division proteins(20). FtsA resides at one pole (the pole opposite to the stalk) in non-dividing *C. crescentus* cells and is recruited to the mid-cell as division begins(20). To study cells at this stage of division, we synchronized cells that express a fluorescent

fusion of the protein Venus-FtsA and treated them with CCCP and DCAP. Treatment of *C. crescentus* cells with CCCP at its minimum inhibitory concentration (5  $\mu$ M) did not alter the localization of FtsA; however, a higher concentration of CCCP (25  $\mu$ M) had a significant effect on the position of FtsA. Most cells treated with DCAP exhibited multiple peaks of FtsA fluorescence ( $\geq 2$ ) instead of a single peak — either at the pole or mid-cell — observed in untreated cells (Figure 8B). The observation that DCAP causes mislocalization of membrane proteins in *B. subtilis* and *C. crescentus* is consistent with the hypothesis that the compound decreases  $\Delta\Psi$ . The effect of DCAP was similar to the ionophore CCCP; however, DCAP causes more severe protein mislocalization at its MIC, which may arise from its influence on membrane permeability.

After confirming the membrane-targeting activity of DCAP, we tested the efficacy of DCAP against other bacterial species. Table 2 demonstrates that DCAP inhibits the growth of *Escherichia coli*, *Pseudomonas aeruginosa*, and other clinical pathogens. We observed that deleting one or more efflux pumps in *E. coli* and *P. aeruginosa* strains increased the sensitivity of cells to DCAP. Efflux pumps are active against a broad range of compounds and typically consist of three components: two transmembrane proteins, one in the inner and the other in the outer membrane, and a periplasmic protein that connects the two transmembrane components(21). Deleting *tolC* in *E. coli* strain BW25113 eliminated a critical component of an efflux pump that is embedded in the outer membrane(22) and reduced the MIC of DCAP by 4-fold. This result suggests that the activity of DCAP in Gram-negative bacteria is largely due to its effect on the inner membrane.

In addition to its activity against actively growing bacteria, DCAP kills cells in stationary phase (Table 3). We tested this property of DCAP against *C. crescentus* and *S. aureus*. We used *S. aureus* as a model Gram-positive bacterium rather than *B. subtilis* for these experiments, as *B. subtilis* can sporulate under starvation conditions and does not form robust biofilms on the plastic surfaces we used as substrates. To ensure that bacteria were deprived of nutrients, we grew the cells to late stationary phase and suspended them in isotonic solutions lacking amino acids or sugars. After treating cells with small molecules, we measured cell viability over time by plating culture aliquots on non-selective, solid growth media. We designated the minimum concentration of antibiotic required to completely eliminate colony formation as the minimum stationary-bactericidal concentration (MSC)(23). To test whether membrane-targeting drugs have a greater efficiency in killing cells that grow slowly, we compared the MSC of membrane-active drugs (CCCP and DCAP) with ampicillin, which is only lethal to cells that are actively growing. We found that the MSC and MIC of DCAP for each organism were similar while the efficacy of ampicillin was significantly reduced for stationary cells of both organisms (Table 3). The MSC of ampicillin for *S. aureus* was 1000-fold higher than its MIC, while the MSC of ampicillin for *C. crescentus* was beyond the range of our measurements. CCCP inhibited the proliferation of *C. crescentus* cells regardless of their physiological status. However, the MSC of CCCP for *S. aureus* was > 300-fold higher than the MIC. This dramatic decrease in the effectiveness of CCCP in *S. aureus* may be due to changes in membrane composition as cells adjust their metabolism in nutrient-deprived conditions(24). Overall, membrane-active CCCP and DCAP were more effective in killing stationary cells than ampicillin whose mechanism of action is more specific towards cells with robust growth.

We found that membrane-active compounds are also efficient at eradicating biofilm-associated cells (Table 3). Biofilms are implicated in a wide range of human diseases, including cystic fibrosis and urinary tract infection, and are particularly recalcitrant to antibiotics(25). The heterogeneity in the physiology of cells in biofilms makes it possible for the bacterial communities to persist in stressful conditions(26). To determine the efficacy of antibiotics against biofilms, we adopted protocols for measuring the minimum biofilm inhibitory concentration (bMIC) and the minimum biofilm eradication concentration (MBEC)(27). First, we formed biofilms on the surface of 96 individual plastic pins that protruded into the 96 wells of a microplate. The biofilms were exposed to compounds for 24 hrs, and we determined the lowest concentration of antibiotic that inhibited planktonic cell growth in the wells (bMIC). Since bMIC is a measurement of the rapid growth of freely suspended cells released from biofilms in the presence of antibiotics, the bMIC and MIC values did not differ significantly (Table 3).

After performing bMIC experiments, we transferred biofilms growing on the pins of the lid to nutrient media devoid of antibiotics to measure the minimum concentration of antibiotic that prevented planktonic growth from biofilms in antibiotic-free nutrient media (MBEC). MBEC indicates whether the exposure to antimicrobial agent used during the bMIC experiment sterilized biofilm-associated cells. MBEC values were generally larger than MICs and indicated an increased tolerance of stress exhibited by cells associated with biofilms.

For *C. crescentus*, the MBEC values recapitulated the trend we observed in the MSC: CCCP and DCAP effectively eradicated biofilm cells while ampicillin was not cytotoxic at the highest concentration tested (400  $\mu$ M). CCCP was the only effective

antibiotic against *S. aureus* biofilms. Since CCCP was not as effective as DCAP at killing stationary *S. aureus* cells, we suspect that this variability in efficacy of membrane-active drugs is caused, in part, by changes in membrane composition (i.e. membrane proteins and lipid content) at different developmental stages of bacterial cells(24). Despite the variations in efficacy, we conclude that the comparison of MIC, bMIC, MSC, and MBEC measurements for the three antibiotics support the hypothesis that membrane-active drugs eradicate slow-growing bacteria more effectively than antibiotics that rely on growth-dependent mechanisms.

To test the toxicity of DCAP against mammalian membranes, we measured the hemolysis of rabbit red blood cells (RBC). We performed these experiments using conditions that closely mimicked the MIC and MSC assays. We treated RBCs with CCCP and DCAP at their MICs for the time periods used (17 h) to determine the MIC of *C. crescentus* and *S. aureus*. After incubation, we measured the absorbance of heme released from lysed RBCs. We found that the MIC concentrations of CCCP and DCAP did not significantly disrupt RBC membranes (Figure 9A) although higher concentrations of DCAP (i.e., 50  $\mu$ M) were moderately toxic to RBCs.

We also reproduced the MSC assay conditions to measure toxicity against RBCs. First we determined the minimum time required to obtain the MSC for DCAP treatment of *C. crescentus* (2 h) and *S. aureus* (6 h; data not shown). Using these times, we performed the hemolysis assay and observed no significant toxicity of DCAP against RBCs (Figure 9B and C). In contrast, CCCP was toxic to RBCs at a high concentration (Figure 9C). These measurements indicate that DCAP does not appreciably perturb RBC membranes in conditions that are lethal to *C. crescentus* and *S. aureus*.

In addition to measuring the toxicity of membrane-active drugs on RBCs, we tested whether DCAP and CCCP dissipated  $\Delta\Psi$  of mitochondria in mammalian cells. We used human epithelial kidney (HEK) cells as a model tissue culture cell line. Similar to the bacterial assays, we used DiOC<sub>2</sub> to probe the changes in  $\Delta\Psi$  in the presence of the compounds. As shown in Figure 10, we found that DCAP and CCCP slowly depolarized the mitochondrial  $\Delta\Psi$  in HEK cells. The efficiency of  $\Delta\Psi$  dissipation was lower in mitochondria compared to bacterial cells: treatment with DCAP and CCCP resulted in approximately 10-fold decrease in bacterial  $\Delta\Psi$  within 20 min (when comparing median values in Figure 6A and B) while the compounds reduced the mitochondrial  $\Delta\Psi$  by 2-fold (the first data point in Figure 10).

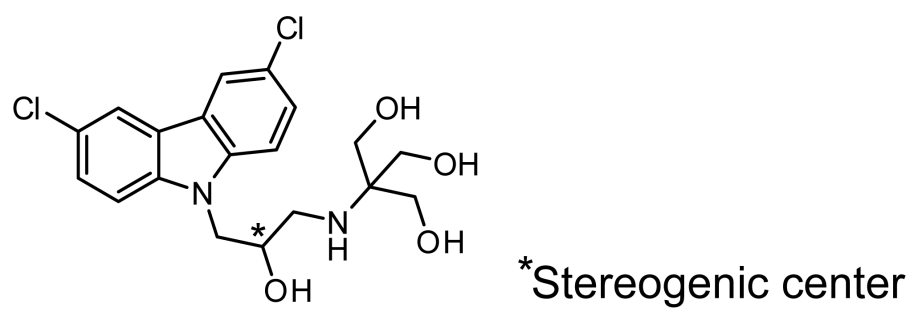
This eventual decrease of mitochondrial  $\Delta\Psi$  in HEK cells prompted us to investigate the viability of these cells when treated with DCAP and CCCP. We observed that the viability of HEK cells was minimally perturbed at short time intervals following treatment (2 h, Figure 11) while longer incubations decreased cell viability. As both CCCP and DCAP were similar in their ability to dissipate the mitochondrial  $\Delta\Psi$  in these cells, we speculate that the toxicity of DCAP on HEK cells may not be caused by its effect on the mitochondrial  $\Delta\Psi$ . We plan to investigate the basis of this toxicity of DCAP in future studies.

## CONCLUSION

In summary, we report the discovery and characterization of a membrane-active antimicrobial agent, DCAP. DCAP kills bacteria by depolarizing  $\Delta\Psi$  and increasing membrane permeability. These activities of the compound disrupt the organization and integrity of the bacterial membrane and mislocalize essential membrane-associated proteins (e.g. MinD and FtsA). DCAP is inert to membranes of red blood cells at concentrations at which it is a potent antibacterial agent. However, DCAP slowly reduces the mitochondrial  $\Delta\Psi$  and becomes toxic to HEK cells. We plan to address the cytotoxicity of DCAP on mammalian cells by synthesizing and testing analogs. Furthermore, studies with DCAP analogs may provide insight into changes in the properties of membranes during the life cycle of bacteria and make it possible to correlate alterations in cell physiology with the vulnerability of cells to membrane-active drugs. Finally, studies of the structure-function relationship of DCAP and other broad-spectrum compounds may provide design rules for potent membrane-targeting drugs that kill bacterial cells specifically.

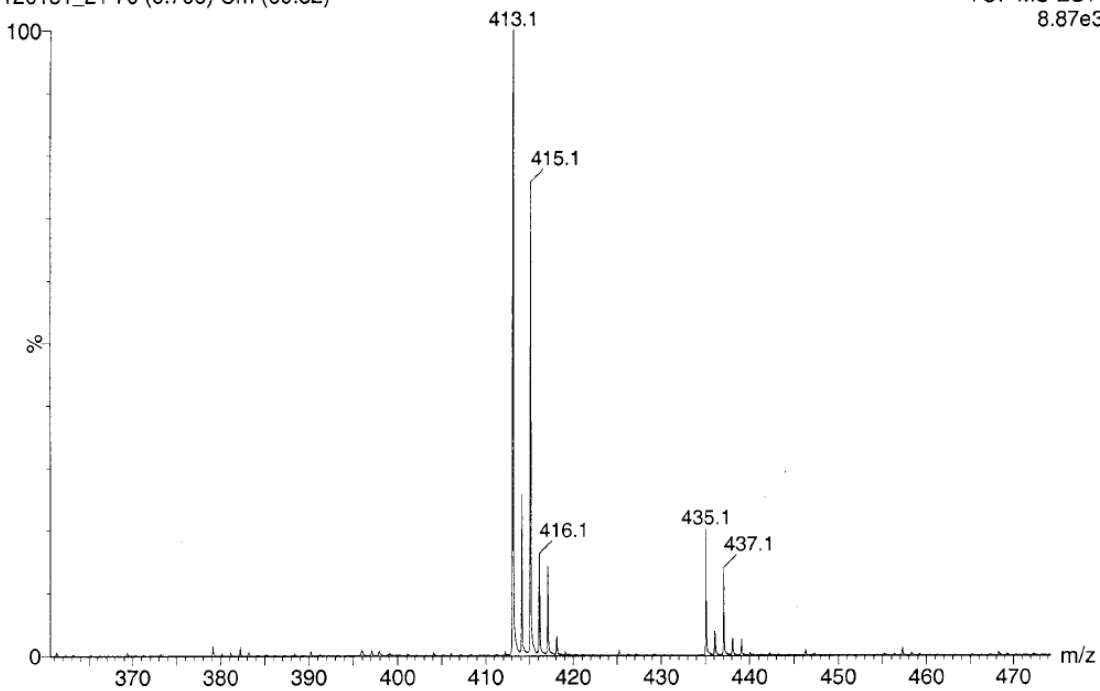
## ACKNOWLEDGMENTS

We thank Keith Poole for *P. aeruginosa* strains and Laura Kiessling for the human epithelial kidney cell line. D.B.W. and M.T. acknowledge the Human Frontiers Science Program (RGY0069/2008-C103). D.B.W also acknowledges the NIH (1DP2OD008735-01) and the Alfred P. Sloan research foundation for financial support of this research. M. T. also acknowledges the LOEWE Center for Synthetic Microbiology (SYNMIKRO).

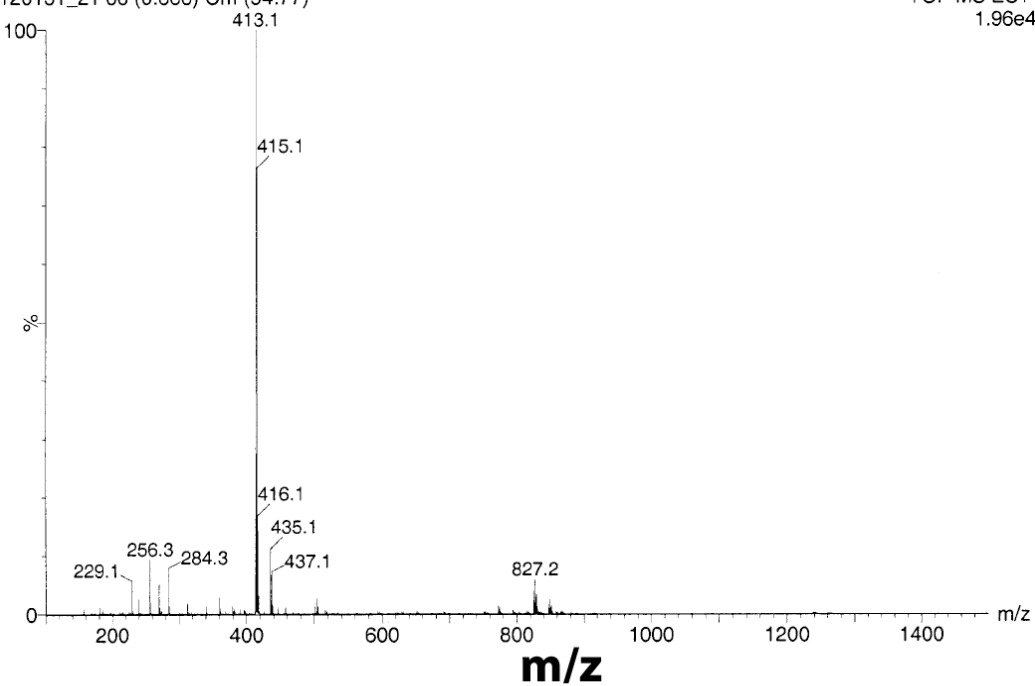


**Figure 1.** Chemical structure of DCAP.

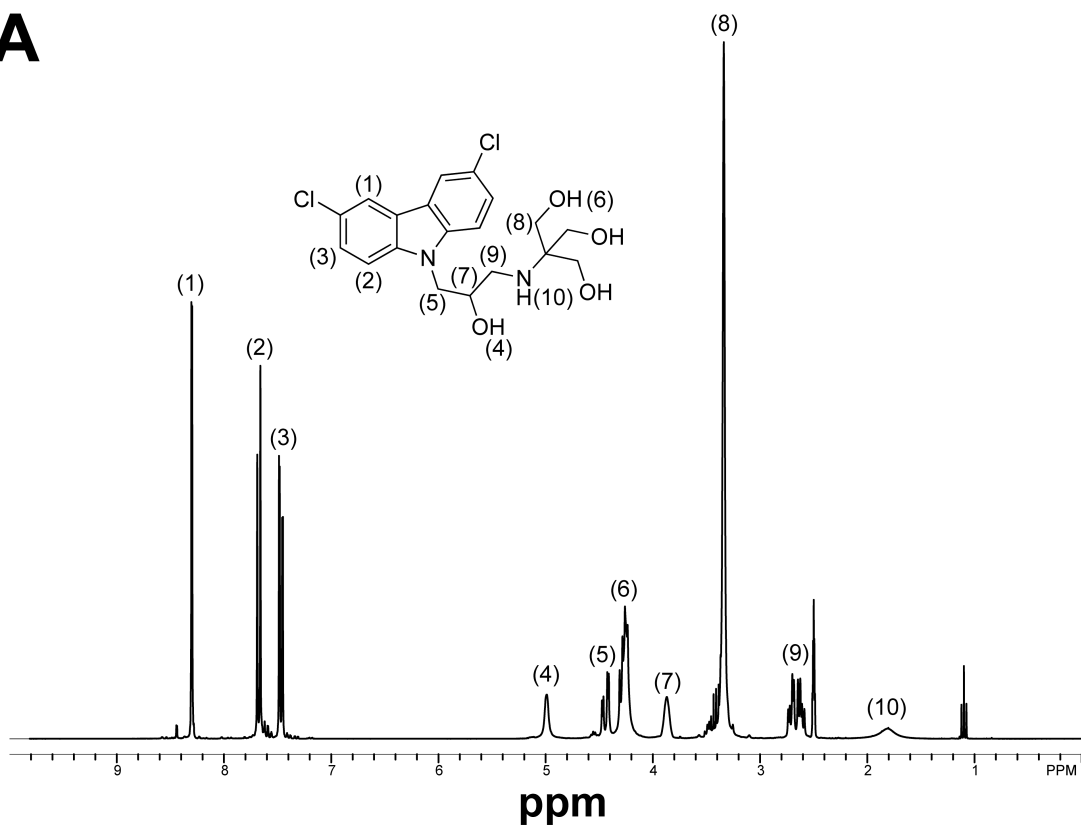
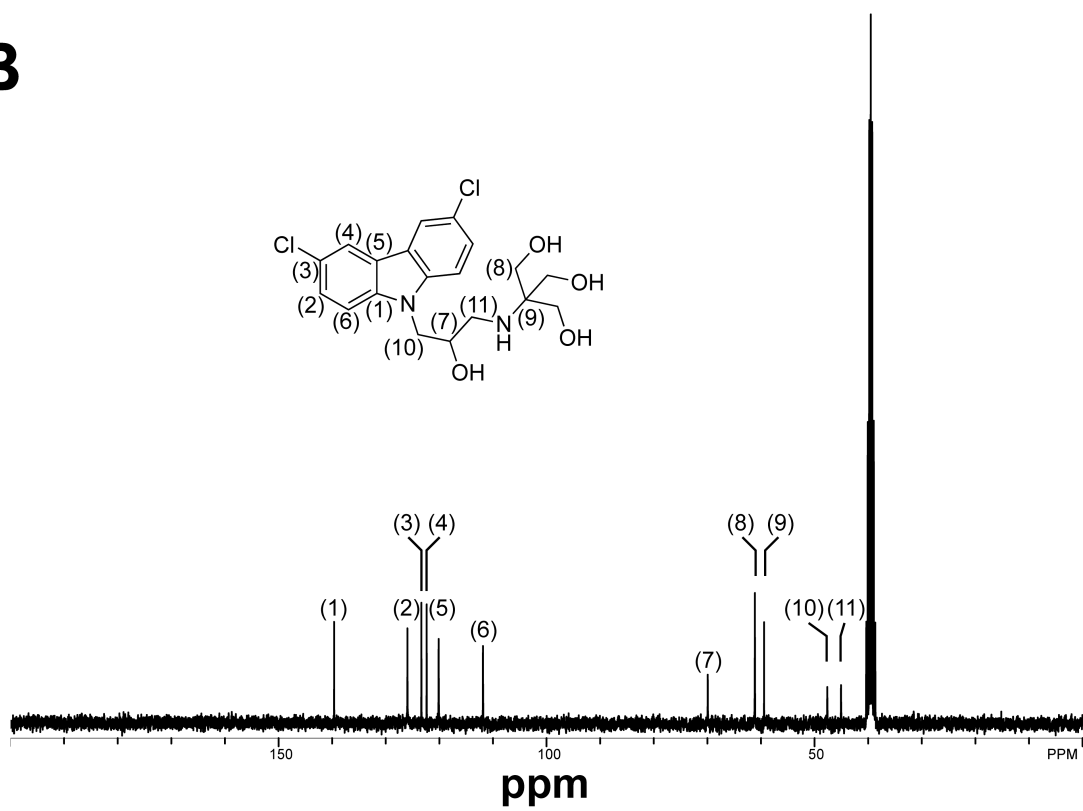
120131\_21 70 (0.706) Cm (69:82)

TOF MS ES+  
8.87e3

120131\_21 66 (0.666) Cm (54:77)

TOF MS ES+  
1.96e4

**Figure 2.** Low-resolution electrospray ionization mass spectra. High-resolution data: expected mass was  $(M+H)^+ = 413.0952$  and  $(M+Na)^+ = 435.0849$ ; observed mass was 435.0832.

**A****B**

**Figure 3.** NMR spectra of DCAP. (A)  $^1\text{H}$  NMR spectrum.  $^1\text{H}$  NMR (299.7 MHz, DMSO)  $\delta$  8.30 (d,  $J = 2.1$  Hz, 2H), 7.68 (d,  $J = 8.8$  Hz, 2H), 7.47 (dd,  $J = 8.8, 2.2$  Hz, 2H), 4.99 (s, 1H), 4.44 (dd,  $J = 14.8, 4.0$  Hz, 2H), 4.27 (m, 3H), 3.87 (s, 1H), 3.34 (s, 6H), 2.67 (m, 2H), 1.81 (s, 1H). (B)  $^{13}\text{C}$  NMR spectrum.  $^{13}\text{C}$  NMR (75.4 MHz, DMSO)  $\delta$  139.6, 126.0, 123.4, 122.4, 120.1, 111.9, 70.0, 61.2, 59.4, 47.6, 45.1

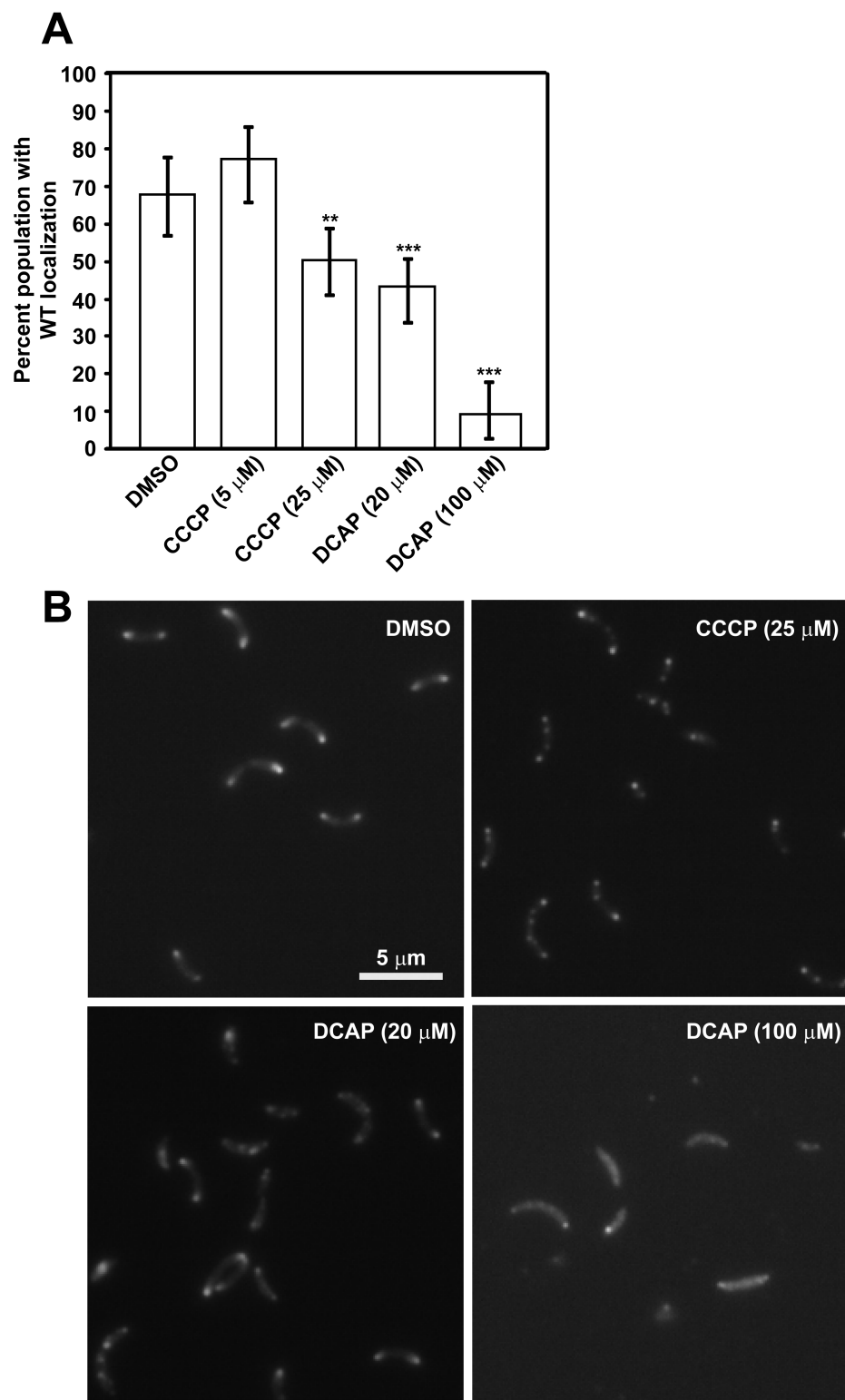


**Figure 4.** Analysis of MipZ-YFP localization. (A) We defined 'wildtype' (WT) localization as 1) unipolar (a single peak of fluorescence signal at a pole) and 2) bipolar (two peaks at poles). All images were acquired 20 min after treating cells with compounds. At least 69 cells were analyzed for each sample. We calculated two-sided p-values using Fisher's exact test in comparison to DMSO:  $p = 0.0075$  (\*\*) for 25  $\mu\text{M}$  of CCCP,  $p = 0.0002$  (\*\*\*) for 20  $\mu\text{M}$  of DCAP, and  $p < 0.0001$  (\*\*\*) for 100  $\mu\text{M}$  of DCAP. (B) Representative fluorescence images of *C. crescentus* cells expressing MipZ-YFP.

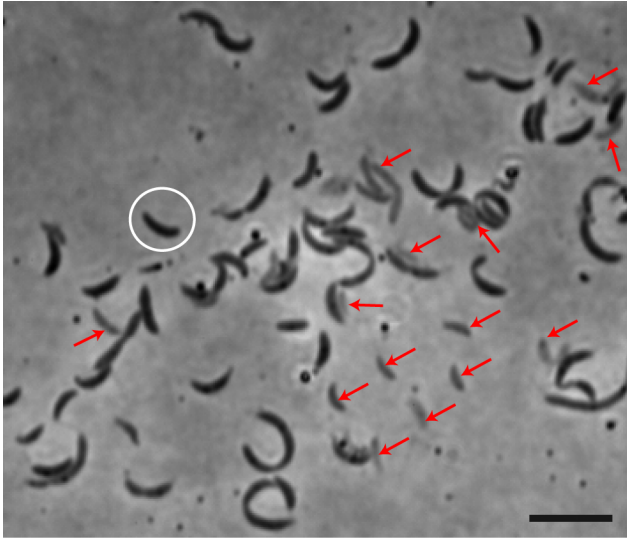


**Figure 5.** *C. crescentus* cells 20-min after treatment with DCAP (100  $\mu$ M). We observed cell lysis in the population (cells with red arrows). The lysed cells look fainter in phase contrast images, compared to cells that did not lyse (e.g. a cell in the white circle). Scale bar, 5  $\mu$ m.

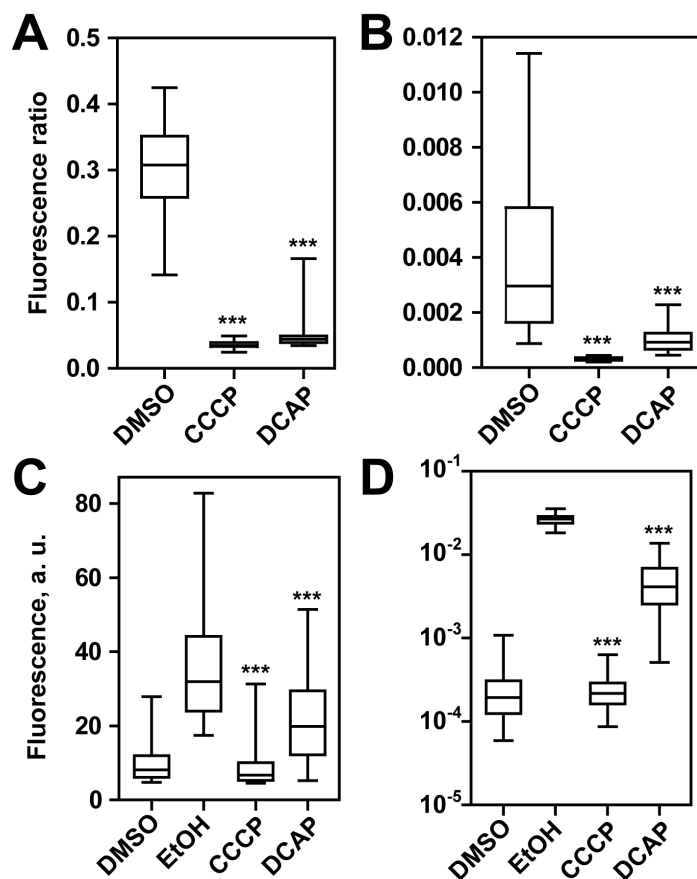


**Figure 6.** (A, B) Measurement of  $\Delta\Psi$  using DiOC<sub>2</sub>. A) *B. subtilis* (n ≥ 8,964 cells). B) *C. crescentus* (n ≥ 158 cells). We calculated *p*-values by comparing data against the DMSO sample. (C, D) Measurement of membrane permeability using PI C) *B. subtilis* (n ≥ 2,546 cells). D) *C. crescentus* (n ≥ 35 cells). We calculated *p*-values by comparing data against the EtOH sample. In box plots, the top whisker represents 95%, the bottom whisker is 5%, the top of the box is 75%, the bottom of the box is 25%, and the line inside the box indicates the median of each sample population. Three asterisks (\*\*\*) refers to *p* < 0.001.

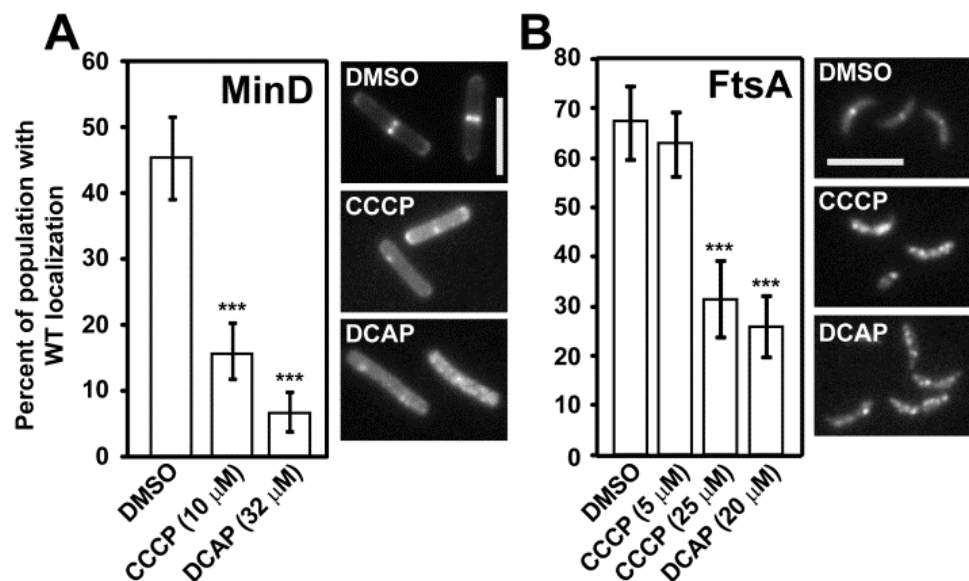


**Figure 7.** Analysis of membrane protein localization in bacteria ( $p < 0.0001 = ***$ , compared to DMSO). Error bars represent the 95% confidence interval of percentages reported. Representative images for each sample are shown (scale bar,  $5\mu\text{m}$ ). (A) GFP-MinD in *B. subtilis* ( $n \geq 252$  cells) and (B) Venus-FtsA in *C. crescentus* ( $n \geq 150$  cells). The middle image shows cells from the treatment with  $25\mu\text{M}$  CCCP.

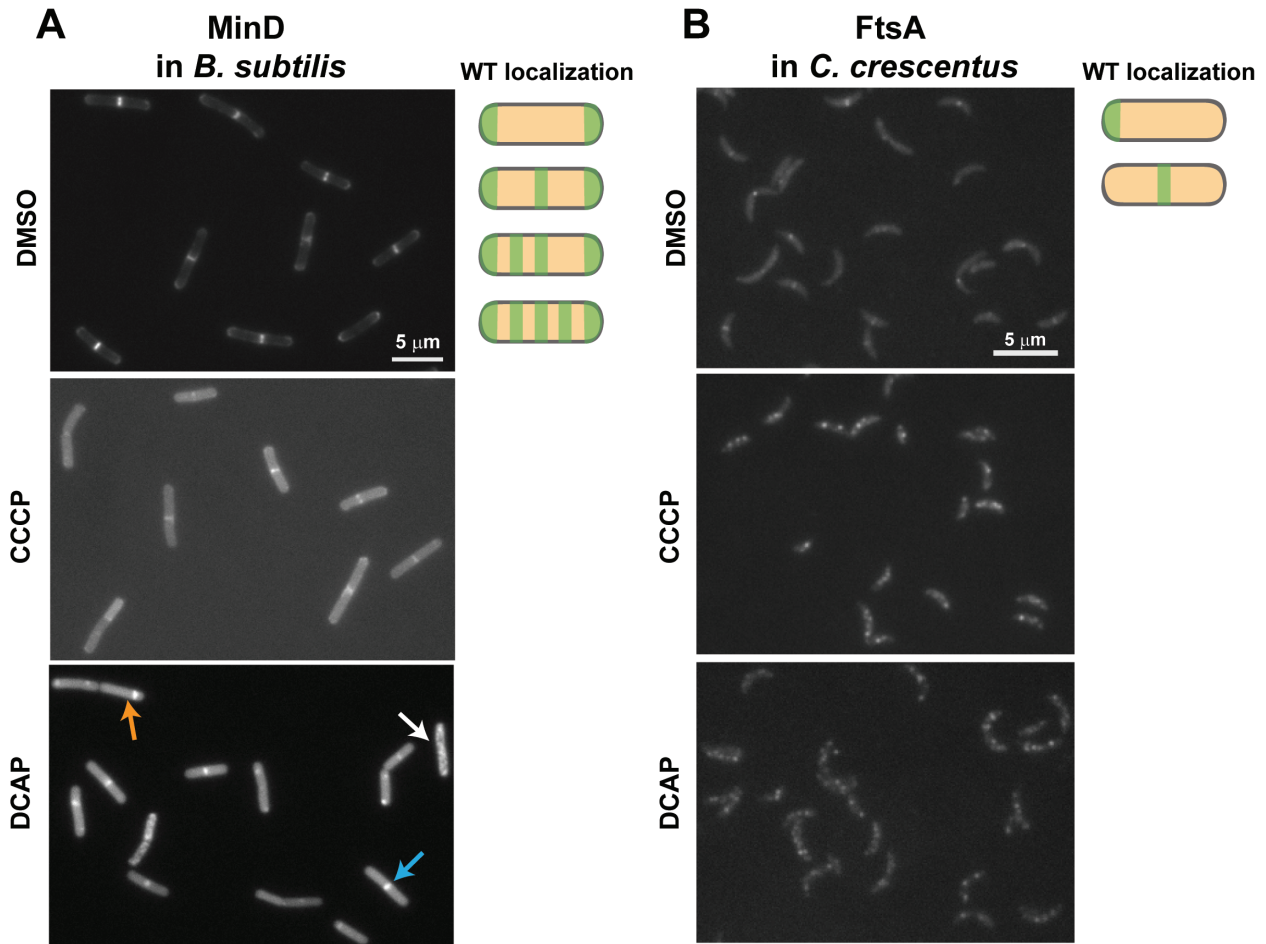


**Figure 8.** Representative fluorescence images of cells treated with DMSO, CCCP, or DCAP for 20 min. To the right of images, cartoons of bacterial cells depict different wildtype (WT) localizations for MinD and FtsA. (A) *B. subtilis* cells expressing GFP-MinD. The DCAP image shows cells with a few peaks mis-localized to random locations in the cell (orange arrows), cells that contain a large number of fluorescent peaks (white arrows), and cells with diffused fluorescence signal throughout the cell and no polar localizations (blue arrows). (B) *C. crescentus* cells expressing Venus-FtsA.

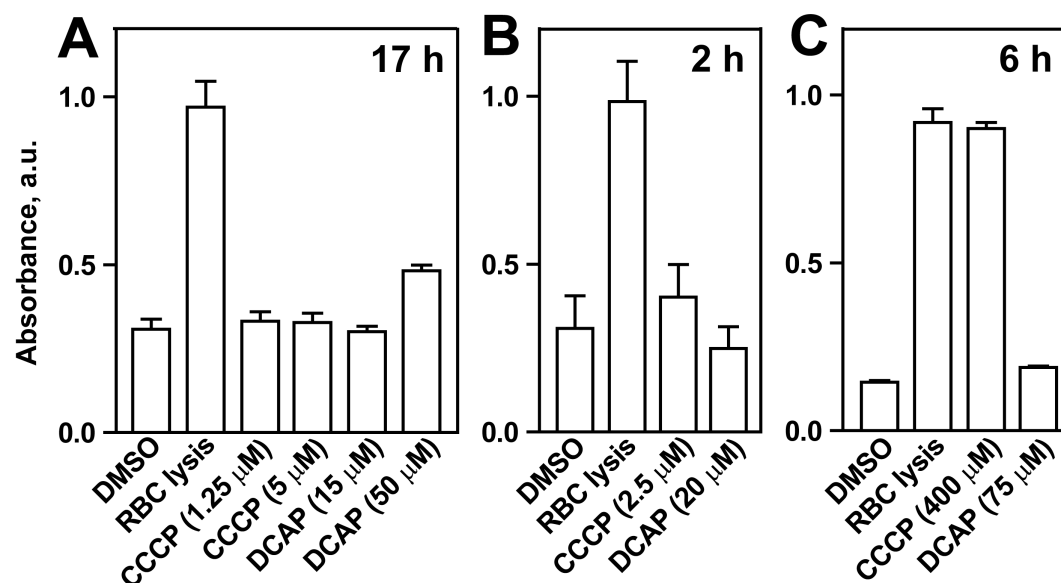


**Figure 9.** Rabbit red blood cell (RBC) hemolysis assay. Columns represent average values, and error bars represent the standard deviation of the mean for three replicates. Assay performed using the MIC conditions for *C. crescentus* and *S. aureus* (A), the MSC for *C. crescentus* (B), and the MSC for *S. aureus* (C).

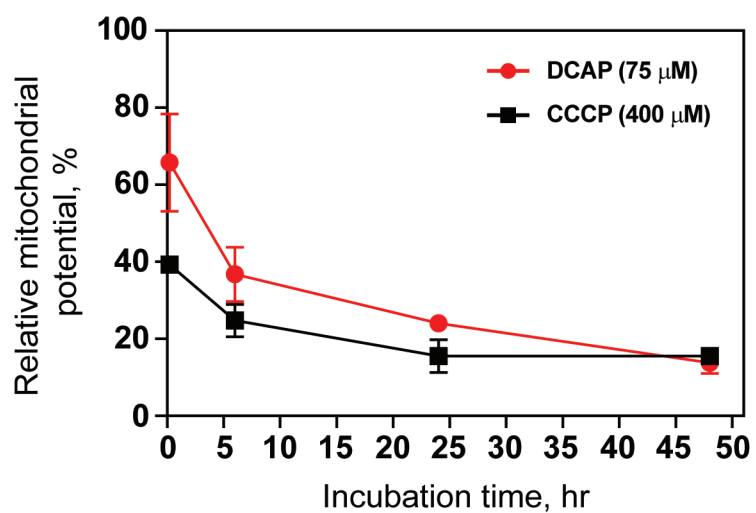


**Figure 10.** Transmembrane potential ( $\Delta\Psi$ ) of mitochondria in HEK cells treated with small molecules. We measured  $\Delta\Psi$  over the course of four time points: 20 min, 6 h, 24 h, and 48 h. Mean values of four independent experiments are plotted. Error bars indicate the standard error of the mean. The percent  $\Delta\Psi$  values plotted are relative to the values obtained from DMSO controls for each compound.

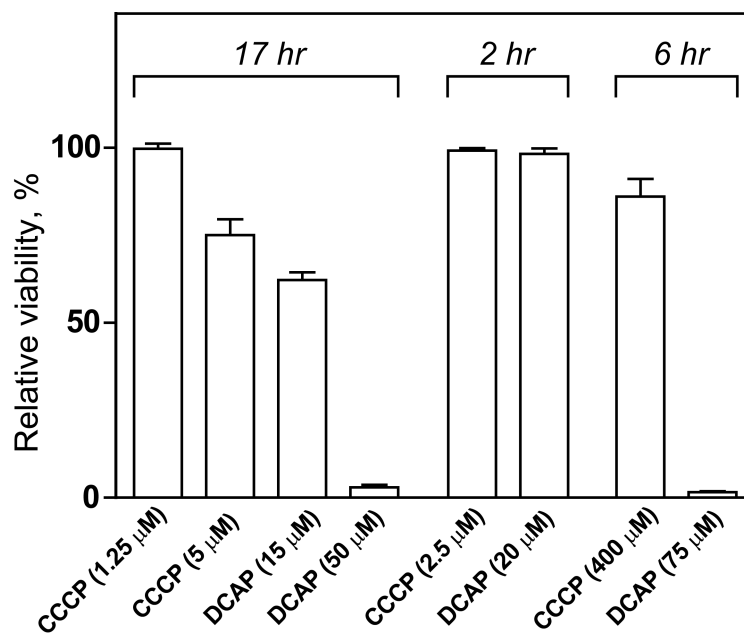


**Figure 11.** Cell viability of human epithelial kidney cells in the presence of membrane-active compounds. Mean values of four independent experiments are plotted. Error bars indicate the standard error of the mean. The percent viability values are relative to the values obtained from DMSO controls for each compound concentration. The duration of compound treatment is indicated above the bars.

**Table 1.** List of strains used in this study.

<i>Organism/Strain</i>	<i>Genotype/Description</i>	<i>Reference</i>
<i>C. crescentus</i> CB15N	synchronizable derivative of wild-type CB15	(9)
<i>C. crescentus</i> MT97	CB15N <i>mipZ-yfp</i>	(9)
<i>C. crescentus</i> AM138	<i>Pxyl-venus-ftsA, kan<sup>R</sup></i>	(28)
<i>S. aureus</i> FRI 100	<i>sea<sup>+</sup> (Tmm<sup>s</sup> Hem<sup>ta</sup> Em<sup>s</sup>)</i>	(29)
<i>E. coli</i> BW25113	$\Delta(\text{araD-araB})567 \Delta\text{lacZ4787}(\text{:rrnB-3})$ $\lambda\text{rph-1 } \Delta(\text{rhaD-rhaB})568 \text{ hsdR514}$	(30)
<i>E. coli</i> BW25113 $\Delta\text{tolC}$	BW25113 <i>tolC::kan<sup>R</sup></i>	(30)
<i>P. aeruginosa</i> PAO1	Prototroph	(31)
<i>P. aeruginosa</i> K1115	<i>ilv-220 thr-9001 leu-9001 met-9011 pur-67</i> <i>aphA ΔmexCD-oprJ ΔmexAB-oprM</i>	(32)
<i>P. aeruginosa</i> K1119	PAO1 $\Delta\text{mexAB-oprM}$	(32)
<i>B. subtilis</i> 168	<i>trpC2</i>	(31)
<i>B. subtilis</i> DS4294	<i>amyE::Pxyl-gfp-minD, cat<sup>R</sup></i>	(12)
<i>Salmonella</i> <i>typhimurium</i>	Clinical isolates from the Department of Medical Microbiology and Immunology (MMI) at the University of Wisconsin– Madison	(33)
<i>Vibrio cholera</i>	Clinical isolates from the Department of Medical Microbiology and Immunology (MMI) at the University of Wisconsin– Madison	(33)
<i>Shigella boydii</i>	Clinical isolates from the Department of Medical Microbiology and Immunology (MMI) at the University of Wisconsin– Madison	(33)
<i>Klebsiella</i> <i>pneumonia</i>	Clinical isolates from the Department of Medical Microbiology and Immunology (MMI) at the University of Wisconsin– Madison	(34)
<i>Enterobacter</i> <i>aerogenes</i>	Clinical isolates from the Department of Medical Microbiology and Immunology (MMI) at the University of Wisconsin– Madison	(33)
<i>Acinetobacter</i> <i>baumannii</i>	Clinical isolates from the Department of Medical Microbiology and Immunology	(33)

	(MMI) at the University of Wisconsin-Madison	
<i>Edwardsiella tarda</i>	Clinical isolates from the Department of Medical Microbiology and Immunology (MMI) at the University of Wisconsin-Madison	(33)
<i>Morganella morganii</i>	Clinical isolates from the Department of Medical Microbiology and Immunology (MMI) at the University of Wisconsin-Madison	(33)

**Table 2.** Minimum inhibitory concentrations (MIC) for DCAP against various pathogenic strains of bacteria. \*Cultures grown in PYE media at 30 °C. §Grown in LB media at 37 °C. †Grown in M8 media at 37 °C.

Organism/Strain	DCAP ( $\mu$ M)
<i>E. coli</i> BW25113†	80
<i>E. coli</i> BW25113 $\Delta$ tolC†	20
<i>P. aeruginosa</i> PAO1†	160
<i>P. aeruginosa</i> K1115§	80
<i>P. aeruginosa</i> K1119†	160
<i>B. subtilis</i> 168§	32
<i>Salmonella typhimurium</i> §	50
<i>Vibrio cholera</i> §	100
<i>Shigella boydii</i> §	100
<i>Klebsiella pneumonia</i> §	100
<i>Enterobacter aerogenes</i> §	200
<i>Acinetobacter baumannii</i> §	200
<i>Edwardsiella tarda</i> §	200
<i>Morganella morganii</i> §	200

**Table 3.** Measurements of the minimum inhibitory concentration of growth (MIC), minimum stationary-bactericidal concentration (MSC), minimum biofilm inhibitory concentration (bMIC), and the minimum biofilm eradication concentration (MBEC).

	<i>C. crescentus</i>			<i>S. aureus</i>		
	DCAP <sup>a</sup>	CCCP <sup>b</sup>	Amp <sup>c</sup>	DCAP <sup>a</sup>	CCCP <sup>b</sup>	Amp <sup>c</sup>
MIC	15	5	50	50	1.25	0.125
MSC	20	2.5	>400	75	>400	100
bMIC	20	5	100	100	2.5	0.8
MBEC	40	5	>400	>200	80	>200

<sup>a,b</sup>Concentration unit,  $\mu\text{M}$ . <sup>c</sup>Concentration unit,  $\mu\text{g/mL}$

## REFERENCES

1. Bush, K., Courvalin, P., Dantas, G., Davies, J., Eisenstein, B., Huovinen, P., Jacoby, G. A., Kishony, R., Kreiswirth, B. N., Kutter, E., Lerner, S. A., Levy, S., Lewis, K., Lomovskaya, O., Miller, J. H., Mobashery, S., Piddock, L. J., Projan, S., Thomas, C. M., Tomasz, A., Tulkens, P. M., Walsh, T. R., Watson, J. D., Witkowski, J., Witte, W., Wright, G., Yeh, P., and Zgurskaya, H. I. (2011) Tackling antibiotic resistance, *Nat Rev Microbiol* 9, 894-896.
2. Coates, A. R., and Hu, Y. (2008) Targeting non-multiplying organisms as a way to develop novel antimicrobials, *Trends Pharmacol Sci* 29, 143-150.
3. Hurdle, J. G., O'Neill, A. J., Chopra, I., and Lee, R. E. (2011) Targeting bacterial membrane function: an underexploited mechanism for treating persistent infections, *Nat Rev Microbiol* 9, 62-75.
4. Falconer, S. B., Czarny, T. L., and Brown, E. D. (2011) Antibiotics as probes of biological complexity, *Nat Chem Biol* 7, 415-423.
5. Chung, H. S., Yao, Z., Goehring, N. W., Kishony, R., Beckwith, J., and Kahne, D. (2009) Rapid beta-lactam-induced lysis requires successful assembly of the cell division machinery, *Proc Natl Acad Sci U S A* 106, 21872-21877.
6. Poetsch, A., and Wolters, D. (2008) Bacterial membrane proteomics, *Proteomics* 8, 4100-4122.
7. Pathania, R., Zlitni, S., Barker, C., Das, R., Gerritsma, D. A., Lebert, J., Awuah, E., Melacini, G., Capretta, F. A., and Brown, E. D. (2009) Chemical genomics in *Escherichia coli* identifies an inhibitor of bacterial lipoprotein targeting, *Nat Chem Biol* 5, 849-856.
8. Ganzle, M. G. (2004) Reutericyclin: biological activity, mode of action, and potential applications, *Appl Microbiol Biotechnol* 64, 326-332.
9. Thanbichler, M., and Shapiro, L. (2006) MipZ, a spatial regulator coordinating chromosome segregation with cell division in *Caulobacter*, *Cell* 126, 147-162.
10. Ely, B. (1991) Genetics of *Caulobacter crescentus*, *Methods Enzymol* 204, 372-384.
11. (2000) *Methods for Dilution Antimicrobial Susceptibility Tests for Bacteria That Grow Aerobically*, Fifth Edition ed., National Committee for Clinical Laboratory Standards, Wayne, PA.

12. Foss, M. H., Eun, Y.-J., Grove, C. I., Pauw, D. A., Rensvold, J. W., Pagliarini, D. J., Shaw, J. T., and Weibel, D. B. (2012) Inhibitors of bacterial tubulin target bacterial membranes in vivo, *MedChemComm*, *Manuscript in press*.
13. Sliusarenko, O., Heinritz, J., Emonet, T., and Jacobs-Wagner, C. (2011) High-throughput, subpixel precision analysis of bacterial morphogenesis and intracellular spatio-temporal dynamics, *Mol Microbiol* 80, 612-627.
14. Orlov, V. N., Antonenko, Y. N., Bulychev, A. A., and Yaguzhinsky, L. S. (1994) Combination of the electrogenic ionophores, valinomycin and CCCP, can lead to non-electrogenic K<sup>+</sup>/H<sup>+</sup> exchange on bilayer lipid membranes, *FEBS Lett* 345, 104-106.
15. Terada, H. (1990) Uncouplers of oxidative phosphorylation, *Environ Health Perspect* 87, 213-218.
16. Shapiro, H. M. (2008) Flow cytometry of bacterial membrane potential and permeability, *Methods Mol Med* 142, 175-186.
17. Waggoner, A. (1976) Optical probes of membrane potential, *J Membr Biol* 27, 317-334.
18. Novo, D. J., Perlmutter, N. G., Hunt, R. H., and Shapiro, H. M. (2000) Multiparameter flow cytometric analysis of antibiotic effects on membrane potential, membrane permeability, and bacterial counts of *Staphylococcus aureus* and *Micrococcus luteus*, *Antimicrob Agents Chemother* 44, 827-834.
19. Strahl, H., and Hamoen, L. W. (2010) Membrane potential is important for bacterial cell division, *Proc Natl Acad Sci U S A* 107, 12281-12286.
20. Goley, E. D., Yeh, Y. C., Hong, S. H., Fero, M. J., Abeliuk, E., McAdams, H. H., and Shapiro, L. (2011) Assembly of the *Caulobacter* cell division machine, *Mol Microbiol* 80, 1680-1698.
21. Poole, K. (2004) Efflux-mediated multiresistance in Gram-negative bacteria, *Clin Microbiol Infect* 10, 12-26.
22. Sharff, A., Fanutti, C., Shi, J., Calladine, C., and Luisi, B. (2001) The role of the TolC family in protein transport and multidrug efflux. From stereochemical certainty to mechanistic hypothesis, *Eur J Biochem* 268, 5011-5026.
23. Coates, A., Hu, Y., Bax, R., and Page, C. (2002) The future challenges facing the development of new antimicrobial drugs, *Nat Rev Drug Discov* 1, 895-910.
24. Zhang, Y. M., and Rock, C. O. (2008) Membrane lipid homeostasis in bacteria, *Nat Rev Microbiol* 6, 222-233.

25. Parsek, M. R., and Singh, P. K. (2003) Bacterial biofilms: an emerging link to disease pathogenesis, *Annu Rev Microbiol* 57, 677-701.
26. Stewart, P. S., and Franklin, M. J. (2008) Physiological heterogeneity in biofilms, *Nat Rev Microbiol* 6, 199-210.
27. Ooi, N., Miller, K., Randall, C., Rhys-Williams, W., Love, W., and Chopra, I. (2010) XF-70 and XF-73, novel antibacterial agents active against slow-growing and non-dividing cultures of *Staphylococcus aureus* including biofilms, *J Antimicrob Chemother* 65, 72-78.
28. Moll, A., and Thanbichler, M. (2009) FtsN-like proteins are conserved components of the cell division machinery in proteobacteria, *Mol Microbiol* 72, 1037-1053.
29. Foss, M. H., and Weibel, D. B. (2010) Oligochlorophens are potent inhibitors of *Bacillus anthracis*, *Antimicrob Agents Chemother* 54, 3988-3990.
30. Baba, T., Ara, T., Hasegawa, M., Takai, Y., Okumura, Y., Baba, M., Datsenko, K. A., Tomita, M., Wanner, B. L., and Mori, H. (2006) Construction of *Escherichia coli* K-12 in-frame, single-gene knockout mutants: the Keio collection, *Mol Syst Biol* 2, 2006 0008.
31. Eun, Y. J., and Weibel, D. B. (2009) Fabrication of microbial biofilm arrays by geometric control of cell adhesion, *Langmuir* 25, 4643-4654.
32. Li, X. Z., Zhang, L., Srikumar, R., and Poole, K. (1998) Beta-lactamase inhibitors are substrates for the multidrug efflux pumps of *Pseudomonas aeruginosa*, *Antimicrob Agents Chemother* 42, 399-403.
33. Ho, J. Y. C., N. J.; Crooks, J. A.; Baeza, J.; and Weibel, D. B. . (2012) Rapid identification of ESKAPE bacterial strains using an autonomous microfluidic device, *Submitted*.
34. Cira, N. J., Ho, J. Y., Dueck, M. E., and Weibel, D. B. (2012) A self-loading microfluidic device for determining the minimum inhibitory concentration of antibiotics, *Lab on a chip* 12, 1052-1059.

## CHAPTER 6

**A bacterial division inhibitor that targets the assembly of the divisome**

Manuscript in preparation

Ye-Jin Eun, Daniela Kiekebusch, Maoquan Zhou, Rishi R. Trivedi, Somenath Bakshi,

Taylor A. Wahlig, James Weisshaar, Martin Thanbichler, and Douglas B. Weibel

## ABSTRACT

Once viewed as a process driven solely by entropy, it is now known that cell division in bacteria involves interactions between more than 10 proteins to achieve a coordinated constriction of the cell envelope and remodeling of the peptidoglycan layer. Bacterial cells regulate the division process to ensure equal distribution of materials between the mother and daughter cells, and to respond to various environmental stresses that cause nutrient deficiency or DNA damage. To study such intricacies in bacterial cell division, we have identified and characterized a small molecule tool. The compound inhibits cell division in Gram-negative organisms; hence, the molecule was named divin (DIVision INhibitor). Treatment with divin causes incomplete constriction in dividing cells and does not affect the segregation of replicated chromosomes. The cells with unfinished constrictions have a cytoplasmic volume that is continuous with the future daughter cells, indicating that the compound blocks the cells from fusing the inner membrane to develop new poles. Using *Caulobacter crescentus* strains that express fluorescently tagged division proteins, we found that Divin perturbs the localization of several late division proteins; FtsI (PBP3) and FtsK were the most sensitive to divin treatment. The perturbation in the assembly of division proteins was also observed in *Escherichia coli* cells. Consistent with these findings, we observed that the intensity of fluorescent vancomycin staining was reduced at the septum of Divin-treated cells, indicating a decrease in the remodeling of the cell wall. In summary, Divin blocks the late stage of cell division by targeting the assembly of division machinery while not affecting FtsZ and segregation of chromosomes. This biological activity makes divin a useful chemical probe to study divisome dynamics.

## INTRODUCTION

Bacterial cell division was historically considered a ‘simple’ process in which cytokinesis occurred in the absence of cytoskeletal elements (1). However, the past two decades of research have transformed this scientific view. More than a dozen different proteins assemble at the division site—including FtsZ, a homolog of eukaryotic tubulin—and the complex is referred to collectively as the ‘divisome’ (2). Deciphering the biochemical and structural roles of the proteins in this complex has lagged behind studies of divisome assembly and cell morphological changes during division (3).

Divisome assembly in *Escherichia coli* is hierarchical and step-wise (4). FtsZ is the first protein to assemble at the site of cell division, and is required for the localization of all downstream division proteins (5). The remaining division proteins arrive in two distinct stages, and are categorized as either ‘early’ or ‘late’ proteins. The dynamics of protein-protein interactions in the divisome are not well understood (2). As divisome assembly occurs, Gram-negative cells constrict several different layers of the cell envelope simultaneously (2). Mutations in division proteins produce various cell morphologies, including smooth filaments, shallow, extended, or deep constrictions (3). It is unclear how these mutations create particular cell morphological phenotypes.

Cell division requires the coordination of several processes in the cell, including DNA synthesis, divisome assembly, and peptidoglycan (PG) remodeling. To orchestrate these processes, bacteria use several mechanisms to regulate the progression of division, including positioning the division site at the mid-cell and responding to various extracellular stresses (6). The majority of these mechanisms block division by targeting FtsZ and altering its properties, including inhibition of its GTPase activity and

protofilament bundling.

FtsZ activity is regulated during cell growth to position the divisome at the mid-cell (7). These regulatory proteins include MipZ in *Caulobacter crescentus*, and MinC and SlmA in *E. coli*. MipZ and MinC bind directly to FtsZ and stimulate the depolymerization of FtsZ protofilaments, and are concentrated at the cell poles. The concentration gradient and activity of MipZ and MinC guide divisome assembly to the mid-cell (7, 8). The DNA-binding protein SlmA also binds to FtsZ, negatively regulates its activity, and ensures that the position of the division site does not overlap with the chromosome (9).

In addition to regulating FtsZ during growth, bacteria may terminate division when available energy is reduced or in response to DNA damage (6). KidO is a homolog of NADH-dependent oxidoreductases in *C. crescentus* and may act as a metabolic sensor to destabilize FtsZ protofilaments when energy levels are low (10). Following DNA damage, *E. coli* cells activate the SOS response to express Sula, which sequesters FtsZ monomers and prevents their polymerization (2). *C. crescentus* uses a different SOS response mechanism in which SidA binds to the late division protein FtsW, interferes with divisome assembly, and inhibits late stages of cell division (11).

Several classes of antimicrobial agents inhibit cell division by activating the regulatory mechanisms described above. The aminocoumarin and quinolone families of antibiotics target DNA gyrase, introduce DNA damage, and disrupt DNA segregation (12). These activities inhibit FtsZ through the SOS response and nucleoid occlusion (13, 14). The  $\beta$ -lactam family of antibiotics blocks PG remodeling at the division site, and simultaneously activates the SOS response by stimulating the DpiBA two-component signal transduction system (15). Overall, these classes of small molecules elicit several

regulatory mechanisms that cause downstream changes in the function and assembly of division machinery. In addition to their therapeutic function, these compounds have enabled studies of bacterial cell division (12). The introduction of new compounds that directly target the divisome may provide deeper insight into the biochemical mechanisms of bacterial division and introduce new classes of clinical antimicrobial agents.

In this manuscript we introduce 2-methyl-1H-Benzimidazole-1-propanoic acid-[(2-hydroxy-1-naphthalenyl)methylene]hydrazide (for brevity, we refer to the compound as 'divin'), a small molecule that targets divisome assembly and inhibits cell division (Figure 1). Divin has a unique mechanism of action compared to antibiotics that block cell division by inhibiting FtsZ indirectly. We have demonstrated that divin is a useful chemical biological probe for studying divisome dynamics and the connection between division protein function and morphological phases of cell division. Lastly, we have shown that divin is a potent antimicrobial agent with low toxicity against mammalian cells.

## EXPERIMENTAL METHODS

### Media and growth conditions

Organisms, strains, and plasmids used in this study, their genotype, experimental conditions, and relevant references are summarized in Tables 1, 2, and 3. We used Luria-Bertani (LB) media (10 g/L tryptone, 10 g/L NaCl, 5 g/L yeast extract, pH 7.2) and M8 minimal media (241 mg/L MgSO<sub>4</sub>, 4 mg/L glucose, 5 mg/L casamino acids, 12.8 g/L Na<sub>2</sub>HPO<sub>4</sub>·7H<sub>2</sub>O, 3 g/L KH<sub>2</sub>PO<sub>4</sub>, and 0.5 g/L NaCl) to grow *V. cholera*, *S. boydii*, *A. baumannii*, and *E. coli* strains at 37 °C. PYE media (2 g/L peptone, 1 g/L yeast extract, 0.8 mM MgSO<sub>4</sub>, and 0.5 mM CaCl<sub>2</sub>) was used to culture *C. crescentus* cells at 30 °C. When growing *C. crescentus* strains that express fluorescent fusions under a xylose-inducible promoter, we supplemented the media with 0.3 % glucose. For induction, we centrifuged the culture and resuspended the pellet in xylose-containing media. All cultures were grown while shaking at 200 rpm with the exception of clinical pathogens, which were statically incubated. For *C. crescentus* cultures, we used the following concentrations (µg/mL; liquid/solid medium): kanamycin (5/25), spectinomycin kanamycin (25/50), ampicillin (50/50), and rifampicin (25/50).

### General methods for optical microscopy

For all microscopy experiments, we transferred a 1 µL cell suspension onto 1%

agarose pads. For brightfield and epifluorescence imaging, we used a Nikon Eclipse TE2000E inverted microscope with an Andor DU-895 EMCCD camera, a Perfect Focus system, and an encoded z-stage for phase contrast and epifluorescence microscopy.

For FITC-vancomycin labeling, we used the protocol described by Laub and co-workers (11). For DNA staining with DAPI, we added the dye at a final concentration of 1  $\mu\text{g}/\text{mL}$  and incubated for 10 min at 25 °C prior to imaging.

### **Assays for measuring the localization of division proteins**

For experiments with *C. crescentus* cells, we prepared the cells by diluting the overnight culture 10 or 20-fold into fresh PYE medium. We pre-incubated the diluted culture for 1 h at 200 rpm and 30 °C, and added divin or DMSO as the solvent control. For experiments with *E. coli* cells, we first diluted overnight cultures to an optical density of 0.1 in M8 media. We incubated the diluted cultures for 30 min prior to compound treatment (DMSO or divin).

Since the experiments with *C. crescentus* cells required long periods of incubation (up to 12 h), we found that the fraction of population that exhibits a normal localization decreased over time in the DMSO control sample. Thus, we grew the DMSO control cells for the same amount of time as the divin-treated cells for a more accurate comparison (e.g. 12 h DMSO sample vs. 12 h divin sample). Experiments with *E. coli*

cells required a shorter incubation (up to 5 h) than *C. crescentus*, and the DMSO control sample was induced immediately after the pre-incubation, imaged, and analyzed for comparison with divin-treated cells.

To quantify the fraction of population with a normal localization, we manually analyzed the images. The manual analysis was necessary since divin-treated cells have an unusual morphology that provides challenges for Matlab-based scripts to segment the cells correctly. In the analysis, we only considered cells with visible constrictions and asked whether fluorescence foci are found at the constriction. Cells with visible constrictions were marked on the brightfield image, which was used as a reference for the fluorescence image to count the cells with a mid-cell localization. Regardless of the intensity of a focus, as long as the fluorescence was discernable at the mid-cell, we categorized the cell as a wildtype phenotype. We counted at least 40 cells per experimental condition, and performed each experiment at least twice to ensure reproducibility of the data. After counting the number of cells displaying a mid-cell localization out of the total number cells analyzed, we calculated two-sided p-values between the DMSO and divin-treated samples using Fisher's exact test (Graphpad Prism).

Furthermore, we used two 'quality control tests', as manual data analysis can be subjective. In one test, a person analyzed several data sets on two different occasions, a

few weeks apart from each other, and asked if the results from the two occasions were the same. We also had two different individuals analyze the same sets of data to compare the results to each other. In both 'quality control tests', we found that the results were very similar to each other and did not change the p-value of the data sets, indicating that the manual analysis was objective and accurate.

### **Fluorescence recovery after photobleaching (FRAP)**

We used MT97 cells for FRAP experiments. This strain expresses YFP, which absorbs green light ( $\lambda_{\max} = 514 \text{ nm}$ ) and fluoresces in the green-yellow region of the electromagnetic spectrum ( $\lambda_{\max} = 533 \text{ nm}$ ). We used a 514 nm Argon ion laser (Melles Griot) to excite the fluorophore. Samples were imaged using a Nikon Eclipse Ti inverted microscope equipped with an oil immersion objective (CFI Plan Apo Lambda DM 100X Oil, 1.45 NA) and a 1.5X tube lens. The yellow emission was collected using a 560/50 emission filter (Chroma). The laser beam was split into two beams using a beam splitter. A focused beam (0.5  $\mu\text{m}$  full width at half-maximum height (FWHM), 30 kW/cm<sup>2</sup> peak intensity, 100 ms in duration) was used to selectively bleach one tip of the cell at  $t = 0$ . A broad probe beam (40  $\mu\text{m}$  FWHM, 100 W/cm<sup>2</sup>) was used to record the fluorescence recovery with time (with 100ms exposure at 1Hz frame rate). The two beams were combined into the microscope in epi illumination mode. The beams were synchronized with the camera frames with fast shutters (Uniblitz LS2, Vincent

Associates). The bleach beam was controlled with an extra home built shutter that was only open at  $t=0$ . We used a back-illuminated EMCCD camera with  $16\ \mu\text{m} \times 16\ \mu\text{m}$  pixels (iXon DV-887, Andor Technology). Each pixel corresponds to  $105 \times 105\ \text{nm}^2$  at the sample (150X magnification).

During the time series of FRAP experiments, we acquired images of a bleached cell and at least one more cell in a same window to compare the fluorescence intensity changes in the bleached cell with the signals in unbleached cells. In addition, we photobleached swarmer cells (with a single focus of MipZ-YFP per cell) in the absence of divin, since it is possible for YFP to slowly recover from the dark state at high laser intensities (16, 17). The laser intensity we used for bleaching did not promote reversible photobleaching. Following data acquisition, fluorescence intensities were measured using ImageJ.

### **NMR spectroscopy**

Divin used in all experiments described in this manuscript was purchased from Ryan Scientific (catalog number F1092-3077). We used a Bruker Avance III 400 MHz instrument (National Magnetic Resonance Facility at Madison) to obtain 1D  $^1\text{H}$  and  $^{13}\text{C}$  NMR spectra for divin at  $25\ ^\circ\text{C}$ . The solvent used was  $\text{CD}_3\text{OD}/\text{CDCl}_3$ .  $^1\text{H}$  and  $^{13}\text{C}$  chemical shifts were referenced to internal solvent resonances. Multiplicities are

indicated by s (singlet), d (doublet), t (triplet), q (quartet), qn (quintet), m (multiplet) and br (broad). Chemical shifts are reported in parts per million (ppm) and coupling constants  $J$  are given in Hz.

### **Determination of compound stability**

We dissolved 1 mg of divin in 400  $\mu\text{L}$  of  $\text{DMSO-d}_6$  and added 600  $\mu\text{L}$  of  $\text{D}_2\text{O}$  to the solution. After 10 min of mixing, the solution was filtered into a NMR tube. The  $^1\text{H}$  NMR was acquired continuously on a Bruker AV III 600 MHz NMR with a cryogenic probe at 37  $^\circ\text{C}$ .

### **Mass spectrometry**

We analyzed divin using high-resolution electrospray ionization mass spectrometry in positive ion mode to determine the exact mass of the compound (Mass Spectrometry Facility, Department of Chemistry at the University of Wisconsin-Madison).

### **Determination of compound solubility**

We determined the solubility of divin using light scattering. We dissolved the compound (0 - 100  $\mu\text{M}$ ) in a buffer solution (50 mM HEPES/NaOH, pH 7.2, 50 mM KCl, 10 mM  $\text{MgCl}_2$ , 1 mM  $\beta$ -mercaptoethanol) that contained different concentrations of DMSO (0 to 8% v/v). We measured the light scattering of the compound solutions

using a PC1 fluorescence spectrophotometer (ISS). Relevant instrument settings include 350 nm for both excitation and emission wavelengths and 1 mm slits. Light scattering from a buffer-only control was subtracted from the sample signal, and the lowest concentration of divin that increased light scattering above background was determined as the solubility limit of the compound at a given DMSO concentration.

### **Measurement of growth over time in the presence of divin**

We measured the growth of *C. crescentus* CB15N and *E. coli*  $\Delta tolC$  cells in the presence of divin. The overnight cultures were diluted 10-fold into fresh media and grown for 30 min prior to compound treatment. After adding divin ( $t = 0$  hr), we serially diluted the culture to test a range of compound concentrations in the assay. During incubation, we took 1 mL aliquots at each time point to measure the optical density at 600 nm.

### **Determination of minimum inhibitory concentration (MIC)**

We determined the MIC of *E. coli* and *C. crescentus* strains in liquid media using the macrodilution method according to the CLSI guidelines. For clinical pathogenic organisms including *V. cholera*, *S. boydii*, and *A. baumannii* strains, we used 96-well microplates (100  $\mu$ L/well) and the microdilution method from the CLSI guidelines.

### **Bacterial viability assay**

We measured the bacterial viability over time in the presence of divin to determine the mode of antibiotic activity of the drug. We used ampicillin and chloramphenicol as bacteriocidal and bacteriostatic antibiotic controls, respectively. We grew an overnight culture of *E. coli* BW25113  $\Delta tolC$  cells in M8 media, and the overnight culture was diluted 500-fold in the same growth media. Antibiotics were added to the cell culture at 4X MIC (50  $\mu\text{g}/\text{mL}$  of ampicillin, 5  $\mu\text{g}/\text{mL}$  of chloramphenicol, and 50  $\mu\text{M}$  of divin) at time zero. At each time point, we took 100  $\mu\text{L}$  of each sample, serially diluted 4 times in PBS, and plated 100  $\mu\text{L}$  of the final dilution onto LB agar plates. After overnight incubation of the plates, we enumerated the colonies on each plate.

### **Radioactive GTPase assay with purified recombinant FtsZ**

Recombinant FtsZ was purified as described previously (18). The final concentration of FtsZ was 2  $\mu\text{M}$  in buffer (50 mM Hepes/NaOH, pH 7.2, 50 mM KCl, 10 mM  $\text{MgCl}_2$ , 1 mM  $\beta$ -mercaptoethanol, 8% v/v DMSO). We mixed [ $\alpha$ - $^{32}\text{P}$ ]-GTP (PerkinElmer) with a cold GTP stock solution to achieve a final radioactivity of 0.027-0.67  $\mu\text{Ci}/\mu\text{L}$  in each reaction (a final volume of 50  $\mu\text{L}$ ). All assays were performed at 25  $^\circ\text{C}$ . At different time points during the reaction, we spotted 0.5  $\mu\text{L}$  of a reaction onto PEI-cellulose F thin-layer chromatography plates (EMD Chemicals). We developed the

plates in a solvent system containing 1 M LiCl and 0.5 M formic acid in H<sub>2</sub>O, air-dried, and exposed them to a phosphor screen (Kodak). After scanning the screen in a Typhoon FLA 9000 imager (GE Healthcare), we quantified the amount of GDP using ImageQuant 5.2 (Molecular Dynamics) and calculated the concentration of GDP generated in the reactions.

To measure the  $K_M$  and  $V_{max}$  of the recombinant FtsZ, we tested nine different concentrations in the range of 0.8 and 500  $\mu$ M. For experiments in which we tested the inhibitory activity of divin against FtsZ, the final concentration of GTP was 80  $\mu$ M.

### **Co-treatment with cephalixin assay**

We tested whether the presence of divin changes the amount of cell lysis induced by cephalixin. We used a protocol similar to the one described by Chung et al., (19). First we diluted an overnight culture of BW25113  $\Delta tolC$  cells in M8 media to an optical density of 0.1. The diluted culture was grown at 37 °C for 1 h. At this time, cephalixin (10  $\mu$ g/mL) and divin (0, 3.13, 6.25, and 12.5  $\mu$ M by serial dilution) were added. Prior to the treatment, fresh cephalixin solution in 1M HCl was prepared for each around of experiment. After adding the compounds, we measured the optical density and imaged the cells to observe cell filamentation and lysis at each time point.

### **Bocillin-binding assay**

We assayed the ability of divin to compete with bocillin for binding the active site of penicillin binding proteins (PBPs). Bocillin is fluorescent derivative of penicillin, and is labeled with BODIPY FL (Invitrogen). Prior to the competition assay, the membrane fraction was isolated from a culture of BW25113  $\Delta tolC$  cells. An overnight culture (20 mL) of the *E. coli* strain was used to inoculate 2 L of LB growth medium to achieve an initial optical density of 0.1. The inoculum was incubated at 37 °C to reach an optical density of 0.7, and we harvested the cells by centrifugation at 12,000 g for 20 min at 4 °C. The cell pellet was frozen at -80 °C overnight and resuspended in buffer solution (25 mM Tris-HCl, 25 mM NaCl, 1 mM EDTA at pH 8) the next day. We added DNaseI (50 µg/mL), β-mercaptoethanol (1 mM), phenylmethanesulfonylfluoride (50 µM), and lysozyme (250 µg/mL) to the resuspension. The solution was homogenized with a sterile syringe and 16-gauge needle. We incubated the solution at 4 °C overnight. After incubation, the un-lysed cells were removed by centrifugation at 12,000 g for 20 min at 4 °C. We centrifuged the supernatant at 100,000 g for 40 min at 4 °C, resuspended the pellet in 10 mL of the Tris-HCl buffer, and centrifuged again. The resulting pellet was resuspended in 800 µL of the buffer, and we stored 100 µL aliquots at -80 °C. A Bradford assay was used to determine the protein concentration in the membrane preparation. Membranes from *C. crescentus* cells were extracted using the

procedure identical to *E. coli* cells, except the growth medium was PYE medium.

For the bocillin-binding assay, the frozen membrane fraction was thawed and pre-warmed at 37 °C for 5 min. We made a working stock solution of bocillin (0.15 mM in water). For one reaction, 10 µL of the membrane fraction was mixed with an antibiotic (ampicillin or divin) and incubated for 30 min at 37 °C. After this incubation, 1 µL of the stock bocillin was added to each reaction and further incubated for 30 min at 37 °C. At the end of the incubation, a loading buffer was added to stop the reaction, and the entire reaction volume was loaded onto a 4-20% gradient Tris-HCl Ready Gel (BioRad) for electrophoresis. After running the gel, we imaged the gel using a Typhoon FLA 9000 (GE Healthcare) scanner using the FITC filter setting (500 volts for gain; 50 µm resolution). We subsequently stained the gel using the coomassie dye to check for consistent sample loading.

### **Red blood cell hemolysis assay**

We used sheep red blood cells from Lampire Biological Laboratories. The assay was performed as previously described (20) using 25 µM of divin. The cells were treated with the compound for 17 h.

### **Mammalian cytotoxicity assay**

We measured the cytotoxicity of small molecules on human epithelial kidney

(HEK) cells using the CellTiterGlo Luminescent Cell Viability Assay (Promega). The assay was performed as previously described (20) using 25  $\mu$ M of divin. The cells were treated with the compound for 17 h, and the final concentration of DMSO was 0.082 % v/v.

## RESULTS

### Discovery and general characterization of divin

We identified divin in a high-throughput screen of small molecule libraries to isolate chemical inhibitors of MipZ. In *C. crescentus* cells, MipZ spatially and temporally coordinates cell division, and its ATP hydrolysis activity is critical for polar localization (18, 20). Using a primary fluorescence-based assay in vitro, we identified candidate inhibitors of the ATPase activity of recombinant MipZ. To narrow down candidate inhibitors, we used a secondary fluorescence microscopy-based assay to quantify the mislocalization of MipZ translationally fused to yellow fluorescent protein (MipZ-YFP) in *C. crescentus* cells (20). We identified divin as a weak inhibitor of the ATPase activity of MipZ and found that it does not perturb the polar localization of the protein in vivo (Figure 2). Interestingly, treating *C. crescentus* and *E. coli* cells with divin arrested cell division after the initiation of the mid-cell constriction (Figure 3). We concluded that divin does not target MipZ in vivo, as the division arrest occurs in *E. coli* cells which lack *mipZ* in their genome. The inhibition of cell division in Gram-negative bacteria inspired us to name the compound, divin (division inhibitor).

Inhibition of cell division appeared 6 h after treating *C. crescentus* cells with divin at its minimum inhibitory concentration (MIC) of 5  $\mu$ M (Table 4). Treating *E. coli* cells with a concentration of divin that was 2 or 4-fold higher than the MIC (12.5  $\mu$ M; Table 4) produced a similar phenotype after 4 h of incubation. It is unclear why several hours of incubation were necessary for compound-treated cells to exhibit the division defect. In contrast to the delay in presenting the morphological phenotype, the presence of divin

immediately influenced the growth rate of bulk cultures (Figure 4).

We confirmed the identity of divin using NMR spectroscopy and mass spectrometry (Figures 5 and 6, respectively). Divin was stable in aqueous solutions for >24 h (Figure 7) and had a solubility of 0.02 mg/mL in aqueous solutions (Table 5). The low solubility of divin prevented us from preparing agar plates containing a high concentration of the small molecule, and using the solid growth medium to isolate suppressor mutations that cause resistance to the drug. Despite this challenge, we characterized several properties of divin, including its biological activity. We determined that divin is a bacteriostatic agent by measuring the time-dependent viability of bacteria treated with compound (Figure 8). Consistent with this observation, we found that the inhibition of division was reversible—cells resumed division after divin was removed (Figure 9). Monitoring cells after removal of the compound, we observed that the newly formed daughter cells have sharp, pointed poles (Figure 9, 105 and 135 min), in contrast to the oblate shapes that are typical of new poles in *C. crescentus* cells (Aaron 2007). The shape of the poles of drug-treated *C. crescentus* cells indicates that divin disturbs the balance between elongation of the mid-cell and constriction at the division site.

As the cytoplasm of *C. crescentus* cells is compartmentalized prior to the physical separation of mother and daughter cells (21), we determined whether the cytoplasm is continuous between the two halves of a dividing cell after divin treatment. We performed fluorescence recovery after photobleaching (FRAP) experiments with *C. crescentus* strain MT97 cells by bleaching MipZ-YFP molecules at one pole and measuring the change of fluorescence in both poles of cells undergoing division. All of the cells treated with divin demonstrated a recovery of fluorescence after bleaching,

which indicated that the cytoplasm in the mother and daughter cells was continuous (Figure 10). From the time scale of the recovery (~30 sec), we concluded that fluorescence recovery is not due to newly translated MipZ-YFP. In summary, the recovery of fluorescence in compound-treated *C. crescentus* cells suggests that arrested division caused by divin occurs prior to compartmentalization of the cytoplasm. Thus, it is unlikely that divin targets amidases, which are activated after the cytoplasm compartmentalization to sever a joined PG layer between the mother and daughter cells (22).

#### **Divin does not bind to, or activate regulatory mechanisms that target FtsZ.**

To test the hypothesis that divin targets FtsZ directly, we measured the enzymatic activity of recombinant *C. crescentus* FtsZ in the presence of divin. Using radioactive GTPase assays, we determined a Michaelis equilibrium constant,  $K_M$  ( $80 \pm 36$   $\mu\text{M}$ ) and rate constant,  $k_{cat}$  ( $4 \pm 0.5$   $\text{min}^{-1}$ ) of the recombinant FtsZ. The  $k_{cat}$  value was consistent with published data for *C. crescentus* FtsZ (18); the  $K_M$  was ~2-fold higher than values reported for *E. coli* and *Bacillus subtilis* FtsZ (23). When testing the potential inhibitory activity of divin, we kept the final concentration of GTP at the  $K_M$  to increase the sensitivity of the enzyme assays. We found that divin does not inhibit *C. crescentus* FtsZ, which indicates the compound targets another division protein (Figure 11).

As divin may target FtsZ indirectly by triggering the regulatory mechanisms described above, we studied FtsZ localization in divin-treated cells. We treated *C. crescentus* MT196 cells expressing FtsZ-YFP with divin and observed FtsZ localization to the mid-cell (Figure 12). In cells with an extended constriction, we occasionally observed more than one focus/band of FtsZ-YFP at the constriction site. These

observations are consistent with FtsZ protofilaments assembling at the division site and the maintenance of its structure after divin treatment. Thus, divin does not activate regulatory mechanisms that target FtsZ directly, since those pathways would hinder FtsZ protofilament assembly in cells (6).

Furthermore, we tested whether divin inhibits segregation of replicated chromosomes. Cells nearing the end of DNA replication separate the two copies of the chromosome and segregate them to each half of a dividing cell. This process involves topoisomerases (e.g. TopoIV) that control the topology of the DNA and some components of the divisome (e.g. FtsK) that participate in chromosome partitioning (24, 25). The chromosome in *C. crescentus* is oriented with the origin of replication located at the pole with a stalk or flagellum, and the terminus at the other end of the cell. The two chromosome termini are the last regions of the DNA to separate during division (26). We visualized DNA near the termini using a fluorescence repressor operator system in *C. crescentus*, and observed that the chromosome termini were well resolved in both DMSO and divin-treated samples (cells with arrows; Figure 13a). Two fluorescent foci were usually located in the mid-cell region, one focus near one half of the cell and the other towards the other half of the cell (cells with asterisks; Figure 13a). In some cells, the two foci were both located in the same half of the cell (cells with plus signs; Figure 13a). This 'mis-segregation' of termini was observed in 20% of cells (n = 111) treated with DMSO, and 31% of the cells treated with divin (n = 133). The modest difference in mis-segregation was not statistically significant.

To rule out chromosome mis-segregation and nucleoid occlusion as a mechanism of action of divin, we observed the distribution of DNA in *E. coli* cells. We treated cells with divin and labeled the DNA with DAPI (Figure 13b). Divin-treated cells typically

contained two regions of DNA with a clear physical separation between the regions. The empty space between the regions of DNA corresponded to the partially constricted site of the cell wall in divin-treated cells. Overall, these data from *C. crescentus* and *E. coli* cells suggest that the chromosome replication and segregation are not affected by divin.

### **Divin inhibits the normal assembly of the divisome**

As temperature-sensitive mutations in several division proteins produce partial constrictions that are similar to the divin-induced phenotype (1, 3, 27, 28), we explored whether divisome assembly was altered in cells treated with the antibiotic. By expressing translational fusions of fluorescent proteins to 11 different division proteins in *C. crescentus*, we quantified the temporal disassembly of the divisome after divin treatment (Table 6 and Figure 14). We found that FtsK and FtsI were the first proteins to delocalize in *C. crescentus* cells (6 h after treatment). We did not observe any significant delocalization of the two proteins prior to the 6 h time point, and increasing the compound concentration to 20  $\mu$ M did not expedite delocalization.

FtsK is an essential division protein that plays a role in partitioning replicated chromosomes to ensure that the site of cell division is devoid of DNA (24). FtsK delocalized after divin treatment; however we did not observe any abnormalities in chromosome segregation in *C. crescentus* and *E. coli* cells (Figure 13). Thus, the disassembly of FtsK from the divisome in the presence of divin likely occurs after the completion of chromosome partitioning.

The other protein that delocalized with FtsK was FtsI (i.e., PBP3). FtsI is

specifically required for PG remodeling at the site of cell division. To better understand the influence of divin on the division site, we visualized PG remodeling in *C. crescentus* cells using fluorescently labeled vancomycin (11) (Figure 15). Consistent with the delocalization of FtsI from the division site, we observed that the constriction site in divin-treated *C. crescentus* cells incorporated lower amounts of fluorescent vancomycin compared to untreated cells. This result indicates that PG remodeling is reduced in the elongated, constricted region of divin-treated cells.

Delocalization of FtsI suggests that the transpeptidase activity of FtsI may be reduced or altered in divin-treated cells, as its localization in *C. crescentus* cells requires its enzymatic activity (29). To test this hypothesis, we purified *C. crescentus* and *E. coli* cell membranes and performed a competitive binding assay with divin and bocillin-FL, a fluorescent derivative of penicillin (Figure 16). We found that the presence of divin did not change the labeling of PBPs with bocillin-FL, while ampicillin (a positive control) reduced the binding of bocillin-FL to PBPs. These results suggested that divin does not directly inhibit PBPs, including FtsI. However, it is possible that divin indirectly perturbs the activity of PG remodeling enzymes.

Following the disassembly of FtsK and FtsI, a group of division proteins—FtsQ, FtsL, FtsW, and FtsB—dissociated from the divisome after divin treatment (Table 6; Figure 14). Most of these proteins normally assemble after the arrival of FtsK and FtsI at the site of cell division, although they do not require FtsK and FtsI for their localization (3). FtsW, FtsI, and FtsN form a subcomplex within the cytokinetic ring in *C. crescentus* (11). Thus, the departure of FtsI from the divisome may have influenced the delocalization of FtsW. However, we found that FtsN was localized at the division site up until 12 h after divin treatment, despite the disassembly of FtsI and FtsW within this

time frame.

FtsL, FtsB, and FtsQ delocalized in *C. crescentus* cells after 8 h of divin treatment. In *C. crescentus*, FtsB and FtsQ require FtsL for localization to the mid-cell (3). In *E. coli*, FtsL, FtsB, and FtsQ form a subcomplex, and their interactions are independent of other division proteins (30, 31). Thus, their simultaneous departure from the divisome in divin-treated *C. crescentus* cells is consistent with previous observations.

Six hours after the dispersion of FtsI and FtsK in *C. crescentus* cells, we observed that several early division proteins remained stable at the constriction site, with the exception of DipM (Table 6 and Figure 14). DipM delocalization may have been triggered by a prior departure of a particular protein from the divisome, or a gradual loss in divisome integrity. Another possible cause for DipM delocalization is reduction in PG remodeling at the constriction site (Figure 15). DipM binds to PG directly (32-34), and associates more strongly with septal PG than with PG in other regions in the cell (34). DipM localization may be influenced by substrate availability at the division site (32, 34), and the reduced PG remodeling at the constriction site in divin-treated cells (Figure 15) may explain the loss of DipM.

Overall, localization studies of 11 division proteins in *C. crescentus* demonstrated that divin reduces PG remodeling at the constriction site, and disrupts divisome assembly with a preference for disassembling late division proteins from the complex. Moreover, we found that the sensitivity of late division proteins to divin treatment was similar in *E. coli* cells (Figure 17 and Table 7). Four division proteins we tested in *E. coli* dispersed from the division plane in an order comparable to proteins in *C. crescentus*, starting with delocalization of FtsK and followed by FtsL, FtsQ, and FtsN. The disassembly of late division proteins after divin treatment, however, does not

necessarily support a direct, physical interaction of divin with these proteins in *C. crescentus* and *E. coli* cells.

To complement the localization studies in *C. crescentus* and *E. coli*, we tested the sensitivity of *E. coli* cells to cephalixin in the presence of divin. In *E. coli* cells, cephalixin specifically inhibits FtsI, and the compound treatment does not interfere with FtsI localization at the division site and recruitment of downstream division proteins, including amidases that remove PG crosslinks (19). Thus, cephalixin treatment produces an imbalance of PG remodeling, as amidases continue to hydrolyze peptide crosslinks while FtsI is unable to create new linkages. The imbalance in PG remodeling causes rapid cell lysis (19). We hypothesized that the co-treatment of cephalixin and divin may decrease the amount of cell lysis, since divin perturbs the assembly of late division proteins to the division site. We co-administered the two antibiotics, characterized cell morphology using microscopy, and quantified cell lysis by measuring growth in bulk cultures. The presence of both drugs reduced cell lysis and filamentation (Figure 18). These results are similar to previous observations in which *E. coli* strains that carry mutations in division proteins exhibit resistance to cell lysis induced by cephalixin (35). Thus, the reduced sensitivity to cephalixin in the presence of divin supports a model in which divin disrupts divisome assembly.

Lastly, we tested the sensitivity of divin in  $\Delta sidA$  cells. In *C. crescentus*, the SOS response triggered by DNA damage leads to expression of SidA (11). The protein inhibits cell division by interacting with FtsW directly and blocking the constriction of cells. As SidA does not perturb the localization of FtsW (11), we hypothesized that it is unlikely that divin activates the SidA pathway to inhibit division. However, we reasoned SidA might be activated prior to FtsW delocalization (Table 6). We examined

whether  $\Delta sidA$  cells exhibit unfinished constrictions similar to wildtype *C. crescentus* cells. We found that  $\Delta sidA$  cells showed a comparable morphology to wild type cells after divin treatment (Figure 19), indicating that the small molecule does not alter division through the primary SOS response pathway in *C. crescentus* (11).

### **Divin as a potential therapeutic for infectious diseases**

Our experiments demonstrated that divin effectively blocks reproduction of model Gram-negative bacteria. We explored whether the compound inhibits the growth of clinically relevant strains of bacteria. We found that divin has an MIC of 0.8  $\mu\text{M}$  against the Gram-negative pathogen *Vibrio cholera*, (Table 4). Divin is also toxic to clinical isolates of *Shigella boydii* and *Acinetobacter baumannii* (Table 4).

The antibiotic activity of divin against bacterial pathogens prompted us to measure its toxicity in mammalian cells. We quantified the hemolysis of red blood cells (RBCs) and the viability of human epithelial kidney (HEK) cells at the concentration of divin that killed bacteria (50  $\mu\text{M}$ ). RBCs treated with divin did not display a significant increase in hemolysis (Figure 20), although the HEK cells treated with divin showed a slight decrease in viability ( $72 \pm 5\%$  viable, compared to the DMSO control). Overall, the specificity of antibiotic activity of divin against Gram-negative bacterial pathogens makes the compound a promising starting point for developing a clinical therapeutic.

## DISCUSSION

We have demonstrated that divin inhibits cell division by perturbing divisome assembly. This biological activity makes divin a useful chemical probe to study divisome dynamics. By studying the spatial and temporal localization of different division proteins, we found that divin weakens the association of several late division proteins with the divisome, without influencing early proteins (Table 6 and Figure 14). The difference in drug sensitivity between early and late proteins may be useful when characterizing new proteins associated with the divisome.

Furthermore, studies of the relationship between localization and function of individual proteins at the divisome may benefit from using divin as a chemical biological probe (36). Some division proteins such as FtsI in *C. crescentus* require function for localization to the mid-cell (29), while other proteins (e.g. FtsN and DipM) have separate domains for activity and divisome localization (33, 37). Thus, it is possible that the activity of some early division proteins is altered despite their normal localizations after divin treatment. As the biochemical/ structural roles of individual division proteins are elucidated, divin and other chemical probes may help investigate the connection between protein localization and activity.

An important conclusion from this study is that divin causes a partial constriction of dividing cells without affecting FtsZ (Figures 3, 11, and 12). This result supports a model in which there are multiple morphological stages of the constriction at the mid-cell. Temperature-sensitive mutants and depletion strains of division proteins produce shallow, extended, or deep constrictions at the division site (3). For example, mutations in *ftsI*, *ftsQ* and *ftsN* generate shallow constrictions, and mutations in *ftsA*

and *ftsK* produce deep constrictions. Divin causes extended, deep constrictions in *C. crescentus* cells, while it arrests constrictions at different stages in *E. coli* cells. Overall, previous genetic studies and our current study suggest that 1) different stages of constrictions do not follow the order of division protein assembly (4, 27); and 2) constrictions must progress through several stages/checkpoints, rather than advancing to completion once initiated. Along with the genetic tools, divin may enable the investigation of the relationship between divisome assembly and progression of cell constrictions (38).

Finally, the incomplete constriction due to divin suggests that the presence of FtsZ and other early proteins at the division site is not sufficient for cytoplasm compartmentalization (Table 6, and Figures 10 and 14). This result supports a model in which FtsZ is influenced by and must work with other division proteins for constriction during division. Studies of recombinant FtsZ and liposomes have demonstrated that FtsZ generates physical forces to constrict membranes in vitro, although the mechanism is not well understood (39, 40). On the other hand, several studies have suggested that cell wall growth (e.g., PG and beta-glucan) may provide some of the energy for constricting prokaryotic and eukaryotic cells (34, 41, 42). Our results support this model, as a reduction in PG remodeling at the septum and the dissociation of late division proteins produced an incomplete, deep constriction at the division site in which FtsZ activity was unaffected by divin and cytoplasm remained continuous between the mother and daughter cells. Using divin in combination with high-resolution imaging may provide clues about the mechanisms by which PG remodeling generates force and/or provides feedback that influences the activity and structure of FtsZ (43).

## CONCLUSION

Drawing lessons from eukaryotic cell biology, the development of chemical tools may have a significant impact on the study of prokaryotic cytoskeletons and their associated proteins (44). To further develop divin as a chemical tool, we are investigating the structure activity relationship of the compound to identify its molecular target, improve its solubility and biological activity, and explore its potential as an antibiotic. In summary, our studies with divin have revealed the complexity of bacterial division, and future investigations may elucidate the molecular mechanisms that underlie this fascinating process.

## ACKNOWLEDGEMENTS

We thank Christine Jacobs-Wagner, Michael T. Laub, Yves V. Brun, Thomas G. Bernhardt, Erin D. Goley, and Lucy Shapiro for providing bacterial strains used in this study. We are grateful to Marie H. Foss, Susan Schlimpert, William M. Westler, Kurt J. Amann, and David J. Pagliarini for providing technical support. We acknowledge the financial support from the University of Wisconsin-Madison Graduate School (Senator Robert Caldwell Graduate Fellowship to Y.-J. E.), Alfred P. Sloan Foundation (fellowship to D.B.W.), NIH (grant 1DP2OD008735-01 to D.B.W.), Wisconsin Alumni Research Foundation (D.B.W.), and Human Frontiers Science Program (grant RGY0069/2008-C103 to M.T. and D.B.W.).

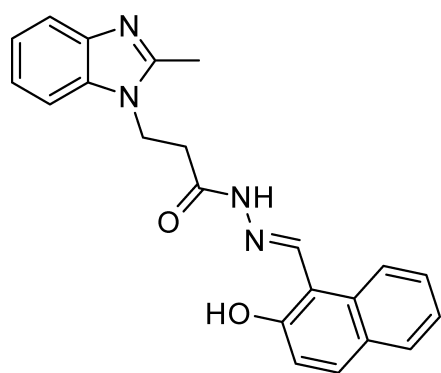


**Figure 1.** Structure of divinin

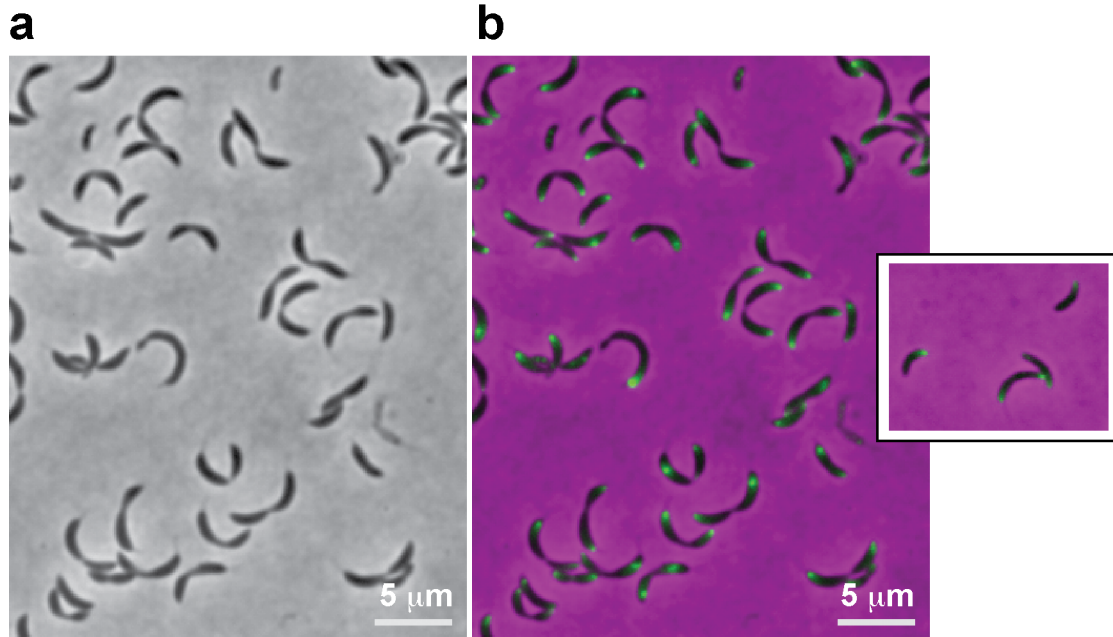


**Figure 2.** Divin does not perturb the polar localization of MipZ-YFP in *C. crescentus*. (a) A brightfield image of *C. crescentus* MT97 cells treated with 5  $\mu$ M divin for 6 h. (b) An overlay of brightfield and YFP channels (in green). The inset image shows the polar localization of MipZ-YFP incubated with DMSO.

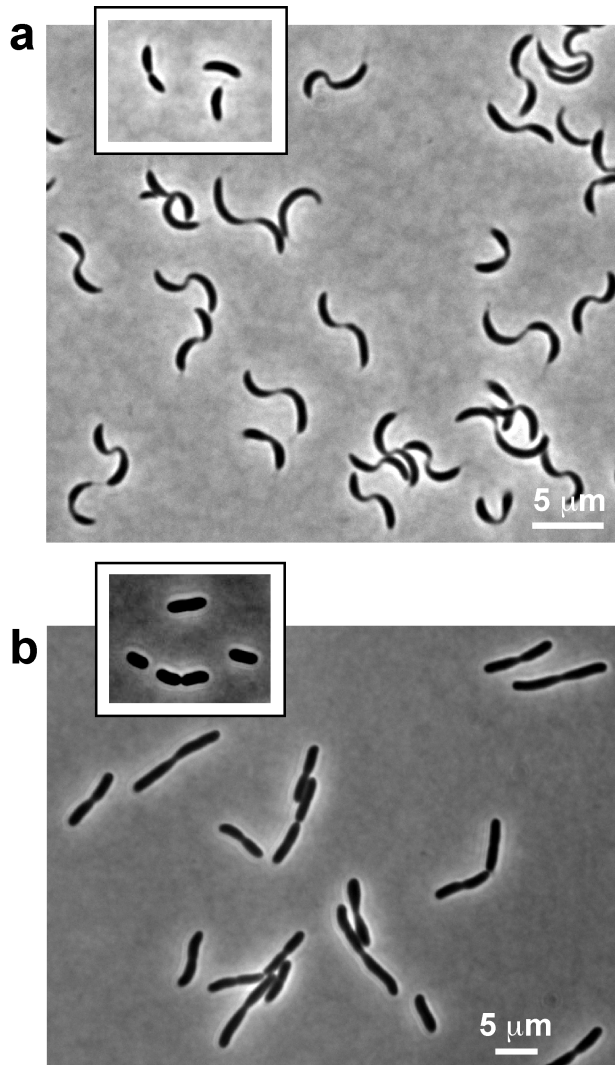


**Figure 3.** Divin causes incomplete constrictions in dividing cells. (a) *C. crescentus* CB15N cells with 5 μM divin after 11 hr of incubation. (b) *E. coli* Δ*tolC* cells with 50 μM divin after 12 hr of incubation.

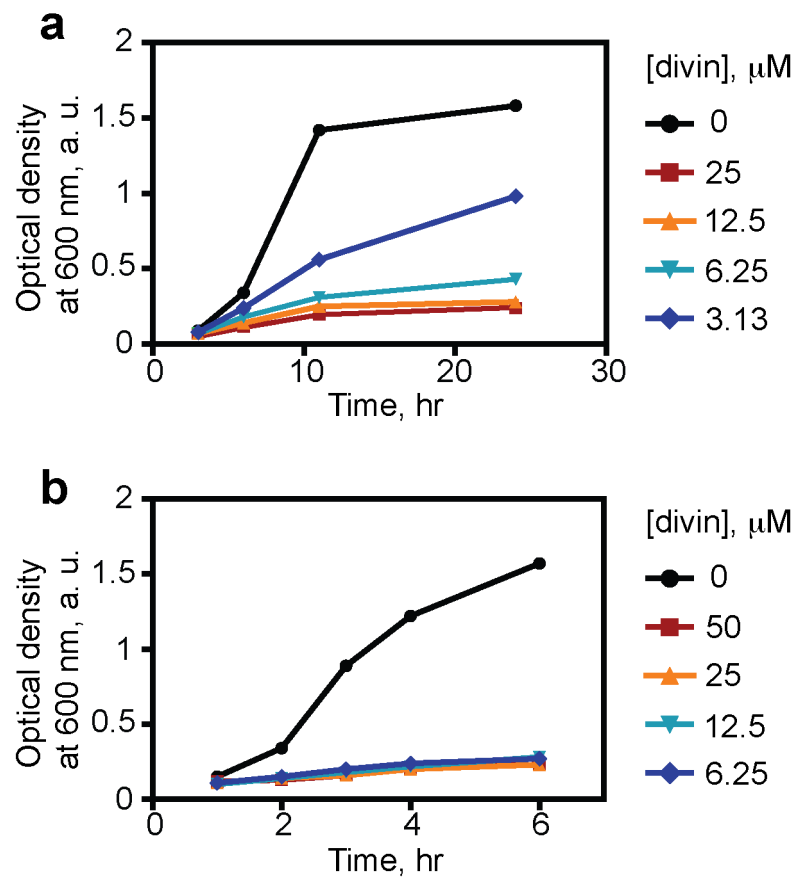


**Figure 4.** The presence of divin immediately influences the growth rate of bacterial cells.

(a) *C. crescentus* CB15N cells. (b) *E. coli*  $\Delta tolC$  cells.

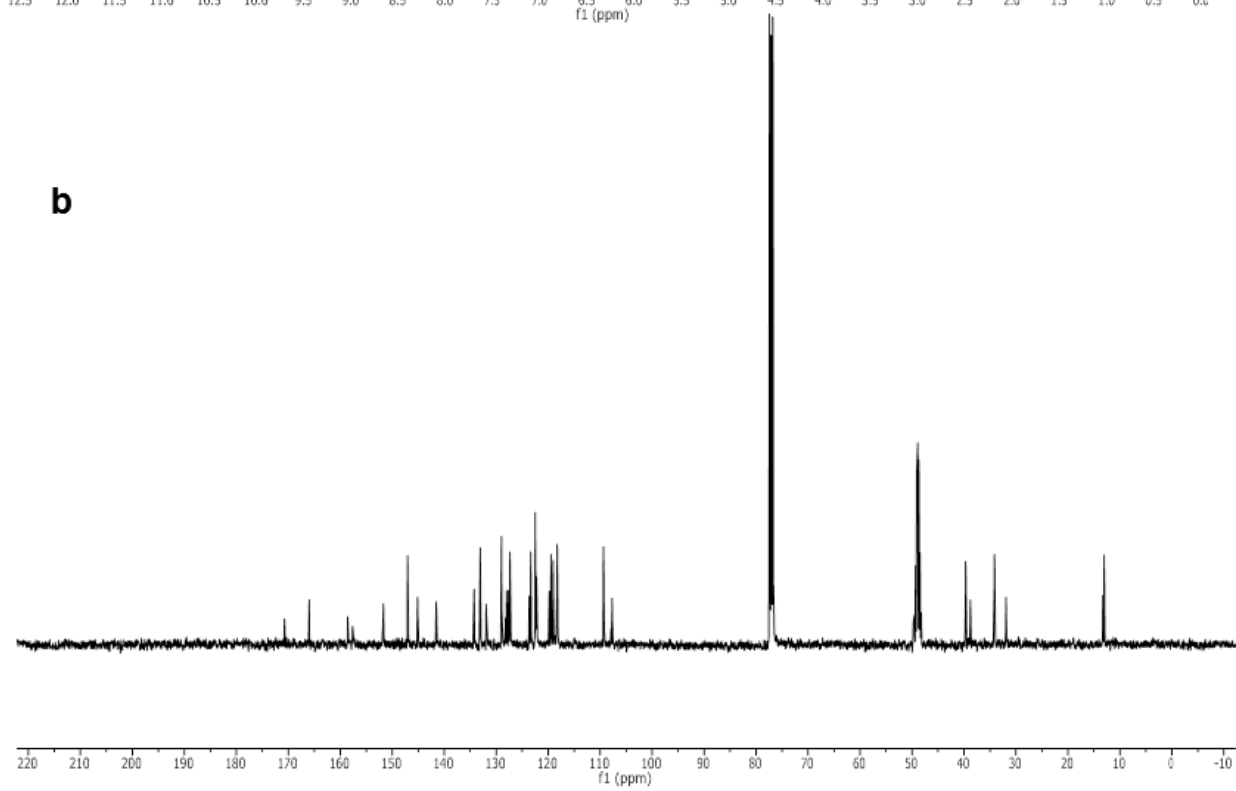
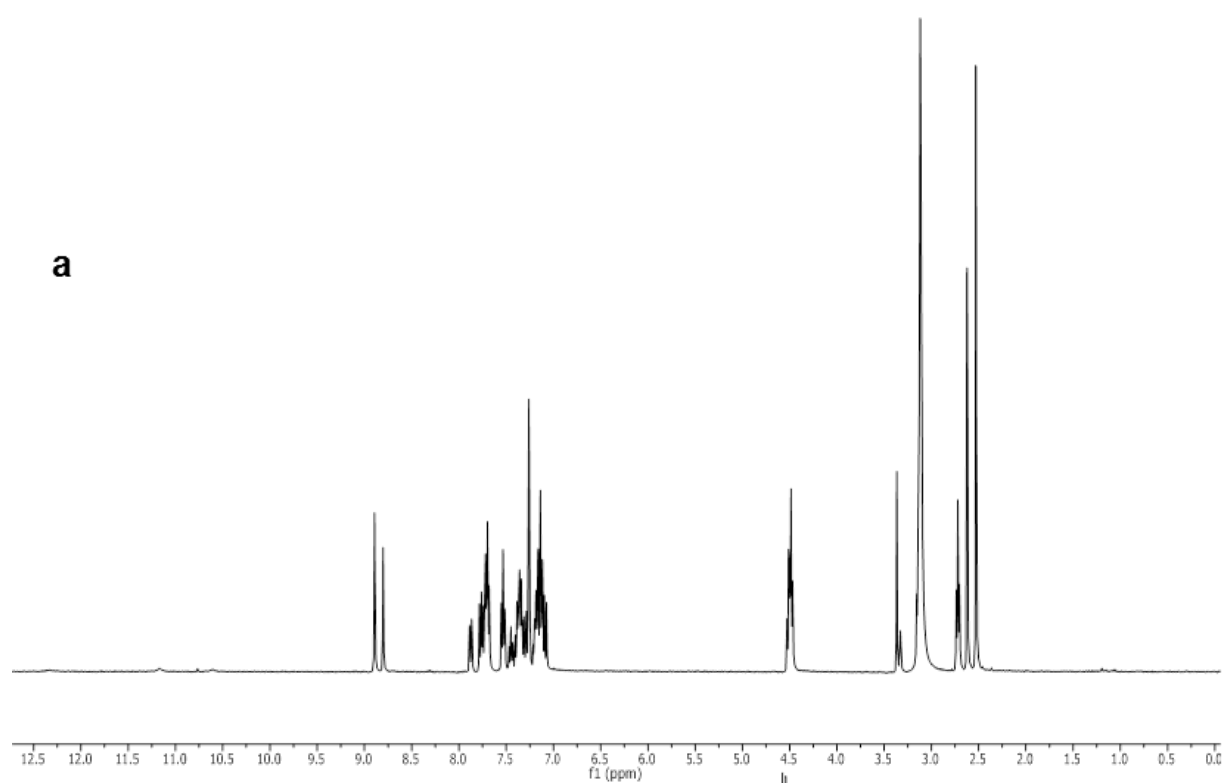


**Figure 5.** NMR spectroscopy of divin. (a)  $^1\text{H}$  spectrum of Divin (400 MHz,  $\text{CD}_3\text{OD}/\text{CDCl}_3$ ).  $^1\text{H}$  NMR (400 MHz,  $\text{CD}_3\text{OD}/\text{CDCl}_3$ )  $\delta$  8.89 (s, 1H,  $-\text{CO}-\text{NH}-\text{N}=\text{}$ ,  $\text{Trans}_{\text{C}(\text{O})-\text{N}}$  isomer), 8.80 (s, 1H,  $-\text{CO}-\text{NH}-\text{N}=\text{}$ ,  $\text{Cis}_{\text{C}(\text{O})-\text{N}}$  isomer), 7.88 (d,  $J = 8.6$  Hz, 1H,  $-\text{NH}-\text{N}=\text{CH}-$ ,  $\text{Cis}_{\text{C}(\text{O})-\text{N}}$  isomer), 7.78 (d,  $J = 8.5$  Hz, 1H,  $-\text{NH}-\text{N}=\text{CH}-$ ,  $\text{Trans}_{\text{C}(\text{O})-\text{N}}$  isomer), 7.75 – 7.65 (m, 3H), 7.58 – 7.05 (m, 7H), 4.50 (m, 2H,  $-\text{N}-\text{CH}_2-\text{CH}_2-\text{CO}-$ ), 3.39 – 3.30 (m, 1H,  $-\text{OH}$ ), 3.15 (m, 2H,  $-\text{N}-\text{CH}_2-\text{CH}_2-\text{CO}-$ ,  $\text{Cis}_{\text{C}(\text{O})-\text{N}}$  isomer), 2.72 (m, 2H,  $-\text{N}-\text{CH}_2-\text{CH}_2-\text{CO}-$ ,  $\text{Trans}_{\text{C}(\text{O})-\text{N}}$  isomer), 2.62 (s, 3H,  $-\text{CH}_3$ ,  $\text{Cis}_{\text{C}(\text{O})-\text{N}}$  isomer), 2.53 (s, 3H,  $-\text{CH}_3$ ,  $\text{Trans}_{\text{C}(\text{O})-\text{N}}$  isomer). (b)  $^{13}\text{C}$  NMR spectrum of Divin (100 MHz,  $\text{CD}_3\text{OD}/\text{CDCl}_3$ ). The chemical shifts for the  $\text{Cis}_{\text{C}(\text{O})-\text{N}}$  isomer listed in the parenthesis.  $^{13}\text{C}$  NMR (100 MHz,  $\text{CD}_3\text{OD}/\text{CDCl}_3$ )  $\delta$  165.98 (170.71) ( $-\text{CH}_2-\text{C}=\text{O}$ ), 158.55 (157.6) ( $-\text{C}-\text{OH}$ ), 151.69 (151.76) ( $\text{C}-\text{CH}_3$ ), 147.05 (145.12), 141.6 (141.5), 134.25 (134.25), 133.08 (133.16), 131.95 (131.87) ( $-\text{NH}-\text{N}=\text{CH}-$ ), 128.97 (128.97), 128.00 (128.22), 127.34 (127.61), 123.34 (123.64), 122.47 (122.47), 122.30 (122.23), 119.46 (119.79), 119.04 (118.39), 118.24 (118.30), 109.35 (109.26), 107.7 (107.9), 39.67 (38.78) ( $-\text{N}-\text{CH}_2-\text{CH}_2-\text{CO}-$ ), 34.14 (31.91) ( $-\text{N}-\text{CH}_2-\text{CH}_2-\text{CO}-$ ), 13.02 (13.28) ( $\text{C}-\text{CH}_3$ ).

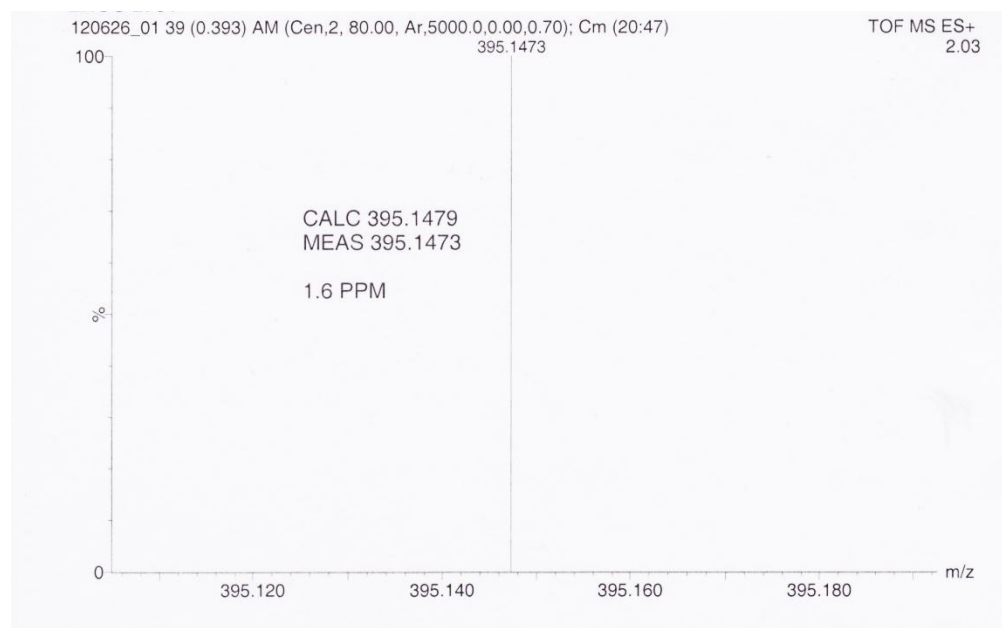


**Figure 6.** High-resolution mass spectrometry data of divin. (Calculated  $[\text{C}_{22}\text{H}_{20}\text{N}_4\text{O}_2\text{Na}]^+$  395.1479; Found 395.1473)

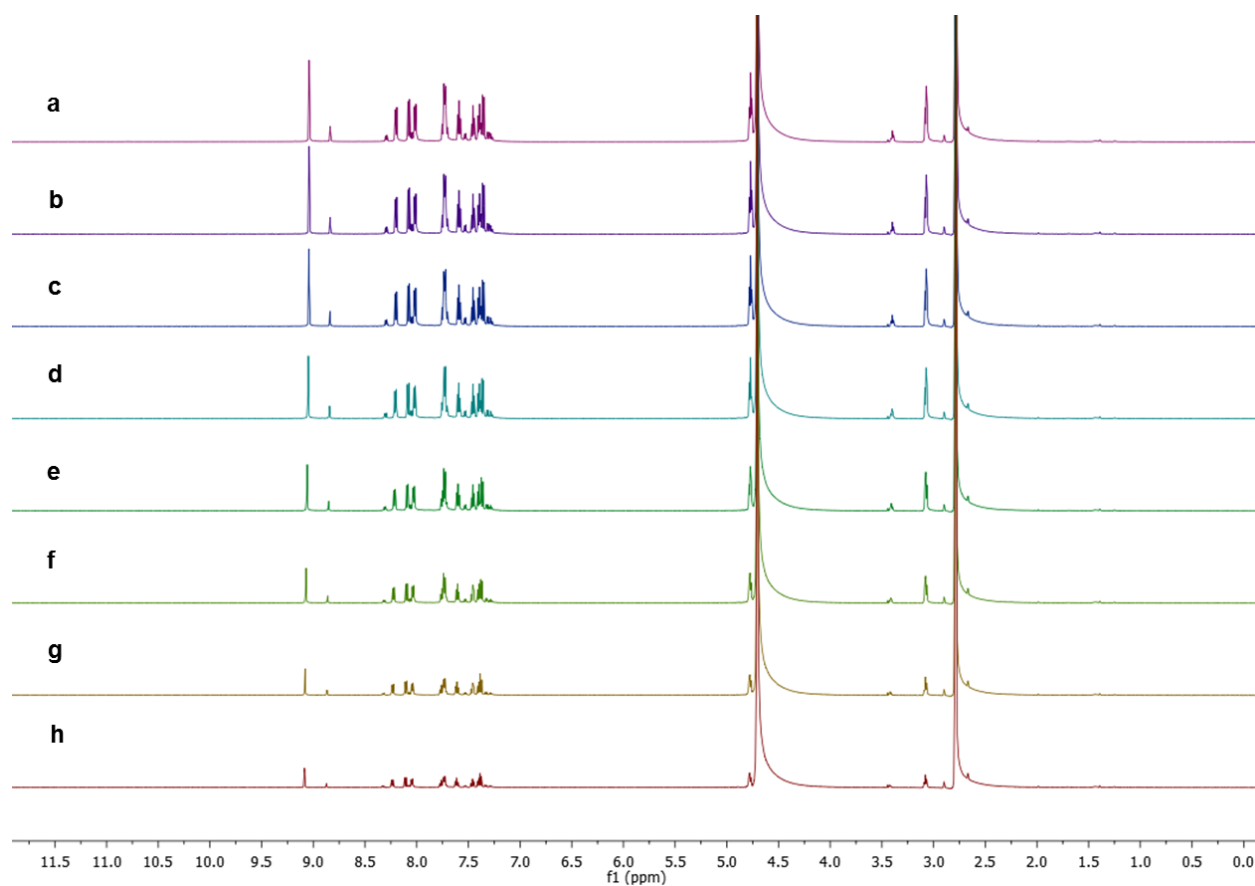


**Figure 7.** Divin is stable in an aqueous solution over a period of 24 h. <sup>1</sup>H NMR spectra (600 MHz) of divin in DMSO-d<sub>6</sub>/D<sub>2</sub>O at 37 °C at (a) 3 h; (b) 6 h; (c) 9 h; (d) 12 h; (e) 15 h; (f) 18 h; (g) 21 h; (h) 24 h.

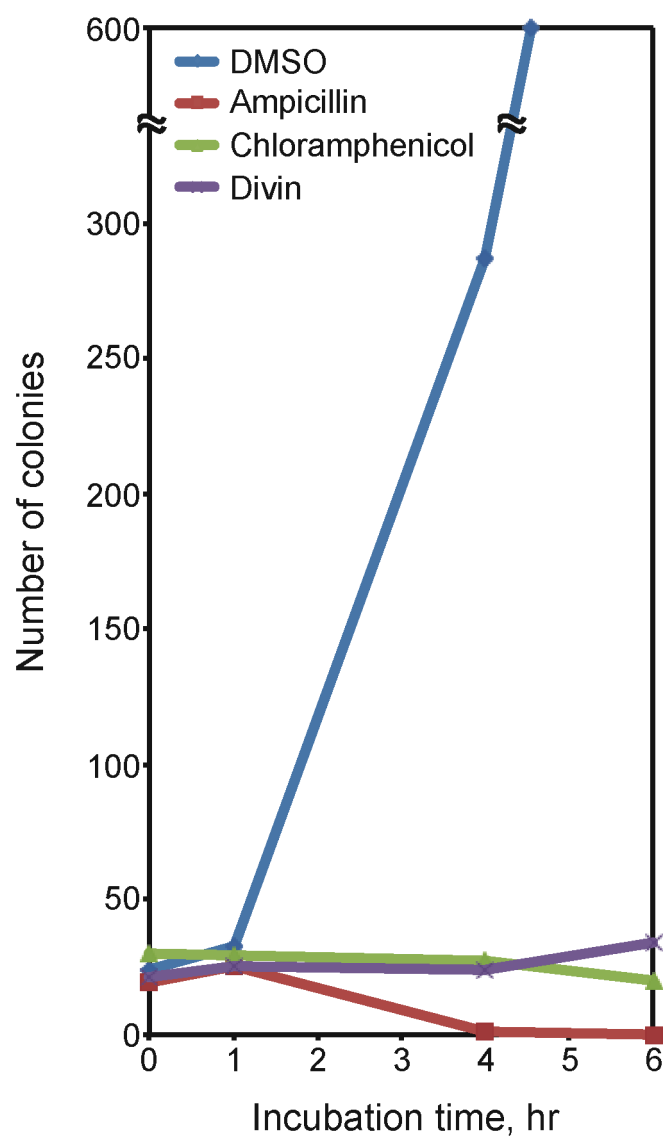


**Figure 8.** Divin is a bacteriostatic antibiotic against *E. coli*  $\Delta tolC$  cells.

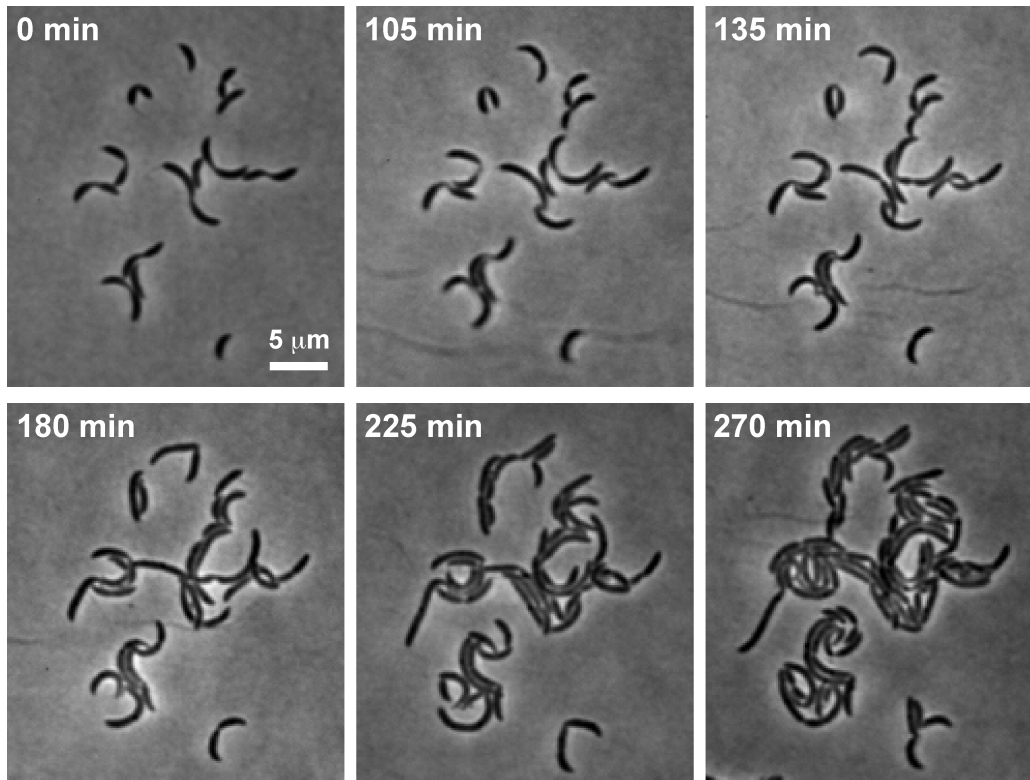


**Figure 9.** Divin reversibly inhibits cell division. *C. crescentus* CB15N cells were treated with 5  $\mu$ M of divin for 6 h, and an aliquot of the culture was inoculated on a 1% agarose 2X PYE pad ( $t = 0$  min). Cells were incubated on the microscope stage at 33  $^{\circ}$ C during image acquisition.

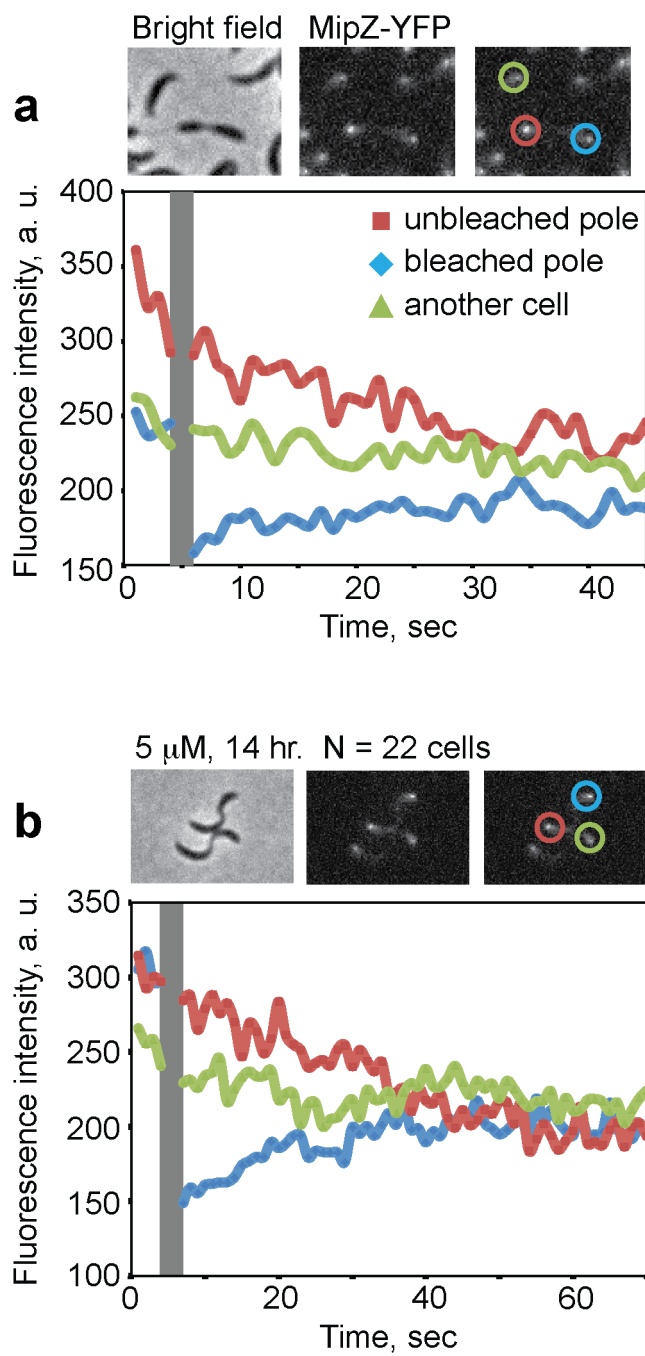


**Figure 10.** Divin-treated *C. crescentus* MT97 cells have a continuous cytoplasm between the mother and daughter cells. Images in each panel show bleached cells and unbleached cells in the imaging field. In the fluorescence image, three colored circles

represent the regions whose fluorescence intensities were plotted. The gray bar in the fluorescence intensity plots represents the bleaching period. (a) DMSO solvent control sample. (b) Cells treated with 5  $\mu\text{M}$  of divin for 14 h.

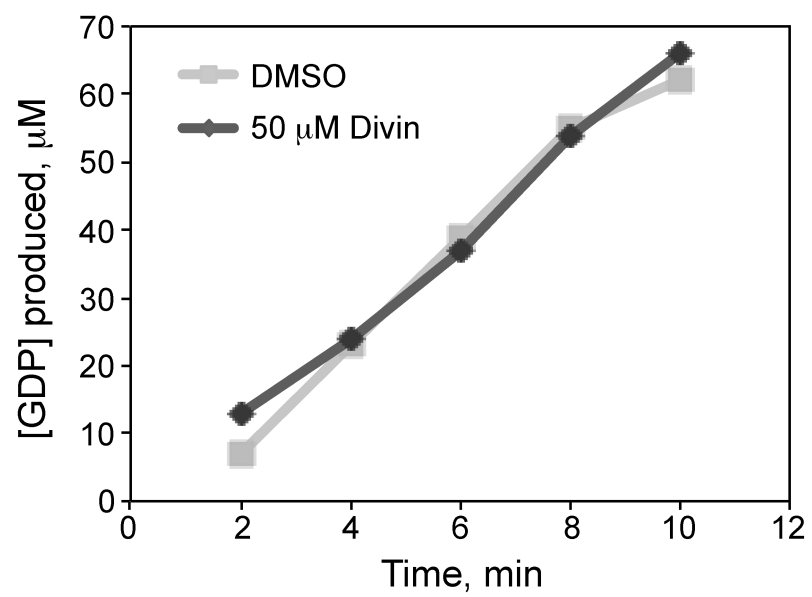


**Figure 11.** Divin does not affect the GTPase activity of recombinant *C. crescentus* FtsZ.

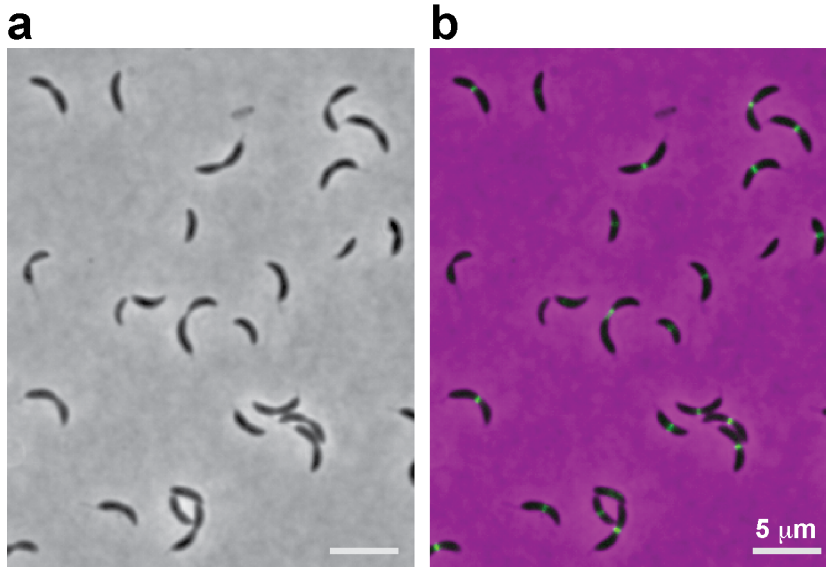


**Figure 12.** Divin does not perturb the FtsZ-YFP localization in *C. crescentus* MT196. (a) A brightfield image of MT196 cells 6 h after treatment with 5  $\mu$ M divin. (b) An overlay of brightfield and fluorescence (in green) channels.

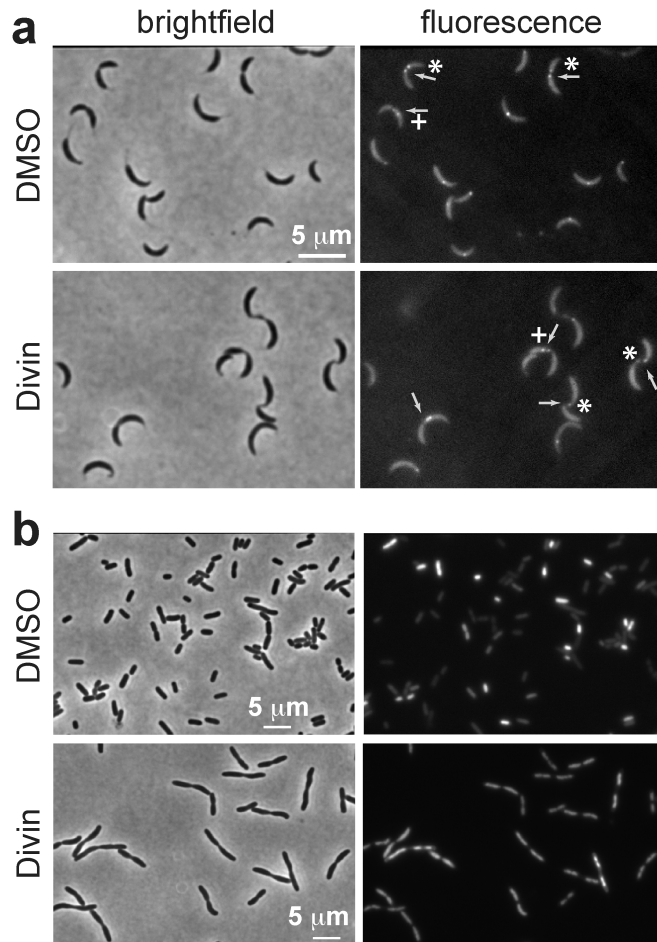


**Figure 13.** Divin does not perturb chromosome segregation of *C. crescentus* and *E. coli* cells. (a) MT20 cells were treated with 5  $\mu$ M divin for 10.5 h. A region of the chromosome near the terminus contains *lacO* arrays and is decorated with LacI-ECFP. Arrows in the fluorescence images point to cells with two fluorescent foci, which indicate two copies of the terminus that are physically separated. Cells that contain one focus per one half of the cell are marked with \*, and cells that have both foci in a same half are marked with +. (b) *E. coli*  $\Delta$ *tolC* cells were treated with 25  $\mu$ M divin for 16.5 h, and labeled with DAPI to visualize the DNA.

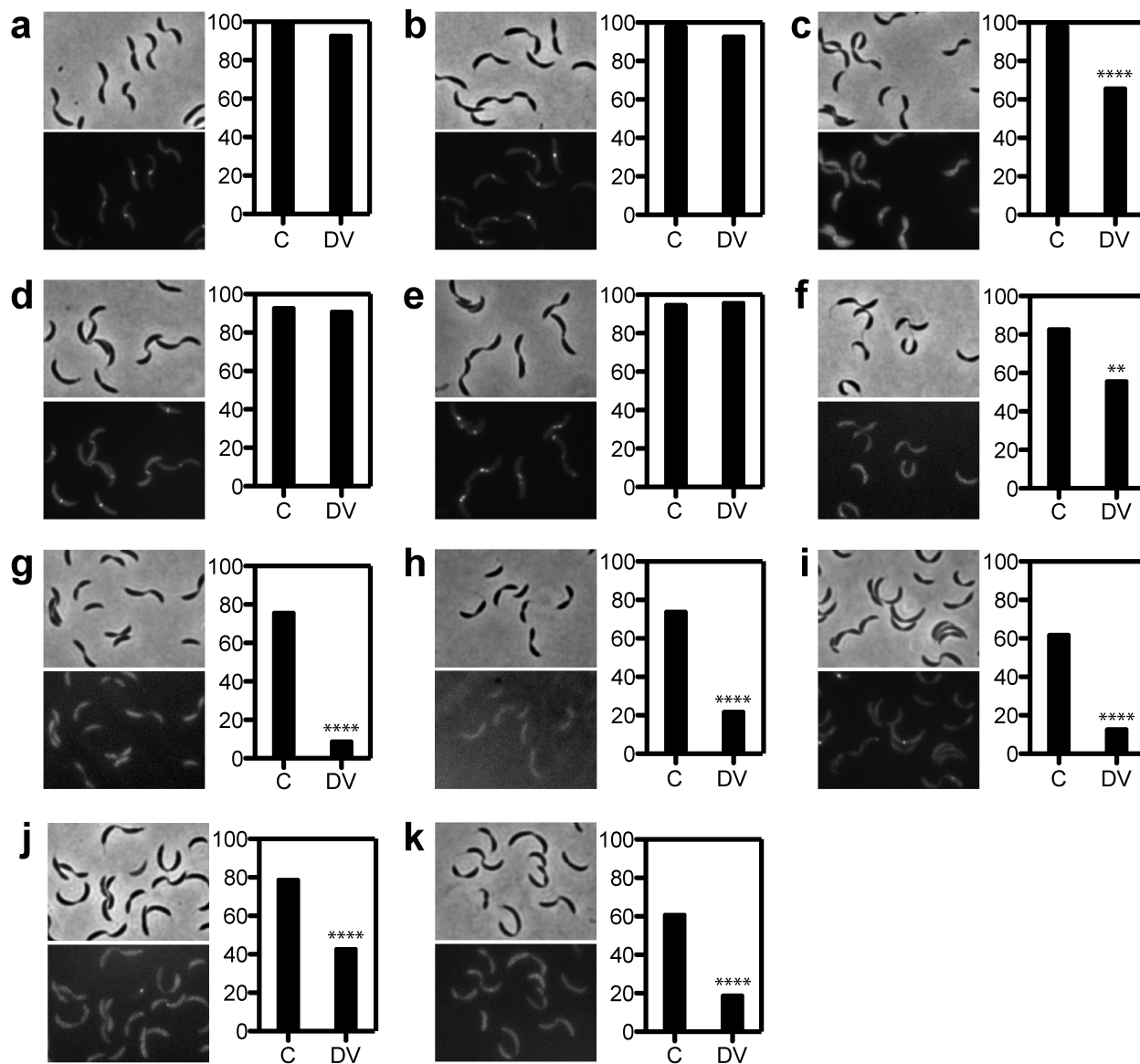


**Figure 14.** Divin perturbs the localization of division proteins in a time-dependent manner. For each division protein listed in Table 6, representative images of *C. crescentus* cells treated with divin (5  $\mu$ M) are shown. Each panel also contains histograms to indicate the percent population with protein localization to the division site. C, control sample; DV, divin-treated sample; \*\*, p-value  $\leq$  0.01; \*\*\*\*, p-value  $\leq$

0.0001. (a) ZapA, 12 h. (b) FzlA, 12 h. (c) DipM, 12 h. (d) FtsA, 12 h. (e) FtsN, 12 h. (f) FtsQ, 8 h. (g) FtsI, 6 h. (h) FtsK, 6 h. (i) FtsL, 8 h. (j) FtsW, 8 h. (k) FtsB, 8 h.

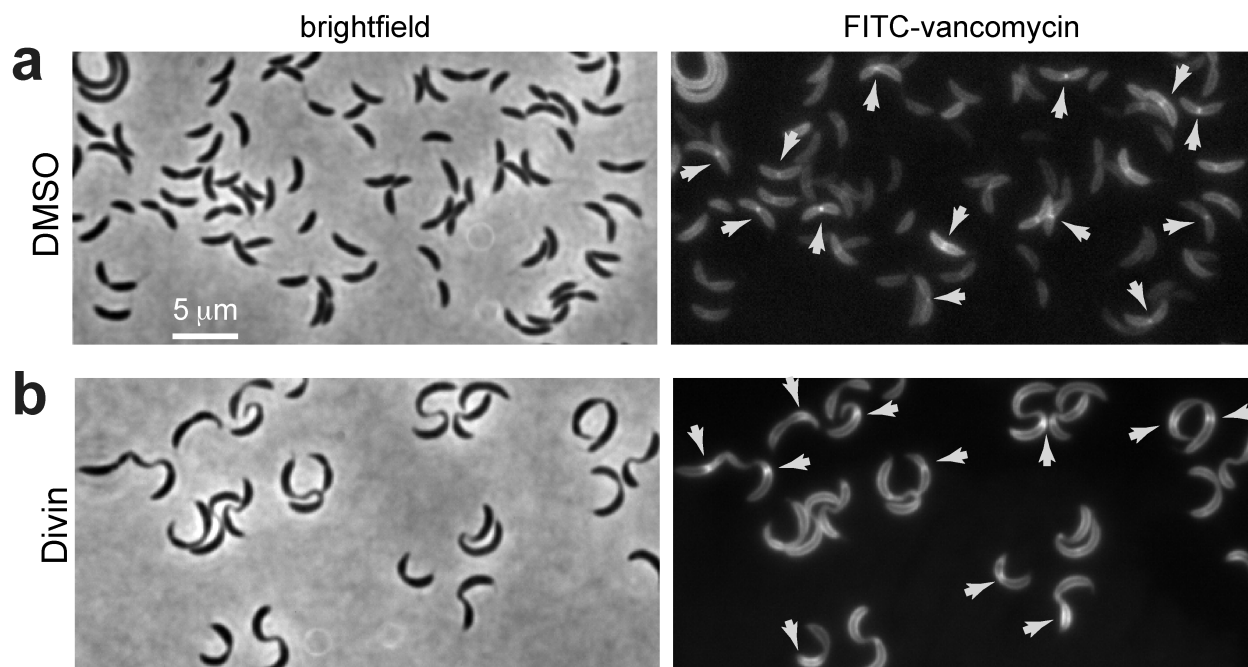


**Figure 15.** Labeling with FITC-vancomycin demonstrates reduced PG remodeling at the division site of divin-treated *C. crescentus* cells. Arrows point to regions of intense FITC-vancomycin labeling in a cell. (a) DMSO control. (b) CB15N cells treated with 5 μM divin for 21 h.

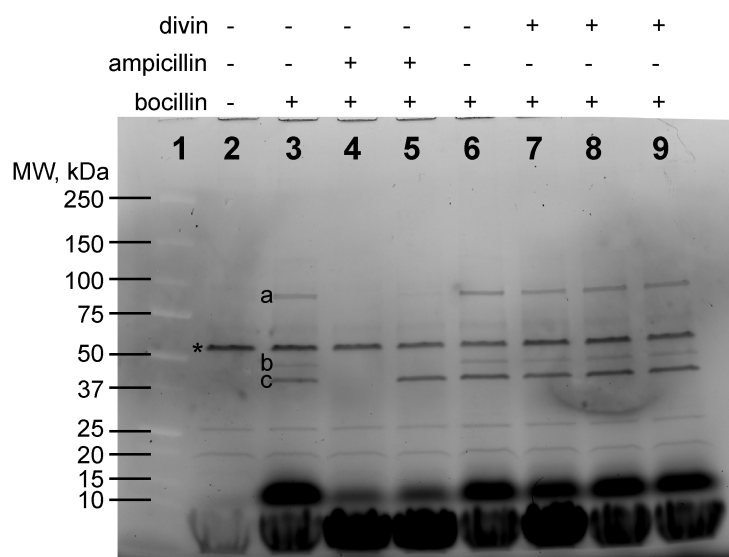


**Figure 16.** Divin does not bind to PBPs. Membrane proteins labeled with bocillin were visualized by gel electrophoresis and fluorescence imaging of the gel. A molecular weight ladder was added to lane 1. Lanes 3 and 6 show solvent-control reactions that had water or DMSO, respectively, instead of antibiotics. We tested two concentrations of ampicillin (5 mg/mL and 50  $\mu$ g/mL, shown in lanes 4 and 5, respectively), and three concentrations of divin (5, 0.5, and 0.05 mM as shown in lanes 7, 8, and 9, respectively). The protein band with \* exhibited autofluorescence (i.e. no bocillin added). Bands denoted with a, b, and c had a reduced labeling with bocillin when co-treated with ampicillin.

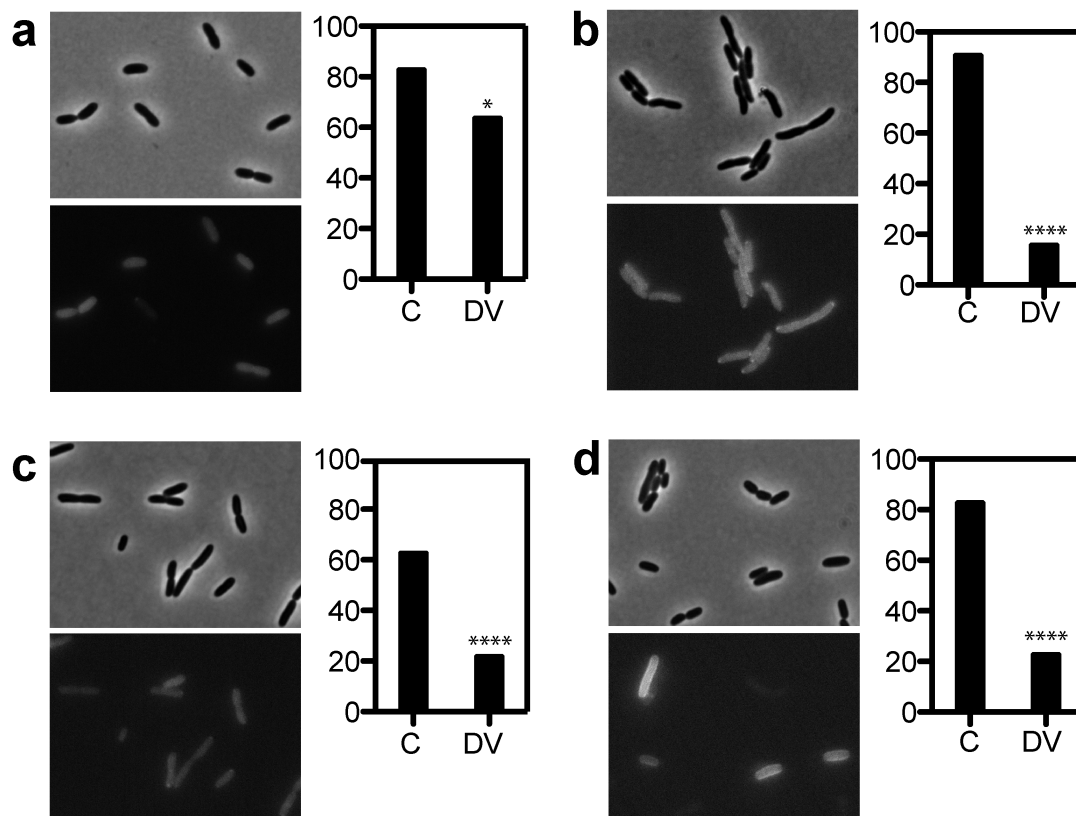


**Figure 17.** Divin perturbs the localization of division proteins in a time-dependent manner. For each division protein listed in Table 7, representative images of *E. coli* cells treated with divin (50  $\mu$ M) are shown. Each panel also contains a histogram to indicate the percent population with protein localization to the division site. C, control sample; DV, divin-treated sample; \*, p-value  $\leq 0.05$ . \*\*\*\*, p-value  $\leq 0.0001$ ; (a) FtsK, 1.5 h; (b) FtsQ, 5 h; (c) FtsL, 3 h; and (d) FtsN, 5 h.

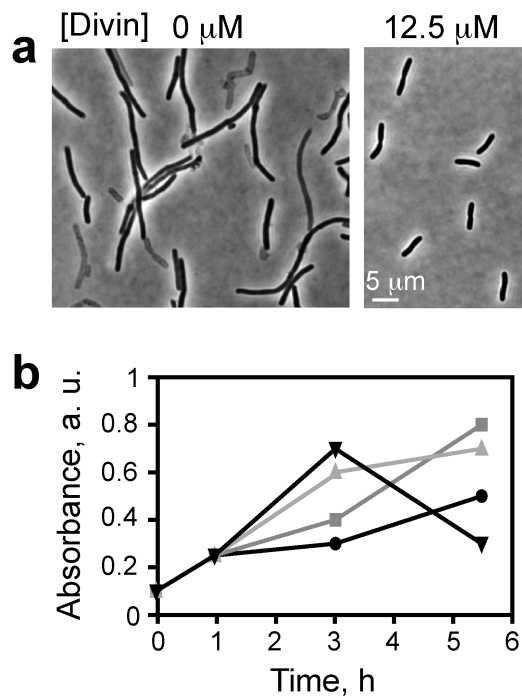


**Figure 18.** Divinin reduced cell lysis and filamentation triggered by cephalaxin. (a) Brightfield images of *E. coli*  $\Delta\text{tolC}$  cells treated with cephalaxin (10  $\mu\text{g}/\text{mL}$ ) and divinin (0 or 12.5  $\mu\text{M}$ ). (b) Absorbance ( $\lambda_{600}$ ) measurements of cell cultures that contained 10  $\mu\text{g}/\text{mL}$  of cephalaxin and different amounts of divinin (▼, 0  $\mu\text{M}$ ; ▲, 3.13  $\mu\text{M}$ ; ■, 6.25  $\mu\text{M}$ ; and ●, 12.5  $\mu\text{M}$ ).

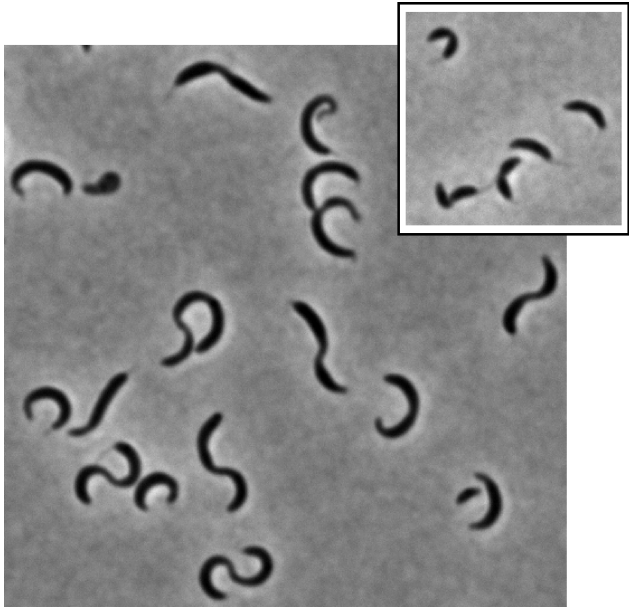


**Figure 19.** Divin inhibits the cell division of *C. crescentus*  $\Delta sidA$  cells. ML1759 cells were treated with 5  $\mu\text{M}$  divin for 24 h. The inset image shows ML1759 cells incubated with DMSO.

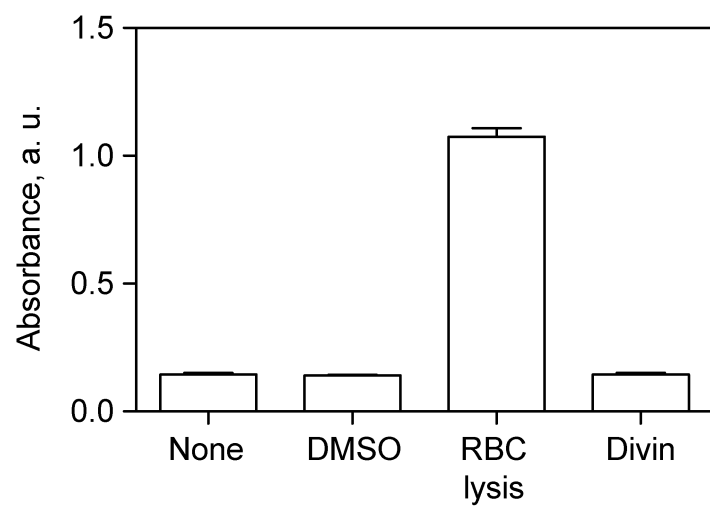


**Figure 20.** Divin is not toxic to red blood cells (RBCs). Hemolysis of RBCs was quantified by measuring the absorbance of heme at  $\lambda=405$  nm. A RBC lysis solution (EpiCentre Biotechnology) was used as a positive control.

Table 1. Strains used in this study.

Organism	Strain	Genotype/description	Resistant marker	Reference/Source
<i>V. cholerae</i>	clinical isolate	clinical isolate	-	(20)
<i>S. boydii</i>	clinical isolate	clinical isolate	-	(20)
<i>A. baumannii</i>	clinical isolate	clinical isolate	-	(20)
<i>C. crescentus</i>	CB15N	synchronizable derivative of wild-type CB15	-	(18)
<i>C. crescentus</i>	MT97	CB15N <i>mipZ::mipZ-yfp</i>	-	(18)
<i>C. crescentus</i>	MT196	CB15N <i>Pvan::Pvan-ftsZ-yfp</i>	kan	(18)
<i>C. crescentus</i>	MT20	CB15N <i>lacO</i> integrated into CC1792, <i>Pxyl::Pxyl-lacI-ecfp, tetR-eyfp</i>	kan, spec, str	This study
<i>C. crescentus</i>	EG050	CB15N <i>Pxyl::Pxyl-venus-ftsW</i>	kan	(3)
<i>C. crescentus</i>	EG081	CB15N <i>Pxyl::Pxyl-yfp-ftsQ</i>	spec	(3)
<i>C. crescentus</i>	EG493	CB15N <i>mipZ::mipZ-cerulean Pxyl::Pxyl-venus-ftsL</i>	kan	(3)
<i>C. crescentus</i>	EG494	CB15N <i>mipZ::mipZ-cerulean Pxyl::Pxyl-venus-ftsB</i>	kan	(3)
<i>C. crescentus</i>	NR1371	CB15N <i>tipN::tipN-egfp</i>	kan	This study
<i>C. crescentus</i>	AM216	CB15N <i>dipM::dipM-mcherry Pxyl::Pxyl-ftsK-ecfp</i>	kan	(33)
<i>C. crescentus</i>	MT46	CB15N <i>ftsN::egfp-ftsN</i>	-	(37)
<i>C. crescentus</i>	CJW1822	CB15N <i>Pxyl::Pxyl-gfp-ftsI</i>	kan	(29)
<i>C. crescentus</i>	SS128	CB15N <i>Pvan::Pvan-gfp-mreB</i>	gent	This study
<i>C. crescentus</i>	SS255	CB15N <i>Pxyl::Pxyl-gfp-fzIA</i>	kan	This study
<i>C. crescentus</i>	SS157	CB15N <i>Pxyl::Pxyl-zapA-gfp</i>	kan	This study
<i>C. crescentus</i>	ML1759	CB15N $\Delta$ <i>sidA</i>	-	(11)
<i>E. coli</i>	JW5503	a part of the Keio collection, BW25113 $\Delta$ <i>tolC</i>	kan	(45)
<i>E. coli</i>	YJE20	JW5503 transformed with the plasmid pCH195	amp	This study
<i>E. coli</i>	YJE21	JW5503 transformed with the plasmid pCH196	amp	This study
<i>E. coli</i>	YJE22	JW5503 transformed with the plasmid pCH201	amp	This study
<i>E. coli</i>	YJE23	JW5503 transformed with the plasmid pCH205	amp	This study

**Table 2.** Plasmids used in this study.

<b>Plasmid</b>	<b>Description</b>	<b>Source</b>
pCH195	<i>Plac::gfp-ftsL AmpR pBR/ColE1</i>	Thomas G. Bernhardt
pCH196	<i>Plac::gfp-ftsQ AmpR pBR/ColE1</i>	Thomas G. Bernhardt
pCH201	<i>Plac::gfp-ftsN AmpR pBR/ColE1</i>	Thomas G. Bernhardt
pCH205	<i>Plac::ftsK[1-266]-gfp AmpR pBR/ColE1</i>	Thomas G. Bernhardt

**Table 3.** Induction conditions for fluorescence microscopy.

<b>Organism</b>	<b>Strain</b>	<b>Induction</b>
<i>C. crescentus</i>	MT196	0.5 mM vanillate, 1.5 h
<i>C. crescentus</i>	MT20	0.3% xylose and 0.5 mM IPTG, 1.5 h
<i>C. crescentus</i>	EG050	0.3% xylose, 1 h
<i>C. crescentus</i>	EG081	0.3% xylose, 1 h
<i>C. crescentus</i>	EG493	0.3% xylose, 1 h
<i>C. crescentus</i>	EG494	0.3% xylose, 1 h
<i>C. crescentus</i>	AM216	0.3% xylose, 1 h
<i>C. crescentus</i>	CJW1822	0.3% xylose, 1 h
<i>C. crescentus</i>	SS255	0.3% xylose, 1 h
<i>C. crescentus</i>	SS157	0.3% xylose, 1 h
<i>E. coli</i>	YJE20	25 $\mu$ M IPTG, 30 m
<i>E. coli</i>	YJE21	25 $\mu$ M IPTG, 30 m
<i>E. coli</i>	YJE22	25 $\mu$ M IPTG, 30 m
<i>E. coli</i>	YJE23	25 $\mu$ M IPTG, 30 m

**Table 4.** Minimum inhibitory concentration (MIC) of divin.

<b>Organism</b>	<b>Strain</b>	<b>MIC (<math>\mu\text{M}</math>)</b>
<i>Escherichia coli</i>	BW25113 $\Delta\text{tolC}$	12.5
<i>Caulobacter crescentus</i>	CB15N	5
<i>Vibrio cholerae</i>	clinical isolate	0.4
<i>Shigella boydii</i>	clinical isolate	50
<i>Acinetobacter baumannii</i>	clinical isolate	25

**Table 5.** Solubility of divin in buffer containing different concentrations of DMSO.

<b>DMSO, % v/v</b>	<b>Solubility, <math>\mu\text{M}</math></b>
2	10
4	10
8	50

**Table 6.** Divin perturbs the localization of division proteins in a time-dependent manner in *C. crescentus* cells. Division proteins are listed in the order of assembly (Goley 2011). A plus sign (+) represents protein localization at the constriction site, and a minus sign (-) for delocalization. Raw images and results from image analysis are shown in Figure 14.

Division proteins	Time		
	6 hr	8 hr	12 hr
ZapA	+	+	+
FzIA	+	+	+
DipM	+	+	-
FtsA	+	+	+
FtsN	+	+	+
FtsQ	+	-	-
FtsI	-	-	-
FtsK	-	-	-
FtsL	+	-	-
FtsW	+	-	-
FtsB	+	-	-

**Table 7.** Divin perturbs the localization of division proteins in a time-dependent manner in *E. coli* cells. Division proteins are listed in the order of assembly (Gonzalez and Beckwith 2010). A plus sign (+) represents protein localization at the constriction site, and a minus sign (-) for delocalization.

Division proteins	Time		
	1.5 hr	3 hr	5 hr
FtsK	-	-	-
FtsQ	+	+	-
FtsL	+	-	-
FtsN	+	+	-

## REFERENCES

1. Taschner, P. E., Huls, P. G., Pas, E., and Woldringh, C. L. (1988) Division behavior and shape changes in isogenic *ftsZ*, *ftsQ*, *ftsA*, *pbpB*, and *ftsE* cell division mutants of *Escherichia coli* during temperature shift experiments, *J Bacteriol* 170, 1533-1540.
2. Adams, D. W., and Errington, J. (2009) Bacterial cell division: assembly, maintenance and disassembly of the Z ring, *Nature reviews. Microbiology* 7, 642-653.
3. Goley, E. D., Yeh, Y.-C., Hong, S.-H., Fero, M. J., Abeliuk, E., McAdams, H. H., and Shapiro, L. (2011) Assembly of the *Caulobacter* cell division machine, *Molecular Microbiology* 80, 1680-1698.
4. Goehring, N. W., and Beckwith, J. (2005) Diverse paths to midcell: assembly of the bacterial cell division machinery, *Current biology : CB* 15, R514-526.
5. Margolin, W. (2005) FtsZ and the division of prokaryotic cells and organelles, *Nature reviews. Molecular cell biology* 6, 862-871.
6. Kirkpatrick, C. L., and Viollier, P. H. (2011) New(s) to the (Z-)ring, *Curr Opin Microbiol* 14, 691-697.
7. Thanbichler, M. (2010) Synchronization of chromosome dynamics and cell division in bacteria, *Cold Spring Harb Perspect Biol* 2, a000331.
8. Renner, L. D., and Weibel, D. B. (2012) MinD and MinE Interact with Anionic Phospholipids and Regulate Division Plane Formation in *Escherichia coli*, *The Journal of biological chemistry* 287, 38835-38844.
9. Wu, L. J., and Errington, J. (2012) Nucleoid occlusion and bacterial cell division, *Nature reviews. Microbiology* 10, 8-12.
10. Radhakrishnan, S. K., Pritchard, S., and Viollier, P. H. (2010) Coupling prokaryotic cell fate and division control with a bifunctional and oscillating oxidoreductase homolog, *Dev Cell* 18, 90-101.
11. Modell, J. W., Hopkins, A. C., and Laub, M. T. (2011) A DNA damage checkpoint in *Caulobacter crescentus* inhibits cell division through a direct interaction with FtsW, *Genes Dev* 25, 1328-1343.
12. Falconer, S. B., Czarny, T. L., and Brown, E. D. (2011) Antibiotics as probes of biological complexity, *Nat Chem Biol* 7, 415-423.

13. Georgopapadakou, N. H., and Bertasso, A. (1991) Effects of quinolones on nucleoid segregation in *Escherichia coli*, *Antimicrob Agents Chemother* 35, 2645-2648.
14. Couturier, M., Bahassi el, M., and Van Melderen, L. (1998) Bacterial death by DNA gyrase poisoning, *Trends Microbiol* 6, 269-275.
15. Miller, C., Thomsen, L. E., Gaggero, C., Mosseri, R., Ingmer, H., and Cohen, S. N. (2004) SOS response induction by beta-lactams and bacterial defense against antibiotic lethality, *Science* 305, 1629-1631.
16. Bakshi, S., Siryaporn, A., Goulian, M., and Weisshaar, J. C. (2012) Superresolution imaging of ribosomes and RNA polymerase in live *Escherichia coli* cells, *Mol Microbiol* 85, 21-38.
17. Deich, J., Judd, E. M., McAdams, H. H., and Moerner, W. E. (2004) Visualization of the movement of single histidine kinase molecules in live *Caulobacter* cells, *Proc Natl Acad Sci U S A* 101, 15921-15926.
18. Thanbichler, M., and Shapiro, L. (2006) MipZ, a spatial regulator coordinating chromosome segregation with cell division in *Caulobacter*, *Cell* 126, 147-162.
19. Chung, H. S., Yao, Z., Goehring, N. W., Kishony, R., Beckwith, J., and Kahne, D. (2009) Rapid beta-lactam-induced lysis requires successful assembly of the cell division machinery, *Proceedings of the National Academy of Sciences of the United States of America* 106, 21872-21877.
20. Eun, Y. J., Foss, M. H., Kiekebusch, D., Pauw, D. A., Westler, W. M., Thanbichler, M., and Weibel, D. B. (2012) DCAP: a broad-spectrum antibiotic that targets the cytoplasmic membrane of bacteria, *J Am Chem Soc* 134, 11322-11325.
21. Judd, E. M., Comolli, L. R., Chen, J. C., Downing, K. H., Moerner, W. E., and McAdams, H. H. (2005) Distinct constrictive processes, separated in time and space, divide *caulobacter* inner and outer membranes, *J Bacteriol* 187, 6874-6882.
22. Uehara, T., and Bernhardt, T. G. (2011) More than just lysins: peptidoglycan hydrolases tailor the cell wall, *Curr Opin Microbiol* 14, 698-703.
23. Chung, K. M., Hsu, H. H., Yeh, H. Y., and Chang, B. Y. (2007) Mechanism of regulation of prokaryotic tubulin-like GTPase FtsZ by membrane protein EzrA, *The Journal of biological chemistry* 282, 14891-14897.
24. Wang, S. C., West, L., and Shapiro, L. (2006) The bifunctional FtsK protein mediates chromosome partitioning and cell division in *Caulobacter*, *J Bacteriol* 188, 1497-1508.

25. Ward, D., and Newton, A. (1997) Requirement of topoisomerase IV parC and parE genes for cell cycle progression and developmental regulation in *Caulobacter crescentus*, *Mol Microbiol* 26, 897-910.
26. Toro, E., and Shapiro, L. (2010) Bacterial chromosome organization and segregation, *Cold Spring Harb Perspect Biol* 2, a000349.
27. Begg, K. J., and Donachie, W. D. (1985) Cell shape and division in *Escherichia coli*: experiments with shape and division mutants, *J Bacteriol* 163, 615-622.
28. Yu, X. C., Tran, A. H., Sun, Q., and Margolin, W. (1998) Localization of cell division protein FtsK to the *Escherichia coli* septum and identification of a potential N-terminal targeting domain, *J Bacteriol* 180, 1296-1304.
29. Costa, T., Priyadarshini, R., and Jacobs-Wagner, C. (2008) Localization of PBP3 in *Caulobacter crescentus* is highly dynamic and largely relies on its functional transpeptidase domain, *Mol Microbiol* 70, 634-651.
30. Gonzalez, M. D., Akbay, E. A., Boyd, D., and Beckwith, J. (2010) Multiple interaction domains in FtsL, a protein component of the widely conserved bacterial FtsLBQ cell division complex, *J Bacteriol* 192, 2757-2768.
31. Gonzalez, M. D., and Beckwith, J. (2009) Divisome under construction: distinct domains of the small membrane protein FtsB are necessary for interaction with multiple cell division proteins, *J Bacteriol* 191, 2815-2825.
32. Goley, E. D., Comolli, L. R., Fero, K. E., Downing, K. H., and Shapiro, L. (2010) DipM links peptidoglycan remodelling to outer membrane organization in *Caulobacter*, *Mol Microbiol* 77, 56-73.
33. Moll, A., Schlimpert, S., Briegel, A., Jensen, G. J., and Thanbichler, M. (2010) DipM, a new factor required for peptidoglycan remodelling during cell division in *Caulobacter crescentus*, *Mol Microbiol* 77, 90-107.
34. Poggio, S., Takacs, C. N., Vollmer, W., and Jacobs-Wagner, C. (2010) A protein critical for cell constriction in the Gram-negative bacterium *Caulobacter crescentus* localizes at the division site through its peptidoglycan-binding LysM domains, *Mol Microbiol* 77, 74-89.
35. de Pedro, M. A., Quintela, J. C., Holtje, J. V., and Schwarz, H. (1997) Murein segregation in *Escherichia coli*, *J Bacteriol* 179, 2823-2834.
36. Foss, M. H., Eun, Y. J., and Weibel, D. B. (2011) Chemical-biological studies of subcellular organization in bacteria, *Biochemistry* 50, 7719-7734.

37. Moll, A., and Thanbichler, M. (2009) FtsN-like proteins are conserved components of the cell division machinery in proteobacteria, *Mol Microbiol* 72, 1037-1053.
38. Hung, D. T., and Rubin, E. J. (2006) Chemical biology and bacteria: not simply a matter of life or death, *Curr Opin Chem Biol* 10, 321-326.
39. Erickson, H. P., Anderson, D. E., and Osawa, M. (2010) FtsZ in Bacterial Cytokinesis: Cytoskeleton and Force Generator All in One, *Microbiology and Molecular Biology Reviews* 74, 504-528.
40. Mingorance, J., Rivas, G., Velez, M., Gomez-Puertas, P., and Vicente, M. (2010) Strong FtsZ is with the force: mechanisms to constrict bacteria, *Trends Microbiol* 18, 348-356.
41. Joseleau-Petit, D., Liebart, J. C., Ayala, J. A., and D'Ari, R. (2007) Unstable *Escherichia coli* L forms revisited: growth requires peptidoglycan synthesis, *J Bacteriol* 189, 6512-6520.
42. Proctor, S. A., Minc, N., Boudaoud, A., and Chang, F. (2012) Contributions of turgor pressure, the contractile ring, and septum assembly to forces in cytokinesis in fission yeast, *Current biology : CB* 22, 1601-1608.
43. Garner, E. C., Bernard, R., Wang, W., Zhuang, X., Rudner, D. Z., and Mitchison, T. (2011) Coupled, Circumferential Motions of the Cell Wall Synthesis Machinery and MreB Filaments in *B. subtilis*, *Science* 333, 222-225.
44. Peterson, J. R., and Mitchison, T. J. (2002) Small molecules, big impact: A history of chemical inhibitors and the cytoskeleton, *Chemistry & Biology* 9, 1275-1285.
45. Baba, T., Ara, T., Hasegawa, M., Takai, Y., Okumura, Y., Baba, M., Datsenko, K. A., Tomita, M., Wanner, B. L., and Mori, H. (2006) Construction of *Escherichia coli* K-12 in-frame, single-gene knockout mutants: the Keio collection, *Mol Syst Biol* 2, 2006 0008.

## **CHAPTER 7**

### **Conclusions and future directions**

Throughout the history of science, new tools and techniques have advanced our understanding of nature. In microbiology, the demand for new tools has increased to keep pace with new discoveries, which include the prevalence of bacterial communities. In these microbial communities, heterogeneity and chemical signaling is essential to adaptation and fitness (1). These discoveries have stimulated research projects that aim to control heterogeneity in bacterial populations, understand variations at the single cell level, and introduce chemicals that modulate biological processes (2-4). New tools can have a transformative impact on these areas of microbiology.

Each chapter in this thesis introduces a new physical or chemical tool for studying microbial physiology. Chapter 2 describes a biofilm stencil fabricated in a biocompatible polymer. This material serves as a physical scaffold for patterning biofilms on surfaces, and growing them reproducibly in a high-throughput manner (5). Based on this approach, another version of the biofilm stencil was developed using a hydrogel that enables the diffusion of small molecules between neighboring biofilms (6). Using the hydrogel stencil, Flickinger et al. studied the effect of a quorum sensing gradient on growth and biofilm formation of *Pseudomonas aeruginosa* cells. Chapter 3 introduces a microfluidic device for encapsulating microbial cells in agarose microparticles. Encapsulation enables isolation and manipulation cells with rare phenotypes (e.g. drug resistance) in a large population (7). Chapter 5 describes DCAP, a small molecule that targets bacterial membranes, reduces their transmembrane potential ( $\Delta\Psi$ ), and increases membrane permeability. The biological activity of DCAP makes it a potent antibiotic against slow-growing and biofilm-associated cells, which are frequently associated with persistent bacterial infections (8). Chapter 6 introduces the small molecule divin, which targets the assembly and maturation of divisome, a

multi-protein complex that drive bacterial cytokinesis. This mechanism of division makes it a valuable tool for studying the dynamics of the divisome and the function of its protein components.

Building upon the characterization and pilot experiments described in this thesis, we propose and summarize several future studies of these physical and chemical tools.

### **Future studies: agarose microparticles**

In chapter 3, we described a microfluidic-based encapsulation technique. One of the highlights of this approach is the small volume of agarose microparticles, which increases the effective concentration of metabolites or other chemicals that are secreted by cells encapsulated within the microparticles (7). This characteristic may be useful for screening soil extracts to identify secondary metabolites with desirable biological activity. For example, some of the most medically important secondary metabolites identified from soil microbes have come from *Streptomyces* spp. *Streptomyces* harbor a large number of cryptic biosynthetic pathways in their genome, which may encode new classes of polyketides and non-ribosomal peptides (9). A fundamental, unanswered question in this area is how this organism activates and regulates the cryptic pathways, and whether these pathways encode fundamentally new classes of secondary metabolites (9).

A growing body of literature suggests that many of the cryptic biosynthetic pathways in *Streptomyces* spp. are regulated at the level of transcription in response to the extracellular environment, and that other soil bacteria may trigger their production (10). To explore this area, we propose to use the agarose microparticle technique to co-encapsulate engineered reporter strains of *Streptomyces coelicolor* with bacterial cells

extracted from soil. The reporter strain and a cell from a soil extract can be co-encapsulated into agarose microparticles at a frequency of  $\sim 10^6$  per hr. Agarose particles can be incubated in an organic phase (e.g. mineral oil) to limit the diffusion of water-soluble metabolites out of particles while supporting the growth of encapsulated microbes. This barrier to retain secondary metabolites and the small volume of particles would increase the effective concentration of secondary metabolite produced from the soil bacterium and enhance the identification of turning on quiescent pathways in *Streptomyces*. Microparticles with high levels of fluorescence can be isolated using fluorescence activated cell sorting (FACS). In summary, the proposed study may enable fundamental research in chemical communication between soil bacteria, transcriptional regulation in *Streptomyces*, natural products chemistry, and medicinal chemistry.

### **Future studies: DCAP**

In chapter 5, we described a membrane-targeting antibiotic DCAP that lowers  $\Delta\Psi$  and increases the membrane permeability in bacteria. It is unclear whether the moderate increase in the membrane permeability is solely responsible for the large decrease in  $\Delta\Psi$  (8). Here we propose a set of experiments to further characterize the mechanism of DCAP.

When investigating the mechanism of DCAP, we treated bacterial cells with the compound for 20 min for both assays measuring the  $\Delta\Psi$  and membrane permeability (8). The first experiment we propose is to revisit these assays and characterize the temporal dependence of changes in the  $\Delta\Psi$  and membrane permeability. A decrease in  $\Delta\Psi$  that occurs before any changes are observed in the membrane potential would indicate that the reduction in  $\Delta\Psi$  was not caused by a leaky membrane. On the other

hand, if changes in  $\Delta\Psi$  and permeability occur simultaneously, there are two possible interpretations of this result. One possibility is that the  $\Delta\Psi$  is lowered due to a leaky membrane, and the other is that DCAP acts both as an ionophore and a permeabilizer of membranes. Although it would be difficult to distinguish between the two scenarios solely by investigating the kinetics of DCAP activity, this experiment would be straightforward to perform and may provide a valuable insight on the biological activity of this compound.

In addition to the time-course experiment, we suggest revisiting the membrane permeability assay to include more positive controls for comparison. Initially we used ethanol solutions (50 or 70% v/v) to prepare 'permeabilized' cells that would be labeled with propidium iodide (8). Along with this positive control, we propose using other antibiotics such as daptomycin and televancin for comparison. The extent of membrane permeability of other small molecules with known activities would serve as useful controls to compare with the activity of DCAP.

Furthermore, it would be helpful to test the ability of DCAP to permeabilize liposomes containing natural or synthetic lipids. Creating liposomes with different lipid compositions is straightforward, and the lipid content of the membrane may be an important parameter for DCAP activity. We have found that the efficacy of DCAP varies depending on the metabolic/developmental stages of bacterial cells (8), and it is known that the composition of bacterial membranes changes during growth and throughout the life cycle to exhibit different physical and chemical properties (11). Performing in vitro assays with liposomes of varying composition may reveal a particular lipid content that increases DCAP activity. This finding would enable our understanding of the molecular basis for the activity of DCAP for certain physiological

states of bacteria, and aid the development the compound as a potential probe for lipids in living cells.

To measure membrane permeability *in vitro*, we propose a fluorescence-based liposome assay. When creating liposomes by extrusion, a fluorescent dye (e.g. carboxyfluorescein and calcein) can be added to the lipid suspension for incorporation into liposomes (12). Free diffusion of dye molecules across the lipid bilayer is insignificant in stable liposomes, and any unincorporated fluorophores should be washed away prior to the assay. At high fluorophore concentrations (e.g. > 200 mM), the dye molecules inside of the liposome are quenched (13). As dye molecules escape the liposome, they emit fluorescence and an increase in fluorescence over time is a useful diagnostic of membrane permeability. Another fluorophore, ANTS, can be used in a similar manner by co-encapsulating ANTS with its quencher, DPX (14). As ANTS leaves the liposome, it is freed from the quencher and its fluorescence intensity increases.

The last study we propose for DCAP is to investigate the structure activity relationship (SAR) of the compound. Katie Hurley is a graduate student in the Weibel lab who has worked out a synthetic route for the compound and is synthesizing different DCAP analogs. Katie found that the enantiomerically pure DCAP stereoisomers have an identical minimum inhibitory concentration, indicating that the compound most likely does not interact directly with a specific protein target. Testing different DCAP analogs may help untangle the 'dual activity' of DCAP on the  $\Delta\Psi$  and membrane permeability. For example, analogs that are not biologically active yet possess the ability to change either the  $\Delta\Psi$  or permeability, would provide insight into which activity is more important for the antibiotic. Furthermore, SAR studies would

guide the modification of the compound structure to reduce toxicity to mammalian cells, and improve the specificity of DCAP for bacterial membranes.

### **Future studies: Divin**

Chapter 6 introduced a chemical inhibitor of bacterial division. Through genetic, biochemical, and cell biological experiments, we have demonstrated that the compound blocks cell division by perturbing the assembly and maturation of the divisome. As a next step, it would be useful to investigate SAR of divin and use this information to identify the molecular target of the compound.

We have previously attempted to find the target of divin by isolating spontaneous and evolved mutants that are resistant to the drug, and characterizing their genotype by genome sequencing. However, these attempts did not lead to a definitive target due to several challenges. First, the compound has a low solubility in aqueous solutions, which makes it difficult to prepare solid growth media containing divin at a concentration that is several folds higher than its MIC, for the selection of resistant mutants. Second, bacterial cells possess multiple strategies to reduce their susceptibility to antibiotics (15). For example, bacteria can increase the production of drug efflux pumps, or modify the pumps to recognize small molecules, which reduces their concentration in cells. Furthermore, cells can change the membrane permeability to lower the drug uptake, or enzymatically modify the drug to inactivate it. Finally, the evolution of resistance through passaging leads to an accumulation of multiple mutations in the genome. These mutations need to be tested in isolation in a wildtype background to investigate which gene product is a direct target of the antibiotic. When we isolated individual mutations from the evolution experiment, we found that a single

mutation did not confer resistance, suggesting that several mutations in a genome may work synergistically to increase resistance to divin. Taking lessons from the previous efforts, SAR studies on divin is necessary to optimize the compound structure for better solubility and potency, and thus enable a successful isolation of spontaneous mutants.

In addition to compound optimization, SAR investigations of divin would make it possible to design reactive probes for biochemical isolation of the target protein. In contrast to a genetic approach where a change in drug sensitivity serves as a clue to target identification, a biochemical approach hinges on the separation of the protein-drug complex to identify the target through subsequent mass spectrometry and bioinformatics (16). The biochemical separation requires modification of the compound structure, and the derivatives should be tested for their efficacy compared to the original compound, prior to its usage for target identification.

To provide a suitable analog for divin for the biochemical approach, we propose adding two modifications to the compound structure. One modification will add a functional group that forms a covalent bond to the protein target. For example, diazirine-modified compounds can be photo-activated to crosslink with nearby amino acids (17). The crosslinking would be useful during chromatography for purification of the protein-drug complex, since a stringent wash is necessary to reduce the number of false-positives (18). The other modification is to add an azide or alkyne to divin for click chemistry. This functional group can react with another small molecule tag (e.g. fluorescein, rhodamine, or biotin) derivatized for click chemistry. The tag serves as a molecular handle to separate the protein-drug complex, and would be used to label the protein-drug complex immediately prior to chromatography to minimize a possible interference from the tag with the bioactivity of the drug in vivo (19).

Although the biochemical approach with a probe containing crosslinking and click chemistry groups has been demonstrated for detecting protein-drug and protein-lipid interactions in vivo (20), the proposed experiments for target identification of divin are not trivial. Target identification has been recognized as the most time-consuming and challenging part of development of chemical tools (18, 21, 22). However, knowing the target of the small molecule would facilitate establishing divin as a reliable and predictable chemical tool for studying bacterial cell biology (23). Dr. Maoquan Zhou is a postdoctoral fellow in the Weibel lab, has devised a synthetic route for divin, and has synthesized and characterized ~20 different divin analogs. Testing these analogs has already provided insight into the SAR of divin. Dr. Zhou has identified small changes in the structure that cause a complete loss of the bioactivity. The inactive analogs would also be useful in the biochemical approach for target identification, since it can be used in parallel to eliminate false-positive hits (18).

## REFERENCES

1. Weibel, D. B., DiLuzio, W. R., and Whitesides, G. M. (2007) Microfabrication meets microbiology, *Nature Reviews Microbiology* 5, 209-218.
2. Muralimohan, A., Eun, Y. J., Bhattacharyya, B., and Weibel, D. B. (2009) Dissecting microbiological systems using materials science, *Trends Microbiol* 17, 100-108.
3. Ward, G. E., Carey, K. L., and Westwood, N. J. (2002) Using small molecules to study big questions in cellular microbiology, *Cellular Microbiology* 4, 471-482.
4. Hung, D. T., and Rubin, E. J. (2006) Chemical biology and bacteria: not simply a matter of life or death, *Curr Opin Chem Biol* 10, 321-326.
5. Eun, Y. J., and Weibel, D. B. (2009) Fabrication of microbial biofilm arrays by geometric control of cell adhesion, *Langmuir : the ACS journal of surfaces and colloids* 25, 4643-4654.
6. Flickinger, S. T., Copeland, M. F., Downes, E. M., Braasch, A. T., Tuson, H. H., Eun, Y. J., and Weibel, D. B. (2011) Quorum sensing between *Pseudomonas aeruginosa* biofilms accelerates cell growth, *J Am Chem Soc* 133, 5966-5975.
7. Eun, Y. J., Utada, A. S., Copeland, M. F., Takeuchi, S., and Weibel, D. B. (2011) Encapsulating bacteria in agarose microparticles using microfluidics for high-throughput cell analysis and isolation, *ACS Chem Biol* 6, 260-266.
8. Eun, Y. J., Foss, M. H., Kiekebusch, D., Pauw, D. A., Westler, W. M., Thanbichler, M., and Weibel, D. B. (2012) DCAP: a broad-spectrum antibiotic that targets the cytoplasmic membrane of bacteria, *J Am Chem Soc* 134, 11322-11325.
9. Medema, M. H., Breitling, R., and Takano, E. (2011) Synthetic biology in *Streptomyces* bacteria, *Methods in enzymology* 497, 485-502.
10. Takano, E., Kinoshita, H., Mersinias, V., Bucca, G., Hotchkiss, G., Nihira, T., Smith, C. P., Bibb, M., Wohlleben, W., and Chater, K. (2005) A bacterial hormone (the SCB1) directly controls the expression of a pathway-specific regulatory gene in the cryptic type I polyketide biosynthetic gene cluster of *Streptomyces coelicolor*, *Mol Microbiol* 56, 465-479.
11. Zhang, Y. M., and Rock, C. O. (2008) Membrane lipid homeostasis in bacteria, *Nature reviews. Microbiology* 6, 222-233.

12. Hernandez, J., Estelrich, J., and Pouplana, R. (1987) Determination of the encapsulation efficiency in liposomes obtained by the 'extruder method', *J Microencapsul* 4, 315-320.
13. Chen, R. F., and Knutson, J. R. (1988) Mechanism of fluorescence concentration quenching of carboxyfluorescein in liposomes: energy transfer to nonfluorescent dimers, *Anal Biochem* 172, 61-77.
14. Duzgunes, N., Faneca, H., and Lima, M. C. (2010) Methods to monitor liposome fusion, permeability, and interaction with cells, *Methods in molecular biology (Clifton, N.J.)* 606, 209-232.
15. Lomovskaya, O., and Watkins, W. J. (2001) Efflux pumps: their role in antibacterial drug discovery, *Current medicinal chemistry* 8, 1699-1711.
16. Rix, U., and Superti-Furga, G. (2009) Target profiling of small molecules by chemical proteomics, *Nat Chem Biol* 5, 616-624.
17. Bond, M. R., Zhang, H., Kim, J., Yu, S. H., Yang, F., Patrie, S. M., and Kohler, J. J. (2011) Metabolism of diazirine-modified N-acetylmannosamine analogues to photo-cross-linking sialosides, *Bioconjug Chem* 22, 1811-1823.
18. Burdine, L., and Kodadek, T. (2004) Target identification in chemical genetics: the (often) missing link, *Chem Biol* 11, 593-597.
19. Tashiro, E., and Imoto, M. (2012) Target identification of bioactive compounds, *Bioorg Med Chem* 20, 1910-1921.
20. Gubbens, J., and de Kroon, A. I. (2010) Proteome-wide detection of phospholipid-protein interactions in mitochondria by photocrosslinking and click chemistry, *Mol Biosyst* 6, 1751-1759.
21. Hart, C. P. (2005) Finding the target after screening the phenotype, *Drug discovery today* 10, 513-519.
22. Zheng, X. S., Chan, T. F., and Zhou, H. H. (2004) Genetic and genomic approaches to identify and study the targets of bioactive small molecules, *Chem Biol* 11, 609-618.
23. Kodadek, T. (2010) Rethinking screening, *Nat Chem Biol* 6, 162-165.

**APPENDIX**

**Deterministic and stochastic modeling of the bipolar MipZ gradient  
in *Caulobacter crescentus***

Ye-Jin Eun, Brian T. Castle, and David J. Odde

Based on a project from the Physiology Course at the Marine Biological Laboratory

## ABSTRACT

The cytoplasm of a bacterial cell is spatially organized at the level of several different classes of biomolecules, including proteins, RNA, and DNA. Spatial organization enables the localized regulation of molecular pathways and sensing of the cellular geometry. In dividing *Caulobacter crescentus* cells, MipZ protein forms a bipolar gradient that determines the mid-point along the long axis of the bacterium. This sensing mechanism using the MipZ gradient is critical for producing two equal-sized daughter cells at the end of division. In this appendix, I describe a reaction and diffusion model to explain the origins of the MipZ gradient. The model is simulated using deterministic and stochastic approaches, and the simulations are remarkably consistent with in vivo observations. This study demonstrates that minimal components in the reaction and diffusion model are sufficient to reproduce the behavior of MipZ in vivo.

## INTRODUCTION

Francois Jacobs once said, “the dream of a bacterium is to become two bacteria” (1). This quote is supported by observations that reproductive forces influence evolution, and that bacterial cells invest an enormous amount of energy in cell growth and division. Under many different conditions, bacterial cells faithfully divide into two equal-sized daughter cells. The mechanistic underpinnings of this process are currently unclear. An important aspect of this process involves spatial recognition within the cell, as the dividing cell needs to precisely position its division machinery while ensuring that each daughter cell receives a copy of the chromosome.

*Caulobacter crescentus* appears to use an elegant solution to the challenge of spatial positioning of the divisome (2). An inhibitor protein, MipZ forms a concentration gradient from the poles of the cells such that the highest activity of inhibition is at the poles and the lowest in the middle of the cell (Figure 1). MipZ directly targets FtsZ, which is the ‘master’ component in the divisome. The interaction with the inhibitor leads to depolymerization of FtsZ filaments, dismantling the physical scaffold for the division machinery. Thus, the bipolar gradient forces the divisome to move to the region at which there is the least amount of inhibition. MipZ has a Walker-type active site and belongs to the superfamily of MinD/ParA ATPases (2).

The protein gradient formed by MipZ is striking, considering the size of a bacterium and the rate of protein diffusion in the cytoplasm. For a diffusion coefficient of  $10 \mu\text{m}^2 \text{sec}^{-1}$  (3), it takes less than one second to explore the entire length of a typical bacterium ( $2 \mu\text{m}$ ). This spatial and temporal scale implies that protein gradients in small cells such as bacteria must be achieved using a different mechanism, compared to

the process of establishing a morphogen gradient across an animal tissue. In the *Drosophila* embryo, the Bicoid gradient is established by localized synthesis and uniform degradation of the morphogen (4). Due to the size of the embryo ( $\geq 100 \mu\text{m}$  in length), the time scale for degradation of the signal is shorter than the time it takes to deliver the morphogen to the opposite place of signal synthesis by molecular diffusion. For intracellular gradients in single cells, a typical rate of protein degradation is slower than the diffusion rate in the cytoplasm, making this mechanism of 'local synthesis and uniform degradation' unsuitable (4).

Then what are the molecular mechanisms that enable a cell to form intracellular gradients of biomolecules? Several protein gradients have been discovered in both eukaryotic and prokaryotic cells, and a prevalent theme for gradient establishment has emerged from quantitative modeling and biological experiments (5-9). This common mechanism states that a protein gradient is generated when different 'states' of the protein have different diffusive behaviors (10, 11). For example, the Pom1 kinase forms a bipolar gradient in a dividing *Schizosaccharomyces pombe* cell (4, 5). The kinase has two states: phosphorylated and dephosphorylated. The dephosphorylated form of the kinase has a higher affinity for the lipid membrane than the other form, which is responsible for the different diffusion coefficients of the protein depending on its phosphorylation state. The switch between the two states is self-regulated, as the kinase auto-phosphorylates itself.

Similar to Pom1, other proteins including Mex-5 (6) and PIE-1 (8) in *Caenorhabditis elegans*, MinD in *Escherichia coli* (9), and Soj in *Bacillus subtilis* (7) form intracellular gradients. The mechanisms underlying their gradients share the same theme as Pom1, while having their own variations in protein states, regulation of changes in states, and

molecular basis for the different diffusive behaviors. MinD and Soj are Walker-type enzymes that hydrolyze ATP; thus the enzymes have apo, ATP-bound, and ADP-bound states (7, 9). Changes from one state to another can be influenced by interactions with proteins and other biomolecules, which may be positioned at a particular location in the cell (6, 7, 9). Differences in the apparent diffusion coefficients typically arises from its interaction with a macromolecule(s), such as DNA (7), RNA (6, 8), or the bilayer membrane (7, 9). Regardless of these variations, the mechanisms share a common theme, which is generally referred to as a reaction and diffusion model (7, 8).

In this appendix, I describe how reaction and diffusion models can be applied to explain the origins of the MipZ gradient in *C. crescentus*. Using deterministic and stochastic simulations, I demonstrate that this simple model successfully reproduces MipZ gradients observed in in vivo in wildtype and mutant strains.

## THE MODEL

According to the reaction and diffusion model, different states of MipZ should exhibit different diffusive behaviors. Since MipZ is an ATPase, we considered apo, ATP-bound, and ADP-bound states of the enzyme. A schematic diagram that summarizes the model is shown in Figure 2. We assumed that only one part of the ATP hydrolysis reaction is reversible, which is the substrate ATP binding event. ATP-bound MipZ forms a dimer with the substrate residing at the interface of the dimer. The ATP-bound dimeric MipZ interacts non-specifically with the chromosome, which is spread throughout the cytoplasm (12). To simplify the reaction rate equations in simulations, we omitted the dimerization reaction in the model. Furthermore, we assumed that the rate of ATP binding is increased when MipZ is interacting with ParB at the pole. Although there is no current experimental evidence supporting ParB acting as a nucleotide exchange factor, ParB may serve as a physical sink for MipZ and increase the local concentration of the enzyme at the pole (12). A high effective concentration of MipZ at the pole may promote dimerization and ATP binding. Lastly, we assumed that ParB maintains a static position in the cell since the protein is anchored at the pole via a polymeric network of PopZ (13).

## RESULTS AND DISCUSSION

### *Deterministic simulation*

We used a deterministic simulation of the model to define reaction constants necessary to create a gradient similar to the observed MipZ gradient. A total of five rate constants and three diffusion coefficients were derived from this simulation (Figure 1 and Table 1). For each species, we expressed its changes in concentration in both time and one-dimensional space using partial differential equations.

$$\frac{\partial[MipZ]}{\partial t} = D_{MipZ} \frac{\partial^2[MipZ]}{\partial x^2} + k_{-1}[MipZ \cdot ATP] + k_3[MipZ \cdot ADP] - k_1[MipZ]$$

$$\frac{\partial[MipZ \cdot ATP]}{\partial t} = D_{MipZ \cdot ATP} \frac{\partial^2[MipZ \cdot ATP]}{\partial x^2} + k_1[MipZ] - (k_{-1} + k_2)[MipZ \cdot ATP]$$

$$\frac{\partial[MipZ \cdot ADP]}{\partial t} = D_{MipZ \cdot ADP} \frac{\partial^2[MipZ \cdot ADP]}{\partial x^2} + k_2[MipZ \cdot ATP] - k_3[MipZ \cdot ADP]$$

These equations incorporate terms for the diffusion of each species and assume that there is no directed transport to bias the direction of the motion. The partial derivatives were solved using Matlab for reactions at equilibrium (i.e. the left side of the equations is zero). Since the reactions are identical at both poles, only one half of the cell was simulated (a total cell length of 2.4  $\mu\text{m}$ ). The region of ParB localization was set from 0.2 to 0.3  $\mu\text{m}$  and the pole was defined as 0  $\mu\text{m}$ . Within the ParB region, the rate constant  $k_1$  was substituted with  $k_{1B}$  to reflect the increase in dimerization rate in the presence of ParB. We adjusted the boundary conditions to make the total protein

concentration similar to the cellular concentration of MipZ ( $\sim 3.5 \mu\text{M}$ ), which was determined using quantitative western blot (2).

We determined a set of values for the parameters used in the simulation that mimicked the MipZ gradients observed in vivo (Figures 1 and 3A and Table 1). We adjusted their values in the simulation and evaluated the sensitivity of each parameter. We found that  $D_{MipZ \cdot ATP}$ ,  $k_{-1}$ , and  $k_{1B}$  were very sensitive to changes, which significantly affected the shape of the MipZ gradient in the simulation. Both  $k_{-1}$  and  $k_{1B}$  directly modulate the concentration of  $MipZ \cdot ATP$ , which is the most prevalent state of the protein in the simulation (Figure 3A). The rate constant  $k_1$  was sensitive only to changes that increase its value. This directional sensitivity suggests that maintaining a large difference between  $k_1$  and  $k_{1B}$  (e.g. a 100-fold as shown in Table 1) is critical for the gradient shape. Other parameters including  $k_2$ ,  $k_3$ ,  $D_{MipZ}$ , and  $D_{MipZ \cdot ADP}$  were the least sensitive to changes.

The values of some parameters determined from this simulation corresponded well with previous experimental data, indicating the validity of the model. The rate constant  $k_1$  was reported to be  $0.07 \mu\text{M}^{-1} \text{s}^{-1}$ , which was measured using stopped-flow spectrometry (12). This value is very similar to the results of our simulations ( $0.1 \mu\text{M}^{-1} \text{s}^{-1}$ ; Table 1). Furthermore, the product of simulated rate constants  $k_2$  and  $k_3$  were equivalent to the experimentally determined  $k_{cat}$  (2). In conditions where initial velocity of the enzyme is measured,  $k_{cat}$  represents the rate of product formation from the enzyme and substrate complex. Thus, this rate constant corresponds to the product of two constants  $k_2$  and  $k_3$ . The product of simulated  $k_2$  and  $k_3$  is  $0.005 \text{s}^{-1}$  and is similar

to the reported value of  $k_{cat}$  (2). Lastly, the diffusion coefficients of simulated species were comparable to the diffusive behaviors observed in vivo. The fold difference between slow ( $MipZ \cdot ATP$ ) and fast species ( $MipZ$  and  $MipZ \cdot ADP$ ) was two orders of magnitude (0.01 verses  $5 \mu\text{m}^2 \text{s}^{-1}$ , respectively; Table 1). This difference in magnitude was measured in fluorescence recovery after photobleaching (FRAP) experiments using cells that express either dimeric or monomeric MipZ mutants (12). The dimeric mutant (D42A) is locked in the  $MipZ \cdot ATP$  state, as it is unable to hydrolyze ATP. The recovery time of D42A was 157 s, compared to 2 s for the monomeric mutant (G14V) that does not bind DNA.

While the parameters described above had simulated values that matched well with experimental data, the rate constant  $k_{-1}$  had a discrepancy between simulation and biochemical data. The simulated rate was 10-fold smaller than the experimentally determined value (12). Using a larger  $k_{-1}$  in the simulation sharpens the polar localization of MipZ, and eliminates the gradual tail of the MipZ gradient.

Another parameter that lacks experimental support is the rate constant  $k_{1B}$ . To biochemically determine  $k_{1B}$ , it would be necessary to characterize the kinetics of ATP binding to dimeric MipZ in the presence of ParB and DNA. Currently this experimental data does not exist to compare to simulation since fluorescently labeled ATP interferes dimerization of the protein (12). Despite this lack of biochemical information, in vivo FRAP experiments suggest that the presence of ParB is critical for MipZ dimerization. In these experiments, the recovery time of wildtype MipZ was similar to the monomeric mutant when ParB is depleted in the cell (12). This observation indicates that most MipZ stays as a monomer when there is no ParB to increase the dimerization rate.

Following the simulation of wildtype MipZ gradients, we tested whether the model recapitulated the behavior of MipZ mutants. The D42A mutation in MipZ abolishes the gradient, and the mutant protein is diffused throughout the cytoplasm (2). Several biochemical experiments demonstrated that MipZ D42A is predominately in the ATP-bound dimeric state (12). Thus the hydrolysis rate ( $k_{cat}$ ) of the mutant is 10-fold slower than that of the wildtype (2). To mimic this behavior, we lowered the rate constant  $k_3$  by 100-fold, which effectively destroyed the gradient (Figure 3A). We found that any decrease in  $k_3$  that is less than 100-fold is too small to significantly change the gradient. This observation suggests that the model is able to reproduce the mutant behavior, although it requires more dramatic changes to the parameter than the changes measured experimentally.

The mutant MipZ K13A has a different distribution pattern compared to wildtype and D42A strains. The K13A mutant displays intense polar foci overlapping with the localization of ParB. In addition to the microscopy data *in vivo*, this mutant exists as monomers *in vitro* (12). Therefore, we chose to increase the rate constant  $k_{-1}$  to mimic the behavior of the mutant. A 10-fold increase in the parameter made the gradient shaper and reduced the tail, which is consistent with the *in vivo* observations of this mutant MipZ. In summary, the deterministic simulation demonstrated that the simple model of reaction and diffusion (Figure 1) captures several critical features of the experimental data, including the *in vivo* behavior of wildtype and mutant MipZ.

### *Stochastic simulation*

In addition to the deterministic simulation, we used Monte Carlo simulation to

investigate how the stochastic nature of biological reactions influences the MipZ gradient. To capture the noisiness of biological processes, we transformed the reaction rates from the deterministic simulation into probabilities of events for individual protein molecules in the stochastic simulation. We simulated 1,000 molecules in a two-dimensional space with a typical width (1  $\mu\text{m}$ ) and length (2.4  $\mu\text{m}$ ) of a dividing cell. This concentration of MipZ in the simulation is consistent with the amount of MipZ in a single cell, measured by quantitative Western blot (2). The region of ParB was defined as the space between each pole and 0.3  $\mu\text{m}$  away from the pole in length. The total simulation time was 1,000 s with a time increment of 0.01 s. At the beginning of the simulation, all molecules were in the free protein state (without any bound nucleotides) and scattered at random positions in the cell. The final state of molecules with their positions were recorded and plotted at the end of the simulation.

In the stochastic simulation, the reaction probabilities of both wildtype and mutant MipZ produced protein distributions in agreement with the deterministic simulation (Figure 4). Utilizing the positional information of individual molecules from the stochastic simulation (14), we created a corresponding image of a virtual cell to visualize the simulated gradient of fluorescent MipZ (Figure 5). This model convolution is useful to determine whether the simulated protein gradient matches the *in vivo* protein distribution observed by fluorescence microscopy (14). We measured the intensity of fluorescent MipZ from both *in silico* and *in vivo* experiments, and overlaid their intensities (Figure 5). The plots show that the simulated cells have a protein distribution very similar to that observed *in vivo* experiments for wildtype, K13A, D42A strains.

## CONCLUSION

In this appendix, we have demonstrated that reaction and diffusion models can successfully recapitulate the MipZ distribution observed in wildtype and mutant strains of *C. crescentus*. Although the model (Figure 1) simplified several aspects of the MipZ hydrolysis cycle, simulations of the model show that the MipZ gradients were effectively reproduced (Figure 5B). This demonstration illustrates the minimal components necessary to create an intracellular gradient in a bacterial cell.

Despite the successful recapitulation of the protein gradient, the current model has several limitations. 1) The assumption that the affinity of MipZ to ADP is insignificant contradicts the experimental finding that monomeric MipZ has an equal affinity to ATP and ADP ( $K_D$  of  $\sim 30 \mu\text{M}$ , 2012). However, the kinetics of nucleotide binding to dimeric MipZ has not yet been characterized (12), and the dimeric MipZ may have a significant bias towards binding ATP over ADP. 2) The model does not take into account the dimerization reaction of MipZ. While this assumption did not restrain the model from demonstrating a MipZ gradient similar to in vivo observations, incorporation of the dimerization step in the model may improve the deterministic simulation to obtain kinetic parameters that more closely match the experimental data (Table 1). However, the incorporation would require significantly greater computing power for the stochastic simulation, as the positional information for individual molecules would need to be stored for each time increment.

In conclusion, the reaction and diffusion model of MipZ show that modeling and simulation make it possible to identify of minimal components to produce a phenotype, and modulate the interactions between different biochemical processes to predict

outcomes that are not intuitive. Insights obtained from the modeling can help design follow-up experiments *in vitro* and *in vivo* (15, 16). The cyclic process and feedback between modeling and experimentation serve a useful approach for quantitative biology (17).

## ACKNOWLEDGEMENTS

Y.-J. E. thanks Marine Biological Laboratory for providing scholarships to attend the Physiology Course, and Prof. Douglas B. Weibel who has enthusiastically supported the author's participation in the course. Y.-J. E. is grateful to the course directors, Drs. Dyche Mullins and Clare Waterman, and other participants in the course.

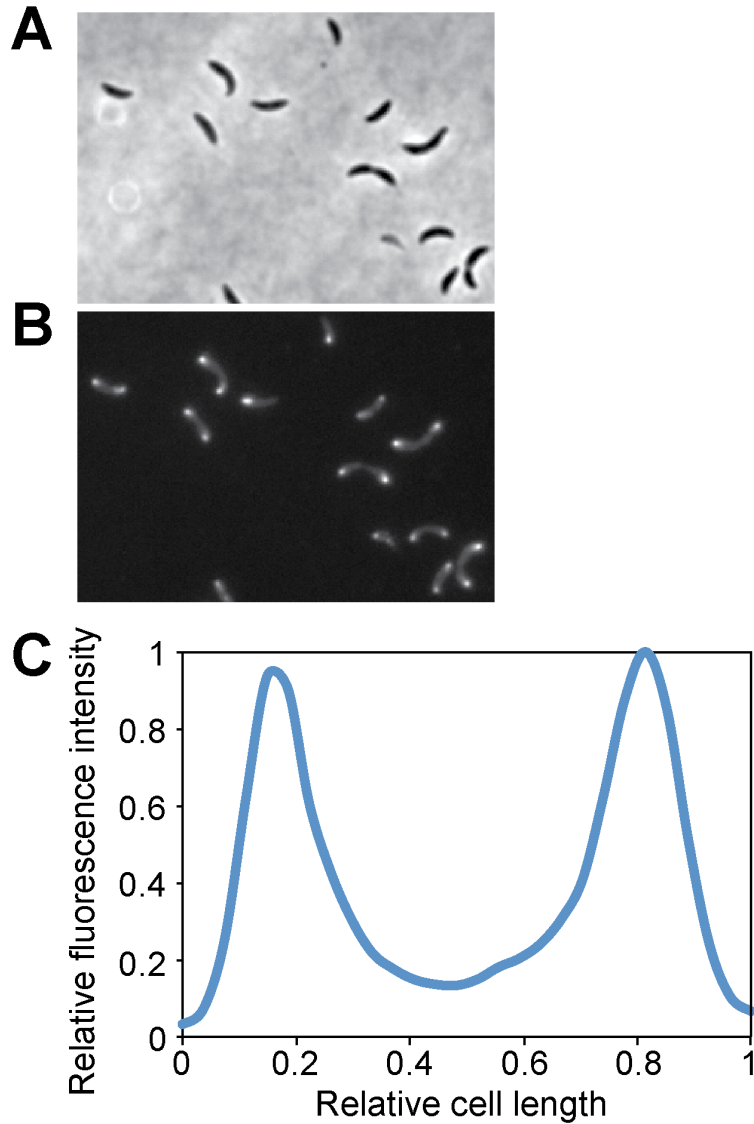


**Figure 1.** Intracellular gradient of MipZ in *C. crescentus*. A bright-field image of *C. crescentus* cells (A) and the corresponding fluorescence image of MipZ-YFP (B). A typical line scan of MipZ-YFP in a single *C. crescentus* cell (C). The fluorescence intensity has been scaled to the highest signal in the cell, after subtracting the background signal. The cell length has been scaled so that the poles have relative positions of 0 and 1. The mid-cell is at position 0.5.

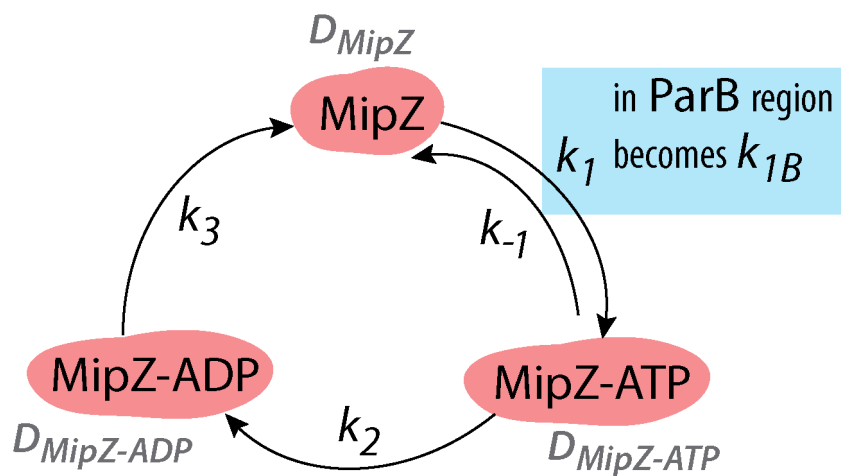


**Figure 2.** A schematic diagram of the model.

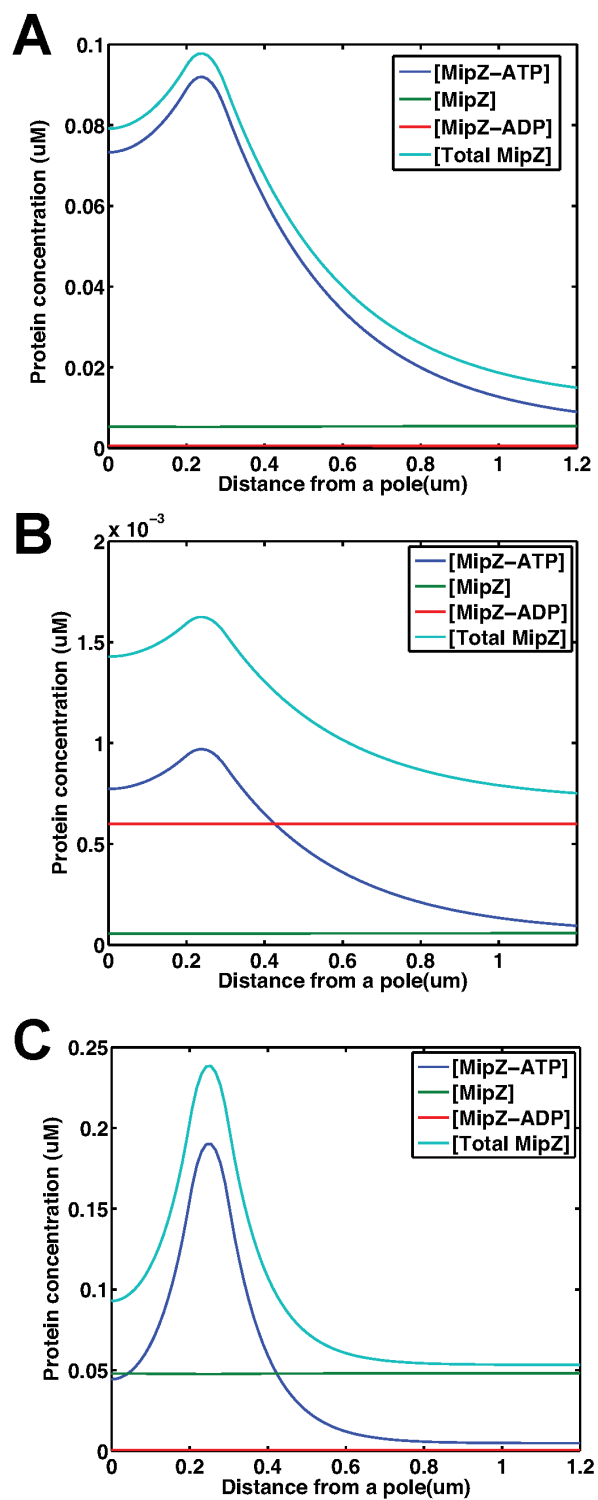


**Figure 3.** Deterministic simulations. (A) wildtype MipZ, (B) D42A mutant, and (C) K13A mutant.

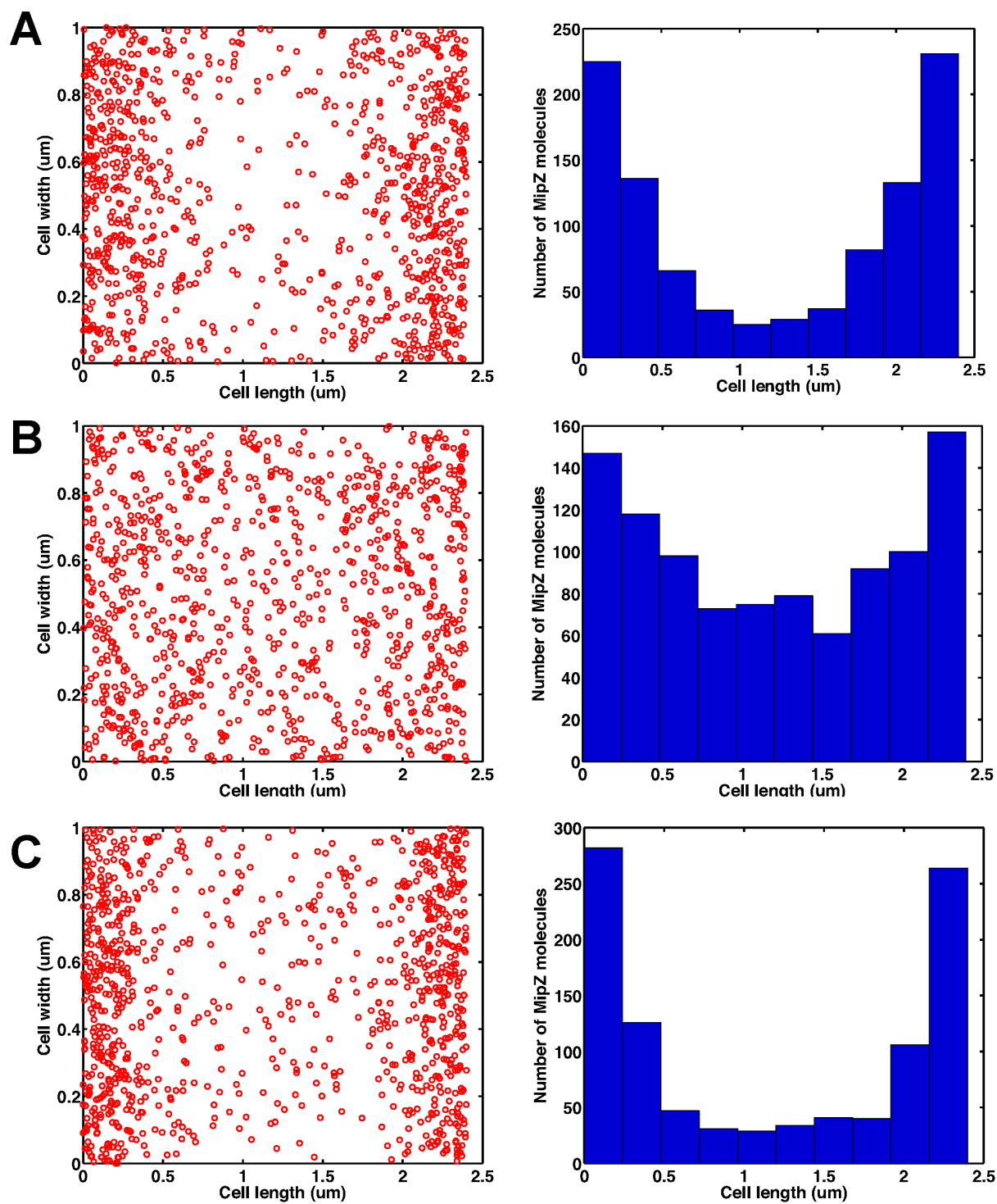
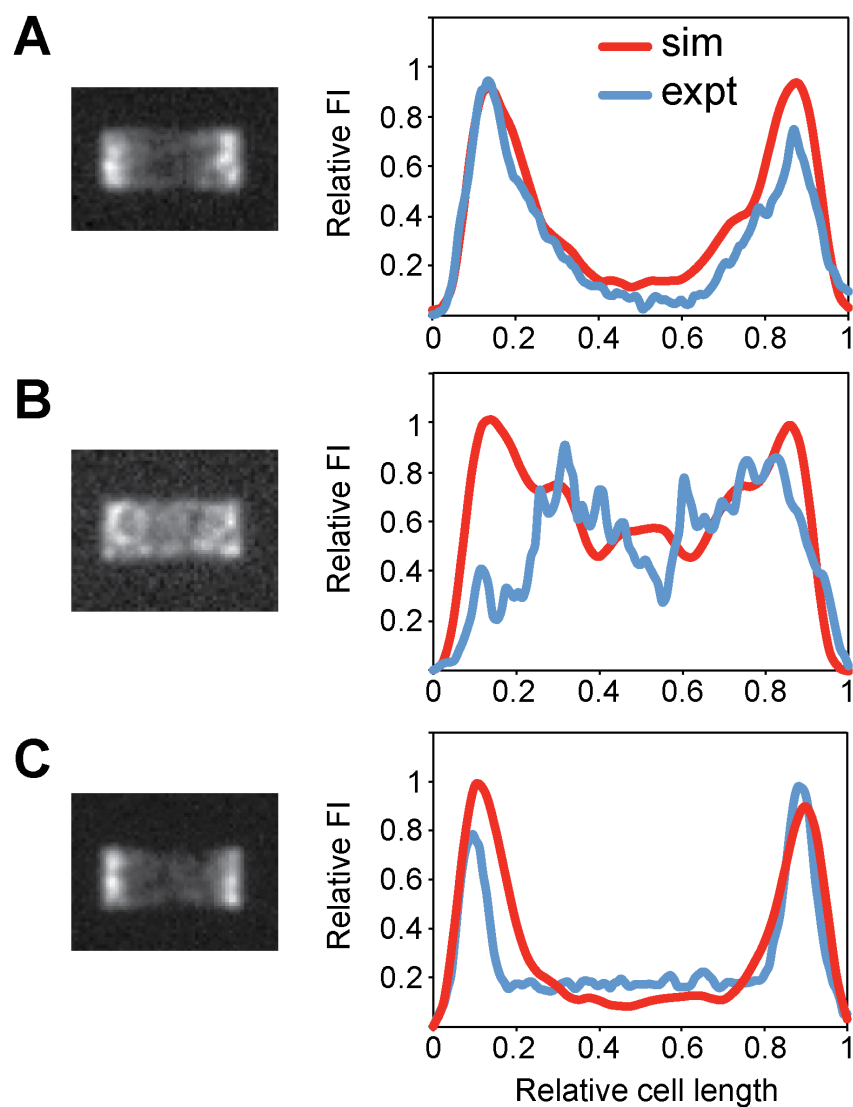


Figure 4. Stochastic simulations. (A) wildtype MipZ, (B) D42A, and (C) K13A mutants.



**Figure 5.** Model convolution of stochastic simulations. Images of virtual cells are shown on the left side, and the corresponding line scans are on the right. Line scans of real cells from in vivo experiments were taken from fluorescence micrographs in the Reference #12. In the line scan plots, the fluorescence intensity has been scaled to the highest signal in the cell, after subtracting the background signal. The cell length has been scaled so that the poles have relative positions of 0 and 1. The mid-cell is at position 0.5. (A) wildtype MipZ, (B) D42A mutant, and (C) K13A mutant.

**Table 1.** Parameters from the deterministic simulation for wildtype MipZ.

Parameter	Simulation	Experimental Data*	Reference
$k_1$	$0.1 \mu\text{M}^{-1} \text{s}^{-1}$	$0.07 \mu\text{M}^{-1} \text{s}^{-1}$	(12)
$k_{1B}$	$10 \mu\text{M}^{-1} \text{s}^{-1}$	N.A.	–
$k_{-1}$	$0.1 \text{s}^{-1}$	$2 \text{s}^{-1}$	(12)
$k_2$	$0.01 \text{s}^{-1}$	N.A.	–
$k_3$	$0.5 \text{s}^{-1}$	N.A.	–
$D_{MipZ}$	$5 \mu\text{m}^2 \text{s}^{-1}$	N.A.	–
$D_{MipZ-ATP}$	$0.01 \mu\text{m}^2 \text{s}^{-1}$	N.A.	–
$D_{MipZ-ADP}$	$5 \mu\text{m}^2 \text{s}^{-1}$	N.A.	–

\*Values for monomeric MipZ.

## REFERENCES

1. Sclafani, R. A., and Holzen, T. M. (2007) Cell cycle regulation of DNA replication, *Annual review of genetics* 41, 237-280.
2. Thanbichler, M., and Shapiro, L. (2006) MipZ, a spatial regulator coordinating chromosome segregation with cell division in *Caulobacter*, *Cell* 126, 147-162.
3. Elowitz, M. B., Surette, M. G., Wolf, P. E., Stock, J. B., and Leibler, S. (1999) Protein mobility in the cytoplasm of *Escherichia coli*, *J Bacteriol* 181, 197-203.
4. Howard, M. (2012) How to build a robust intracellular concentration gradient, *Trends Cell Biol* 22, 311-317.
5. Moseley, J. B., Mayeux, A., Paoletti, A., and Nurse, P. (2009) A spatial gradient coordinates cell size and mitotic entry in fission yeast, *Nature* 459, 857-860.
6. Griffin, E. E., Odde, D. J., and Seydoux, G. (2011) Regulation of the MEX-5 gradient by a spatially segregated kinase / phosphatase cycle, *Cell* 146, 955-968.
7. Dubrovinski, K., and Howard, M. (2005) Stochastic model for Soj relocation dynamics in *Bacillus subtilis*, *Proc Natl Acad Sci U S A* 102, 9808-9813.
8. Daniels, B. R., Perkins, E. M., Dobrowsky, T. M., Sun, S. X., and Wirtz, D. (2009) Asymmetric enrichment of PIE-1 in the *Caenorhabditis elegans* zygote mediated by binary counterdiffusion, *The Journal of cell biology* 184, 473-479.
9. Huang, K. C., Meir, Y., and Wingreen, N. S. (2003) Dynamic structures in *Escherichia coli*: spontaneous formation of MinE rings and MinD polar zones, *Proc Natl Acad Sci U S A* 100, 12724-12728.
10. Lipkow, K., and Odde, D. J. (2008) Model for Protein Concentration Gradients in the Cytoplasm, *Cellular and molecular bioengineering* 1, 84-92.
11. Tropini, C., Rabbani, N., and Huang, K. C. (2012) Physical constraints on the establishment of intracellular spatial gradients in bacteria, *BMC biophysics* 5, 17.
12. Kiekebusch, D., Michie, K. A., Essen, L. O., Lowe, J., and Thanbichler, M. (2012) Localized dimerization and nucleoid binding drive gradient formation by the bacterial cell division inhibitor MipZ, *Molecular cell* 46, 245-259.
13. Bowman, G. R., Comolli, L. R., Zhu, J., Eckart, M., Koenig, M., Downing, K. H., Moerner, W. E., Earnest, T., and Shapiro, L. (2008) A polymeric protein anchors the chromosomal origin / ParB complex at a bacterial cell pole, *Cell* 134, 945-955.

14. Gardner, M. K., Sprague, B. L., Pearson, C. G., Cosgrove, B. D., Bicek, A. D., Bloom, K., Salmon, E. D., and Odde, D. J. (2010) Model Convolution: A Computational Approach to Digital Image Interpretation, *Cellular and molecular bioengineering* 3, 163-170.
15. Mogilner, A., Allard, J., and Wollman, R. (2012) Cell polarity: quantitative modeling as a tool in cell biology, *Science* 336, 175-179.
16. Wilkinson, D. J. (2009) Stochastic modelling for quantitative description of heterogeneous biological systems, *Nature reviews. Genetics* 10, 122-133.
17. Phair, R. D., and Misteli, T. (2001) Kinetic modelling approaches to in vivo imaging, *Nature reviews. Molecular cell biology* 2, 898-907.